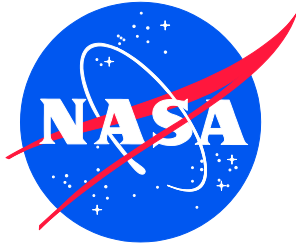


NASA/TM–2020-220568/Volume II/Part 3



Nondestructive Evaluation (NDE) Methods and Capabilities Handbook

Volume II Appendices — Appendix E Volume 2

*Patricia A. Howell, Editor
Langley Research Center, Hampton, Virginia*

APPROVED FOR PUBLIC RELEASE

February 2020

NASA STI Program . . . in Profile

Since its founding, NASA has been dedicated to the advancement of aeronautics and space science. The NASA scientific and technical information (STI) program plays a key part in helping NASA maintain this important role.

The NASA STI program operates under the auspices of the Agency Chief Information Officer. It collects, organizes, provides for archiving, and disseminates NASA's STI. The NASA STI program provides access to the NTRS Registered and its public interface, the NASA Technical Reports Server, thus providing one of the largest collections of aeronautical and space science STI in the world. Results are published in both non-NASA channels and by NASA in the NASA STI Report Series, which includes the following report types:

- **TECHNICAL PUBLICATION.** Reports of completed research or a major significant phase of research that present the results of NASA Programs and include extensive data or theoretical analysis. Includes compilations of significant scientific and technical data and information deemed to be of continuing reference value. NASA counter-part of peer-reviewed formal professional papers but has less stringent limitations on manuscript length and extent of graphic presentations.
- **TECHNICAL MEMORANDUM.** Scientific and technical findings that are preliminary or of specialized interest, e.g., quick release reports, working papers, and bibliographies that contain minimal annotation. Does not contain extensive analysis.
- **CONTRACTOR REPORT.** Scientific and technical findings by NASA-sponsored contractors and grantees.

- **CONFERENCE PUBLICATION.** Collected papers from scientific and technical conferences, symposia, seminars, or other meetings sponsored or co-sponsored by NASA.
- **SPECIAL PUBLICATION.** Scientific, technical, or historical information from NASA programs, projects, and missions, often concerned with subjects having substantial public interest.
- **TECHNICAL TRANSLATION.** English-language translations of foreign scientific and technical material pertinent to NASA's mission.

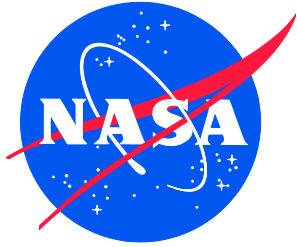
Specialized services also include organizing and publishing research results, distributing specialized research announcements and feeds, providing information desk and personal search support, and enabling data exchange services.

For more information about the NASA STI program, see the following:

- Access the NASA STI program home page at <http://www.sti.nasa.gov>
- E-mail your question to help@sti.nasa.gov
- Phone the NASA STI Information Desk at 757-864-9658

- Write to:
NASA STI Information Desk
Mail Stop 148
NASA Langley Research Center
Hampton, VA 23681-2199

NASA/TM–2020-220568/Volume II/Part 3



Nondestructive Evaluation (NDE) Methods and Capabilities Handbook

Volume II Appendices — Appendix E Volume 2

*Patricia A. Howell, Editor
Langley Research Center, Hampton, Virginia*

National Aeronautics and
Space Administration

Langley Research Center
Hampton, Virginia 23681-2199

APPROVED FOR PUBLIC RELEASED

February 2020

**The material is based upon work supported by NASA under Award Nos.
NNL09AA00A and 80LARC17C0004**

The use of trademarks or names of manufacturers in the report is for accurate reporting and does not constitute an official endorsement, either expressed or implied, of such products or manufacturers by the National Aeronautics and Space Administration.

Available from:

NASA STI Program / Mail Stop 148
NASA Langley Research Center
Hampton, VA 23681-2199
Fax: 757-864-6500

Table of Contents

E.21 Specimen #21 – Not Manufactured	1
E.22 Specimen #22: NASA-RP-01MP.....	1
E.22.1 Method: Single-Sided Infrared (IR) Thermography (SSIR)	1
E.22.2 Method: Through-Transmission Infrared Thermography (TTIR)	4
E.22.3 Method: Single-Side Flash Thermography (SSFT-TSR).....	7
E.23 Specimen #23 - Not Manufactured	9
E.24 Specimen #24 - Not Manufactured	9
E.25 Specimen #25 - Not Manufactured	9
E.26 Specimen #26: NASA-RP-10MP.....	9
E.26.1 Method: SSIR	10
E.26.2 Method: TTIR	12
E.26.3 Method: SSFT-TSR	15
E.27 Specimen #27 - Not Manufactured	18
E.28 Specimen #28: NASA-RP-20MP.....	18
E.28.1 Method: Single-Sided Infrared Thermography (SSIR).....	19
E.28.2 Method: Through-Transmission Infrared Thermography (TTIR)	22
E.28.3 Method: Single-Side Flash Thermography (SSFT-TSR).....	25
E.29 Specimen #29 - Not Manufactured	27
E.30 Specimen #30: NASA-RP-40MP 4.0-inch radial curve medium porosity.....	27
E.30.1 Method: Pulse-Echo Ultrasonic Testing (PEUT).....	28
E.30.2 Method: Guided Wave Ultrasonic Testing (GWUT).....	29
E.31 Specimen #31: Wrinkle A1.....	33
E.31.1 Method: Pulse-Echo Ultrasound Testing (PEUT)	33
E.31.2 Method: X-ray Computed Tomography (XCT).....	36
E.31.3 Method: Single-Sided Infrared Thermography (SSIR).....	40
E.32 Specimen #32: Wrinkle A2.....	42
E.32.1 Method: Pulse-Echo Ultrasound Testing (PEUT)	42
E.32.2 Method: X-ray Computed Tomography (XCT).....	45
E.32.3 Method: Guided Wave Ultrasonic Testing (GWUT).....	48
E.32.4 Method: Single-Sided Infrared Thermography (SSIR).....	59
E.33 Specimen #33: Wrinkle A3.....	61
E.33.1 Method: Pulse-Echo Ultrasound Testing (PEUT)	62
E.33.2 Method: X-ray Computed Tomography (XCT).....	65
E.33.3 Method: Guided Wave Ultrasonic Testing (GWUT).....	69
E.33.4 Method: Single-Sided Infrared Thermography (SSIR).....	74
E.34 Specimen #34: Wrinkle A4.....	76
E.34.1 Method: Pulse-Echo Ultrasonic Testing (PEUT).....	77
E.34.2 Method: X-ray Computed Tomography (XCT).....	79
E.34.3 Method: Guided Wave Ultrasonic Testing (GWUT).....	83
E.34.4 Method: Single-Sided Infrared Thermography	86
E.35 Specimen #35: Boeing 8276-200-58-8A	88
E.35.1 Method: X-ray Computed Tomography (XCT).....	89
E.35.2 Method: Through-Transmission Ultrasound Testing (TTUT).....	93
E.35.3 Method: Single-Sided Infrared Thermography (SSIR).....	95
E.35.4 Method: X-ray Digital Radiography (DR).....	97
E.35.5 Method: X-ray Computed Radiography (CR)	100
E.36 Specimen #36: Boeing 8276-200-58-26A	104
E.36.1 Method: X-ray Computed Tomography (XCT).....	104
E.36.2 Method: Through-Transmission Ultrasound Testing (TTUT).....	108

E.36.3	Method: Single-Sided Infrared Thermography (SSIR).....	110
E.36.4	Method: X-ray Digital Radiography (DR).....	112
E.36.5	Method: Computed Radiography (CR).....	115
E.36.6	Method: X-ray Backscatter	118
E.37	Specimen #37: Boeing 8276-200-58-48A	120
E.37.1	Method: Pulse-Echo Ultrasound Testing (PEUT)	120
E.37.2	Method: X-ray Computed Tomography (XCT).....	122
E.37.3	Method: Through-Transmission Ultrasound Testing (TTUT).....	126
E.37.4	Method: Single-Sided Infrared Thermography (SSIR).....	128
E.37.5	Method: X-ray Digital Radiography (DR).....	130
E.37.6	Method: Computed Radiography (CR).....	133
E.38	Specimen #38: Boeing 8276-200-56-48A	135
E.38.1	Method: X-ray Computed Tomography (XCT).....	136
E.38.2	Method: Through-Transmission Ultrasound Testing (TTUT).....	140
E.38.3	Method: X-ray Digital Radiography (DR).....	142
E.38.4	Method: X-ray Computed Radiography (CR)	144
E.39	Specimen #39: Boeing 8276-200-59-48A	147
E.39.1	Method: X-ray Computed Tomography (XCT).....	147
E.39.2	Method: Through-Transmission Ultrasound Testing (TTUT).....	151
E.39.3	Method: X-ray Digital Radiography (DR).....	153
E.39.4	Method: X-ray Computed Radiography (CR)	156
E.40	Specimen #40: Boeing-8276-200-58-8B – Not Tested.....	158

List of Figures

Figure E.22-1.	Photographs of Specimen #22: NASA-RP-01MP.	1
Figure E.22-2.	SSIR setup.....	1
Figure E.22-3.	NASA-RP-01MP sample.	3
Figure E.22-4.	SSIR inspection of NASA-RP-01MP sample’s left, center, and right section processed with PCA from frame 100 (1.66s) to 1000 (16.66s).	3
Figure E.22-5.	TTIR setup.	4
Figure E.22-6.	NASA-RP-01MP sample.	6
Figure E.22-7.	TTIR inspection of NASA-RP-01MP sample’s left, center, and right section processed with PCA from frame 100 (1.66s) to 1500 (25s).	6
Figure E.22-8.	SSFT system with TSR.	8
Figure E.22-9.	TSR 2 nd derivative at 4.87sec of NASA-RP-01MP.	9
Figure E.26-1.	Photographs of Specimen #26: NASA-RP-10MP.	9
Figure E.26-2.	SSFT setup.....	10
Figure E.26-3.	NASA-RP-10MP sample.	11
Figure E.26-4.	SSFT inspection of NASA-RP-10MP sample’s left, center, and right section processed with PCA from frame 100 (1.66s) to 500 (8.33s).	12
Figure E.26-5.	TTIR setup.	13
Figure E.26-6.	NASA-RP-10MP sample.	14
Figure E.26-7.	TTIR inspection of NASA-RP-10MP sample’s left, center, and right section processed with PCA from frame 100 (1.66s) to 1500 (25s).	15
Figure E.26-8.	SSFT system with TSR.	17
Figure E.26-9.	TSR 2 nd derivative at 3.53 sec of NASA-RP-10MP.....	18
Figure E.28-1.	Photographs of Specimen #26: NASA-RP-2.	18
Figure E.28-2.	SSIR setup.....	19
Figure E.28-3.	SSFT inspection of NASA-RP-20MP sample.	20

Figure E.28-4.	SSFT inspection of NASA-RP-20MP sample's left, center, and right section processed with PCA from frame 150 (2.5s) to 1000 (16.67s).....	21
Figure E.28-5.	TTIR setup.	22
Figure E.28-6.	SSFT inspection of NASA-RP-20MP sample.	23
Figure E.28-7.	TTIR inspection of NASA-RP-20MP sample's left, center, and right section processed with PCA from frame 100 (1.67s) to 1500 (25s).	24
Figure E.28-8.	SSFT system with TSR.	26
Figure E.28-9.	TSR 2 nd derivative at 6.13 sec of NASA-RP-20MP.	27
Figure E.30-1.	Photographs of specimen #30: NASA-RP-40MP.	27
Figure E.30-2.	Ultrasonic system components.	28
Figure E.30-3.	Picture of specimen NASA-RP-40MP.	29
Figure E.30-4.	Schematic design of the PZT-SLDV system.	30
Figure E.30-5.	Experimental setup of the PZT-SLDV system.	30
Figure E.30-6.	Experimental setup.	31
Figure E.30-7.	Wavefield imaging on the outside surface with excitation location at: a) O ₁ , b) O ₂ , and c) O ₃	32
Figure E.30-8.	Wavefield imaging on the inside surface with excitation location at: a) O ₁ , b) O ₂ , and c) O ₃	32
Figure E.31-1.	Photograph of specimen #31: Boeing Wrinkle A1.	33
Figure E.31-2.	Ultrasonic system components.	34
Figure E.31-3.	UT image showing near surface indications of fiber waviness.	35
Figure E.31-4.	UT image showing indications of fiber waviness within the material bulk.	35
Figure E.31-5.	XCT system components.	36
Figure E.31-6.	Slice direction nomenclature.	37
Figure E.31-7.	Microfocus XCT system showing orientation of Specimen #31: Boeing-Wrinkles A1... ..	37
Figure E.31-8.	3D X-ray generated view of specimen #31: Boeing-Wrinkles using a small viewing window showing the y-normal direction (center), z-normal direction (top) and x-normal direction (right).	39
Figure E.31-9.	3D X-ray generated view of specimen #31: Boeing-Wrinkles from the z-normal direction.	39
Figure E.31-10.	SSIR system components.	40
Figure E.31-11.	IR inspection system.	41
Figure E.31-12.	Greyscale 1.6 sec IR image of Composite Wrinkle Standard A1 side 1 (a) and side 2 (b).	42
Figure E.32-1.	Photographs of Specimen #33: Boeing Wrinkle A3.	42
Figure E.32-2.	Ultrasonic system components.	43
Figure E.32-3.	UT image showing near surface indications of fiber waviness.	44
Figure E.32-4.	UT image showing indications of fiber waviness within the material bulk.	45
Figure E.32-5.	XCT system components.	46
Figure E.32-6.	Slice direction nomenclature.	46
Figure E.32-7.	Microfocus XCT system showing orientation of Specimen #32: Boeing-Wrinkles A2... ..	47
Figure E.32-8.	3D X-ray generated view of specimen #32: Boeing-Wrinkles using a small viewing window showing the y direction (center), z direction (top) and x direction (right).	48
Figure E.32-9.	Picture of Specimen A2. (a) front side (side 1), (b) back side (side 2); (c) side view.	49
Figure E.32-10.	Schematic Design of the PZT-SLDV System.	49
Figure E.32-11.	Experimental Setup of the PZT-SLDV System.	50
Figure E.32-12.	Experimental setup for Specimen A2 along 0°/180° direction w.r.t actuation on side 1: (a) 1D line inspection, and (b) 2D area inspection.	51
Figure E.32-13.	Experimentally Acquired Dispersion Curves.	52
Figure E.32-14.	Comparison between 1D inspection results along W and R.	53
Figure E.32-15.	Energy map of wrinkle region at excitation frequency.	54

Figure E.32-16. Experimental setup of 2D inspection from different actuation (location O ₁ for a left view).	55
Figure E.32-17. Energy map of wrinkle region with actuation at location O ₁ for left view.	55
Figure E.32-18. Reference region 2D inspection scanning setup with actuation at different locations: inspection with excitation at O for a left view, at O ₂ for a right view, and at O ₃ for another right view	56
Figure E.32-19. Energy map of the reference region with different actuations.	56
Figure E.32-20. Energy map of wrinkle region.	57
Figure E.32-21. Energy map of the reference region with different actuations.	58
Figure E.32-22. Flash IRT system components.	60
Figure E.32-23. IR inspection system.	60
Figure E.32-24. Greyscale 1.6 sec IR image of Composite Wrinkle Standard A2 side 1 (a) and side 2 (b).	61
Figure E.33-1. Photograph of Specimen #33: Boeing-Wrinkle-A3.	61
Figure E.33-2. Ultrasonic system components.	62
Figure E.33-3. UT image showing near surface indications of fiber waviness.	63
Figure E.33-4. UT image showing indications of fiber waviness within the material bulk.	64
Figure E.33-5. UT image showing indications of fiber waviness within the material bulk.	65
Figure E.33-6. XCT System Components	66
Figure E.33-7. Slice Direction Nomenclature.	66
Figure E.33-8. Microfocus XCT system showing orientation of Specimen #33: Boeing-Wrinkles A3.	67
Figure E.33-9. 3D X-ray generated view of Specimen #33: Boeing-Wrinkles using a small viewing window showing the y direction (center), z direction (top) and x direction (right).	68
Figure E.33-10. 3D X-ray generated view of Specimen #33: Boeing-Wrinkles from the z direction.	68
Figure E.33-11. Picture of specimen A3.	69
Figure E.33-12. Schematic design of the PZT-SLDV system.	70
Figure E.33-13. Experimental setup of the PZT-SLDV system.	70
Figure E.33-14. Experimental setup along 0°/180° direction w.r.t actuation on side 1.	71
Figure E.33-15. 1D Inspection results wavefield results with excitation at (a) 120 kHz, (b) 240 kHz, and (c) 300 kHz; frequency-wavenumber spectra with excitation at (d) 120 kHz, (e) 240 kHz, and (f) 300 kHz, showing that wave-wrinkle interaction becomes obvious with excitation frequency increase.	72
Figure E.33-16. Wavefield images obtained on side-1 with excitation.	73
Figure E.33-17. Wavefield images obtained on side-2 with excitation.	73
Figure E.33-18. Flash IRT system components.	75
Figure E.33-19. IR inspection system.	75
Figure E.33-20. Greyscale 1.6 sec IR image of Composite Wrinkle Standard A3 side 1 (a) and side 2 (b).	76
Figure E.34-1. Photograph of Specimen #34: Boeing-Wrinkle-A4.	76
Figure E.34-2. Ultrasonic system components.	77
Figure E.34-3. UT image showing near surface indications of fiber waviness.	78
Figure E.34-4. UT image showing indications of fiber waviness within the material bulk.	79
Figure E.34-5. XCT system components.	80
Figure E.34-6. Slice direction nomenclature.	80
Figure E.34-7. Microfocus XCT system showing orientation of Specimen #34: Boeing-Wrinkles A4.	81
Figure E.34-8. 3D X-ray generated view of specimen #32: Boeing-Wrinkles using a small viewing window showing the y direction (center), z direction (top) and x direction (right).	82
Figure E.34-9. 3D X-ray generated view of specimen #34: Boeing-Wrinkles from the z direction.	83
Figure E.34-10. Picture of specimen A4. (a) front side (side 1), and (b) back side (side 2).	83
Figure E.34-11. Schematic design of the PZT-SLDV system.	84
Figure E.34-12. Experimental setup of the PZT-SLDV system.	84

Figure E.34-13. 2D area inspection setup.	85
Figure E.34-14. Wavefield images obtained on: (a) side-1, and (b) side-2.	85
Figure E.34-15. Flash IRT system components.	87
Figure E.34-16. IR inspection system.	87
Figure E.34-17. Greyscale 1.0 sec IR image of Composite Wrinkle Standard A4 side 1 (a) and side 2 (b).	88
Figure E.35-1. Photographs of Angle Panel Reference Standard	89
Figure E.35-2. XCT system components.	89
Figure E.35-3. Slice direction nomenclature.	90
Figure E.35-4. Microfocus XCT setup for Radii Delamination Standard.	91
Figure E.35-5. CT slice view showing PT (a), RPF (b), and brass (c) inserts.	92
Figure E.35-6. CT slice view showing PT and RPF inserts.	93
Figure E.35-7. TTUT Scanning schematic with water pump.	94
Figure E.35-8. TTUT scans showing PT (a), RPF (b), and brass (c) inserts.	95
Figure E.35-9. Flash IRT system components.	96
Figure E.35-10. IR inspection system.	96
Figure E.35-11. Greyscale IR image of Radii Delamination Standard inserts (Top: PT and RPF, Bottom: brass).	97
Figure E.35-12. X-ray DR imaging.	98
Figure E.35-13. Laboratory setup of angle plate standard for DR imaging.	98
Figure E.35-14. DR Image of RPF inserts with close up.	100
Figure E.35-15. DR images of PT (a), RPF (b), and brass (c) insert locations in 8276-200-58-8 standard.	100
Figure E.35-16. X-ray CR imaging.	101
Figure E.35-17. Laboratory setup of angle plate standards for CR imaging.	102
Figure E.35-18. CR image of RPF inserts with close up (filter applied).	103
Figure E.35-19. CR images of PT (a), RPF (b), and brass (c) insert locations for 8276-200-58-8 standard (filter applied).	103
Figure E.36-1. Photographs of Angle Panel Reference Standard.	104
Figure E.36-2. XCT system components.	104
Figure E.36-3. Slice direction nomenclature.	105
Figure E.36-4. Microfocus XCT setup for Radii Delamination Standard.	106
Figure E.36-5. CT slice view showing PT (a), RPF (b), and brass (c) inserts.	107
Figure E.36-6. CT slice view showing PT and RPF inserts.	108
Figure E.36-7. TTU Scanning schematic with water pump.	109
Figure E.36-8. TTUT scans showing PT (a), RPF (b), and brass (c) inserts.	110
Figure E.36-9. Flash IRT system components.	111
Figure E.36-10. IR inspection system.	111
Figure E.36-11. Greyscale IR image of Radii Delamination Standard inserts (Top: PT and RPF, Bottom: brass).	112
Figure E.36-12. X-ray DR imaging.	113
Figure E.36-13. Laboratory setup of angle plate standard for DR imaging.	113
Figure E.36-14. DR images of PT (a), RPF (b), and brass (c) insert locations in 8276-200-58-26 standard.	115
Figure E.36-15. X-ray CR imaging.	116
Figure E.36-16. Laboratory setup of angle plate standards for CR imaging.	116
Figure E.36-17. CR images of PT (a), RPF (b), and brass (c) insert locations for 8276-200-58-26 standard (filter applied).	117
Figure E.36-18. NuSAFE portable X-ray backscatter system.	118
Figure E.36-19. X-ray backscatter imaging.	119
Figure E.36-20. X-ray backscatter image of 8276-200-58-26 standard with brass inserts.	120

Figure E.37-1. Photograph of Specimen #37: Boeing 8276-200-58-48A.....	120
Figure E.37-2. Ultrasonic system components.	121
Figure E.37-3. UT image showing near surface delaminations on the large flat edge.	122
Figure E.37-4. UT image showing delaminations within the bulk of the sample.....	122
Figure E.37-5. UT image showing delaminations within the bulk of the sample.....	122
Figure E.37-6. XCT system components.	123
Figure E.37-7. Slice direction nomenclature.....	123
Figure E.37-8. Microfocus XCT setup for Radii Delamination Standard.	124
Figure E.37-9. CT Slice view showing PT (a), RPF (b), and brass (c) inserts.	125
Figure E.37-10. CT slice view showing PT and RPF inserts.....	126
Figure E.37-11. TTUT scanning schematic with water pump.	127
Figure E.37-12. TTUT scans showing PT (a), RPF (b), and brass (c) inserts.....	128
Figure E.37-13. Flash IRT system components.	129
Figure E.37-14. IR inspection system.	129
Figure E.37-15. Greyscale IR image of Radii Delamination Standard inserts (Top: PT and RPF, Bottom: brass).....	130
Figure E.37-16. X-ray DR imaging.	131
Figure E.37-17. Laboratory setup of angle plate standard for DR imaging.....	131
Figure E.37-18. DR images of PT (a), RPF (b), and brass (c) insert locations in 8276-200-58-48 standard.....	133
Figure E.37-19. X-ray CR imaging.....	134
Figure E.37-20. Laboratory setup of angle plate standards for CR imaging.	134
Figure E.37-21. CR images of PT (a), RPF (b), and brass (c) insert locations for 8276-200-58-48 standard (filter applied).....	135
Figure E.38-1. Photographs of Angle Panel Reference Standard.	136
Figure E.38-2. XCT system components.	136
Figure E.38-3. Slice direction nomenclature.....	137
Figure E.38-4. Microfocus XCT setup for Radii Delamination Standard.	138
Figure E.38-5. CT slice view showing PT (a), RPF (b), and brass (c) inserts.	139
Figure E.38-6. CT Slice view showing PT and RPF inserts.	140
Figure E.38-7. TTUT scanning schematic with water pump.	140
Figure E.38-8. TTUT scans showing PT (a), RPF (b), and brass (c) inserts.....	142
Figure E.38-9. X-ray DR Imaging	142
Figure E.38-10. Laboratory setup of angle plate standard for DR imaging.	143
Figure E.38-11. DR images of PT (a), RPF (b), and brass (c) insert locations in 8276-200-56-48 standard.....	144
Figure E.38-12. X-ray CR imaging.....	145
Figure E.38-13. Laboratory setup of angle plate standards for CR imaging.	145
Figure E.38-14. CR images of PT (a), RPF (b), and brass (c) insert locations for 8276-200-56-48 standard (filter applied).....	146
Figure E.39-1. Photograph of specimen #39: Boeing-8276-200-59-48A.....	147
Figure E.39-2. XCT system components.	148
Figure E.39-3. Slice direction nomenclature.....	149
Figure E.39-4. Microfocus XCT setup for Radii Delamination Standard.	150
Figure E.39-5. CT slice view showing PT (a), RPF (b), and brass (c) inserts.	150
Figure E.39-6. CT slice view showing PT and RPF inserts.....	151
Figure E.39-7. TTUT scanning schematic with water pump.	152
Figure E.39-8. TTUT scans showing PT (a), RPF (b), and brass (c) inserts.....	153
Figure E.39-9. X-ray DR imaging.	154
Figure E.39-10. Laboratory setup of angle plate standard for DR imaging.	154

Figure E.39-11. DR images of PT (a), RPF (b), and brass (c) insert locations in 8276-200-59-48 standard.....	155
Figure E.39-12. X-ray CR imaging.....	157
Figure E.39-13. Laboratory setup of angle plate standards for CR imaging.	157
Figure E.39-14. CR images of PT (a), RPF (b), and brass (c) insert locations for 8276-200-59-48 standard (filter applied).....	158

List of Tables

Table E.30-1. Data collection settings.....	28
Table E.30-2. Equipment/device specifications.	30
Table E.30-3. Data collection settings.....	31
Table E.30-4. Hybrid PZT-SLDV guided wave inspection rating.	33
Table E.31-1. Data collection settings.....	34
Table E.31-2. Data collection settings.....	38
Table E.32-1. Data collection settings.....	43
Table E.32-2. Data collection settings.....	47
Table E.32-3. Equipment/device specifications.	50
Table E.32-4. Data collection settings.....	50
Table E.32-5. Hybrid PZT-SLDV guided wave inspection rating.	59
Table E.33-1. Data collection settings.....	62
Table E.33-2. Data collection settings.....	67
Table E.33-3. Equipment/device specifications.	70
Table E.33-4. Data collection settings.....	70
Table E.33-5. Hybrid PZT-SLDV guided wave inspection rating.	74
Table E.34-1. Data collection settings.....	77
Table E.34-2. Data collection settings.....	81
Table E.34-3. Equipment/device specifications.	84
Table E.34-4. Data collection settings.....	84
Table E.34-5. Hybrid PZT-SLDV guided wave inspection rating.	86
Table E.35-1. Data collection settings.....	91
Table E.35-2. Data collection settings.....	94
Table E.35-3. Imaging and exposure parameters.	96
Table E.35-4. Imaging and exposure parameters.	99
Table E.35-5. Imaging and Exposure Parameters.....	102
Table E.36-1. Data collection settings.....	106
Table E.36-2. Data collection settings.....	109
Table E.36-3. Imaging and exposure parameters.	111
Table E.36-4. Imaging and exposure parameters.	114
Table E.36-5. Imaging and exposure parameters.	117
Table E.36-6. Imaging and exposure parameters.	119
Table E.37-1. Data collection settings.....	121
Table E.37-2. Data collection settings.....	124
Table E.37-3. Data collection settings.....	127
Table E.37-4. Data collection settings.....	129
Table E.37-5. Data collection settings.....	132
Table E.37-6. Data collection settings.....	134
Table E.38-1. Data collection settings.....	138
Table E.38-2. Data collection settings.....	141
Table E.38-3. Imaging and exposure parameters.	143

Table E.38-4.	Imaging and exposure parameters.	146
Table E.39-1.	Data collection settings.	147
Table E.39-2.	Data collection settings.	151
Table E.39-3.	Imaging and exposure parameters.	153
Table E.39-4.	Imaging and exposure parameters.	156

Nomenclature

μA	Microampere
μm	Micrometer/Micron
μs	Microseconds
1D	One-Dimensional
2D	Two-Dimensional
3D	Three-Dimensional
ABS	Acrylonitrile Butadiene Styrene
ACAD	Air Coupled Acoustic Drive
ACC	Advanced Composites Consortium
ACP	Advanced Composites Project
ACT	Air Coupled Transducer
ADR	Assisted Defect Recognition
AFP	Automated fiber placement
AISI	American Iron and Steel Institution
AMT	Active Microwave Thermography
ANSI	American National Standards Institute
APF	Automated Fiber Placement
ARC	Ames Research Center
ASME	American Society of Mechanical Engineers
ASNT	American Society of Nondestructive Testing
ASTM	American Society for Testing and Materials
ATL	Automated Tape Lay-Up
AWG	Arbitrary Waveform Generator
AWS	American Welding Society
BMS	Boeing Material Specification
BSI	British Standards Institution
BVID	Barely Visible Impact Damage
BW	Back Wall
C	Celsius
CAD	Computer-Aided Design
CAFA	Combined Analytical Finite Element Approach
CCD	Charge-coupled Device
CDRH	Center for Devices and Radiological Health
CFRP	Carbon Fiber Reinforced Polymer
CMOS	complementary metal oxide semiconductor
CNN	Convolutional Neural Network
CO_2	Carbon Dioxide
COPV	Composite Over-Wrap Pressure Vessel
CPV	Composite Pressure Vessel
CR	Computed Radiography
CST	Charge Simulation Technique
CT	Computed Tomography
CTE	Coefficient of Thermal Expansion
DAQ	Data Acquisition
dB	Decibel
dB/in	Decibels Per Inch
DDA	Digital Detector Array
DOF	Degree of Freedom
DR	Digital Radiography
DRC	Digital Radiography Center
ECT	Eddy Current Thermography
EFIT	Elastodynamic Finite Integration Technique

FBH	Flat-bottom holes
FD	Finite Difference
FDA	Food and Drug Administration
FEA	Finite Element Analysis
FEM	Finite Element Method
FEP	Fluorinated Ethylene Propylene
FLIR	Forward-looking Infrared
FMC	Full Matrix Capture
FOD	Foreign Object Debris
FOV	Field of View
ft-lbs	Foot Pounds
GE	General Electric
GHz	Gigahertz
GN ₂	Gaseous Nitrogen
gsm	Grams per square meter
GWUT	Guided Wave Ultrasound
Hz	Hertz
ID	Inner Diameter
IDIQ	Indefinite Delivery/Indefinite Quantity
IEC	International Electrotechnical Commission
IML	Inner Mold Line
in	Inch
in/min	Inches per Minute
InSb	Indium Antimonide
ipm	Images per Minute
IR	Infrared
IRT	Infrared Thermography
ISTIS	<i>In Situ</i> Thermal Inspection System
J/cm ²	Joules Per Square Centimeter
K	Kelvin
KeV	Kiloelectron Volt
kg	Kilograms
kg/cm ²	kilogram per square centimeter
kHz	Kilohertz
kV	Kilovolts
kW	kilowatt
LaRC	Langley Research Center
LBI	Laser Bond Inspection
LMCO	Lockheed-Martin Company
LPS	Local Positioning System
LST	Line Scanning Thermography
LT	Lock-In Thermography
m ²	Square Meter
m ² /hr	Meters Square per Hour
mA	Miliampere
MECAD	Mechanically Coupled Acoustic Drive
MGBM	Multi-Gaussian Beam Model
MHz	Megahertz
mHz	Millihertz
mK	Millikelvin
mm	Millimeter
MPa	Megapascals
ms	Meter per Second
MS/s	Megasamples/second

msec	Millisecond
MSFC	Marshall Space Flight Center
NAS	National Aerospace Standard
NASA	National Aeronautics and Space Administration
Nd:Glass	Neodymium Glass Laser
NDE	Nondestructive Evaluation
NDI	Nondestructive Inspection
NDT	Nondestructive Test
NEDT	Noise Equivalent Differential Temperature
NGIS	Northrop Grumman Innovation Systems
nm	Nanometer
ns	Nanosecond
OEM	Original Equipment Manufacturer
OML	Outer Mold Line
ONR	Office of Naval Research
OSHA	Occupational Safety and Health Administration
PA	Phased Array
PCA	Principal Component Analysis
PEUT	Pulse Echo Ultrasound
PMC	Polymer Matrix Composite
PML	Perfectly Matched Layer
POC	Point of Contact
PoD	Probability of Detection
PPT	Pulsed-Phase Thermography
psi	Pounds Per Square Inch
PT	Pressure-Sensitive Tape
PTFE	Polytetrafluoroethylene (Teflon™)
PVDF	polyvinylidene fluoride
PWI	Plane Wave Imaging
PW-UTC	Pratt Whitney – United Technology Corporation
PZT	Piezoelectric Sensors/Transducer
R&D	Research and Development
RAH	Refresh After Heat
RBH	Refresh Before Heat
RGB	Red, Green, and Blue
RMS	Root Mean Squared
ROI	Region of Interest
RPF	Release Ply Fabric
RSG	Rotated-Staggered Grid
RVE	Representative Volume Element
s	Seconds
SAE	Society of Automotive Engineers
SAFE	Semi-Analytical Finite Element
SAR	Synthetic Aperture Radar
sec	Seconds
SHM	Structural Health Monitoring
SLDV	Scanning Laser Doppler Vibrometer
SMAAART	Structures, Materials, Aerodynamics, Aerothermodynamics, and Acoustics Research and Technology
SME	Subject Matter Expert
SNR	Signal to Noise Ratio
SOFI	Spray on Foam Insulation
SoP	State-of-Practice
sq. ft/hr	square foot per hour

SSFT	Single-Side Flash Thermography
SSIR	Single-Sided Infrared Thermography
SVD	Singular Value Decomposition
TC2	Technical Challenge 2
TDRS	Time Domain Reflectometry Systems
TFM	Total Focus Method
T _g	Glass Transition Temperature
THz	Terahertz
TPS	Thermal Protection System
TSR	Thermographic Signal Reconstruction
TT	Through Transmission
TTIR	Through-Transmission Infrared Thermography
TTUT	Through-Transmission Ultrasound
TWI	Thermal Wave Imaging System
USC	University of South Carolina
UT	Ultrasound
VaRTM	Variation Resin Transfer Molding
VSHM	Visualized Structural Health Monitoring
XCT	X-ray Computed Tomography

Appendix E Individual Test Reports by Specimen (Sections 21-40)

☆☆☆	Not Suitable for this Specimen
★★☆	Marginally suitable for this Specimen, or only provides qualitative information
★★★	Highly successful for this Specimen, including quantifiable information

E.21 Specimen #21 – Not Manufactured

E.22 Specimen #22: NASA-RP-01MP

Structure	Material	Details	Dimensions (inches)	Partner Methods	
Uni-ply (0/90/45)	IM7/8552	0.1-inch radial inside curve. Radius Panel 0.1-inch Curve Rad with medium porosity	4.5 × 2.5 × 4	NASA	E.22.1 SSIR
				TWI	E.22.2 TTIR E.22.3 SSFT

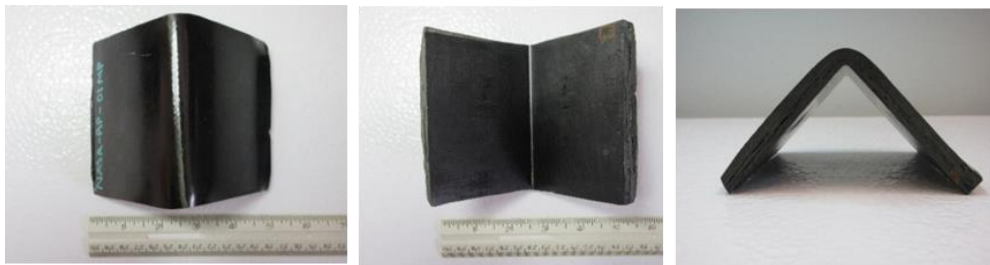


Figure E.22-1. Photographs of Specimen #22: NASA-RP-01MP.

E.22.1 Method: Single-Sided Infrared (IR) Thermography (SSIR)

E.22.1.1 Partner: NASA

E.22.1.2 Technique Applicability: ★★★

Single-sided thermography is capable of detecting few defects that may be due to porosities.

E.22.1.3 Laboratory Setup

A commercially available flash thermography system was used for the inspection. The flash thermography system consisted of two linear flash tubes mounted within a hood. An IR camera was mounted at the back of the hood viewing through a circular hole between the flash tubes and were positioned to view the hood opening. In this configuration, the flash lamps heated an area equal to the hood opening and the IR camera captured the thermal response. The IR camera operates in the mid-wave IR band (3–5 μm) and is configured with a 25-mm germanium lens. The focal plane array size for the camera is 640 × 512 with a detector pitch size of 14 × 14 μm .

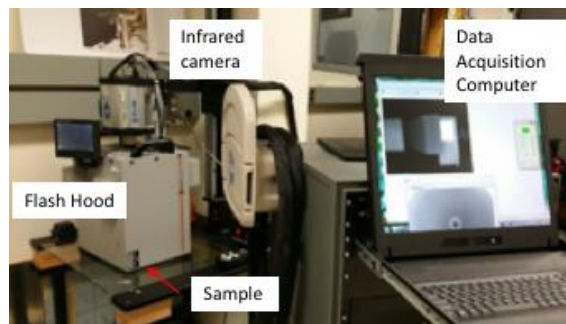


Figure E.22-2. SSIR setup.

E.22.1.4 Equipment List and Specifications:

- Thermal Wave Imaging System (TWI)
- TWI flash heat source using Speedotron power supplies.
- SC6000 FLIR IR camera, 640 × 512 Indium Antimonide (InSb) array, Noise Equivalent Differential Temperature (NEDT) < 20 mK
- 50 mm Germanium Optics

E.22.1.5 Settings:

- 60 Hz Frame Rate
- Flash on frame #10
- Total number of Frames 3000
- Total data acquisition time of 50 sec
- The camera/hood was positioned to view the entire sample

E.22.1.6 Principal Component Analysis

PCA is common for processing of thermal data [1–3]. This algorithm is based on decomposition of the thermal data into its principal components or eigenvectors. Singular value decomposition is a routine used to find the singular values and corresponding eigenvectors of a matrix. Since thermal NDE signals are slowly decaying waveforms, the predominant variations of the entire data set are usually contained in the first or second eigenvectors, and thus account for most of the data variance of interest. The principle components are computed by defining a data matrix A , for each data set, where the time variations are along the columns and the spatial image pixel points are row-wise. The matrix A is adjusted by dividing the maximum value (normalization) and subtracting the mean along the time dimension. The covariance matrix is defined as the $A^T * A$. The covariance matrix is now a square matrix of number of images used for processing. The covariance matrix can then be decomposed using singular value decomposition as:

$$\text{covariance matrix} = A^T A = V * S * V^T$$

Where S is a diagonal matrix containing the square of the singular values and V is an orthogonal matrix, which contains the basis functions or eigenvectors describing the time variations. The eigenvectors can be obtained from the columns of V . The PCA inspection image is calculated by dot product multiplication of the selected eigenvector times the temperature response (data matrix A), pixel by pixel.

E.22.1.7 Inspection Results

The 3000 frames of data (50 sec) were processed using iterations of different time windows. The processing of frames 100 to 1000 corresponding to a time window of 1.67–16.67 sec yielded the best results. Sections A to D, shown in Figure E.22-4, were the most visible compared the surrounding area. A time delay of 1.67 sec allowed enough time after the flash for the heat to flow into the sample and 16.67 sec was sufficient to provide good contrast of the defects. No apparent defects were noticed in the specimen's apex. The second eigenvector was used to produce the final inspection images shown in Figure E.22-3.

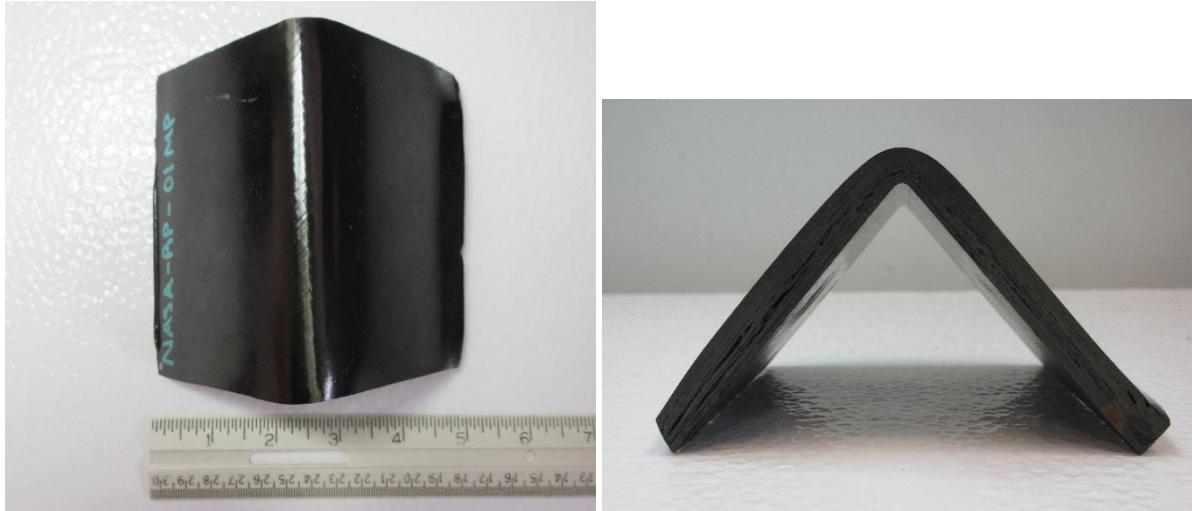


Figure E.22-3. NASA-RP-01MP sample.

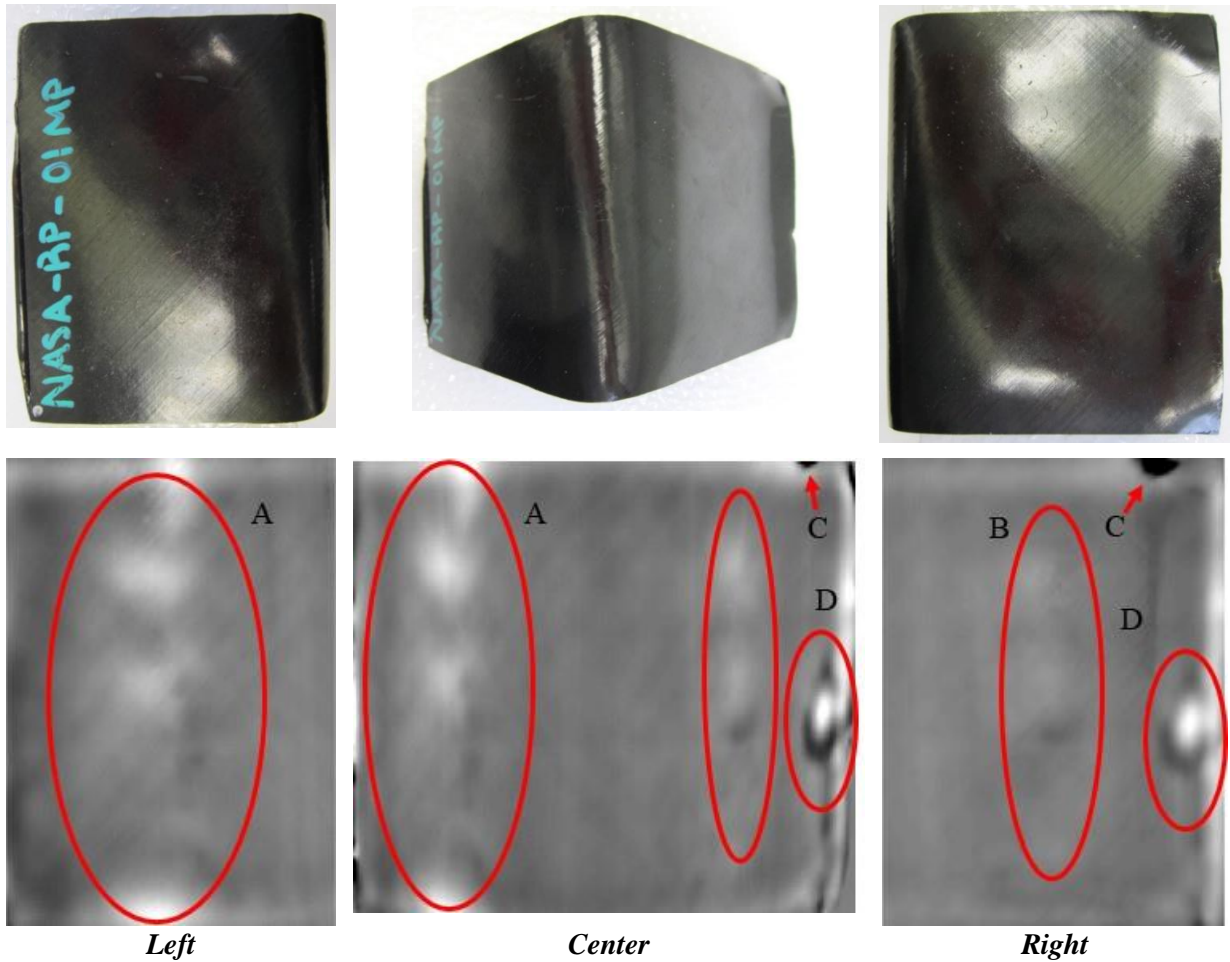


Figure E.22-4. SSIR inspection of NASA-RP-01MP sample's left, center, and right section processed with PCA from frame 100 (1.66s) to 1000 (16.66s).

E.22.1.8 References

- [1] Rajic, N.: “Principal Component Thermography for Flaw Contrast Enhancement and Flaw Depth Characterization in Composite Structures,” *Composite Structures*, Vol. 58, pp. 521-528, 2002.
- [2] Zalameda, J. N.; Bolduc S.; and Harman R.: “Thermal Inspection of a Composite Fuselage Section using a Fixed Eigenvector Principal Component Analysis Method,” *Proc. SPIE 10214, Thermosense: Thermal Infrared Applications XXXIX*, 102140H, 5 May 2017.
- [3] Cramer, K. E.; and Winfree, W. P.: “Fixed Eigenvector Analysis of Thermographic NDE Data”, *Proceedings of SPIE, Thermosense XXXIII*, edited by Morteza Safai and Jeff Brown, Vol. 8013, 2011.

E.22.2 Method: Through-Transmission Infrared Thermography (TTIR)

E.22.2.1 Partner: NASA

E.22.2.2 Technique Applicability: ★★☆

TTIR Thermography is capable of detecting defects that may be due to porosities.

E.22.2.3 Laboratory Setup

The TT thermal inspection system setup is shown in Figure E.22-5. The test specimen is placed between the heat source and the IR camera. The lamp used to induce the heat was a commercially available photographic flash lamp powered by a 6,400-Joule power supply (manufactured by Balcar). The camera used was a FLIR SC6000 with a 640×512 InSb array operating in the 3- to 5- μm IR band. The image data frame rate was 60 image frames per second. The computer records the IR image of the specimen immediately prior to the firing of the flash lamp (for emissivity correction), and then the thermal response of the specimen at a user defined sampling rate and for a user defined duration is acquired.

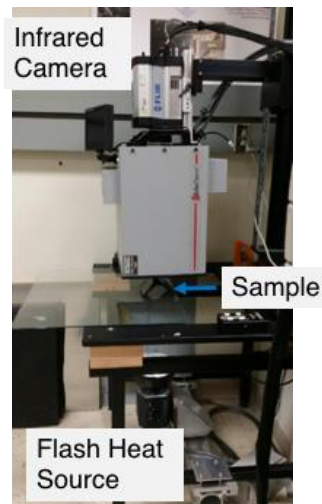


Figure E.22-5. TTIR setup.

E.22.2.4 Equipment List and Specifications:

- TWI
- TWI flash heat source using Balcar power supply externally triggered by TWI system.
- SC6000 FLIR IR camera, 640×512 InSb array, NEDT < 20 mK

- 50 mm Germanium Optics

E.22.2.5 Settings:

- 60Hz Frame Rate
- Flash on frame #10
- Total number of frames: 3500
- Total data acquisition time of 58.33 sec
- Infrared camera was positioned to view the entire sample

E.22.2.6 Principal Component Analysis

PCA is common for processing of thermal data [1–3]. This algorithm is based on decomposition of the thermal data into its principal components or eigenvectors. Singular value decomposition is a routine used to find the singular values and corresponding eigenvectors of a matrix. Since thermal NDE signals are slowly decaying waveforms, the predominant variations of the entire data set are usually contained in the first or second eigenvectors, and thus account for most of the data variance of interest. The principle components are computed by defining a data matrix A , for each data set, where the time variations are along the columns and the spatial image pixel points are row-wise. The matrix A is adjusted by dividing the maximum value (normalization) and subtracting the mean along the time dimension. The covariance matrix is defined as the $A^T * A$. The covariance matrix is now a square matrix of number of images used for processing. The covariance matrix can then be decomposed using singular value decomposition as:

$$\text{covariance matrix} = A^T A = V * S * V^T$$

Where S is a diagonal matrix containing the square of the singular values and V is an orthogonal matrix, which contains the basis functions or eigenvectors describing the time variations. The eigenvectors can be obtained from the columns of V . The PCA inspection image is calculated by dot product multiplication of the selected eigenvector times the temperature response (data matrix A), pixel by pixel.

E.22.2.7 Inspection Results

The 3500 frames of data (58.33 sec) were processed using iterations of different time windows. The processing of frames 100 to 1500 corresponding to a time window of 1.67–25 sec yielded the best results, shown in Figure E.22-7. Possible porosities, labeled A through G were detected. The different point of views (left, center, right) from which data were taken allow for different perspectives on the possible defects. Notably, C, D, and E, show linear indications of possible defects that have clear contrast with the surrounding areas.

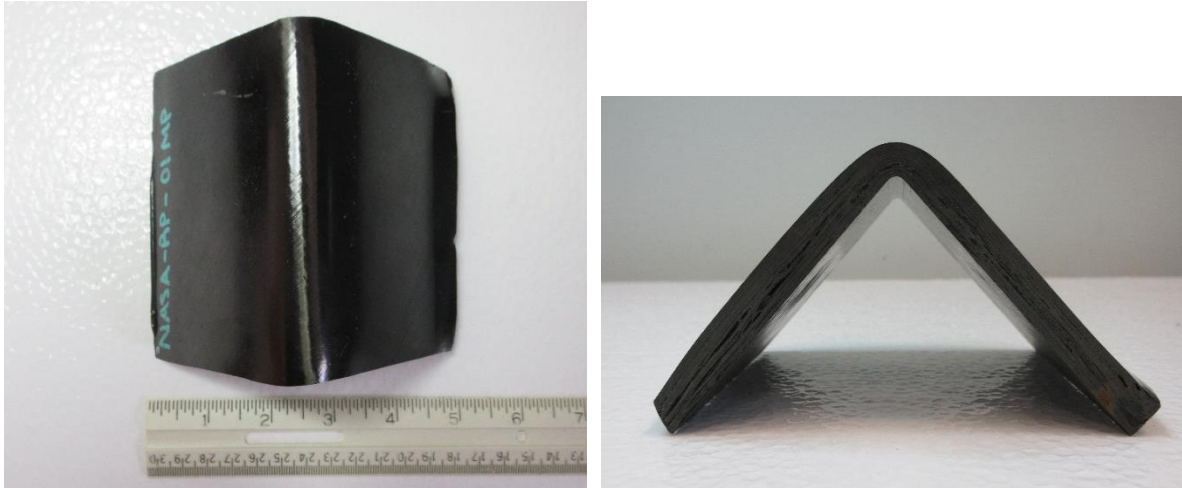


Figure E.22-6. NASA-RP-01MP sample.

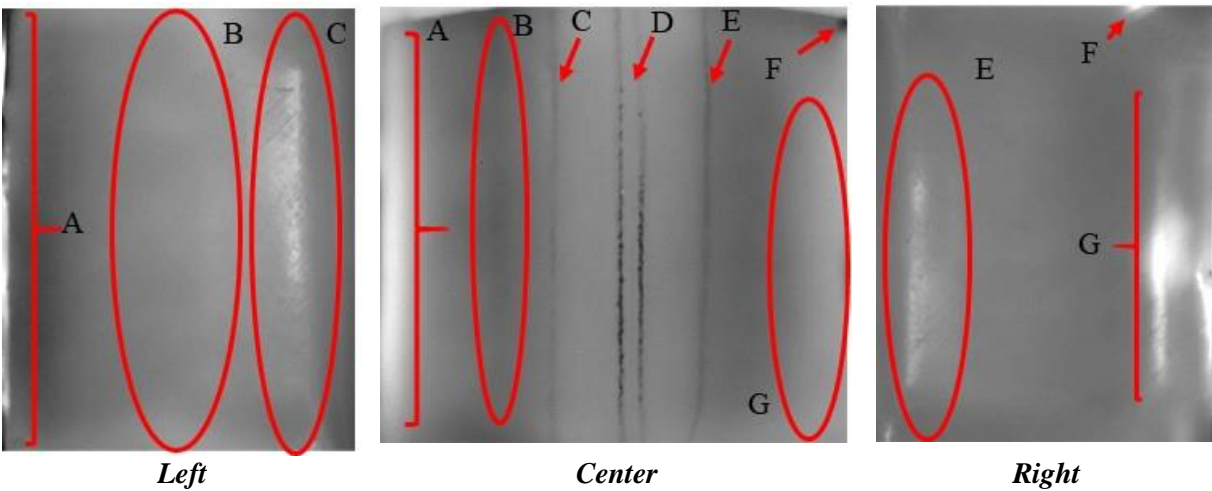
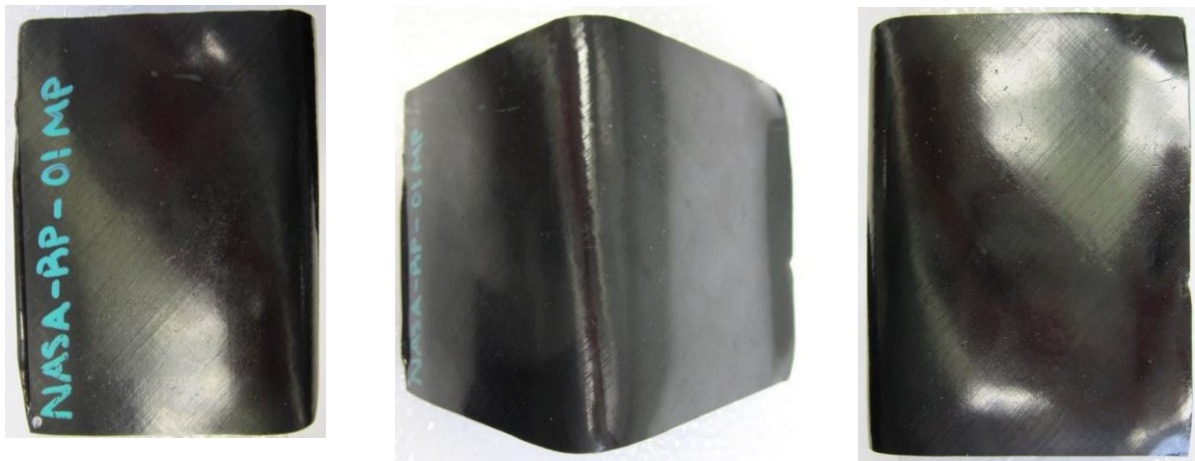


Figure E.22-7. TTIR inspection of NASA-RP-01MP sample's left, center, and right section processed with PCA from frame 100 (1.66s) to 1500 (25s).

E.22.2.8 References

- [1] Rajic, N.: “Principal Component Thermography for Flaw Contrast Enhancement and Flaw Depth Characterization in Composite Structures,” *Composite Structures*, Vol. 58, pp. 521-528, 2002.
- [2] Zalameda, J. N.; Bolduc S.; and Harman R.: “Thermal Inspection of a Composite Fuselage Section using a Fixed Eigenvector Principal Component Analysis Method,” Proc. *SPIE* 10214, *Thermosense: Thermal Infrared Applications XXXIX*, 102140H, 5 May 2017.
- [3] Cramer, K. E.; and Winfree, W. P.: “Fixed Eigenvector Analysis of Thermographic NDE Data”, Proceedings of *SPIE, Thermosense XXXIII*, edited by Morteza Safai and Jeff Brown, Vol. 8013, 2011.

E.22.3 Method: Single-Side Flash Thermography (SSFT-TSR)

E.22.3.1 Partner: Thermal Wave Imaging, Inc.*

*TWI was not part of the ACC but reviewed specimens.

E.22.3.2 Technique Applicability: ★★★

Single-Side Flash Thermography (SSFT) Thermographic Signal Reconstruction (TSR) is capable of detecting subsurface anomalies in this specimen that could be the result of delamination, voids or porosity. All indications appear in the head-on image, but more accurate sizing is achieved by inspecting the flat surfaces separately.

E.22.3.3 Laboratory Setup:

The sample was inspected with a commercially available flash thermography system (EchoTherm®, Thermal Wave Imaging, Inc.), equipped with 2 linear xenon flash/reflector assemblies mounted in a reflective hood optimized to provide uniform output at the 10 × 14-inch exit aperture. Each lamp is powered by a 6 kJ power supply that allows truncation of the flash to a rectangular pulse with duration <1 msec. A cryogenically cooled IR camera is mounted to view the plane of the hood exit aperture, with the camera lens positioned at the plane of the flashlamps. Excitation, data capture and processing and analysis using Thermographic Signal Reconstruction (TSR) are controlled at the system console using Virtuoso software.

E.22.3.4 Equipment List and Specifications:

- EchoTherm® Flash Thermography System
- 2 linear xenon flash lamps and power supplies (6 kJ each)
- TWI Precision Flash Control (truncation to 4 msec rectangular pulse)
- A6751sc FLIR IR camera, 640x512 InSb array, NEDT < 20 mK
- 25 mm Germanium Lens
- TWI Virtuoso® software

E.22.3.5 Settings:

- 15 Hz Frame Rate
- 10 Preflash Frames
- 2700 total frames
- 7 Polynomial order
- 180 sec data acquisition time

- Field of View (FOV): 10 × 14-inch

Settings were determined following the recommendations in ASTM E2582-14. Acquisition duration was set according to the time of the break from linearity ($t^* \sim 90$ sec) due to the back wall for typical points in the log time history. The acquisition period was then set to 180 sec ($3 \times t^*$), per ASTM E2582-14.

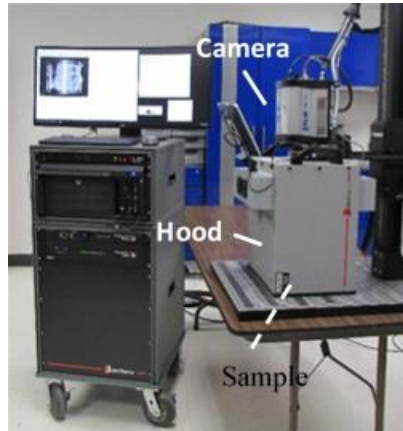


Figure E.22-8. SSFT system with TSR.

E.22.3.6 Thermographic Signal Reconstruction (TSR)

After acquisition, captured data are processed using TSR to reduce temporal noise, enhance deviation from normal cooling behavior and allow segmentation of the data based on signal attributes. For each pixel, the average of 10 frames immediately preceding the flash pulse is subtracted from the pixel time history, and a 7th order polynomial is fit to the logarithmically scaled result using least squares. First and 2nd derivatives of the result are calculated and the derivative images are displayed in the Virtuoso software. Derivative signals associated normal areas of the sample exhibit minimal activity over the duration of the acquisition. Signals associated with subsurface anomalies typically behave identically to the normal signals until a particular time (dependent on host material characteristics and the depth of the feature) after which their behavior deviates from normal (the degree of the deviation depends on the relative difference in the thermal properties of the anomaly and the surrounding normal matrix).

E.22.3.7 Inspection Results

Five clusters of subsurface indications were observed and confirmed to be subsurface by their late divergence in the logarithmic temperature time plot. All indications appear in the head-on (center) image; however, the full spatial extent of the indications is displayed in the left and right images, where the optical axis is normal to the sample surface. No apparent defects were noticed in the specimen's apex. The 2nd derivative at 4.87 sec was used to produce the final inspection images shown in Figure E.22-9.

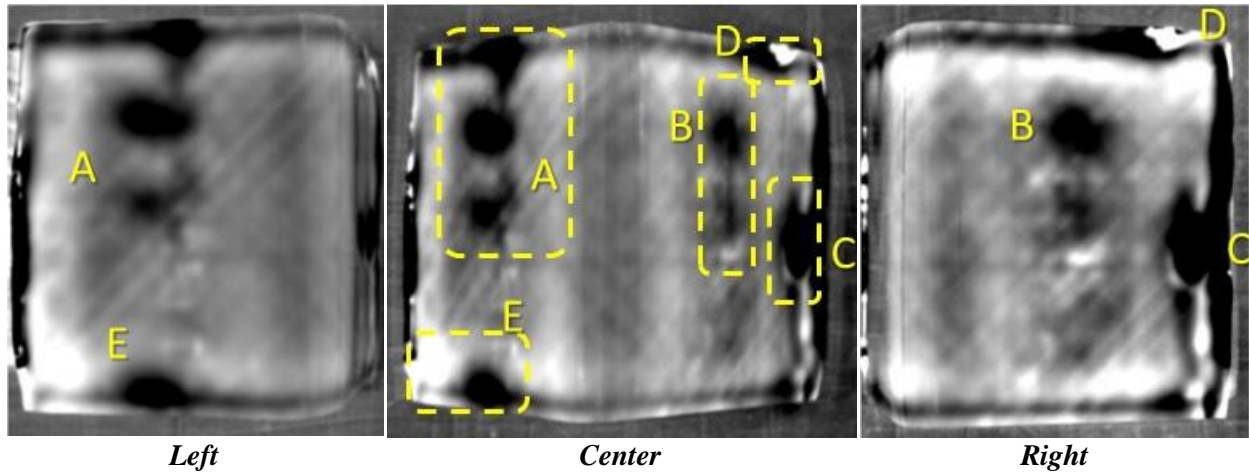


Figure E.22-9. TSR 2nd derivative at 4.87sec of NASA-RP-01MP.

E.22.3.8 References

- [1] ASNT: *ASNT Aerospace NDT Industry Handbook*, Chapter 11, “Thermography,” Nov 2014.
- [2] ASTM International: “Standard Practice for Infrared Flash Thermography of Composite Panels and Repair Patches,” *ASTM E2582–07*, 2007.
- [3] Shepard, S.; and Frenberg, M.: “Thermographic Detection and Characterization of Flaws in Composite Materials,” *Materials Evaluation*, ASNT, July 2014.
- [4] Hou, Y.; Lhota, J. R.; and Golden, T. J. M.: “Automated processing of thermographic derivatives for quality assurance,” *Opt. Eng.*, Vol. 46, 051008, 2007.
- [5] *Temporal noise reduction, compression and analysis of data sequences*, U.S. Patent 6,516,084.

E.23 Specimen #23 - Not Manufactured

E.24 Specimen #24 - Not Manufactured

E.25 Specimen #25 - Not Manufactured

E.26 Specimen #26: NASA-RP-10MP

Structure	Material	Details	Dimensions (inches)	Partner Methods	
Uni-ply (0/90/45)	IM7/8552	1.0-inch radial inside curve. Radius Panel 1.0-inch Curve Rad with medium porosity.	4.5 × 2.5 × 4	NASA	E.26.1 SSIR E.26.2 TTIR
				TWI	E.26.3 SSFT

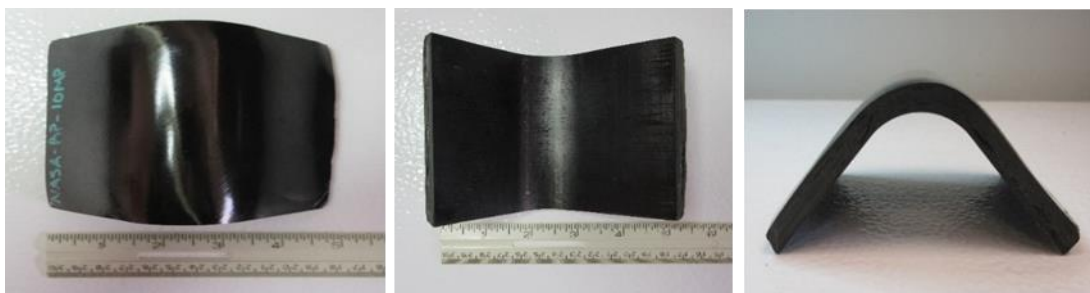


Figure E.26-1. Photographs of Specimen #26: NASA-RP-10MP.

E.26.1 Method: SSIR

E.26.1.1 Partner: NASA

E.26.1.2 Technique Applicability: ★☆☆

SSIR is capable of detecting few defects that may be due to porosities.

E.26.1.3 Laboratory Setup

A commercially available flash thermography system was used for the inspection. The flash thermography system consisted of two linear flash tubes mounted within a hood. An IR camera was mounted at the back of the hood viewing through a circular hole between the flash tubes and were positioned to view the hood opening. In this configuration, the flash lamps heated an area equal to the hood opening and the IR camera captured the thermal response. The IR camera operates in the mid-wave IR band (3–5 μm) and is configured with a 25 mm germanium lens. The focal plane array size for the camera is 640×512 with a detector pitch size of $14 \times 14 \mu\text{m}$.

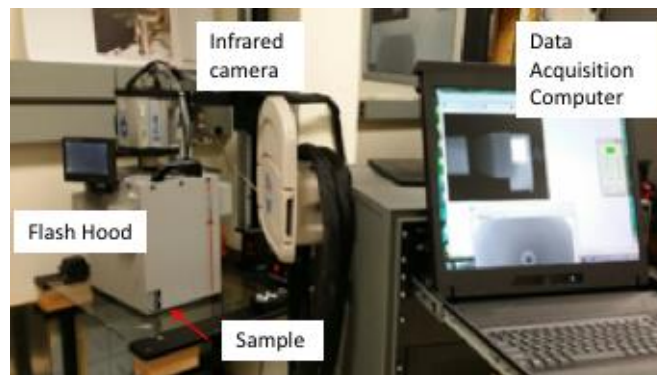


Figure E.26-2. SSFT setup.

E.26.1.4 Equipment List and Specifications:

- TWI
- TWI flash heat source using Speedotron power supplies
- SC6000 FLIR IR camera, 640×512 InSb array, NEDT $< 20 \text{ mK}$
- 50 mm Germanium Optics

E.26.1.5 Settings:

- 60Hz Frame Rate
- Flash on frame #10
- Total number of Frames 3000
- Total data acquisition time of 50 sec
- The camera/hood was positioned to view the entire sample

E.26.1.6 Principal Component Analysis

PCA is common for processing of thermal data [1–3]. This algorithm is based on decomposition of the thermal data into its principal components or eigenvectors. Singular value decomposition is a routine used to find the singular values and corresponding eigenvectors of a matrix. Since thermal NDE signals are slowly decaying waveforms, the predominant variations of the entire data set are usually contained in the first or second eigenvectors, and thus account for most of the data variance

of interest. The principle components are computed by defining a data matrix A , for each data set, where the time variations are along the columns and the spatial image pixel points are row-wise. The matrix A is adjusted by dividing the maximum value (normalization) and subtracting the mean along the time dimension. The covariance matrix is defined as the $A^T * A$. The covariance matrix is now a square matrix of number of images used for processing. The covariance matrix can then be decomposed using singular value decomposition as:

$$\text{covariance matrix} = A^T A = V * S * V^T$$

Where S is a diagonal matrix containing the square of the singular values and V is an orthogonal matrix, which contains the basis functions or eigenvectors describing the time variations. The eigenvectors can be obtained from the columns of V . The PCA inspection image is calculated by dot product multiplication of the selected eigenvector times the temperature response (data matrix A), pixel by pixel.

E.26.1.7 Inspection Results

The 3000 frames of data (50 sec) were processed using iterations of different time windows. The processing of frames 100 to 500 corresponding to a time window of 1.67–8.33 sec yielded the best results. Sections A, B, C, D and E shown in Figure E.26-4 were detected. A time delay of 1.67 sec allowed enough time after the flash for the heat to flow into the sample and 8.33 sec was sufficient to provide good contrast of the defects. All different time windows detected the five defects. However, when including later frames (e.g. frame 100 to 1000) section A was more perceptible. Excluding later frames, as it is the case here, made section D more apparent. No apparent defects were noticed in the specimen's apex. The second eigenvector was used to produce the final inspection images shown in Figure E.26-3.

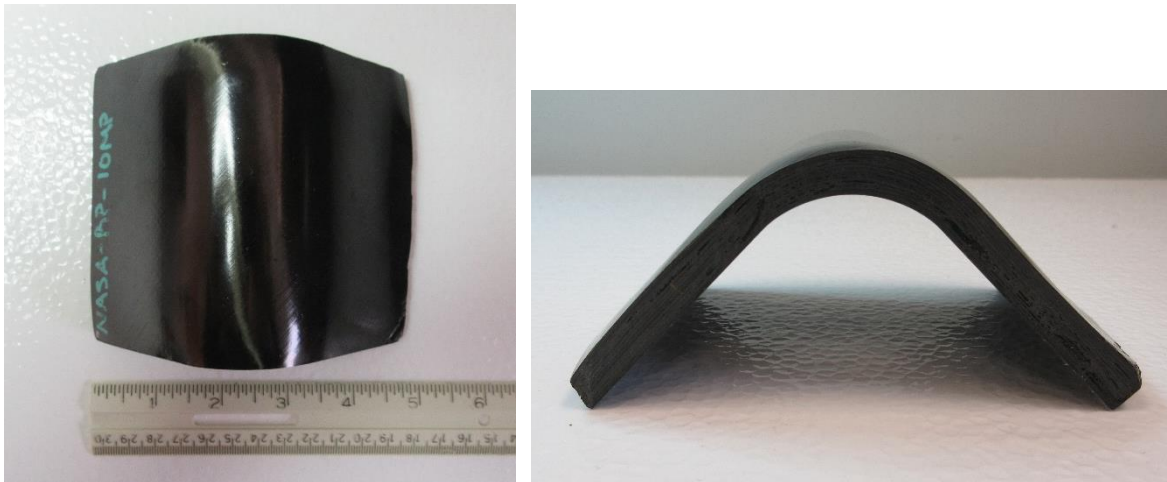


Figure E.26-3. NASA-RP-10MP sample.

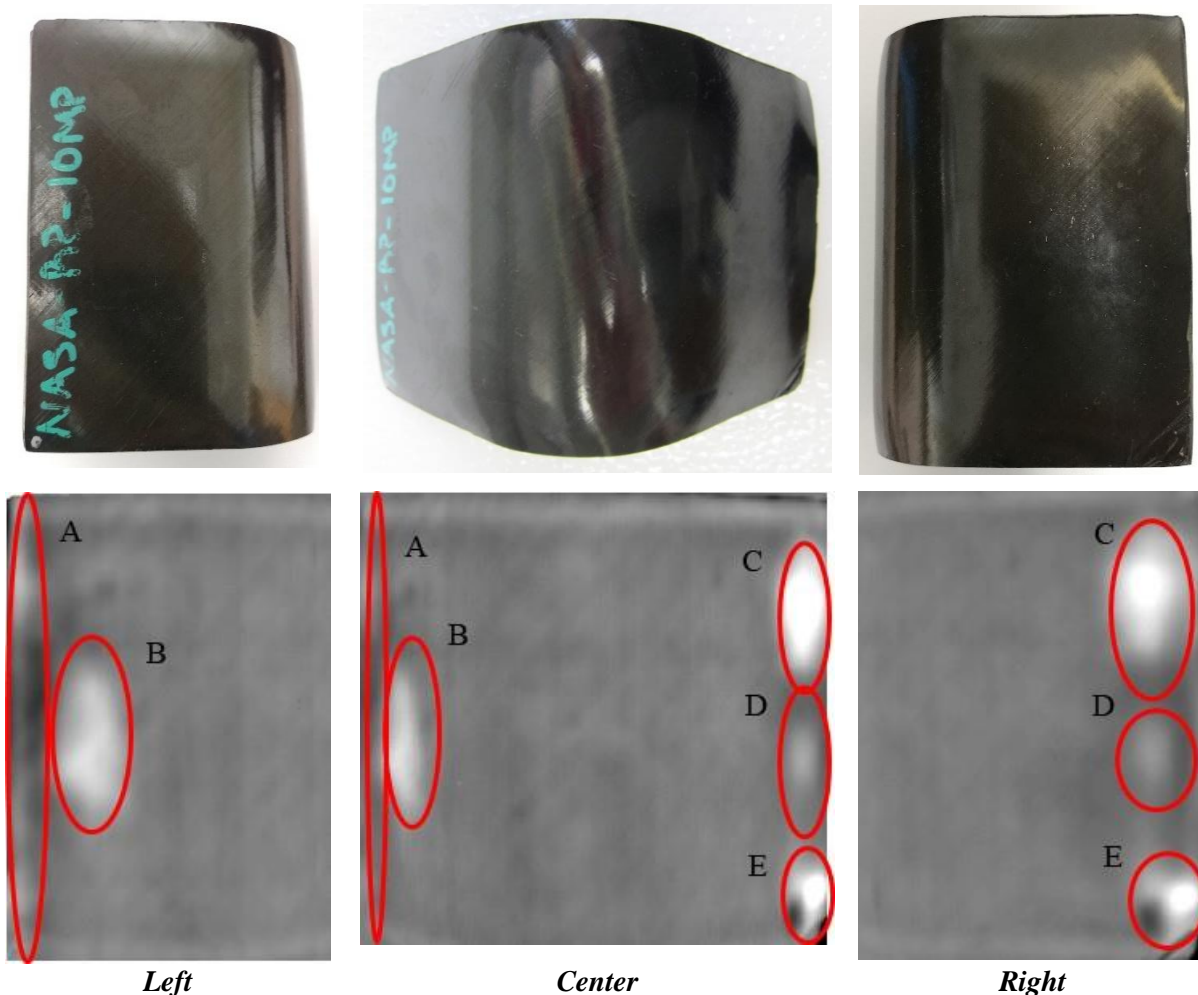


Figure E.26-4. SSFT inspection of NASA-RP-10MP sample's left, center, and right section processed with PCA from frame 100 (1.66s) to 500 (8.33s).

E.26.1.8 References

- [1] Rajic, N.: "Principal Component Thermography for Flaw Contrast Enhancement and Flaw Depth Characterization in Composite Structures," *Composite Structures*, Vol. 58, pp. 521-528, 2002.
- [2] Zalameda, J. N.; Bolduc S.; and Harman R.: "Thermal Inspection of a Composite Fuselage Section using a Fixed Eigenvector Principal Component Analysis Method," Proc. *SPIE* 10214, *Thermosense: Thermal Infrared Applications XXXIX*, 102140H, 5 May 2017.
- [3] Cramer, K. E.; and Winfree, W. P.: "Fixed Eigenvector Analysis of Thermographic NDE Data", Proceedings of *SPIE, Thermosense XXXIII*, edited by Morteza Safai and Jeff Brown, Vol. 8013, 2011.

E.26.2 Method: TTIR

E.26.2.1 Partner: NASA

E.26.2.2 Technique Applicability: ★★★

TTIR is capable of detecting defects that may be due to porosities.

E.26.2.3 Laboratory Setup

The TT thermal inspection system setup is shown in Figure E.26-5. The test specimen is placed between the heat source and the IR camera. The lamp used to induce the heat was a commercially available photographic flash lamp powered by a 6,400-Joule power supply (manufactured by Balcar). The camera used was a FLIR SC6000 with a 640×512 InSb array operating in the 3- to 5- μm IR band. The image data frame rate was 60 image frames per second. The computer records the IR image of the specimen immediately prior to the firing of the flash lamp (for emissivity correction), and then the thermal response of the specimen at a user defined sampling rate and for a user defined duration is acquired.

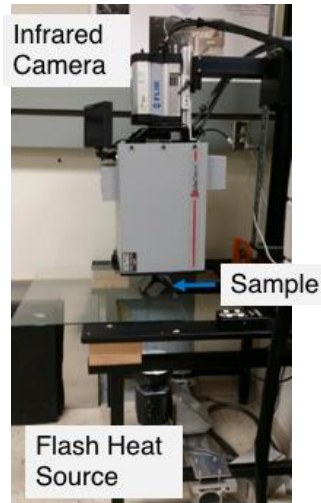


Figure E.26-5. TTIR setup.

E.26.2.4 Equipment List and Specifications:

- TWI
- TWI flash heat source using Balcar power supply externally triggered by TWI system
- SC6000 FLIR IR camera, 640×512 InSb array, NEDT < 20 mK
- 50 mm Germanium Optics

E.26.2.5 Settings:

- 60Hz Frame Rate
- Flash on frame #10
- Total number of frames: 3500
- Total data acquisition time of 58.33 sec
- Infrared camera was positioned to view the entire sample

E.26.2.6 Principal Component Analysis

PCA is common for processing of thermal data [1–3]. This algorithm is based on decomposition of the thermal data into its principal components or eigenvectors. Singular value decomposition is a routine used to find the singular values and corresponding eigenvectors of a matrix. Since thermal NDE signals are slowly decaying waveforms, the predominant variations of the entire data set are usually contained in the first or second eigenvectors, and thus account for most of the data variance of interest. The principle components are computed by defining a data matrix A , for each data set, where the time variations are along the columns and the spatial image pixel points are row-wise.

The matrix A is adjusted by dividing the maximum value (normalization) and subtracting the mean along the time dimension. The covariance matrix is defined as the $A^T * A$. The covariance matrix is now a square matrix of number of images used for processing. The covariance matrix can then be decomposed using singular value decomposition as:

$$\text{covariance matrix} = A^T A = V * S * V^T$$

Where S is a diagonal matrix containing the square of the singular values and V is an orthogonal matrix, which contains the basis functions or eigenvectors describing the time variations. The eigenvectors can be obtained from the columns of V . The PCA inspection image is calculated by dot product multiplication of the selected eigenvector times the temperature response (data matrix A), pixel by pixel.

E.26.2.7 Inspection Results

The 3500 frames of data (58.33 sec) were processed using iterations of different time windows. The processing of frames 100 to 1500 corresponding to a time window of 1.67–25 sec yielded the best results, shown in Figure E.26-7. Possible porosities, labeled A through I were detected. The different point of views (left, center, right) from which data were taken allow for different perspectives on the possible defects. Notably, C, D, and E, show linear indications of possible defects that have clear contrast with the surrounding areas.

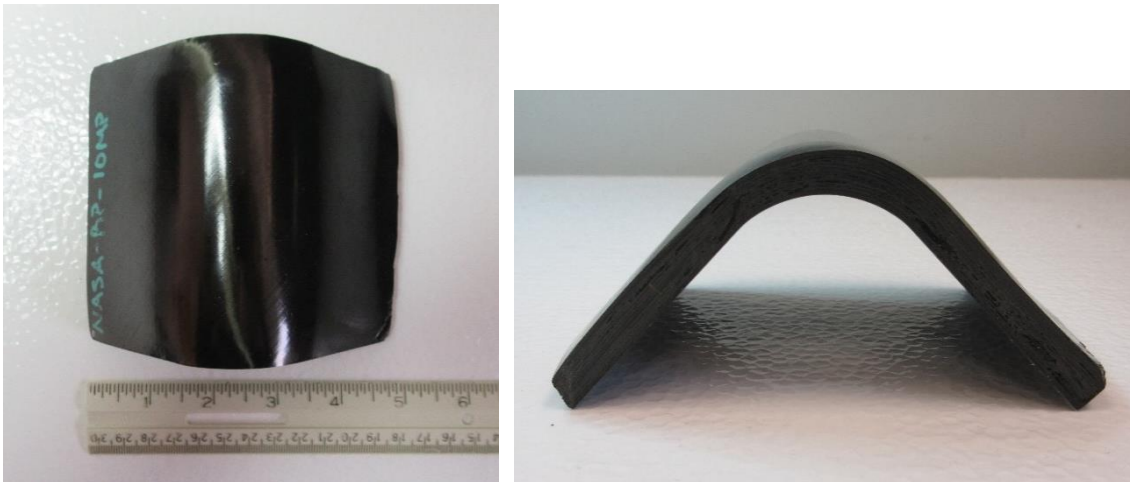


Figure E.26-6. NASA-RP-10MP sample.

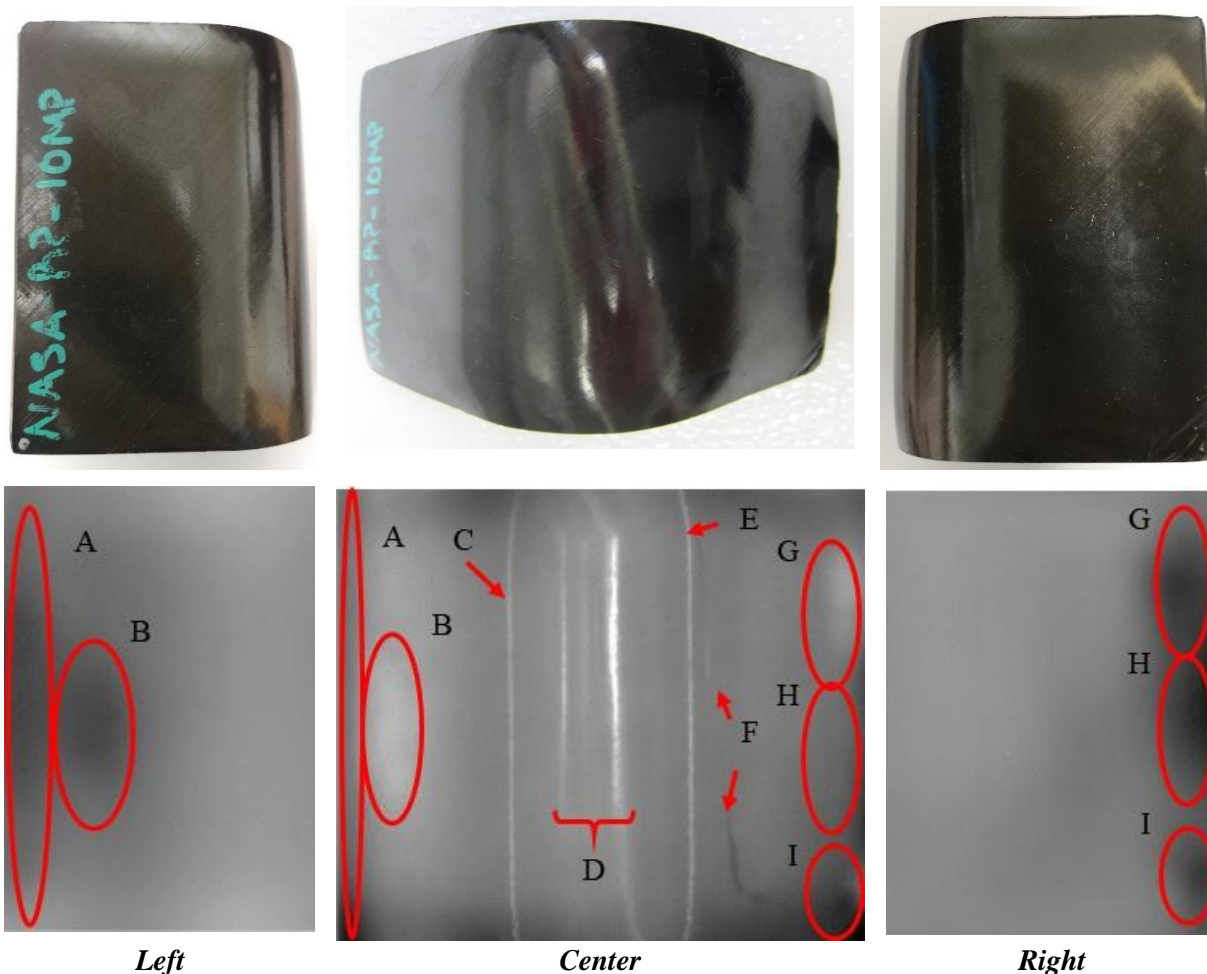


Figure E.26-7. TTIR inspection of NASA-RP-10MP sample's left, center, and right section processed with PCA from frame 100 (1.66s) to 1500 (25s).

E.26.2.8 References

- [1] Rajic, N.: "Principal Component Thermography for Flaw Contrast Enhancement and Flaw Depth Characterization in Composite Structures," *Composite Structures*, Vol. 58, pp. 521-528, 2002.
- [2] Zalameda, J. N.; Bolduc S.; and Harman R.: "Thermal Inspection of a Composite Fuselage Section using a Fixed Eigenvector Principal Component Analysis Method," Proc. *SPIE* 10214, *Thermosense: Thermal Infrared Applications XXXIX*, 102140H, 5 May 2017.
- [3] Cramer, K. E.; and Winfree, W. P.: "Fixed Eigenvector Analysis of Thermographic NDE Data", Proceedings of *SPIE*, *Thermosense XXXIII*, edited by Morteza Safai and Jeff Brown, Vol. 8013, 2011.

E.26.3 Method: SSFT-TSR

E.26.3.1 Partner: Thermal Wave Imaging, Inc.*

*TWI was not part of the ACC but reviewed specimens.

E.26.3.2 Technique Applicability: ★★★

SSFT-TSR is capable of detecting subsurface anomalies in this specimen that could be the result of delamination, voids or porosity. All indications appear in the head-on image, but more accurate sizing is achieved by inspecting the flat surfaces separately.

E.26.3.3 Laboratory Setup:

The sample was inspected with a commercially available flash thermography system (EchoTherm®, Thermal Wave Imaging, Inc.), equipped with 2 linear xenon flash/reflector assemblies mounted in a reflective hood optimized to provide uniform output at the 10 × 14-inch exit aperture. Each lamp is powered by a 6 kJ power supply that allows truncation of the flash to a rectangular pulse with duration <1 msec. A cryogenically cooled IR camera is mounted to view the plane of the hood exit aperture, with the camera lens positioned at the plane of the flashlamps. Excitation, data capture and processing and analysis using TSR are controlled at the system console using Virtuoso software.

E.26.3.4 Equipment List and Specifications:

- EchoTherm® Flash Thermography System
- 2 linear xenon flash lamps and power supplies (6 kJ each)
- TWI Precision Flash Control (truncation to 4 msec rectangular pulse)
- A6751sc FLIR IR camera, 640 × 512 InSb array, NEDT < 20 mK
- 25 mm Germanium Lens
- TWI Virtuoso® software

E.26.3.5 Settings:

- 15 Hz Frame Rate
- 10 Preflash Frames
- 2700 total frames
- 7 Polynomial order
- 180 sec data acquisition time
- FOV: 10 × 14-inch

Settings were determined following the recommendations in ASTM E2582-14. Acquisition duration was set according to the time of the break from linearity ($t^* \sim 90$ sec) due to the back wall for typical points in the log time history. The acquisition period was then set to 180 sec ($3 \times t^*$), per ASTM E2582-14.

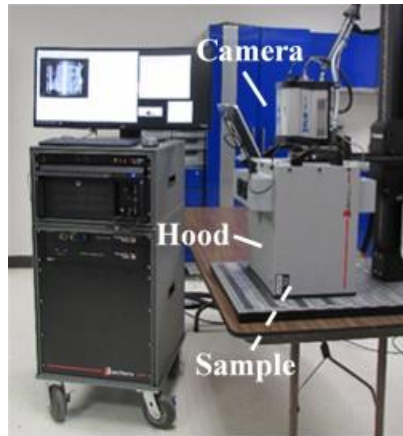


Figure E.26-8. SSFT system with TSR.

E.26.3.6 Thermographic Signal Reconstruction (TSR)

After acquisition, captured data are processed using TSR to reduce temporal noise, enhance deviation from normal cooling behavior and allow segmentation of the data based on signal attributes. For each pixel, the average of 10 frames immediately preceding the flash pulse is subtracted from the pixel time history, and a 7th order polynomial is fit to the logarithmically scaled result using least squares. First and 2nd derivatives of the result are calculated and the derivative images are displayed in the Virtuoso software. Derivative signals associated normal areas of the sample exhibit minimal activity over the duration of the acquisition. Signals associated with subsurface anomalies typically behave identically to the normal signals until a particular time (dependent on host material characteristics and the depth of the feature) after which their behavior deviates from normal (the degree of the deviation depends on the relative difference in the thermal properties of the anomaly and the surrounding normal matrix).

E.26.3.7 Inspection Results

Four clusters of subsurface indications were observed and confirmed to be subsurface by their late divergence in the logarithmic temperature time plot. All indications appear in the head-on (center) image; however, the full spatial extent of the indications is displayed in the left and right images, where the optical axis is normal to the sample surface. No apparent defects were noticed in the specimen's apex. The 2nd derivative at 3.53 sec was used to produce the final inspection images shown in Figure E.26-9.

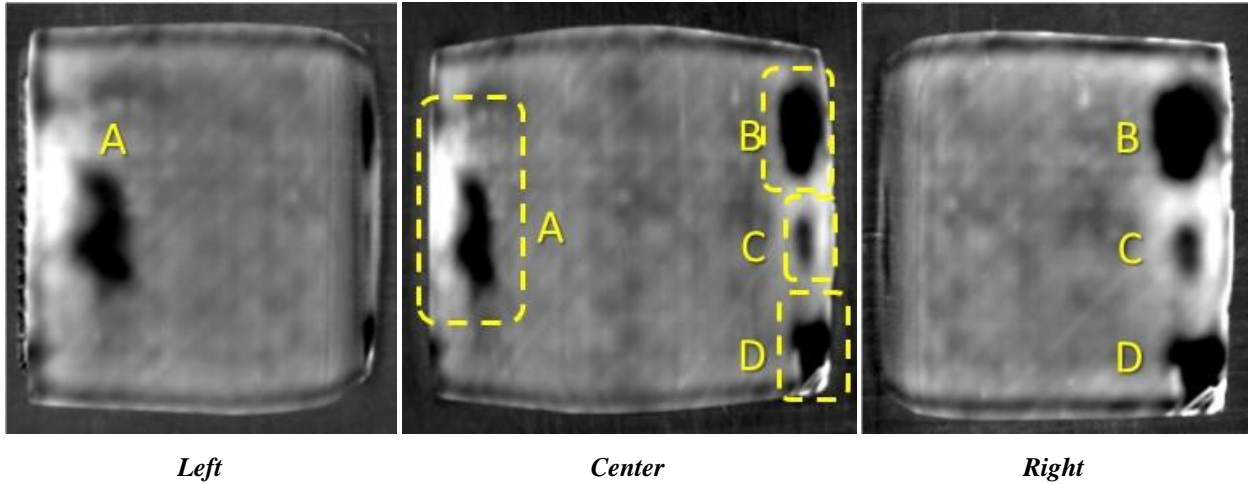


Figure E.26-9. TSR 2nd derivative at 3.53 sec of NASA-RP-10MP.

E.26.3.8 References

- [1] ASNT: *ASNT Aerospace NDT Industry Handbook*, Chapter 11, “Thermography,” Nov 2014.
- [2] ASTM International: “Standard Practice for Infrared Flash Thermography of Composite Panels and Repair Patches,” *ASTM E2582–07*, 2007.
- [3] Shepard, S.; and Frenberg, M.: “Thermographic Detection and Characterization of Flaws in Composite Materials,” *Materials Evaluation*, ASNT, July 2014.
- [4] Hou, Y.; Lhota, J. R.; and Golden, T. J. M.: “Automated processing of thermographic derivatives for quality assurance,” *Opt. Eng.*, Vol. 46, 051008, 2007.
- [5] *Temporal noise reduction, compression and analysis of data sequences*, U.S. Patent 6,516,084.

E.27 Specimen #27 - Not Manufactured

E.28 Specimen #28: NASA-RP-20MP

Structure	Material	Details	Dimensions (inches)	Partner Methods	
Uni-ply (0/90/45)	IM78552	2.0-inch radial inside curve. Radius Panel 2.0 in Curve Rad with medium porosity.	4.5 × 2.5 × 4	NASA	E.28.1 SSIR E.28.2 TTIR
				TWI	E.28.3 SSFT

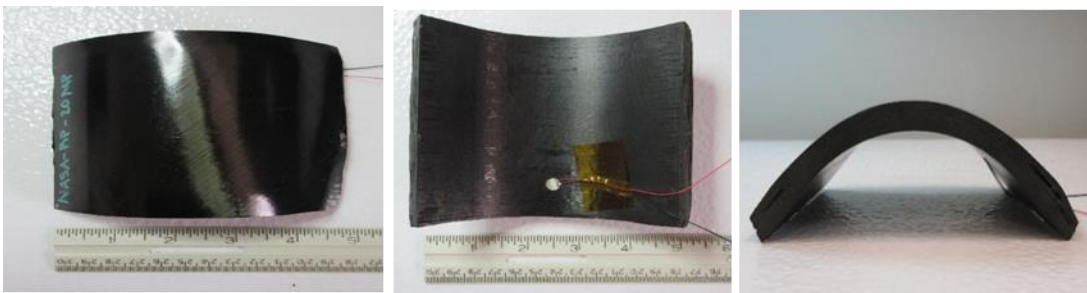


Figure E.28-1. Photographs of Specimen #26: NASA-RP-2.

E.28.1 Method: Single-Sided Infrared Thermography (SSIR)

E.28.1.1 Partner: NASA

E.28.1.2 Technique Applicability: ★☆☆

SSIR Thermography is capable of detecting few defects that may be due to porosities.

E.28.1.3 Laboratory Setup

A commercially available flash thermography system was used for the inspection. The flash thermography system consisted of two linear flash tubes mounted within a hood. An IR camera was mounted at the back of the hood viewing through a circular hole between the flash tubes and were positioned to view the hood opening. In this configuration, the flash lamps heated an area equal to the hood opening and the IR camera captured the thermal response. The IR camera operates in the mid-wave IR band (3–5 μm) and is configured with a 25-mm germanium lens. The focal plane array size for the camera is 640×512 with a detector pitch size of $14 \times 14 \mu\text{m}$.

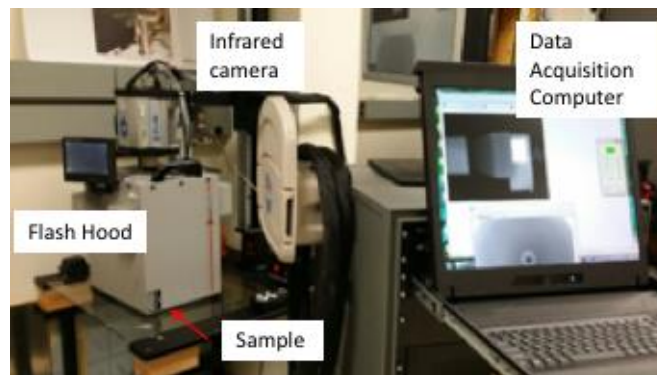


Figure E.28-2. SSIR setup.

E.28.1.4 Equipment List and Specifications:

- TWI
- TWI flash heat source using Speedotron power supplies
- SC6000 FLIR IR camera, 640×512 InSb array, NEDT < 20 mK
- 50 mm Germanium Optics

E.28.1.5 Settings:

- 60 Hz Frame Rate
- Flash on frame #10
- Total number of frames: 3000
- Total data acquisition time of 50 sec
- The camera/hood was positioned to view the entire sample

E.28.1.6 Principal Component Analysis

PCA is common for processing of thermal data [1–3]. This algorithm is based on decomposition of the thermal data into its principal components or eigenvectors. Singular value decomposition is a routine used to find the singular values and corresponding eigenvectors of a matrix. Since thermal NDE signals are slowly decaying waveforms, the predominant variations of the entire data set are usually contained in the first or second eigenvectors, and thus account for most of the data variance

of interest. The principle components are computed by defining a data matrix A , for each data set, where the time variations are along the columns and the spatial image pixel points are row-wise. The matrix A is adjusted by dividing the maximum value (normalization) and subtracting the mean along the time dimension. The covariance matrix is defined as the $A^T * A$. The covariance matrix is now a square matrix of number of images used for processing. The covariance matrix can then be decomposed using singular value decomposition as:

$$\text{covariance matrix} = A^T A = V * S * V^T$$

Where S is a diagonal matrix containing the square of the singular values and V is an orthogonal matrix, which contains the basis functions or eigenvectors describing the time variations. The eigenvectors can be obtained from the columns of V . The PCA inspection image is calculated by dot product multiplication of the selected eigenvector times the temperature response (data matrix A), pixel by pixel.

E.28.1.7 Inspection Results

The 3000 frames of data (50 sec) were processed using iterations of different time windows. The processing of frames 150 to 1000 corresponding to a time window of 2.5–16.67 sec yielded the best results. Ten possible defects shown in Figure E.28-4 were detected. A time delay of 2.5 sec allowed enough time after the flash for the heat to flow into the sample and 16.67 sec was sufficient to provide good contrast of the defects. All iterations of different time windows would detect the five defects. No apparent defects were noticed in the specimen's apex. The second eigenvector was used to produce the final inspection images shown in Figure E.28-3.

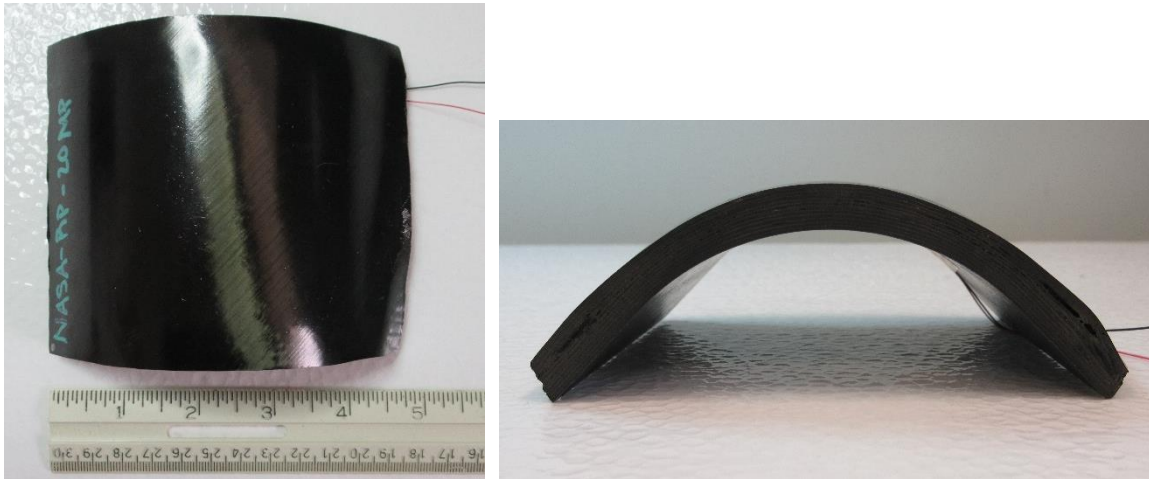
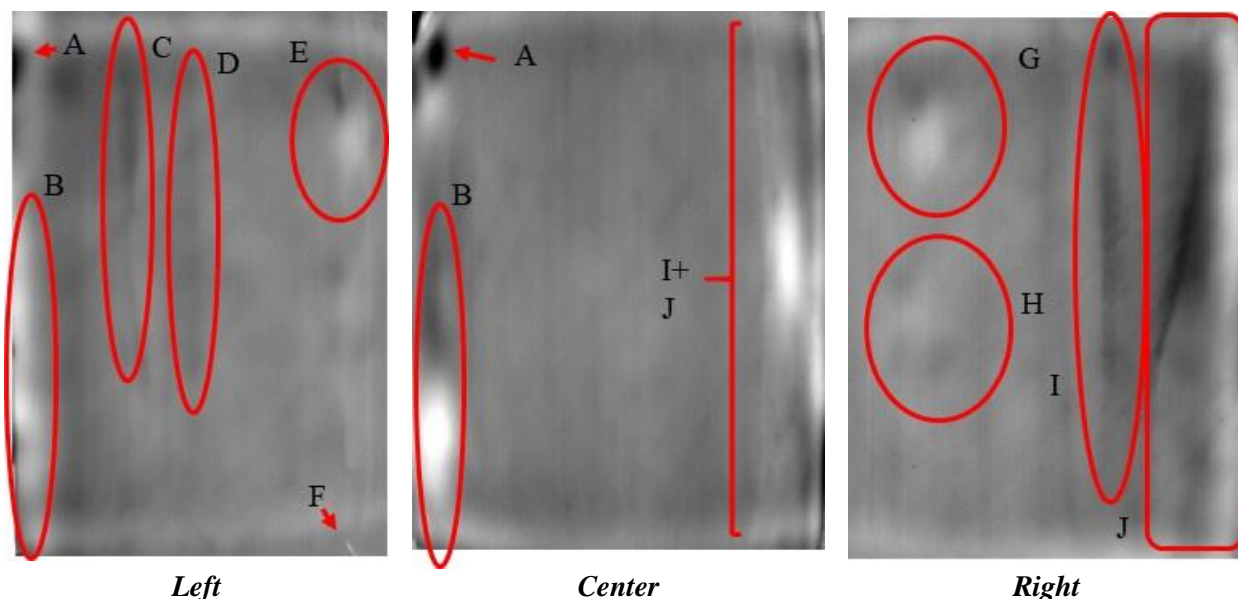
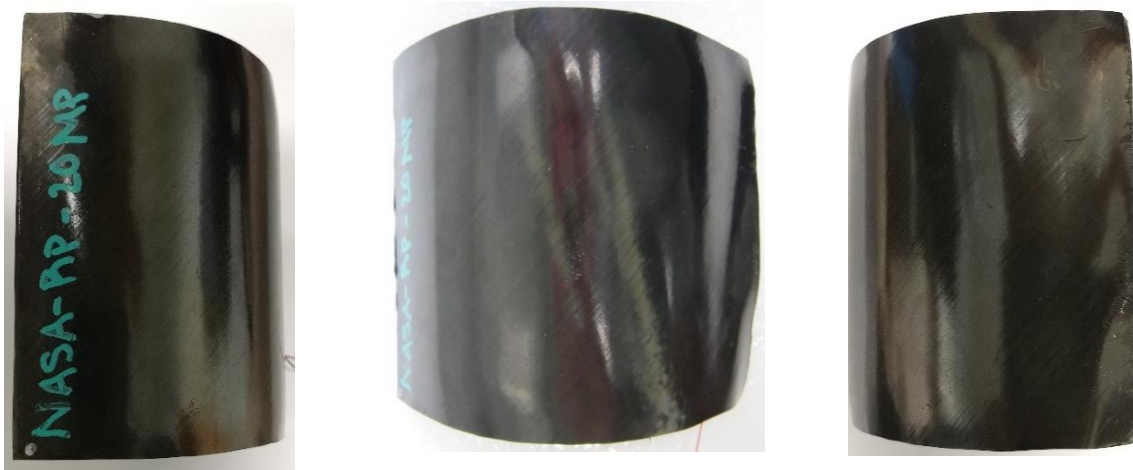


Figure E.28-3. SSFT inspection of NASA-RP-20MP sample.



Left
Center
Right

Figure E.28-4. SSFT inspection of NASA-RP-20MP sample's left, center, and right section processed with PCA from frame 150 (2.5s) to 1000 16.67s).

E.28.1.8 References

- [1] Rajic, N.: "Principal Component Thermography for Flaw Contrast Enhancement and Flaw Depth Characterization in Composite Structures," *Composite Structures*, Vol. 58, pp. 521-528, 2002.
- [2] Zalameda, J. N.; Bolduc S.; and Harman R.: "Thermal Inspection of a Composite Fuselage Section using a Fixed Eigenvector Principal Component Analysis Method," Proc. *SPIE* 10214, *Thermosense: Thermal Infrared Applications XXXIX*, 102140H, 5 May 2017.
- [3] Cramer, K. E.; and Winfree, W. P.: "Fixed Eigenvector Analysis of Thermographic NDE Data", Proceedings of *SPIE*, *Thermosense XXXIII*, edited by Morteza Safai and Jeff Brown, Vol. 8013, 2011.

E.28.2 Method: Through-Transmission Infrared Thermography (TTIR)

E.28.2.1 Partner: NASA

E.28.2.2 Technique Applicability: ★☆☆

TTIR is capable of imaging few defects that may be due to porosities.

E.28.2.3 Laboratory Setup

The TT thermal inspection system setup is shown in Figure E.28-5. The test specimen is placed between the heat source and the IR camera. The lamp used to induce the heat was a commercially available photographic flash lamp powered by a 6,400-Joule power supply (manufactured by Balcar). The camera used was a FLIR SC6000 with a 640×512 InSb array operating in the 3–5-micron IR band. The image data frame rate was 60 image frames per second. The computer records the IR image of the specimen immediately prior to the firing of the flash lamp (for emissivity correction), and then the thermal response of the specimen at a user defined sampling rate and for a user defined duration is acquired.

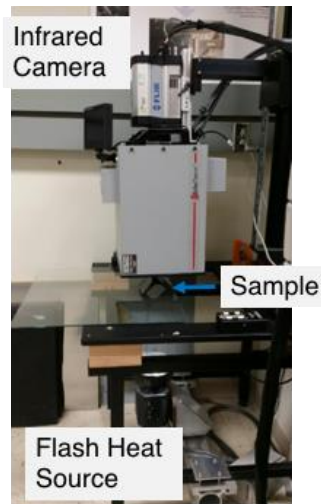


Figure E.28-5. TTIR setup.

E.28.2.4 Equipment List and Specifications:

- TWI
- TWI flash heat source using Balcar power supply externally triggered by TWI system
- SC6000 FLIR IR camera, 640×512 InSb array, NEDT < 20 mK
- 50 mm Germanium Optics

E.28.2.5 Settings:

- 60Hz Frame Rate
- Flash on frame #10
- Total number of frames: 3500
- Total data acquisition time of 58.33 sec
- Infrared camera was positioned to view the entire sample

E.28.2.6 Principal Component Analysis

PCA is common for processing of thermal data [1–3]. This algorithm is based on decomposition of the thermal data into its principal components or eigenvectors. Singular value decomposition is a routine used to find the singular values and corresponding eigenvectors of a matrix. Since thermal NDE signals are slowly decaying waveforms, the predominant variations of the entire data set are usually contained in the first or second eigenvectors, and thus account for most of the data variance of interest. The principle components are computed by defining a data matrix A , for each data set, where the time variations are along the columns and the spatial image pixel points are row-wise. The matrix A is adjusted by dividing the maximum value (normalization) and subtracting the mean along the time dimension. The covariance matrix is defined as the $A^T * A$. The covariance matrix is now a square matrix of number of images used for processing. The covariance matrix can then be decomposed using singular value decomposition as:

$$\text{covariance matrix} = A^T A = V * S * V^T$$

Where S is a diagonal matrix containing the square of the singular values and V is an orthogonal matrix, which contains the basis functions or eigenvectors describing the time variations. The eigenvectors can be obtained from the columns of V . The PCA inspection image is calculated by dot product multiplication of the selected eigenvector times the temperature response (data matrix A), pixel by pixel.

E.28.2.7 Inspection Results

The 3500 frames of data (58.33 sec) were processed using iterations of different time windows. The processing of frames 100 to 1500 corresponding to a time window of 1.67–25 sec yielded the best results, shown in Figure E.28-7. Possible porosities, labeled A through O were detected. The different point of views (left, center, right) from which data were taken allow for different perspectives on the possible defects. Notably, F, H, and I, show linear indications of possible defects that have clear contrast with the surrounding areas. Due to the discrepancies between the curved specimen and the 2D representation of the thermography data, it can be hard to correlate the possible defects from the different point of views. Hence, A, B, and E are possibly the same feature being displayed differently. The same with C and F.

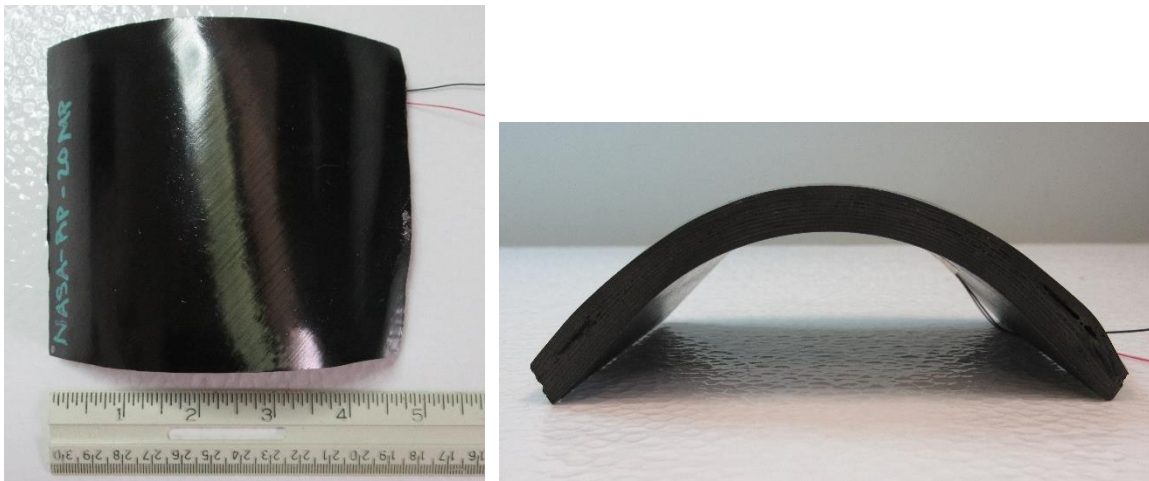


Figure E.28-6. SSFT inspection of NASA-RP-20MP sample.

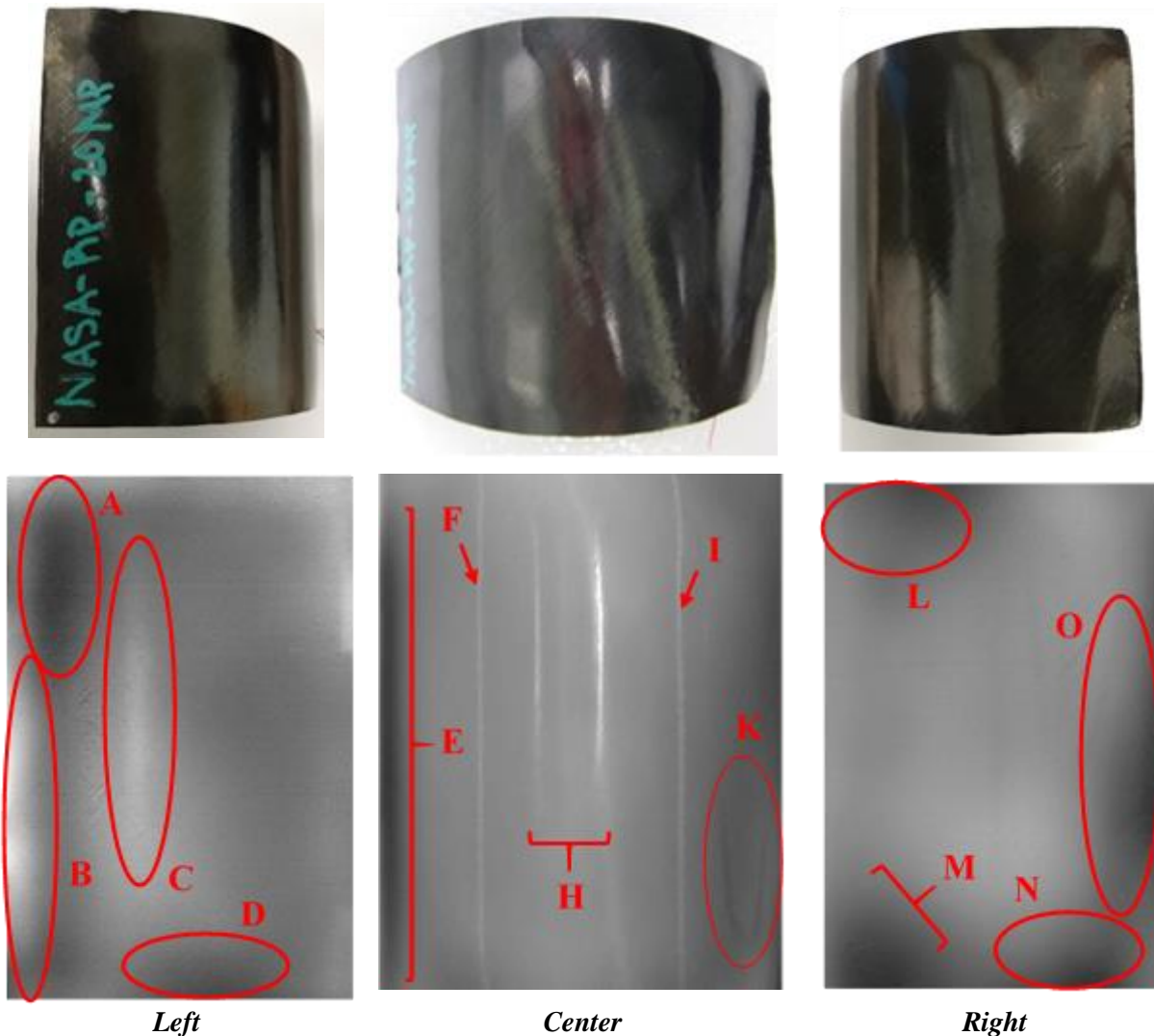


Figure E.28-7. TTIR inspection of NASA-RP-20MP sample's left, center, and right section processed with PCA from frame 100 (1.67s) to 1500 (25s).

E.28.2.8 References

- [1] Rajic, N.: "Principal Component Thermography for Flaw Contrast Enhancement and Flaw Depth Characterization in Composite Structures," *Composite Structures*, Vol. 58, pp. 521-528, 2002.
- [2] Zalameda, J. N.; Bolduc S.; and Harman R.: "Thermal Inspection of a Composite Fuselage Section using a Fixed Eigenvector Principal Component Analysis Method," Proc. *SPIE* 10214, *Thermosense: Thermal Infrared Applications XXXIX*, 102140H, 5 May 2017.
- [3] Cramer, K. E.; and Winfree, W. P.: "Fixed Eigenvector Analysis of Thermographic NDE Data", Proceedings of *SPIE*, *Thermosense XXXIII*, edited by Morteza Safai and Jeff Brown, Vol. 8013, 2011.

E.28.3 Method: Single-Side Flash Thermography (SSFT-TSR)

E.28.3.1 Partner: Thermal Wave Imaging, Inc.*

*TWI was not part of the ACC but reviewed specimens.

E.28.3.2 Technique Applicability: ★★★

SSFT-TSR is capable of detecting subsurface anomalies in this specimen that could be the result of delamination, voids or porosity. All indications appear in the head-on image, but more accurate sizing is achieved by inspecting the flat surfaces separately.

E.28.3.3 Laboratory Setup:

The sample was inspected with a commercially available flash thermography system (EchoTherm®, Thermal Wave Imaging, Inc.), equipped with 2 linear xenon flash/reflector assemblies mounted in a reflective hood optimized to provide uniform output at the 10 × 14-inch exit aperture. Each lamp is powered by a 6 kJ power supply that allows truncation of the flash to a rectangular pulse with duration <1 msec. A cryogenically cooled IR camera is mounted to view the plane of the hood exit aperture, with the camera lens positioned at the plane of the flashlamps. Excitation, data capture and processing and analysis using TSR are controlled at the system console using Virtuoso software.

E.28.3.4 Equipment List and Specifications:

- EchoTherm® Flash Thermography System
- 2 linear xenon flash lamps and power supplies (6 kJ each)
- TWI Precision Flash Control (truncation to 4 msec rectangular pulse)
- A6751sc FLIR IR camera, 640 × 512 InSb array, NEDT < 20 mK
- 25 mm Germanium Lens
- TWI Virtuoso® software

E.28.3.5 Settings:

- 15 Hz Frame Rate
- 10 Preflash Frames
- 2700 total frames
- 7 Polynomial order
- 180 sec data acquisition time
- FOV: 10 × 14-inch

Settings were determined following the recommendations in ASTM E2582-14. Acquisition duration was set according to the time of the break from linearity ($t^* \sim 90$ sec) due to the back wall for typical points in the log time history. The acquisition period was then set to 180 sec ($3 \times t^*$), per ASTM E2582-14.

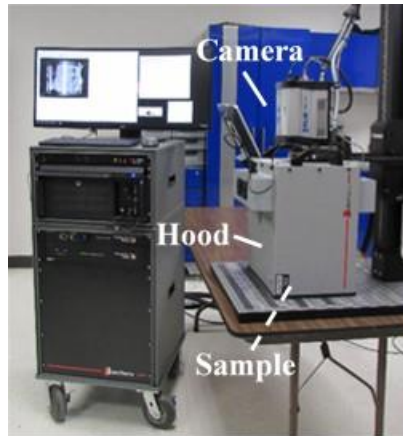


Figure E.28-8. SSFT system with TSR.

E.28.3.6 Thermographic Signal Reconstruction (TSR)

After acquisition, captured data are processed using TSR to reduce temporal noise, enhance deviation from normal cooling behavior and allow segmentation of the data based on signal attributes. For each pixel, the average of 10 frames immediately preceding the flash pulse is subtracted from the pixel time history, and a 7th order polynomial is fit to the logarithmically scaled result using least squares. First and 2nd derivatives of the result are calculated and the derivative images are displayed in the Virtuoso software. Derivative signals associated normal areas of the sample exhibit minimal activity over the duration of the acquisition. Signals associated with subsurface anomalies typically behave identically to the normal signals until a particular time (dependent on host material characteristics and the depth of the feature) after which their behavior deviates from normal (the degree of the deviation depends on the relative difference in the thermal properties of the anomaly and the surrounding normal matrix).

E.28.3.7 Inspection Results

Four clusters of subsurface indications were observed and confirmed to be subsurface by their late divergence in the logarithmic temperature time plot. All indications appear in the head-on (center) image; however, the full spatial extent of the indications is displayed in the left and right images, where the optical axis is normal to the sample surface. The 2nd derivative at 6.13 sec was used to produce the final inspection images shown in Figure E.28-9.

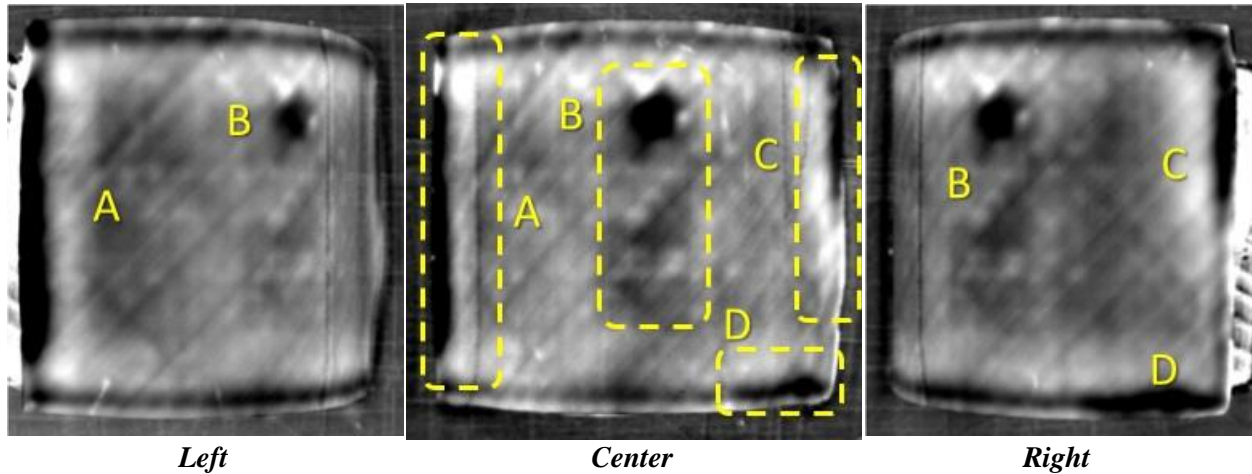


Figure E.28-9. TSR 2nd derivative at 6.13 sec of NASA-RP-20MP.

E.28.3.8 References

- [1] ASNT: *ASNT Aerospace NDT Industry Handbook*, Chapter 11, “Thermography,” Nov 2014.
- [2] ASTM International: “Standard Practice for Infrared Flash Thermography of Composite Panels and Repair Patches,” *ASTM E2582–07*, 2007.
- [3] Shepard, S.; and Frenberg, M.: “Thermographic Detection and Characterization of Flaws in Composite Materials,” *Materials Evaluation*, ASNT, July 2014.
- [4] Hou, Y.; Lhota, J. R.; and Golden, T. J. M.: “Automated processing of thermographic derivatives for quality assurance,” *Opt. Eng.*, Vol. 46, 051008, 2007.
- [5] *Temporal noise reduction, compression and analysis of data sequences*, U.S. Patent 6,516,084.

E.29 Specimen #29 - Not Manufactured

E.30 Specimen #30: NASA-RP-40MP 4.0-inch radial curve medium porosity

Structure	Material	Details	Dimensions (inches)	Partners Methods	
Uni-ply (0/90/45)	8552/IM7	4.0-inch radial inside curve, medium porosity	4.5 × 1.25 × 6	NASA	E.30.1 PEUT
				USC	E.30.2 GWUT



Figure E.30-1. Photographs of specimen #30: NASA-RP-40MP.

E.30.1 Method: Pulse-Echo Ultrasonic Testing (PEUT)

E.30.1.1 Partner: NASA

E.30.1.2 Technique Applicability: ☆☆☆

PEUT cannot characterize porosity in this sample.

E.30.1.3 Laboratory Setup

Immersion Ultrasonic Testing: NASA Langley Research Center (LaRC) uses a custom designed single probe ultrasonic scanning system. The system has an 8-axis motion controller, a multi-axis gantry robot mounted above a medium-size water tank, a dual-channel, 16-bit, high-speed digitizer, and an off-the-shelf ultrasonic pulser receiver. The system can perform TTUT and PEUT inspections. TT inspection employs two aligned ultrasonic probes, one transmitter and one receiver, placed on either side of a test specimen. Pulse-echo inspection is a single-sided method where a single ultrasonic probe is both transmitter and receiver. In each method, data are acquired while raster scanning the ultrasonic probe(s) in relation to a part. Figure E.30-2 shows a simplified block diagram of a scanning Pulse-echo inspection.

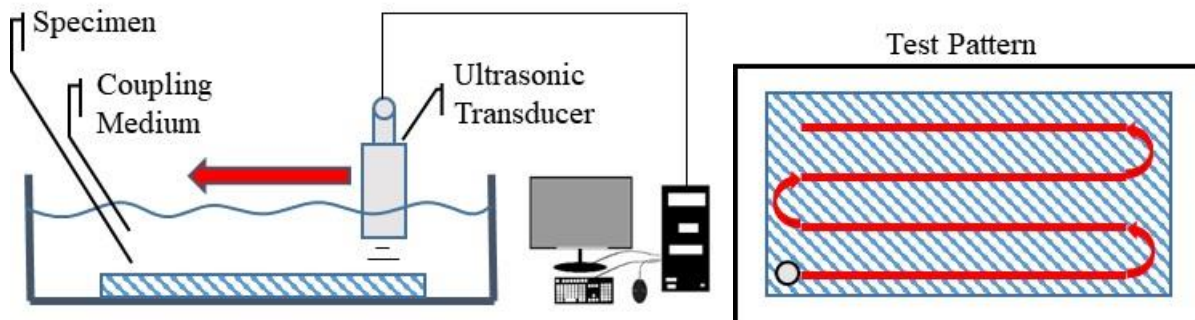


Figure E.30-2. Ultrasonic system components.

E.30.1.4 Equipment List and Specifications:

- Pulser/Receiver: Olympus 5073PR
- Digitizer: AlazarTech ATS9462, dual channel, 16 bit, 180 MS/s
- Sensor: Olympus 2-inch spherical focus immersion ultrasonic transducer
- Motion system: open looped stepper motor based X-YY-Z gantry robot
- Motion Controller: Galil DMC-4183
- Acquisition Software: FastScan, custom developed at NASA LaRC
- Signal Processing Software: DataViewer, custom developed at NASA LaRC

E.30.1.5 Settings

Table E-30-1. Data collection settings.

Resolution (horizontal) [in/pixel]	0.01
Resolution (vertical) [in/pixel]	0.02
Probe frequency [MHz]	5–10
Focal Length [in]	2
Array Dimensions [pixels]	311 × 301

The specimen is placed flat against the zero position of the tank raised above the glass bottom by several metal washers. The test probe is computer-controlled and correlated to the position on the

sample. It is also focused to a point 1 mm below the surface of the test material. The specimen remains in place while the transducer follows a preprogrammed test grid across the surface as indicated in Figure E.30-2. At each point, ultrasonic data are collected from individual pulses. Larger step sizes between data collection result in lower image resolution. These data points are reconstructed into a data cube displaying spatial coordinates as time progresses. 2D reconstruction of the collection of ultrasonic responses create flattened slices at varying depths within the material.

E.30.1.6 Inspection Results

A back-wall echo could not be resolved with either 5 or 10 MHz transducers. Therefore, it was not possible to characterize the porosity with PEUT at 5 or 10 MHz. Sample curvature presented further complications. A contact method at lower frequencies or a TTUT method may provide better results.

E.30.2 Method: Guided Wave Ultrasonic Testing (GWUT)

E.30.2.1 Partner: USC

E.30.2.2 Technique Applicability: ★☆☆

GWUT employs ultrasonic waves that propagate along waveguides by its boundaries, e.g. pipes, rods and plate-like structures, which allows waves propagate a long distance with little energy loss. GWUT shows advantage in many types of defect inspection, e.g. crack in metallic structures [1], and delamination in composite structures [2].

The Specimen, NASA-RP-40MP (herein referred to as 40MP), is inspected using hybrid PZT-SLDV GWUT method in this report. General information of 40MP is illustrated in the paragraph below. The relative inspection, results and system rating are illustrated in the inspection results.

The front view and side view Specimen 40MP are shown in Figure E.30-3a and Figure E.30-3b respectively. The height of the specimen is 101 mm, and the thickness is around 9.54 mm. The length between the specimen edges is 148 mm for outer surface and 143 mm for inner surface. The arc length of outer surface is 160 mm as shown in Figure E.30-3c. The actuator is attached at O_1 , O_2 , and O_3 in order to inspect the specimen from different views. No other information about 40 MP is available to the inspectors.

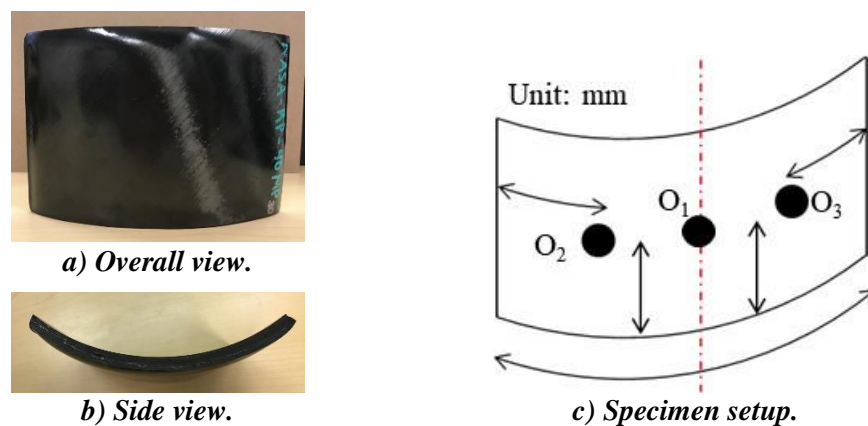


Figure E.30-3. Picture of specimen NASA-RP-40MP.

E.30.2.3 Laboratory Set up

The same hybrid PZT-SLDV system is employed for 40MP inspection, where contact type PZT is used as actuator and SLDV as sensor to excite and receive guided waves in the testing plate (Lamb waves) [1]. The overall setup also remains the same as reported previously shown in Figure E.30-4 and Figure E.30-5 [3].

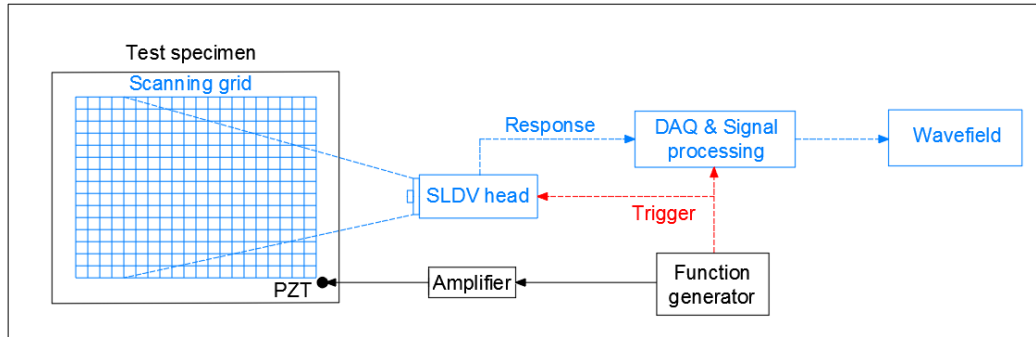


Figure E.30-4. Schematic design of the PZT-SLDV system.

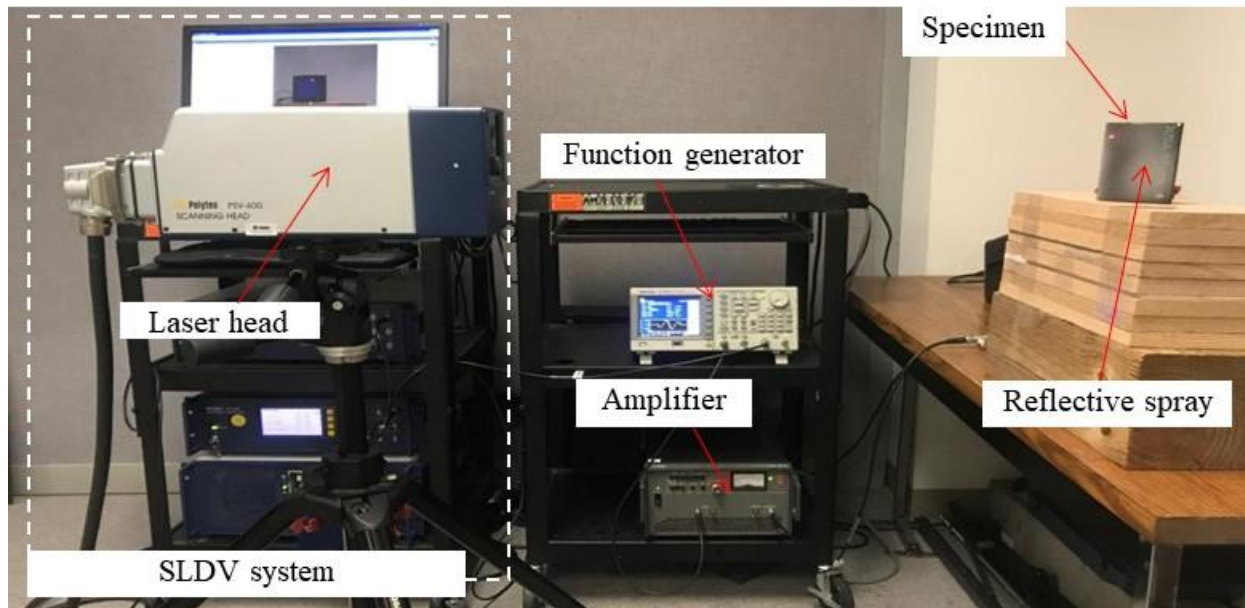


Figure E.30-5. Experimental setup of the PZT-SLDV system.

E.30.2.4 Equipment List and Specifications

The detailed specifications of the equipment and devices used for the hybrid PZT-SLDV system at USC Visualized Structural Health Monitoring (VSHM) laboratory are given in Table E.30-2. Data acquisition settings are shown in Table E.30-3.

Table E.30-2. Equipment/device specifications.

Equipment/device	Specifications
Polytec PSV-400-M2	2D scanning laser Doppler vibrometer with a frequency range up to 1 MHz with specific velocity decoders
PZT	Steminc 7-mm circular 0.5-mm thick piezoelectric transducers
Tektronix AFG3022C	2-channel arbitrary function generator with 1 μ Hz to 25MHz

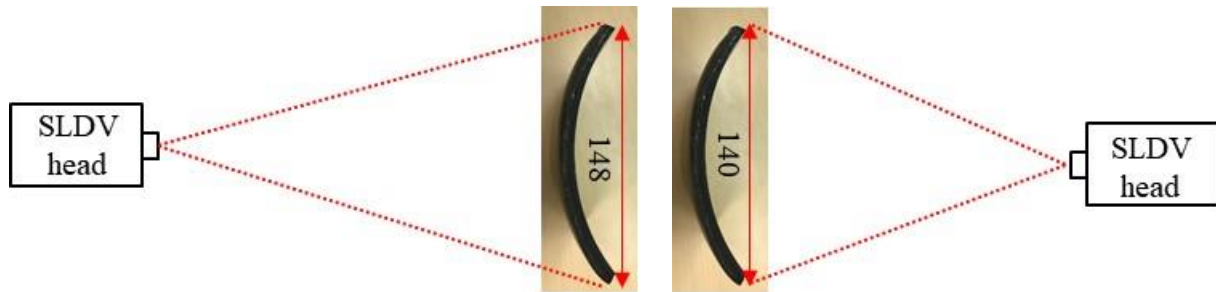
HSA 4014	High speed bipolar amplifier up to 1 MHz and 200 VA
Target Simply Balanced™ organic honey	Natural and organic honey blend performed as couplant
Albedo 100 Reflective Spray	a non-permanent, clear spray with light-reflective properties

Table E.30-3. Data collection settings.

Sampling frequency (MHz)	12.56 MHz
Spatial sampling interval (mm)	1 mm
Average	100
Velocity decoder	VD-07 10mm/s/V
Spray coating	20 layers

E.30.2.5 Settings

A 3-count toneburst at 240 kHz amplified to 50 V_{pp} is used as excitation for each test. 2D area inspection is performed for each part with spatial resolution 1 mm. The inspection is performed with the setup shown in Figure E.30-6. Since the specimen is curved, the inspection is not the same as traditional SLDV scanning. The SLDV head is placed normal to the center of the specimen (O_2), and the scanning angle effect is not considered. 2D area inspection is performed with each actuation locations on both sides. For each inspection, the scanning area covers the accessible surface of the inspected wing: around 120 mm × 90 mm for both sides. For each side, the inspection area differs a little due to the curvature. Note that the scanning area is not identical to the real arc surface, and the measured wavefield is the shrink version of original wavefield in x - z plane due to the curvature.



a) Scanning schematic of outside surface. b) Scanning schematic design of inside surface.

Figure E.30-6. Experimental setup.

E.30.2.6 Inspection Results and Conclusions

Outside surface

2D area inspection is performed on the outside surface first. The 2D time-space wavefields are obtained with O_1 , O_2 , and O_3 as excitation point, and the relative wavefield imaging are generated and plotted in Figure E.30-7. When the excitation is at O_1 , areas with intensified energy is observed while no obvious defects are observed, which means there might be small defects existing in the plate and scattered the energy towards all direction resulting in energy distribution as shown in Figure E.30-8a. When the excitation at O_2 , two areas of possible defects are observed (Figure E.30-7b), while one possible defect is observed with excitation at O_3 .

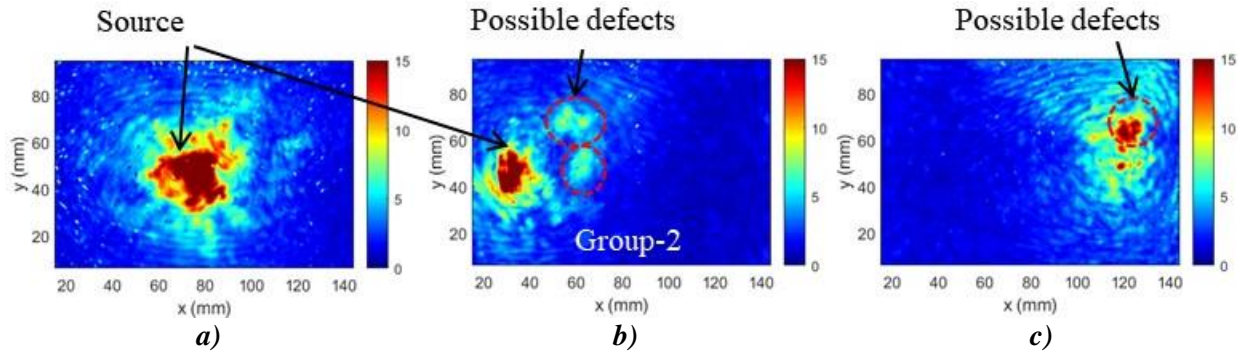


Figure E.30-7. Wavefield imaging on the outside surface with excitation location at: a) O_1 , b) O_2 , and c) O_3 .

Inside surface

On the inside surface, same 2D area inspection is performed. The relative wavefield imaging are generated and plotted in Figure E.30-8. When the excitation is at O_1 , areas with intensified energy are observed while no obvious defects are observed, which matches the results on outside surface. While with the excitation at O_2 and O_3 , no obvious defect is observed (Figure E.30-8b and Figure E.30-8c).

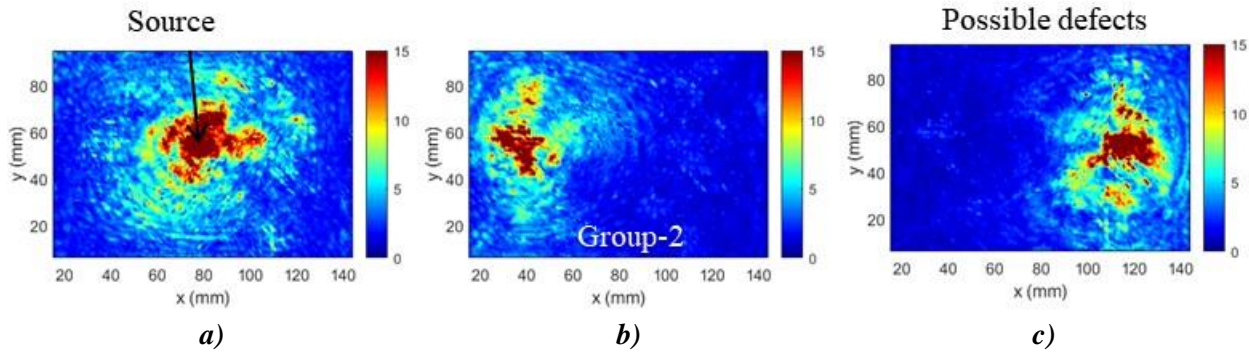


Figure E.30-8. Wavefield imaging on the inside surface with excitation location at: a) O_1 , b) O_2 , and c) O_3 .

In conclusion, defects (porosity) on specimen 40D using the hybrid PZT-SLDV system is detected even without material properties. The detailed rating of the system is shown in Table E.30-4. The defects are successfully detected since areas with intensified energy were observed in the wavefield imaging. However, the locations of the defects cannot be confirmed since the results from the three inspection schemes are not consistent. Thus, three stars are rated for this part. For defect visualization, no obvious defect size and shape is identified, so that part gets two of five stars. For inspection time, the inspection time for one 2D scanning is around 50 minutes for areas illustrated in this test, which is fast. Thus, the inspection time gets four stars overall. Last, the actuator PZT is \$3.60 per piece, which is cost effective. However, the SLDV is an expensive equipment, which costs \$300,000 when purchasing. Thus, this part gets two stars. In the future, expensive SLDV can be replaced by customized fixed LDV and gantry system to reduce the system cost. Overall, this hybrid PZT-SLDV guided wave inspection is very robust in general with two out of five stars.

Table E.30-4. Hybrid PZT-SLDV guided wave inspection rating.

Hybrid PZT-SLDV guided wave inspection		
NASA-RP-40MP Defect: porosity	Rating	
	Detection:	★★★★☆
	Defect visualization	★★☆☆☆
	Inspection time:	★★★★☆
	Equipment cost:	★★☆☆☆
	Overall Performance:	★★☆☆☆

E.30.2.7 References

- [1] Yu, L.; Leckey, C. A.; and Tian, Z.: “Study on crack scattering in aluminum plates with Lamb wave frequency–wavenumber analysis,” *Smart Materials and Structures*, Vol. 22, No. 6, pp065019, 2013.
- [2] Tian, Z.; Yu, L.; and Leckey, C.: “Delamination detection and quantification on laminated composite structures with Lamb waves and wavenumber analysis,” *Journal of Intelligent Material Systems and Structures*, Vol.26, No. 13, 2015, pp. 1723-1738, 2015.
- [3] Guided wave inspection on specimen A1 (A1 report, submitted).

E.31 Specimen #31: Wrinkle A1

Structure	Material	Details	Dimensions (inches)	Partner Methods	
Thin laminates	IM7/8552-1 slit tape	flat wrinkling in flat panels	15 × 12 × 0.15	NASA	E.31.1 PEUT E.31.2 XCT
				Boeing	E.31.3 SSIR

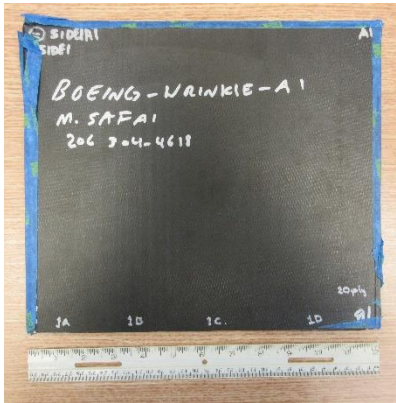


Figure E.31-1. Photograph of specimen #31: Boeing Wrinkle A1.

E.31.1 Method: Pulse-Echo Ultrasound Testing (PEUT)

E.31.1.1 Partner: NASA

E.31.1.2 Technique Applicability: ★★★

PEUT is able to detect the flat wrinkles in this specimen.

E.31.1.3 Laboratory Setup

Immersion Ultrasonic Testing: NASA LaRC uses a custom designed single probe ultrasonic scanning system. The setup has a 8-axis motion controller, a multi-axis gantry robot mounted above a medium-size water tank, a dual-channel 16-bit high speed digitizer, and an off-the-shelf

ultrasonic pulser receiver. The system can perform TTUT and PEUT inspections. TT inspection employs two aligned ultrasonic probes, one transmitter and one receiver, placed on either side of a test specimen. Pulse-echo inspection is a single sided method where a single ultrasonic probe is both transmitter and receiver. In each method, data are acquired while raster scanning the ultrasonic probe(s) in relation to a part. Figure E.31-2 shows a simplified block diagram of a scanning Pulse-echo inspection.

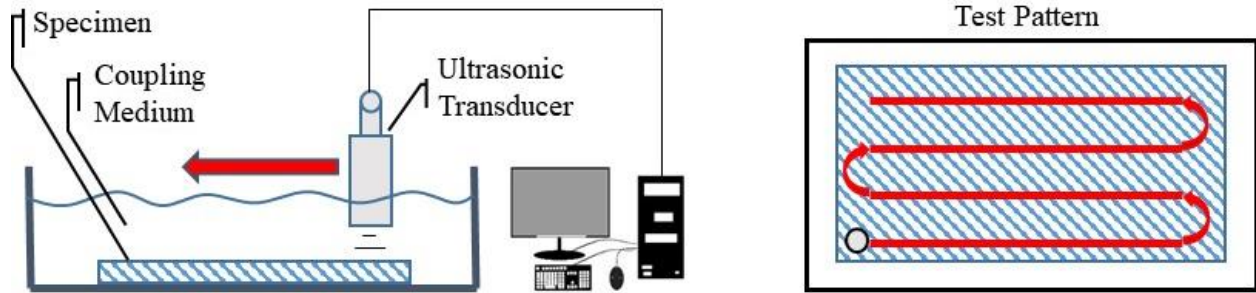


Figure E.31-2. Ultrasonic system components.

E.31.1.4 Equipment List and Specifications:

- Pulser/Receiver: Olympus 5073PR
- Digitizer: AlazarTech ATS9462, dual channel, 16 bit, 180 MS/s
- Sensor: Olympus 2-inch spherical focus immersion ultrasonic transducer
- Motion system: open looped stepper motor based X-YY-Z gantry robot
- Motion Controller: Galil DMC-4183
- Acquisition Software: FastScan, custom developed at NASA LaRC
- Signal Processing Software: DataViewer, custom developed at NASA LaRC

E.31.1.5 Settings

Table E-31-1. Data collection settings.

Resolution horizontal [in/pixel]	.01
Resolution vertical [in/pixel]	.01
Probe frequency [mHz]	10
Focal Length [in]	2
Array Dimensions [pixels]	451 × 351

The specimen is placed flat against the zero position of the tank raised above the glass bottom by several metal washers. The test probe is computer-controlled and correlated to the position on the sample. It is also focused to a point 1 mm below the surface of the test material. The specimen remains in place while the transducer follows a preprogrammed test grid across the surface as indicated in Figure E.31-2. At each point, ultrasonic data are collected from individual pulses. Larger step sizes between data collection result in lower image resolution. These data points are reconstructed into a data cube displaying spatial coordinates as time progresses. 2D reconstruction of the collection of ultrasonic responses create flattened slices at varying depths within the material.

E.31.1.6 Inspection Results

Specimen #31 is fabricated from IM7/8552-1 slit tape with the objective of achieving flat wrinkles within the material. PEUT was performed on this specimen in NASA's immersion tank specified above.

The UT image in Figure E.31-3a is signal amplitude just below the sample top surface. It indicates fiber wrinkling near the surface of the material. The white dots in the image corners are reflections from the metallic standoffs under the sample. The fiber wrinkles cause severe perturbations in the acoustic waves that are easily seen throughout the sample as shown in C-scan image, Figure E.31-3b.

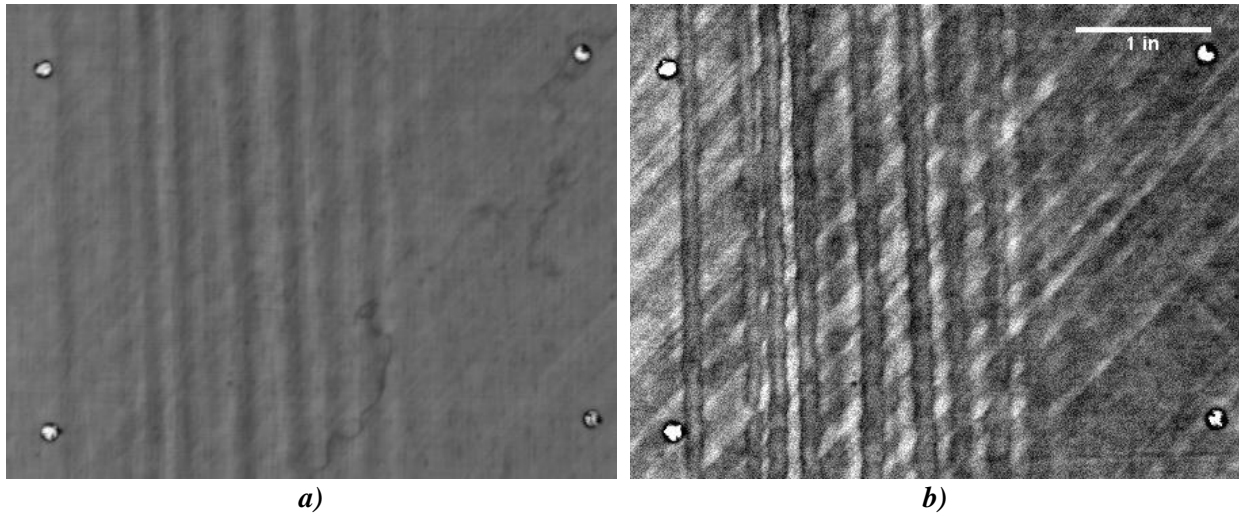


Figure E.31-3. UT image showing near surface indications of fiber waviness.

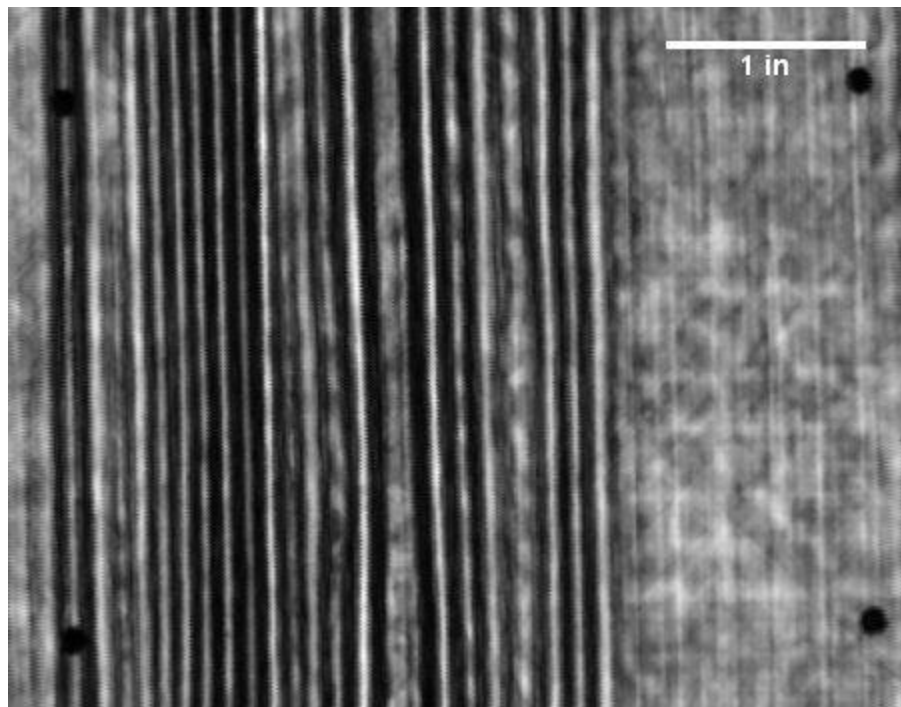


Figure E.31-4. UT image showing indications of fiber waviness within the material bulk.

E.31.2 Method: X-ray Computed Tomography (XCT)

E.31.2.1 Partner: NASA

E.31.2.2 Technique Applicability: ☆☆☆

XCT is does not detect the flat wrinkles in this specimen.

E.31.2.3 Laboratory Setup

The microfocus XCT system at NASA LaRC is a commercially available Avonix (Nikon C2) Metrology System designed for high resolution NDE inspections. The system is an advanced microfocus X-ray system, capable of resolving details down to 5 μm , and with magnifications up to 60X. Supplied as complete, the system is a large-dimension radiation enclosure with X-ray source. The imaging controls are housed in a separate control console. The detector is a Perkin-Elmer, 16-bit, amorphous-silicon digital detector with a 2000 \times 2000-pixel array.

A consistent Cartesian coordinate system is used to define slice direction as illustrated in Figure E.31-6. Slices normal to the X-, Y-, and Z-directions are shown in Figures 31-6a, b, and c, respectively.

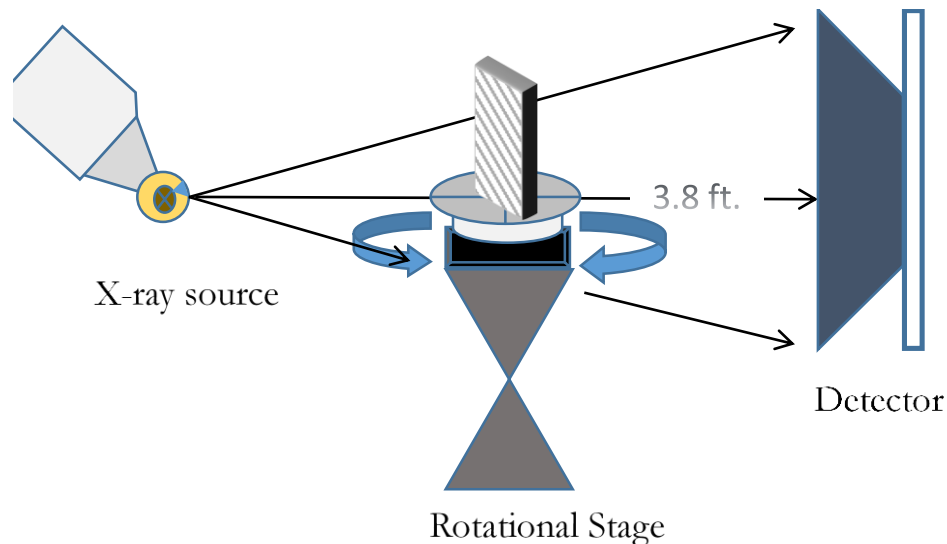


Figure E.31-5. XCT system components.

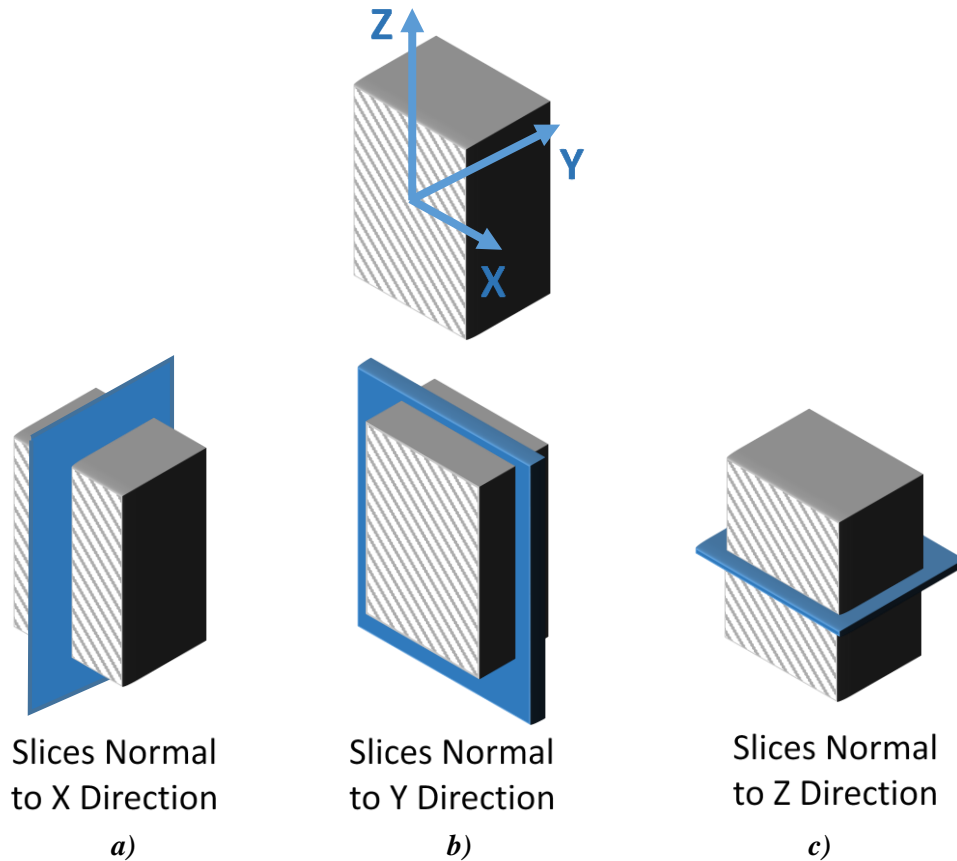


Figure E.31-6. Slice direction nomenclature.

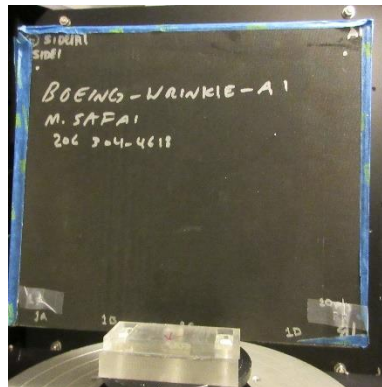


Figure E.31-7. Microfocus XCT system showing orientation of Specimen #31: Boeing-Wrinkles A1.

E.31.2.4 Equipment List and Specifications:

- Avonix 225 CT System
- 225 kV microfocus X-ray source with 5- μ m focal spot size
- 15 or 30kg Capacity, 5-axis, fully programmable manipulator
- Detector: Perkin Elmer XRD 1621 – 2000 \times 2000 pixels with 200 μ m pitch
- 10 μ m spatial resolution for specimens 1.5 cm wide
- Thin panels 10 \times 10 inches – full volume 200 μ m spatial resolution

E.31.2.5 Settings

Table E.31-2. Data collection settings.

Source Energy	120 kV
Current	90 μ A
Magnification	1.65 X
Filter	NF
# Rotational angles	3142
Exposure time / frame	1.0 sec
Max Histogram Grey Level	22 K
# Averages	8
Resolution (μ m)	114.894 μ m
Array Dimensions (pixels)	Set 1: 1999 \times 362 \times 1998 Set 2: 1998 \times 686 \times 1997

The specimen is placed vertically (rotated about the smallest dimension) on the rotational stage located between the radiation source and the detector. The rotational stage is computer-controlled and correlated to the position of the sample. As the sample is rotated the full 360° (~0.11° increments), the detector collects radiographs at each rotated angle as the X-ray path intersects the sample. 3D reconstruction of the collection of radiographs produces a volume of data observed along any plane in the volume. The closer the sample placement to the X-ray source, the higher the spatial resolution obtained.

E.31.2.6 Inspection Results

Section A

Specimen #31 is a panel with flat wrinkles induced within the material. XCT was performed on this specimen in NASA LaRC's large CT system with the settings defined in Section E.31.2.5. The scan was done using a large viewing window encompassing the whole specimen (Figure E.31-8) and a small window covering a smaller area to increase the resolution of the scan (Figure E.31-9). This cannot always be done on larger specimens.

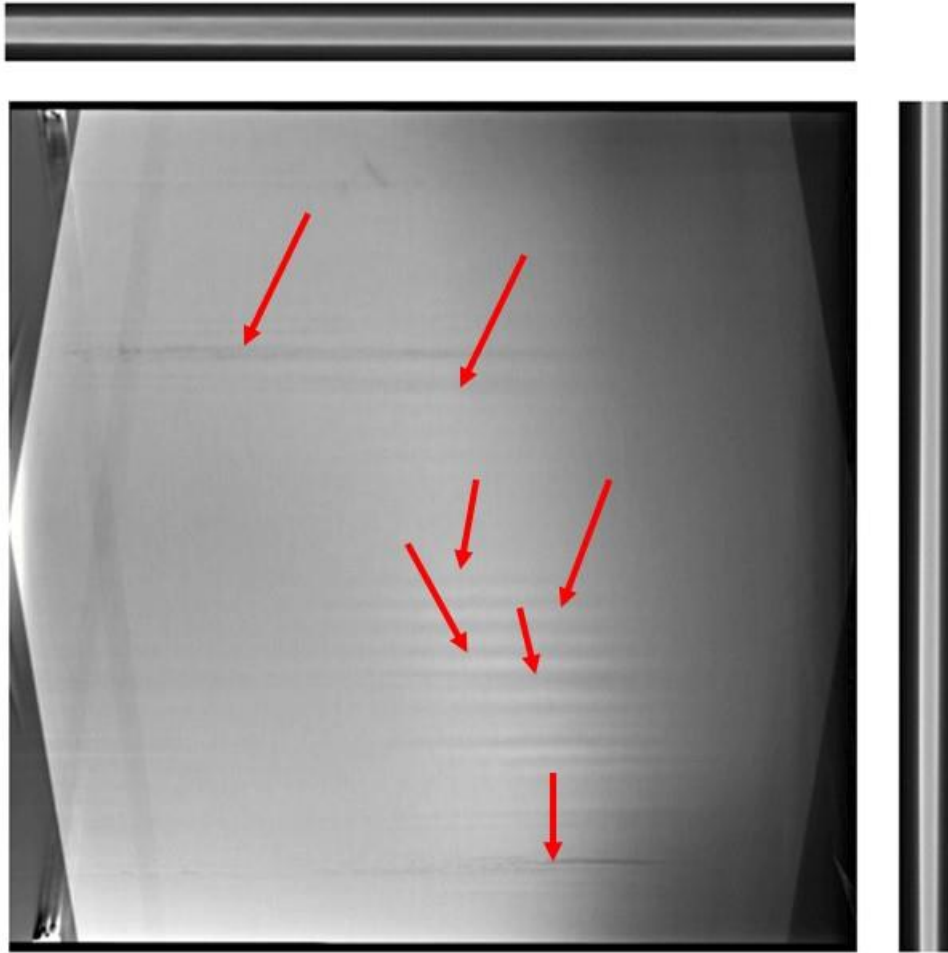


*Figure E.31-8. 3D X-ray generated view of specimen #31: Boeing-Wrinkles using a small viewing window showing the y-normal direction (center), z-normal direction (top) and x-normal direction (right).
Wrinkles are highlighted in the y-normal view with red arrows*

The wrinkles cannot be seen from any viewing directions shown in Figure E.31-8. The y direction shows some dark streaks that are damage as result of the method the fiber wrinkles were introduced; however, they do not represent the wrinkles themselves. Both the x- and z-direction views give little evidence of any fiber waviness. When viewing the higher resolution data the fiber waviness still is not apparent (Figure E.31-9).

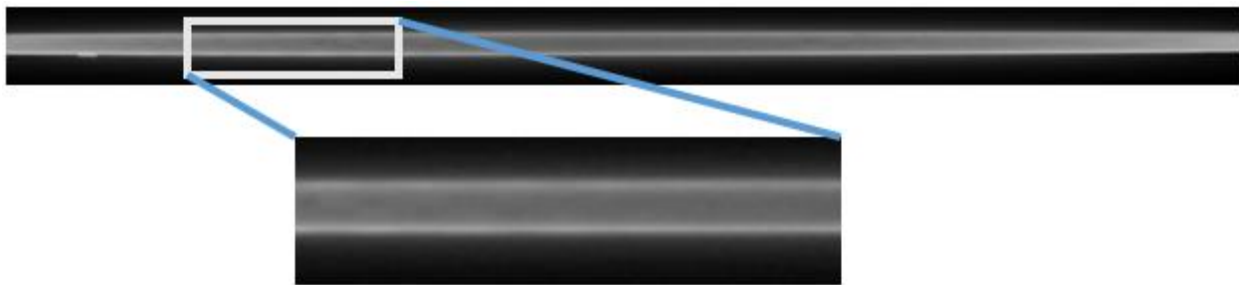


Figure E.31-9. 3D X-ray generated view of specimen #31: Boeing-Wrinkles from the z-normal direction.

E.31.3 Method: Single-Sided Infrared Thermography (SSIR)

E.31.3.1 Partner: Boeing

E.31.3.2 Technique Applicability: ★★★

SSIR Thermography is capable of detecting wrinkles in the composite material.

E.31.3.3 Laboratory Setup

For each inspection, the part was placed in the IR imaging system (Figure E.31-10). For each test, the flash lamp fires, heating the surface of the part uniformly. The IR camera records the heat signature of the part over time to track the diffusion of heat through the part thickness. This test was repeated for the front and backsides of each panel. The wrinkles on the panel cause alternating areas of high and low resin content in the troughs and crest, respectively. Because the resin has a lower thermal conductivity than the carbon fiber, the high content regions (troughs) will retain heat more than the low content regions (crests). As a result, the crests will show as cold spots over time while the troughs show as hot spots.

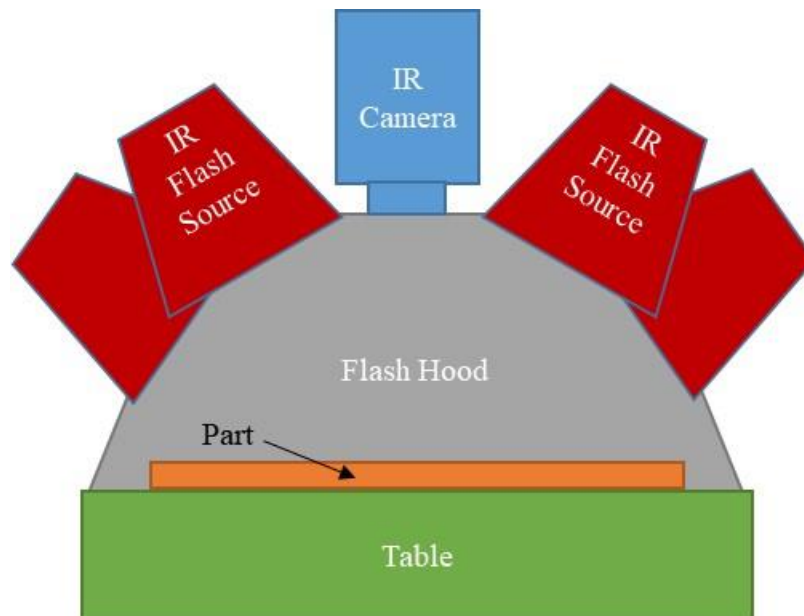


Figure E.31-10. SSIR system components.



Figure E.31-11. IR inspection system.

E.31.3.4 Equipment List and Specifications:

- Thermal Wave VoyageIR system
- SC6000 Series FLIR IR camera
- 4 6400 Watt-sec flash lamps
- Flash Hood
- X-Y gantry system

E.31.3.5 Settings

Data collection settings (i.e., resolution, frame rate, data acquisition time) were not provided by inspector.

E.31.3.6 Inspection Results

Figure E.31-12 shows the IR image of the panel at 1.6 sec. As anticipated, hot and cold spots can be observed (circled in red), corresponding with the manufactured wrinkle locations. Because the panel was uniformly heated on the side that the camera observed, the strongest thermal gradient will come from the wrinkles on that side. Because of this, one can observe fainter, mirrored indications of the wrinkles when observed from the opposite side, such as the left side grouping of wrinkles in Figure E.31-12a appearing fainter on the right side in Figure E.31-12b. From these data, it is possible to measure the wavelength of the wrinkles, though the amplitudes cannot be determined from these data.

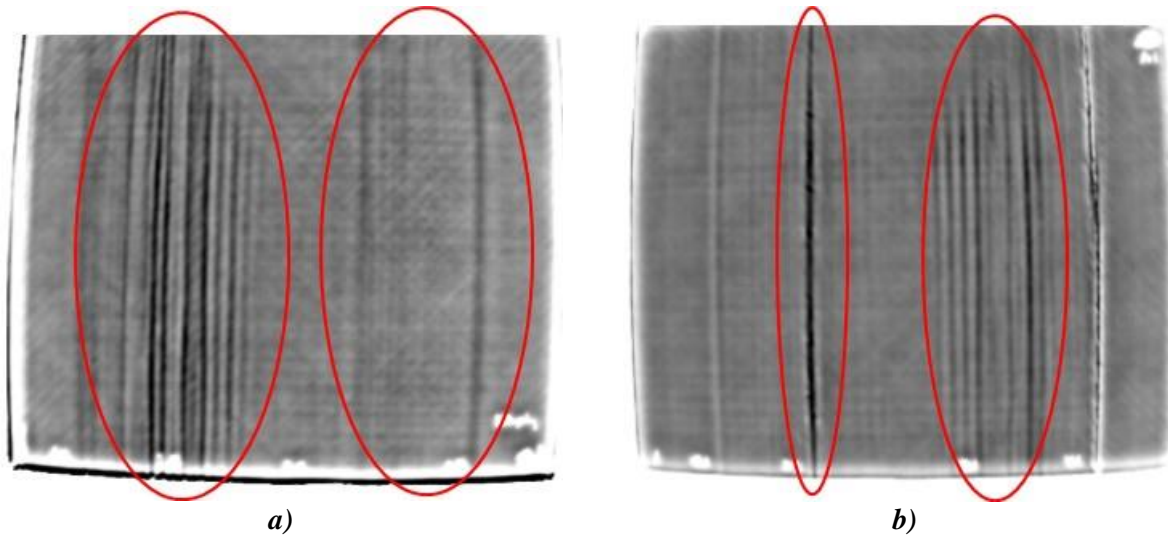


Figure E.31-12. Greyscale 1.6 sec IR image of Composite Wrinkle Standard A1 side 1 (a) and side 2 (b).

E.32 Specimen #32: Wrinkle A2

Structure	Material	Details	Dimensions (inches)	Partner Methods	
Thin laminates	IM7/8552-1 slit tape	flat wrinkling in flat panels	15 × 12 × 0.15	NASA	E.32.1 PEUT E.32.2 XCT
				USC	E.32.3 GWUT
				Boeing	E.32.4 SSIR

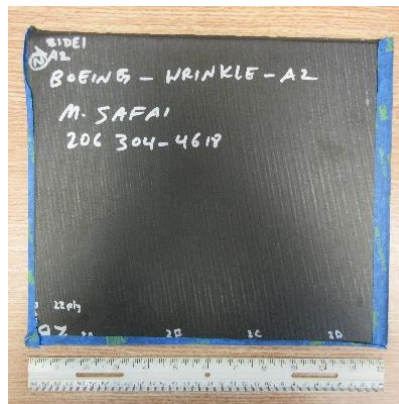


Figure E.32-1. Photographs of Specimen #33: Boeing Wrinkle A3.

E.32.1 Method: Pulse-Echo Ultrasound Testing (PEUT)

E.32.1.1 Partner: NASA

E.32.1.2 Technique Applicability: ★★★

PEUT is capable of detecting the fiber wrinkling within this specimen.

E.32.1.3 Laboratory Setup

Immersion Ultrasonic Testing: NASA LaRC uses a custom designed single probe ultrasonic scanning system. The system has an 8-axis motion controller, a multi-axis gantry robot mounted above a medium-size water tank, a dual-channel, 16-bit, high-speed digitizer, and an off-the-shelf

ultrasonic pulser receiver. The system can perform TTUT and PEUT inspections. TT inspection employs two aligned ultrasonic probes, one transmitter and one receiver, placed on either side of a test specimen. Pulse-echo inspection is a single-sided method where a single ultrasonic probe is both transmitter and receiver. In each method, data are acquired while raster scanning the ultrasonic probe(s) in relation to a part. Figure E.32-2 shows a simplified block diagram of a scanning Pulse-echo inspection.

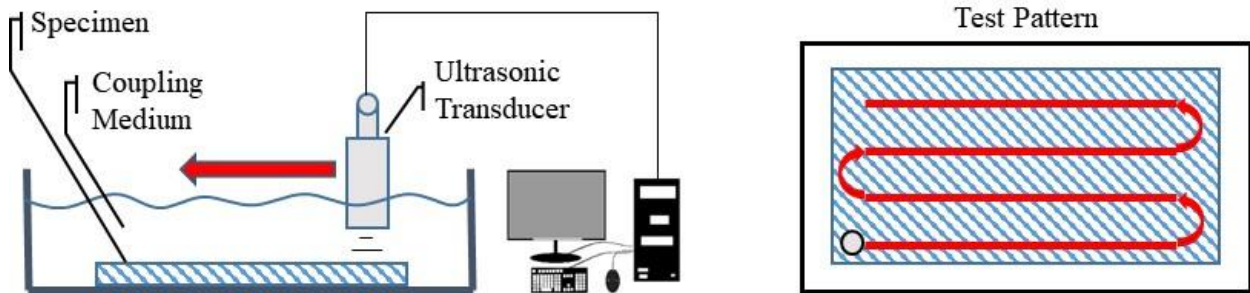


Figure E.32-2. Ultrasonic system components.

E.32.1.4 Equipment List and Specifications:

- Pulser/Receiver: Olympus 5073PR
- Digitizer: AlazarTech ATS9462, dual channel, 16 bit, 180 MS/s
- Sensor: Olympus 2-inch spherical focus immersion ultrasonic transducer
- Motion system: open looped stepper motor based X-YY-Z gantry robot
- Motion Controller: Galil DMC-4183
- Acquisition Software: FastScan, custom developed at NASA LaRC
- Signal Processing Software: DataViewer, custom developed at NASA LaRC

E.32.1.5 Settings

Table E.32-1. Data collection settings.

Resolution horizontal [in/pixel]	0.02
Resolution vertical [in/pixel]	0.05
Probe frequency [MHz]	10
Focal Length [in]	2
Array Dimensions [pixels]	601 × 201

The specimen is placed flat against the zero position of the tank raised above the glass bottom by several metal washers. The test probe is computer-controlled and correlated to the position on the sample. It is also focused to a point 1 mm below the surface of the test material. The specimen remains in place while the transducer follows a preprogrammed test grid across the surface as indicated in Figure E.32-2. At each point, ultrasonic data are collected from individual pulses. Larger step sizes between data collection result in lower image resolution. These data points are reconstructed into a data cube displaying spatial coordinates as time progresses. 2D reconstruction of the collection of ultrasonic responses create flattened slices at varying depths within the material.

E.32.1.6 Inspection Results

Specimen #32 is a panel fabricated from IM7/8552-1 slit tape with the objective of achieving flat wrinkles within the material. PEUT was performed on this specimen in NASA's immersion tank specified above.

In Figure E.32-3, UT images taken at an early time step show the indications of fiber wrinkling near the surface of the material. The wrinkles cause severe perturbations in the acoustic waves that are easily seen throughout the sample as shown in Figure E.32-4.

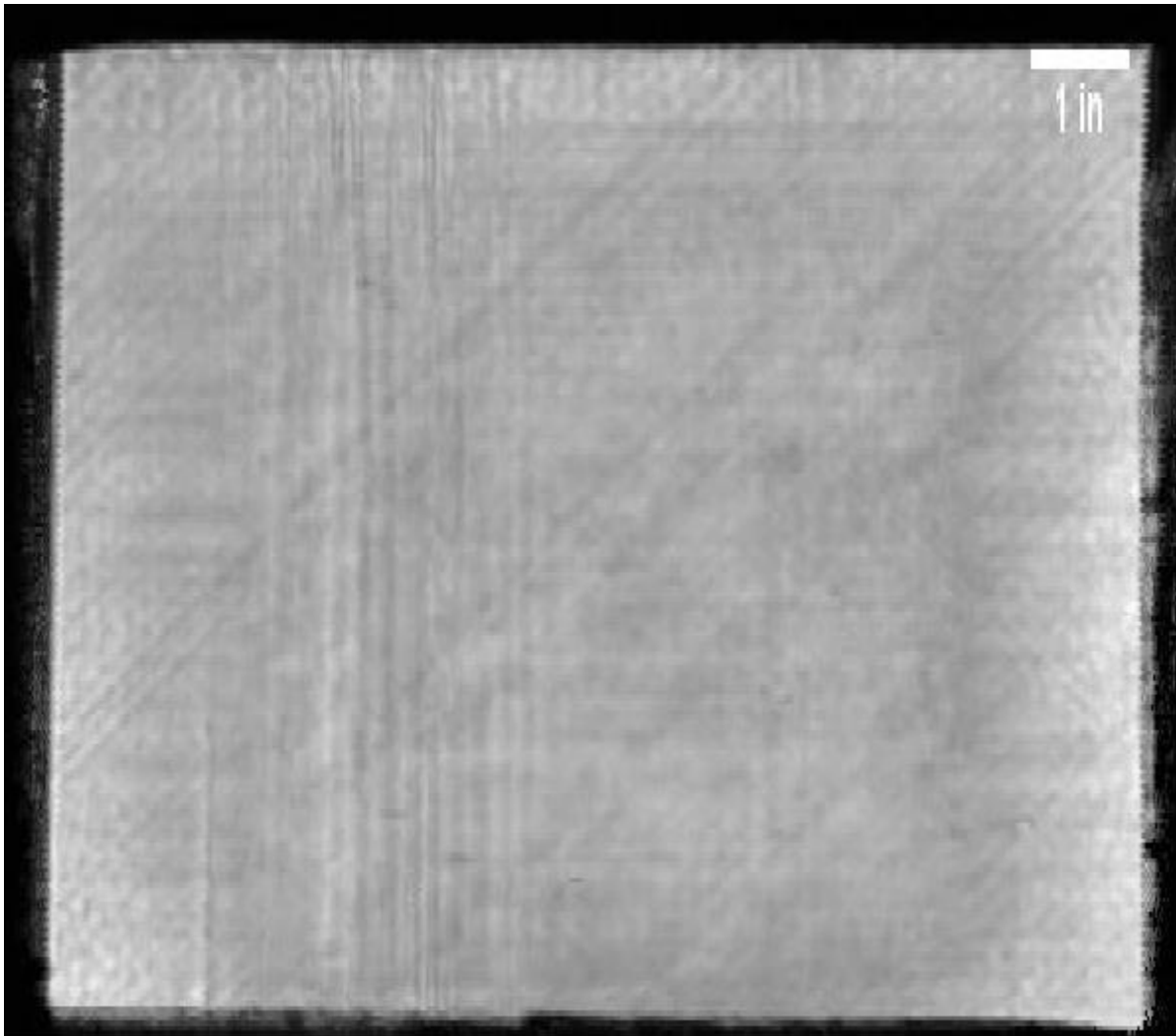


Figure E.32-3. UT image showing near surface indications of fiber waviness.

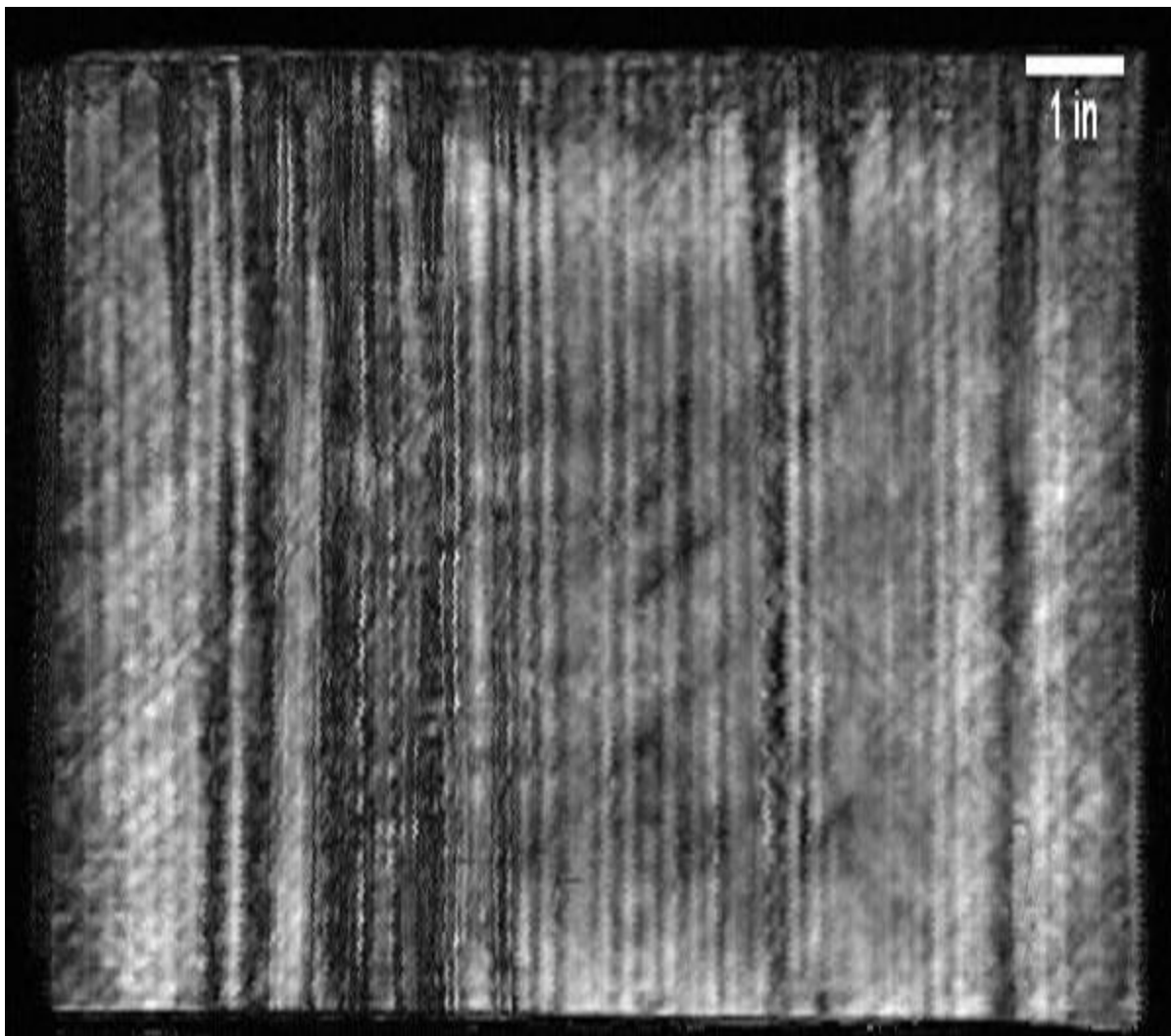


Figure E.32-4. UT image showing indications of fiber waviness within the material bulk.

E.32.2 Method: X-ray Computed Tomography (XCT)

E.32.2.1 Partner: NASA

E.32.2.2 Technique Applicability: ★★☆☆

E.32.2.3 Laboratory Setup

The microfocus XCT system at NASA LaRC is a commercially available Avonix (Nikon C2) Metrology System designed for high resolution NDE inspections. The system is an advanced microfocus X-ray system, capable of resolving details down to 5 μm , and with magnifications up to 60X. Supplied as complete, the system is a large-dimension radiation enclosure with X-ray source, specimen manipulator, and an amorphous silica detector, as shown in Figure E.32-5. The imaging controls are housed in a separate control console. The detector is a Perkin-Elmer, 16-bit, amorphous-silicon digital detector with a 2000 \times 2000-pixel array.

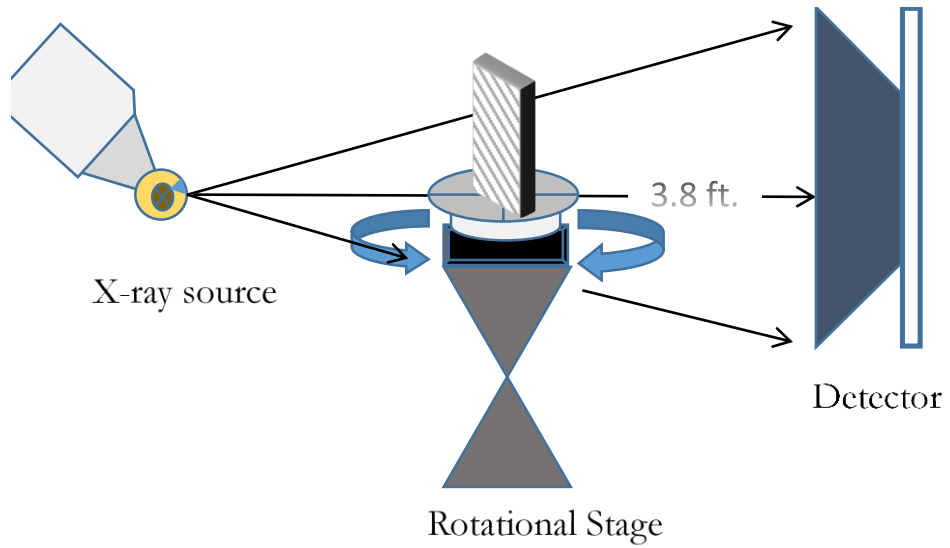


Figure E.32-5. XCT system components

A consistent Cartesian coordinate system is used to define slice direction as illustrated in Figure E.32-6 and Figure E.32-7. Slices normal to the X-, Y-, and Z-directions are shown in Figures E.32-6a, b, and c, respectively.

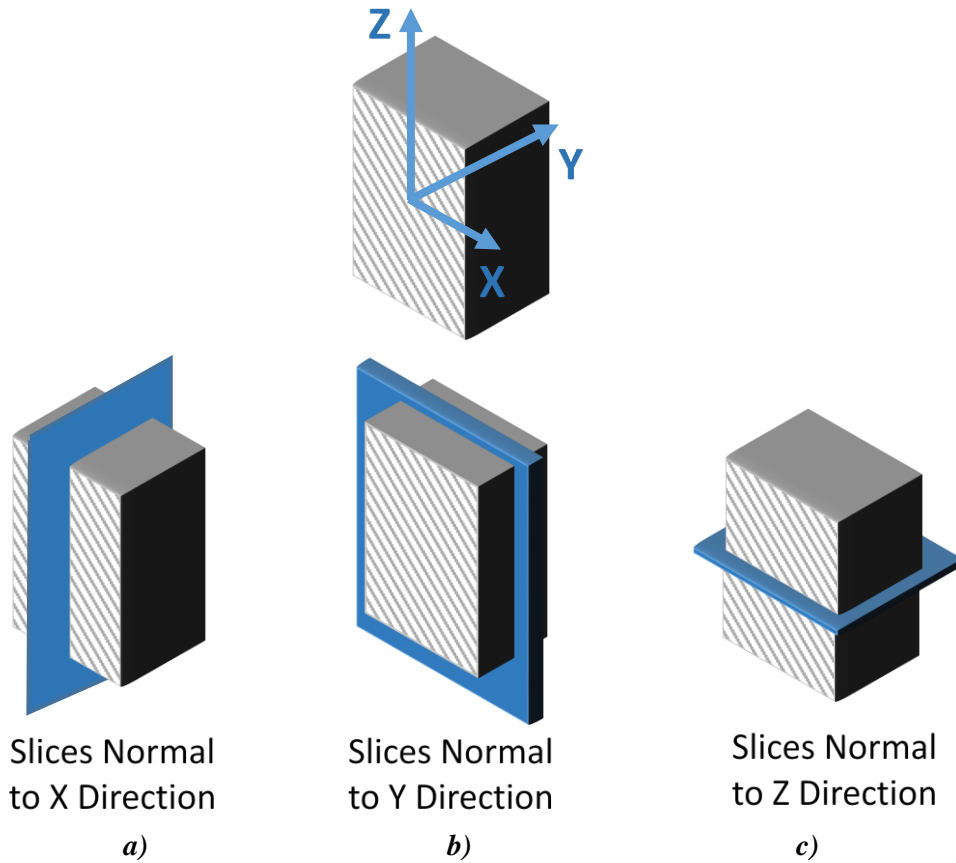


Figure E.32-6. Slice direction nomenclature.

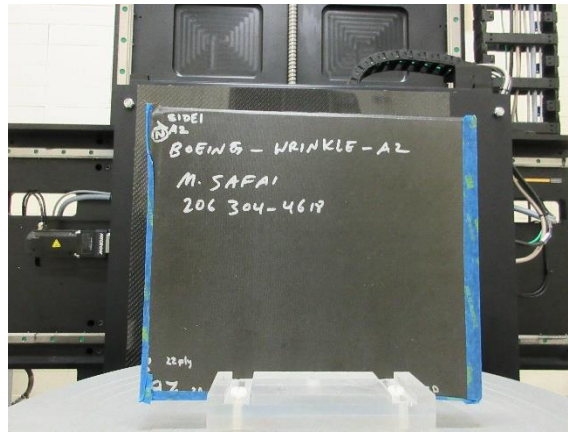


Figure E.32-7. Microfocus XCT system showing orientation of Specimen #32: Boeing-Wrinkles A2.

E.32.2.4 Equipment List and Specifications:

- Avonix 225 CT System
- 225 kV microfocus X-ray source with 5 μm focal spot size
- 15 or 30 kg Capacity, 5-axis, fully programmable manipulator
- Detector: Perkin Elmer XRD 1621 – 2000 \times 2000 pixels with 200 μm pitch
- 10 μm spatial resolution for specimens 1.5 cm wide
- Thin panels 10 \times 10 inches – full volume 200 μm spatial resolution

E.32.2.5 Settings

Table E.32-2. Data collection settings.

Source Energy	120 kV
Current	90 μA
Magnification	1.65 X
Filter	NF
# Rotational angles	3142
Exposure time / frame	1.0 sec
Max Histogram Grey Level	22 K
# Averages	8
Resolution (μm)	114.894 μm
Array Dimensions (pixels)	Set 1: 1999 \times 362 \times 1998 Set 2: 1998 \times 686 \times 1997

The specimen is placed vertically (rotated about the smallest dimension) on the rotational stage located between the radiation source and the detector. The rotational stage is computer-controlled and correlated to the position of the sample. As the sample is rotated the full 360° (~0.11° increments), the detector collects radiographs at each rotated angle as the X-ray path intersects the sample. 3D reconstruction of the collection of radiographs produces a volume of data that can then be viewed along any plane in the volume. The closer the sample placement to the X-ray source, the higher the spatial resolution that obtained.

E.32.2.6 Inspection Results

Specimen #32 is a panel with medium wrinkles induced within the material. XCT was performed on this specimen in NASA LaRC's large CT system with the settings defined in Section E.32.1.5.

The wrinkles are unseen from all viewing directions shown in Figure E.32-6. Both the x- and z-direction views give little evidence of any fiber waviness. In the y direction, the fiber wrinkles are somewhat visible in the form of dark regions that track slowly up and down as they move across the specimen.

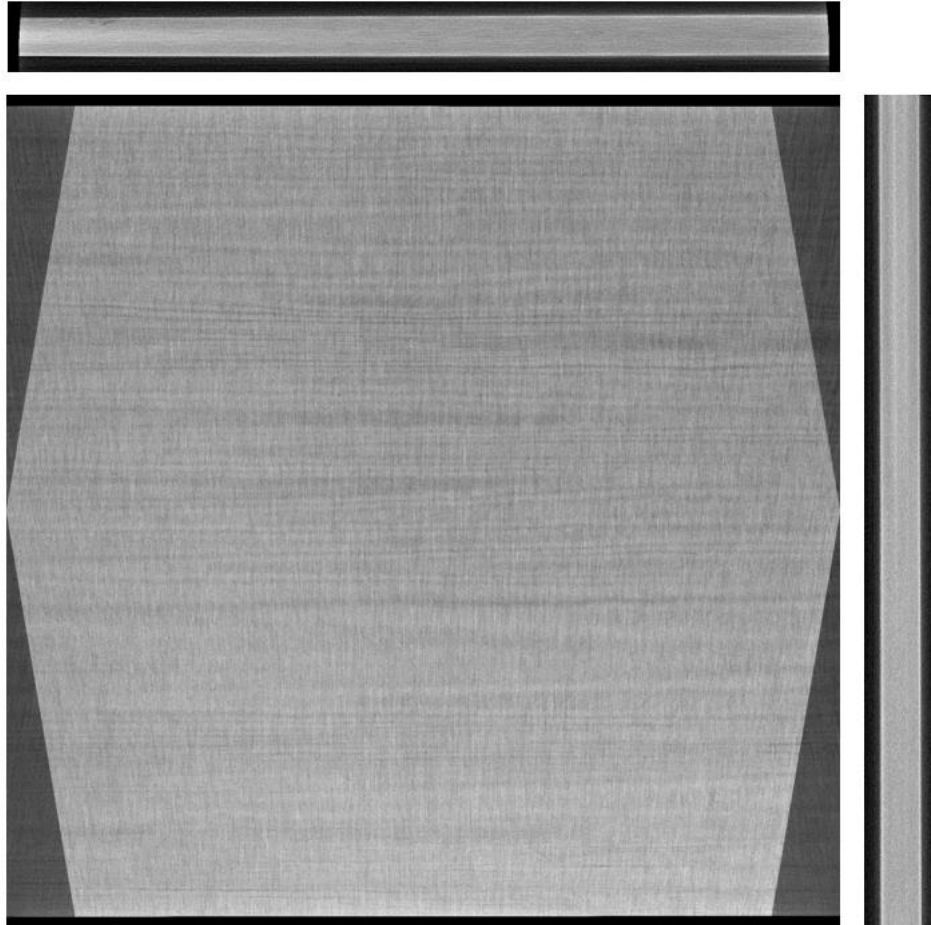


Figure E.32-8. 3D X-ray generated view of specimen #32: Boeing-Wrinkles using a small viewing window showing the y direction (center), z direction (top) and x direction (right).

E.32.3 Method: Guided Wave Ultrasonic Testing (GWUT)

E.32.3.1 Partner: USC

E.32.3.2 Technique Applicability: ★★★

GWUT employs ultrasonic waves that propagate along waveguides by its boundaries, e.g. pipes, rods and plate-like structures, which allows waves propagate a long distance with little energy loss. GWUT shows advantage in many types of defect inspection, e.g. crack in metallic structures [1], and delamination in composite structures [2].

The Specimen, Boeing-wrinkle-A2 (herein referred to as A2), is inspected using hybrid PZT-SLDV GWUT method in this report. General information of A2 and its wrinkle layout are illustrated in the paragraph below. The relative inspection, results and system rating are illustrated in the inspection results.

Specimen A2 is shown in Figure E.32-9 with its front, back and side view. The measured dimension of A2 is $306 \times 260 \times 3.83$ mm. Significant wrinkles are observed from both sides as shown in Figure E.32-9 (pointed by arrows). The wrinkles within areas marked as 2B and 2C while much less or likely no wrinkles within areas marked as 2D. No other information about A2 is available to the inspectors.

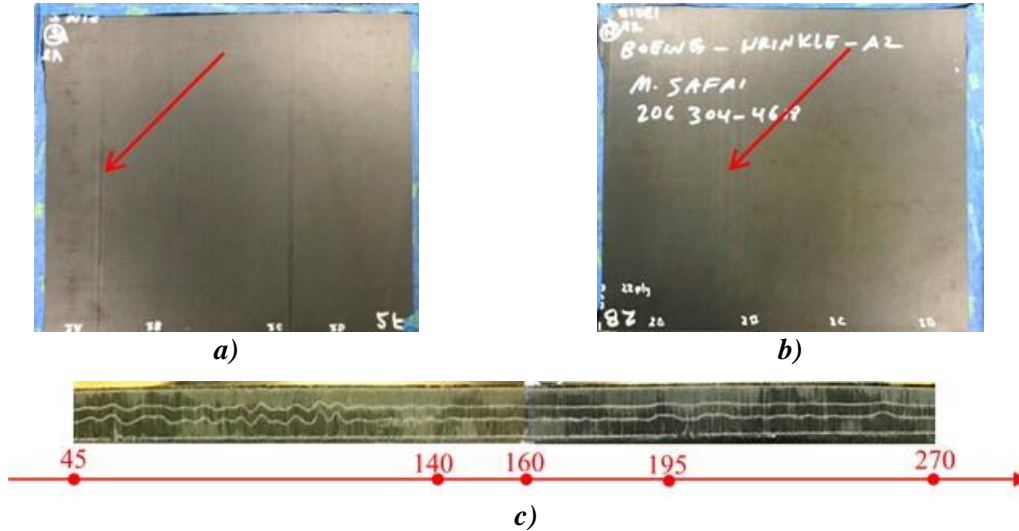


Figure E.32-9. Picture of Specimen A2. (a) front side (side 1), (b) back side (side 2); (c) side view.

E.32.3.3 Laboratory Set Up

The same hybrid PZT-SLDV system is implemented to inspect A2, using contact type PZT as actuator and SLDV as sensor to excite and receive guided waves in the testing plate (Lamb waves) [1]. The overall setup also remains the same as reported previously and shown in Figure E.32-10 and Figure E.32-11 [3].

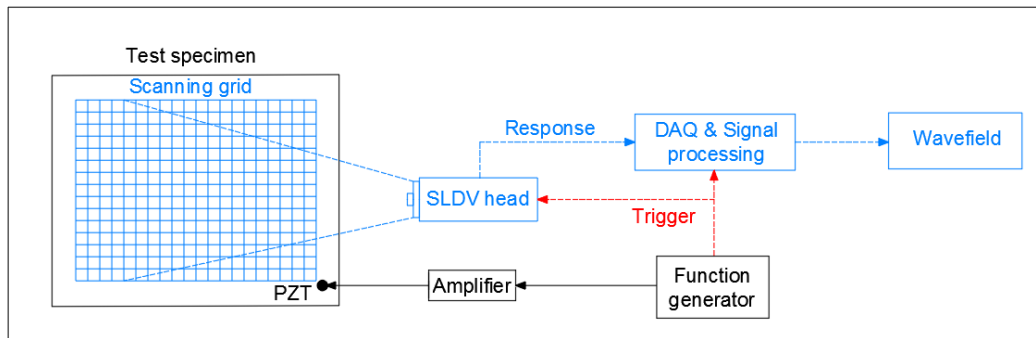


Figure E.32-10. Schematic Design of the PZT-SLDV System.

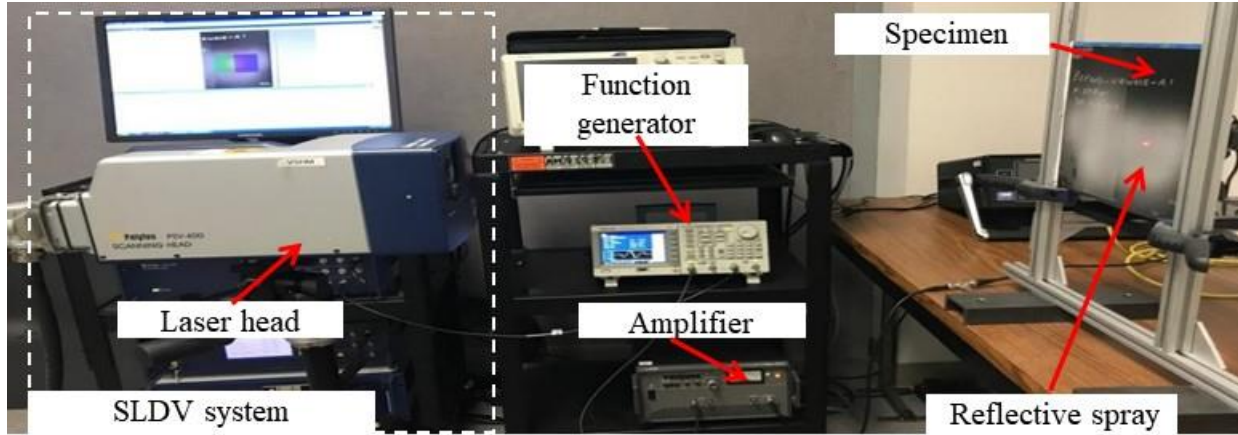


Figure E.32-11. Experimental Setup of the PZT-SLDV System.

E.32.3.4 Equipment List and Specifications

The detailed specifications of the equipment and devices used for the hybrid PZT-SLDV system at USC VSHM laboratory are given in Table E.32-3. Data acquisition settings are shown in Table E.32-4.

Table E.32-3. Equipment/device specifications.

Equipment/device	Specifications
Polytec PSV-400-M2	2D scanning laser Doppler vibrometer with a frequency range up to 1 MHz with specific velocity decoders
PZT	Steminc 7-mm circular 0.5-mm thick piezoelectric transducers
Tektronix AFG3022C	2-channel arbitrary function generator with 1 μ Hz to 25MHz
HSA 4014	High speed bipolar amplifier up to 1 MHz and 200 VA
Target Simply Balanced TM organic honey	Natural and organic honey blend performed as couplant
Albedo 100 Reflective Spray	a non-permanent, clear spray with light-reflective properties

E.32.3.5 Settings

Table E.32-4. Data collection settings.

Sampling frequency (MHz)	12.56 MHz
Spatial sampling interval (mm)	1 mm
Average	200
Velocity decoder	VD-07 10mm/s/V
Spray coating	20 layers

Similar to A1, two regions are predefined for inspection as shown in Figure E.32-12: reference (marked as red) and wrinkle (marked as green) region. Before wrinkle inspection, the dispersion curves of A2 are acquired experimentally by line scanning using chirp excitation along R in the reference region as illustrated in Figure E.32-12a. Since no obvious wrinkle defects are detected along 90°/270° direction (parallel to wrinkle pattern by visual inspection) w.r.t actuation based on the A1 inspection results, the inspection on A2 is only performed along 0°/180° direction (normal to wrinkle pattern by visual inspection).

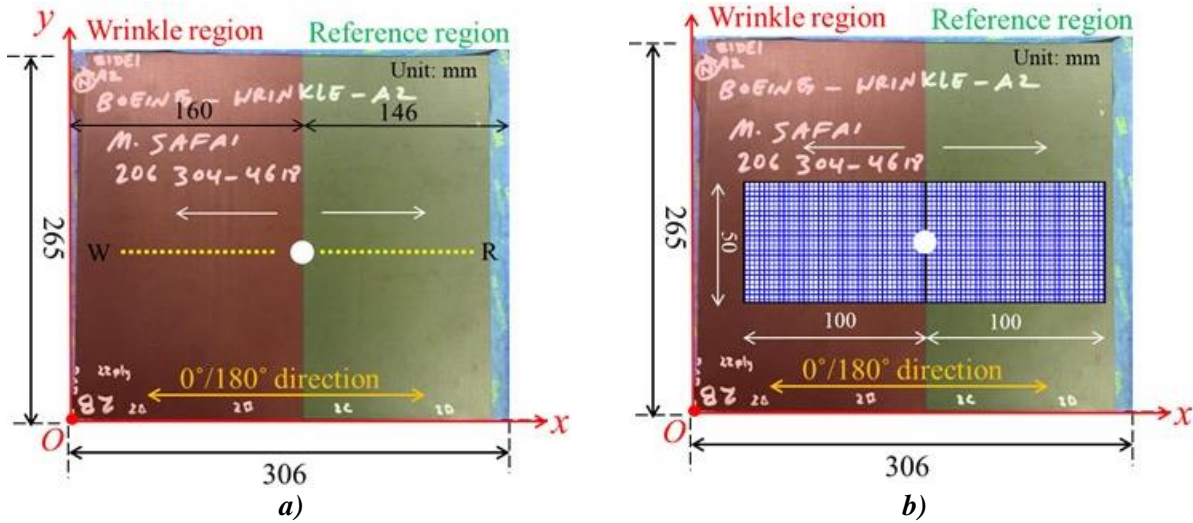


Figure E.32-12. Experimental setup for Specimen A2 along 0°/180° direction w.r.t actuation on side 1: (a) 1D line inspection, and (b) 2D area inspection.

The A2 side 1 was inspected using 3-count toneburst excitation at selected excitation frequencies 180 kHz. 1D inspection is performed at reference region (along R) and wrinkle region (along W) with local excitation origins O (160, 115). The scanning lines are in the range $x = 10-100$ mm with 0.5-mm spatial resolution. With the same excitation point, 2D area inspection is performed in the area 50 mm \times 100 mm Figure E.32-12b with 1-mm spatial resolution. Also performed is actuation at other locations in order to create different inspection perspectives. The detailed illustration is shown in the 2D inspection section.

E.32.3.6 Inspection Results

Experimental Dispersion Curves

The experimental dispersion curves are obtained through 2D Fourier transform of the time-space wavefield, which is shown in Figure E.32-13. One can see that only one mode is observed under low excitation frequency, while multiple and complex modes are observed in higher frequencies. In A2 inspection, excitation frequencies able to excite two Lamb wave modes in the target plate result in better wrinkle detection and visualization. As shown in Figure E.32-13, two Lamb wave modes are excited at 180 kHz. Thus, it is first selected as the excitation frequency while other frequencies are also tested for further evaluation since Lamb waves are frequency dependent.

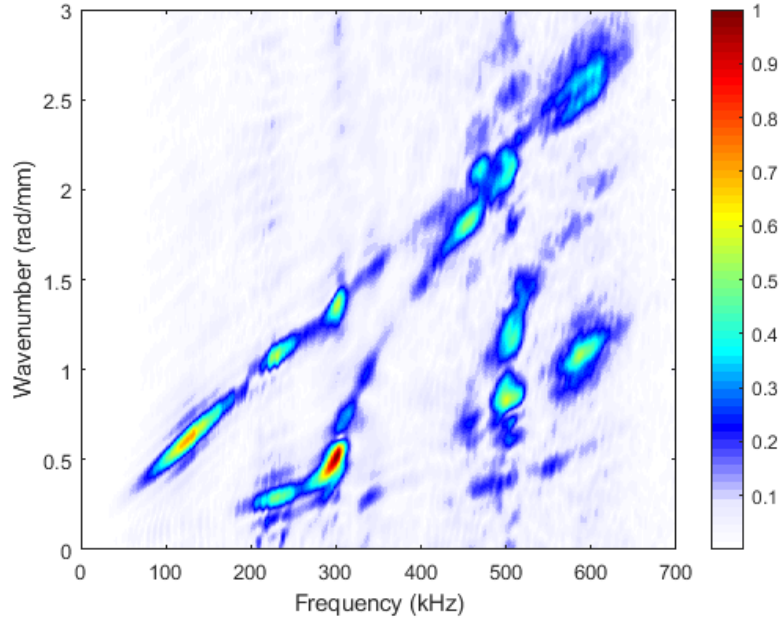


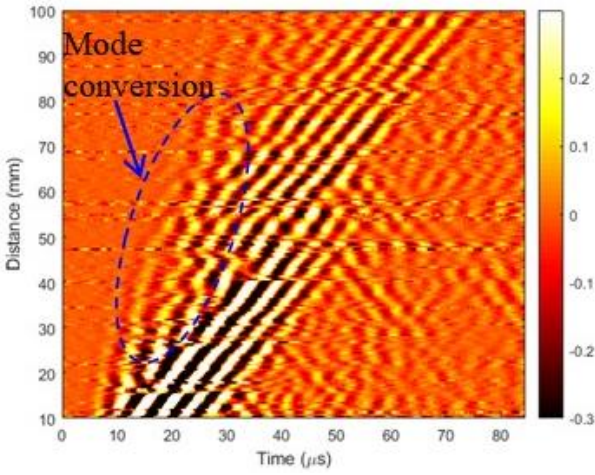
Figure E.32-13. Experimentally Acquired Dispersion Curves

Inspection of A2 Specimen on Side 1

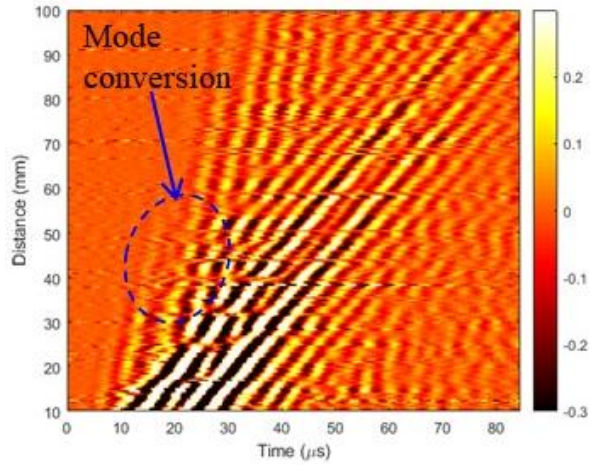
First conducted is the inspection on side 1 at excitation frequency 180 kHz. 1D inspection and 2D inspection are both conducted (area scan given in Figures E.32-12a and b). Time-space wavefields and frequency-wavenumber ($f-k$) spectra are studied and analyzed to detect wrinkles and evaluate its significance. In addition, we compared the wavefields, spectra, and spatial wavenumber distribution between reference and wrinkle regions in the plate. Generation of energy maps based on 2D inspection show the energy change through the inspection area in wrinkle and reference regions, and frequency dependence of the inspection results were explored.

1D Inspection

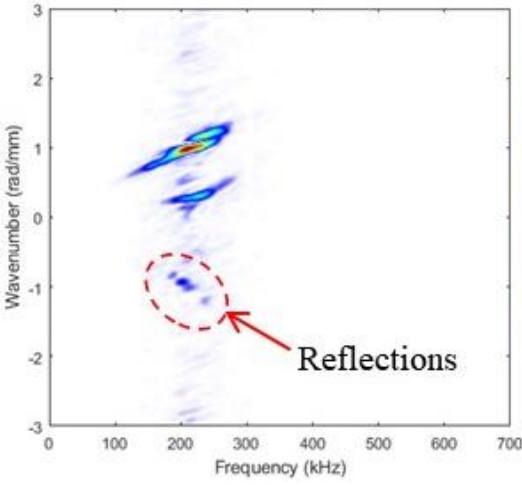
First performed was the 1D inspection along W (in wrinkle region) and R (in reference region). Results in terms of time-space wavefields and ($f-k$ spectra are plotted in Figure E.32-14. One can see that, in both W and R wavefields (Figure E.32-14a and b), strong mode conversion and reflections are observed when the Lamb waves interact with wrinkles. Compared to the R wavefield (Figure E.32-14b) in the reference region, mode conversion appears in a longer propagating distance and reflections are stronger in the W wavefield (Figure E.32-14a). This indicates that in the wrinkle region, larger range of wrinkle exist than that in the reference region. In addition, strong reflections are observed in the W $f-k$ spectrum (Figure E.32-14c) in the wrinkle region than R (Figure E.32-14d) in the reference region. One can also notice that reflections appear at different wavenumber locations between W and R $f-k$ spectrum. Different wrinkle sizes in the two regions may cause this change.



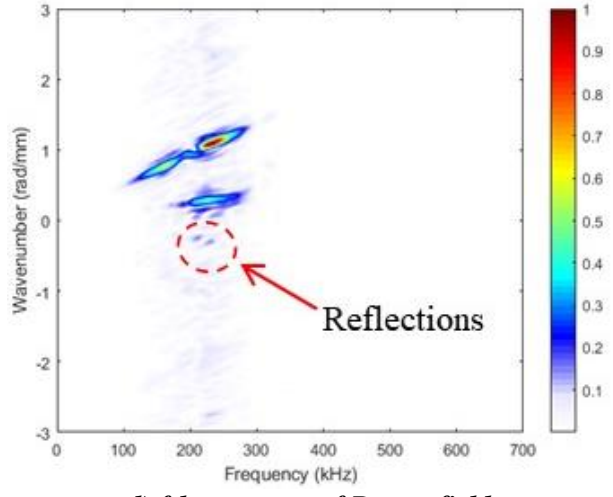
a) Time-space wavefield along W.



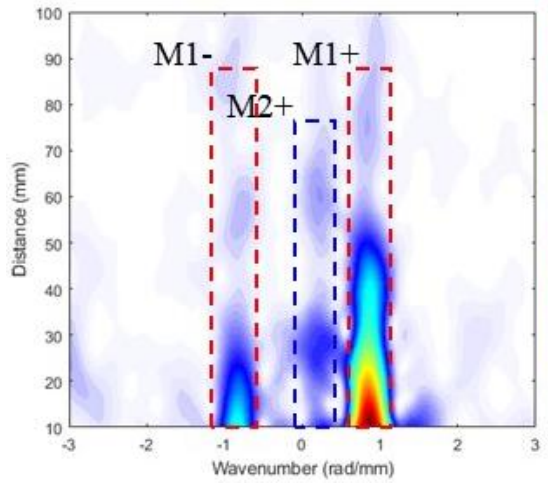
b) Time-space wavefield along R.



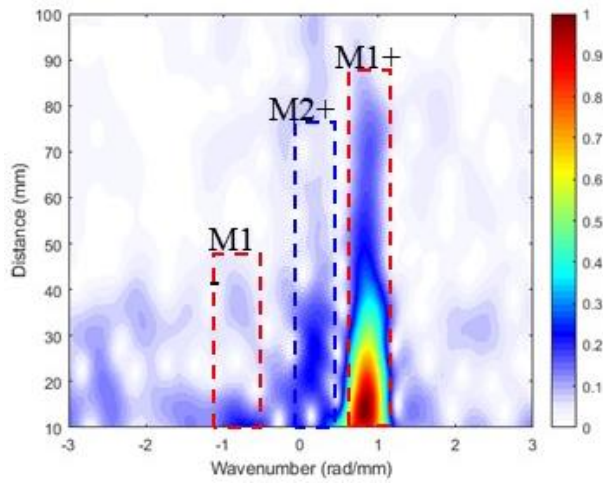
c) f-k spectrum of W wavefield.



d) f-k spectrum of R wavefield.



e) x-k spectrum of W wavefield.



f) x-k spectrum of R wavefield.

Figure E.32-14. Comparison between 1D inspection results along W and R.

In the space-wavenumber (x - k) spectra, shown in Figure E.32-14e for W and f for R , two incident wave modes, positive mode-1 (M1+) and mode-2 (M2+) are observed. Strong reflections (negative wave mode-1, refer as M1-) appears in the range 10–100 mm in the wrinkle region, while weak reflections (M1-) appear in the range 10–50 mm in the reference region.

2D Inspection – Wrinkle Region

The 2D area inspection is performed next under 180 kHz in the wrinkle region. The scanning grid is 50×100 mm as shown in Figure E.32-15b with 1-mm spatial resolution. The corresponding energy map is generated by using the maximum amplitude of the signal in the recording time range, which is shown in Figure E.32-15b. Obvious wrinkle patterns in the range 80–140 mm are observed in the energy map.

Since Lamb waves are frequency dependent, excitation frequency is studied in order to obtain better imaging results. Three frequencies: 120, 240, and 300 kHz are selected for Lamb wave excitation. The corresponding energy maps are plotted in Figure E.32-15a, Figure E.32-15c and Figure E.32-15d respectively. Comparing the four energy maps in Figure E.32-15, vague wrinkle patterns (in the range 100–140 mm) are observed under 120 kHz (Figure E.32-15a) while clear wrinkle patterns (in the range 80–140 mm) are observed with frequency increase to 180 kHz (Figure E.32-15b). The wrinkle patterns become clearer at 240 kHz (Figure E.32-15c) than that at 180 kHz. However, when excitation frequency increase to 300 kHz (Figure E.32-15d), the wrinkle patterns are not as clear as 240 kHz. Thus, 240 kHz is selected as the optimal excitation frequency to achieve better imaging result.

As shown in Figure E.32-15c at 240 kHz, the right edge of the wrinkle range in the wrinkle region is identified as around $x = 140$ mm when inspection from right view, which matches the visual inspection as shown in Figure E.32-9c.

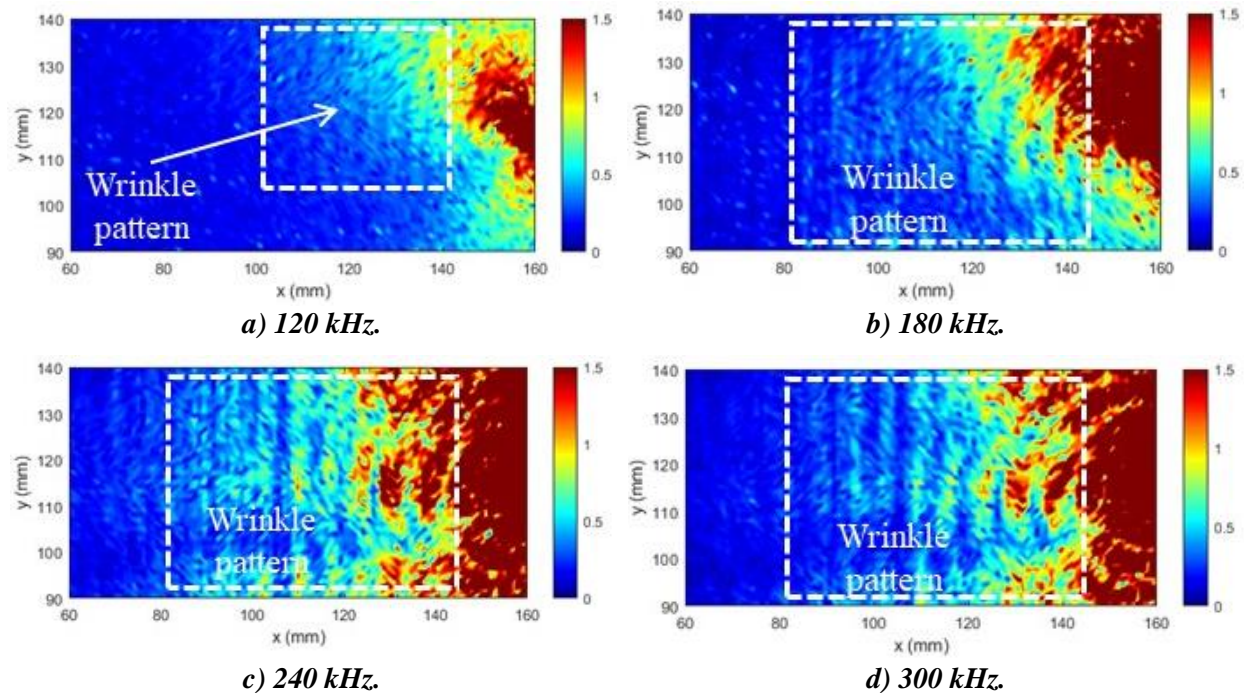


Figure E.32-15. Energy map of wrinkle region at excitation frequency.

The 2D inspection is then performed from different location (location O_1 for a left view) as shown in Figure E.32-16. The PZT actuator is attached on the left edge of the specimen at O_1 (5, 115 mm). The scanning grid is 50 mm \times 140 mm with the same 1-mm spatial resolution. The obtained energy map is plotted in Figure E.32-17. Clear wrinkle patterns are observed along the range 45–120 mm. The left edge of the wrinkle range is at round $x = 45$ mm, which matches the visual inspection in Figure E.32-9c.

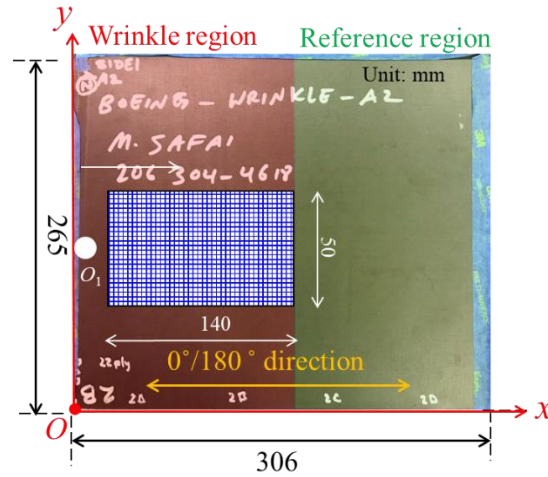


Figure E.32-16. Experimental setup of 2D inspection from different actuation (location O_1 for a left view).

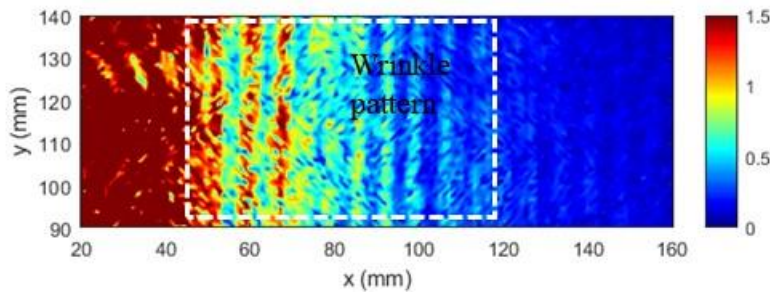


Figure E.32-17. Energy map of wrinkle region with actuation at location O_1 for left view.

With scanning actuation setup (here two actuation location for left and right view respectively), the wrinkle range are approximately quantified as in the range 45–140 mm in the wrinkle region.

2D Inspection - Reference Region

With identified optimal excitation frequency, the reference region is inspected through 2D area scanning with different actuation locations: O (160, 115) for a left view (Figure E.32-12b), and O_2 (240, 115) and O_3 (300, 115) for right views (Figure E.32-18).

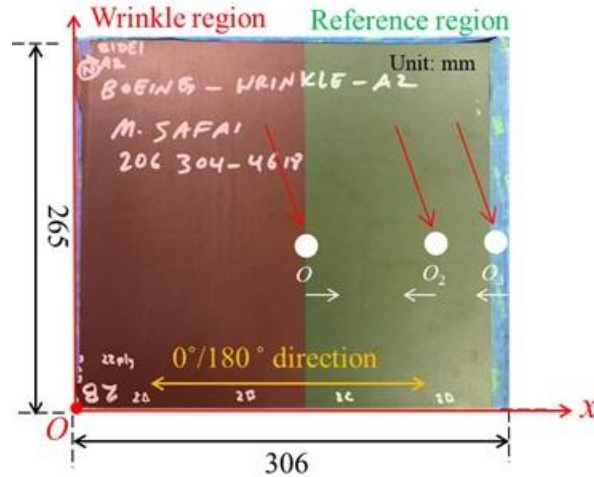


Figure E.32-18. Reference region 2D inspection scanning setup with actuation at different locations: inspection with excitation at O for a left view, at O_2 for a right view, and at O_3 for another right view

The relative energy maps are plotted in Figure E.32-19. In the energy map for a left view (Figure E.32-19a), clear wrinkle patterns are observed along the range 190–220 mm. The left edge of the wrinkle range is at round $x = 190$ mm, which matches the visual inspection in Figure E.32-9c. The same wrinkle range is observed in the energy map for a right view at excitation point O_2 (Figure E.32-19b). When excitation is at O_3 , the inspection result shows that wrinkle pattern appear at ranges 190–220 mm and 230–260 mm, which matches the visual inspection. With the scanning actuation setup (actuation at O , O_2 , and O_3 in this scenario), the wrinkle range is approximately quantified for the reference region.

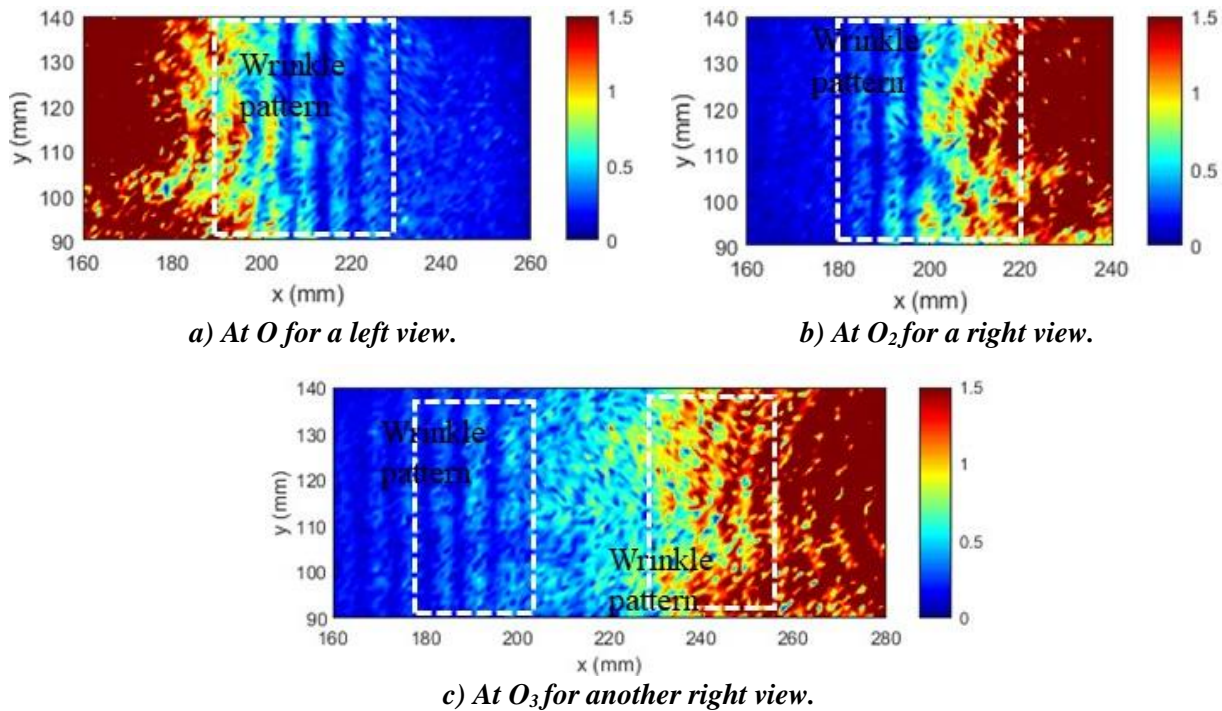


Figure E.32-19. Energy map of the reference region with different actuations.

Inspection of A2 on side 2

Based on the optimized experimental setup and inspection results on side one, only 2D inspection is performed on side two for wrinkle detection. The experimental setup for wrinkle region is the same as A1 in Figure E.32-12b (actuator location 1) and Figure E.32-16 (actuator location 2), while for reference region is the same as A1 in Figure E.32-18 (3 actuator locations).

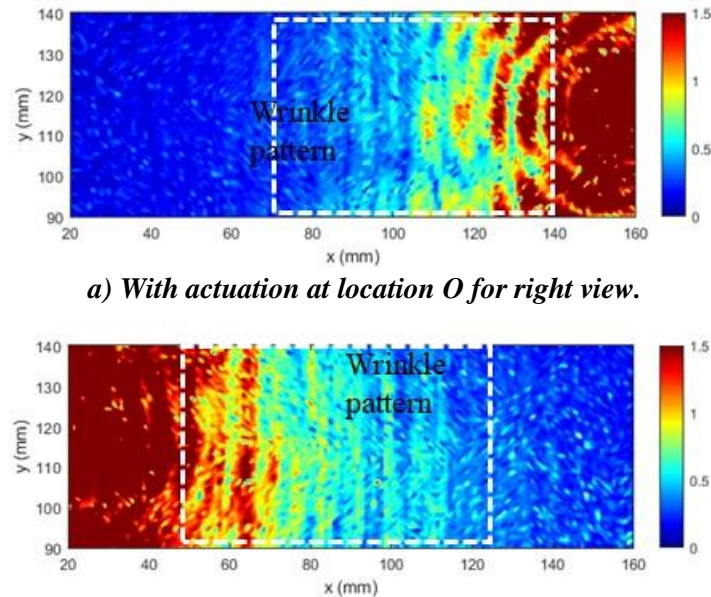
2D Inspection - Wrinkle Region

The 2D inspection is performed from different locations (location O_1 for a left view and O for a right view) as shown in Figure E.32-12b and Figure E.32-16 respectively. The obtained energy map is plotted in Figure E.32-20. Clear wrinkle patterns are observed along the range 70–140 mm in Figure E.32-20a and 45–120 mm in Figure E.32-20b respectively. The left edge of the wrinkle range is at around $x = 45$ mm, and the right edge is around 140 mm, which matches the visual inspection in Figure E.32-9c.

With scanning actuation setup (here two actuation location for left and right view respectively), the wrinkle range are approximately quantified as in the range 45–140 mm in the wrinkle region. The inspection results on side two match the results on side one.

2D Inspection - Reference Region

The reference region is inspected through 2D area scanning with three actuation locations: O (160, 115) for a left view (Figure E.32-12b), and O_2 (240, 115) and O_3 (300, 115) for right views (Figure E.32-18).



b) With actuation at location O_1 for left view.

Figure E.32-20. Energy map of wrinkle region.

The relative energy maps are plotted in Figure E.32-21. In the energy map for a left view (Figure E.32-21a), clear wrinkle patterns are observed along the range 190–220 mm. The left edge of the wrinkle range is at round $x = 190$ mm, which matches the visual inspection in Figure E.32-9c. The same wrinkle range is observed in the energy map for a right view at excitation point O_2 (Figure E.32-21b). When excitation is at O_3 , the inspection result shows that wrinkle pattern appear at ranges 190–220 mm, which also matches the visual inspection. With the scanning actuation setup

(actuation at O , O_2 , and O_3 in this scenario), the wrinkle range is approximately quantified for the reference region. The inspection results are similar to the results on side one except that they are not as clear as on side one. This might be caused that the wrinkle in this area is closer to side one according to visual inspection.

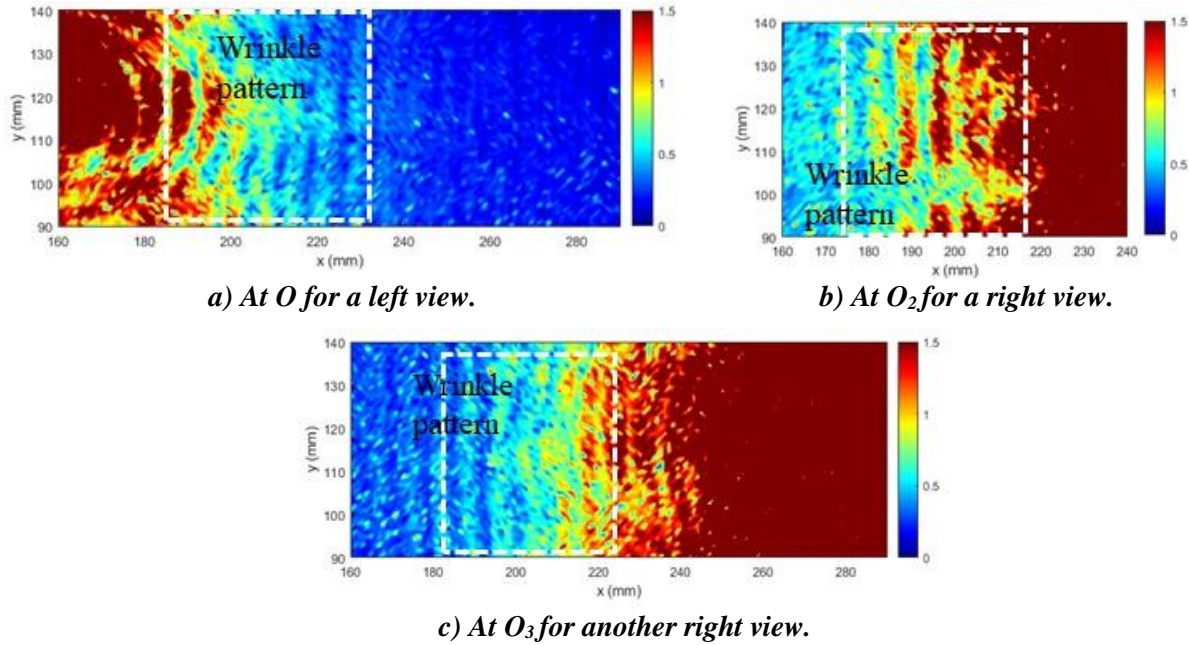


Figure E.32-21. Energy map of the reference region with different actuations.

E.32.3.7 Inspection Results and Conclusions

In conclusion, wrinkle existence on A2 specimen using the hybrid PZT-SLDV system is successful detected and quantified even without material properties. The detailed rating of the system is shown in Table E.32-5. For defect visualization, five out of five stars is rated compared to the four out of five in the A1 report [3]. The reason for this improvement is that the wrinkle pattern is clearly observed, and its range is approximately quantified with different actuation locations. For inspection time, the inspection time for 1D inspection is around one minute, which is very rapid, while the inspection time for 2D inspection is around one hour for areas illustrated in this test, which is still relatively fast. Thus, the inspection time gets four stars overall. Last, the actuator PZT is \$3.60 per piece, which is cost effective. However, the SLDV is an expensive equipment, which costs \$300,000 when purchasing. Thus, this part gets two stars. In the future, expensive SLDV can be replaced by customized fixed LDV and gantry system to reduce the system cost. Overall, this hybrid PZT-SLDV guided wave inspection is very robust in general with four out of five stars.

Table E.32-5. Hybrid PZT-SLDV guided wave inspection rating.

Hybrid PZT-SLDV guided wave inspection		
Sample A2 Defect: wrinkles	Rating	
	Detection:	★★★★★
	Defect visualization	★★★★★
	Inspection time:	★★★★☆
	Equipment cost:	★★☆☆☆
	Overall Performance:	★★★★☆

E.32.3.8 References

- [1] Yu, L.; Leckey, C. A.; and Tian, Z.: “Study on crack scattering in aluminum plates with Lamb wave frequency–wavenumber analysis,” *Smart Materials and Structures*, Vol. 22, No. 6, pp065019, 2013.
- [2] Tian, Z.; Yu, L.; and Leckey, C.: “Delamination detection and quantification on laminated composite structures with Lamb waves and wavenumber analysis,” *Journal of Intelligent Material Systems and Structures*, Vol.26, No. 13, 2015, pp. 1723-1738, 2015.
- [3] Guided wave inspection on specimen A1 (A1 report, submitted).

E.32.4 Method: Single-Sided Infrared Thermography (SSIR)

E.32.4.1 Partner: Boeing

E.32.4.2 Technique Applicability: ★★★

SSIR thermography is capable of detecting wrinkles in the composite material.

E.32.4.3 Laboratory Setup

For each inspection, the part was placed in the IR imaging system (Figure E.32-22). For each test, the flash lamp fires, heating the surface of the part uniformly. The IR camera records the heat signature of the part over time to track the diffusion of heat through the part thickness. This test was repeated for the front and backsides of each panel. The wrinkles on the panel cause alternating areas of high and low resin content in the troughs and crest, respectively. Because the resin has a lower thermal conductivity than the carbon fiber, the high content regions (troughs) will retain heat more than the low content regions (crests). As a result, the crests will show as cold spots over time while the troughs show as hot spots.

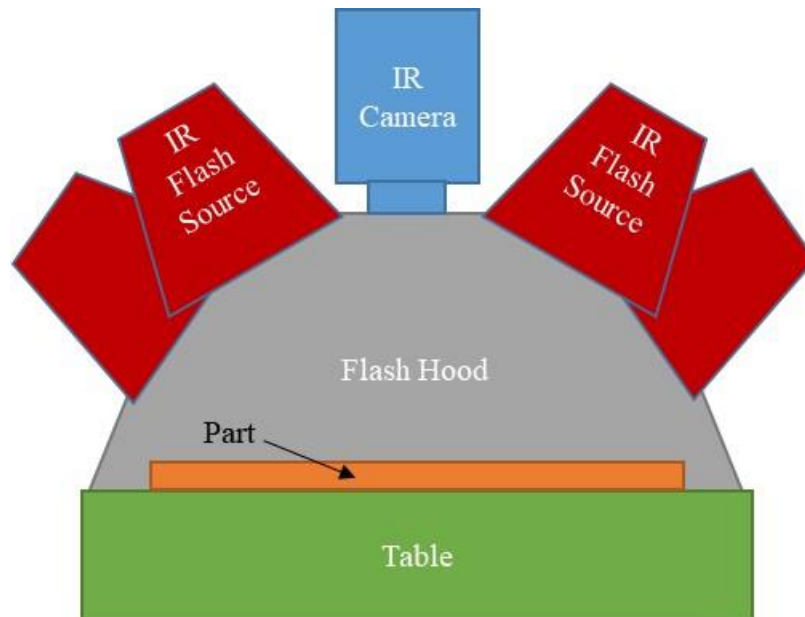


Figure E.32-22. Flash IRT system components.



Figure E.32-23. IR inspection system.

E.32.4.4 Equipment List and Specifications:

- Thermal Wave VoyageIR system
- SC6000 Series FLIR IR camera
- 4 6400 Watt-sec flash lamps
- Flash Hood
- X-Y gantry system

E.32.4.5 Settings

Data collection settings (i.e., resolution, frame rate, data acquisition time) were not provided by inspector.

E.32.4.6 Inspection Results

Figure E.32-24 shows the IR image of the panel at 1.6 sec. As anticipated, hot and cold spots can be observed (circled in red), corresponding with the manufactured wrinkle locations. Because the panel was uniformly heated on the side that the camera observed, the strongest thermal gradient will come from the wrinkles on that side. Because of this, one can observe fainter, mirrored indications of the wrinkles when observed from the opposite side, such as the left side grouping of wrinkles in Figure E.32-24a appearing fainter on the right side in Figure E.32-24b. From these data, it is possible to measure the wavelength of the wrinkles, though the amplitudes cannot be determined from these data.

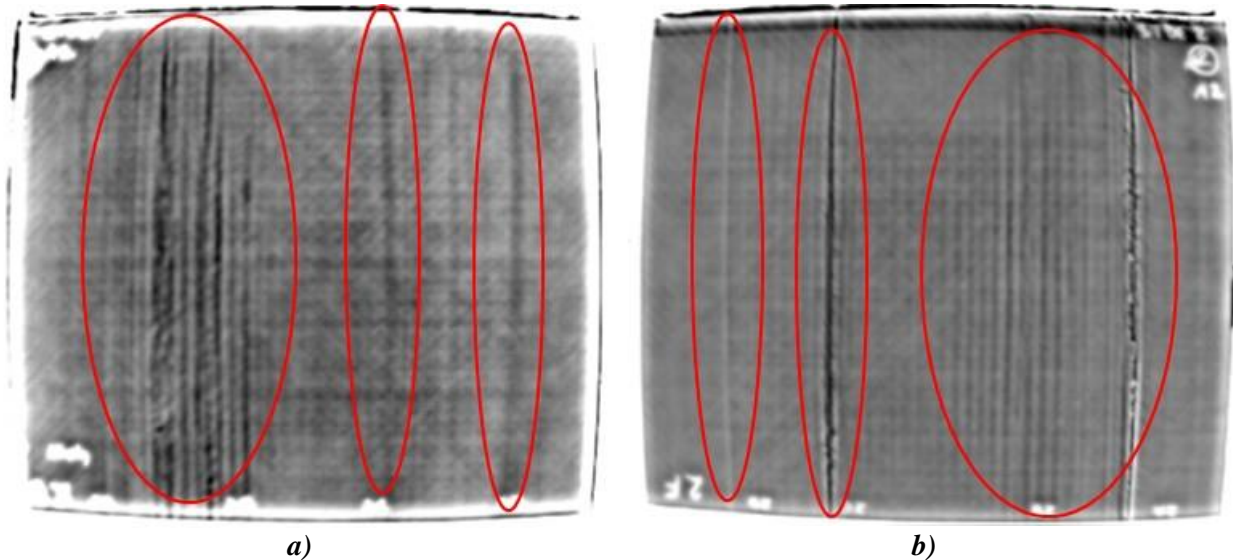


Figure E.32-24. Greyscale 1.6 sec IR image of Composite Wrinkle Standard A2 side 1 (a) and side 2 (b)

E.33 Specimen #33: Wrinkle A3

Structure	Material	Details	Dimensions (inches)	Partner Methods	
Thin laminates	IM7/8552-1 slit tape	Significant wrinkling in flat panels	1.5 × 12 × 0.15	NASA	E.33.1 PEUT
					E.33.2 XCT
				USC	E.33.3 GWUT
				Boeing	E.33.4 SSIR

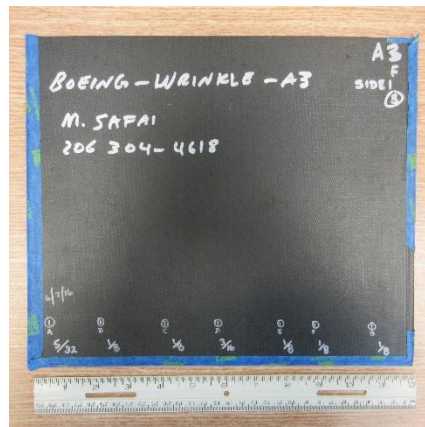


Figure E.33-1. Photograph of Specimen #33: Boeing-Wrinkle-A3.

E.33.1 Method: Pulse-Echo Ultrasound Testing (PEUT)

E.33.1.1 Partner: NASA

E.33.1.2 Technique Applicability: ★★★

PEUT is able to detect the significant fiber wrinkles within the specimen.

E.33.1.3 Laboratory Setup

Immersion Ultrasonic Testing: NASA LaRC uses a custom designed single probe ultrasonic scanning system. The system has an 8-axis motion controller, a multi-axis gantry robot mounted above a medium-size water tank, a dual-channel, 16-bit, high-speed digitizer, and an off-the-shelf ultrasonic pulser receiver. The system can perform TTUT and PEUT inspections. TT inspection employs two aligned ultrasonic probes, one transmitter and one receiver, placed on either side of a test specimen. Pulse-echo inspection is a single-sided method where a single ultrasonic probe is both transmitter and receiver. In each method, data are acquired while raster scanning the ultrasonic probe(s) in relation to a part. Figure E.33-2 shows a simplified block diagram of a scanning Pulse-echo inspection.

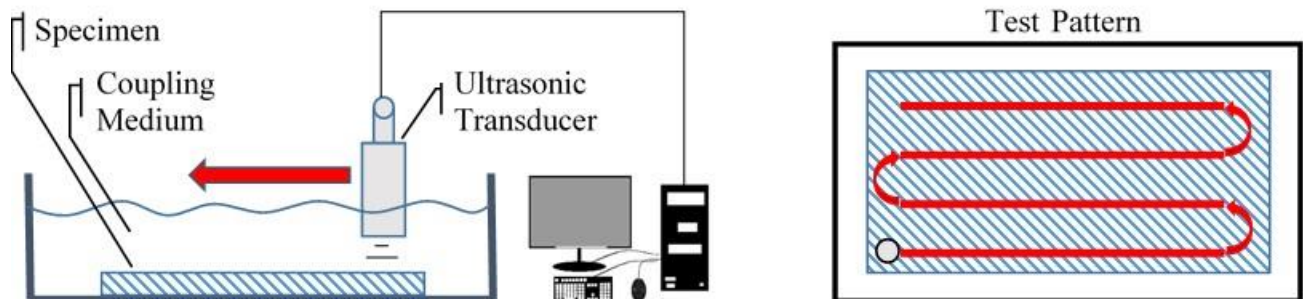


Figure E.33-2. Ultrasonic system components.

E.33.1.4 Equipment List and Specifications:

- Pulser/Receiver: Olympus 5073PR
- Digitizer: AlazarTech ATS9462, dual channel, 16 bit, 180 MS/s
- Sensor: Olympus 2-inch spherical focus immersion ultrasonic transducer
- Motion system: open looped stepper motor based X-YY-Z gantry robot
- Motion Controller: Galil DMC-4183
- Acquisition Software: FastScan, custom developed at NASA LaRC
- Signal Processing Software: DataViewer, custom developed at NASA LaRC

E.33.1.5 Settings

Table E.33-1. Data collection settings

Resolution horizontal [in/pixel]	0.02
Resolution vertical [in/pixel]	0.05
Probe frequency [MHz]	10
Focal Length [in]	2
Array Dimensions [pixels]	601 × 201

The specimen is placed flat against the zero position of the tank raised above the glass bottom by several metal washers. The test probe is computer-controlled and correlated to the position on the

sample. It is also focused to a point 1 mm below the surface of the test material. The specimen remains in place while the transducer follows a preprogrammed test grid across the surface as indicated in Figure E.33-2. At each point, ultrasonic data are collected from individual pulses. Larger step sizes between data collection result in lower image resolution. These data points are reconstructed into a data cube displaying spatial coordinates as time progresses. 2D reconstruction of the collection of ultrasonic responses create flattened slices at varying depths within the material.

E.33.1.6 Inspection Results

Specimen #31 is a panel fabricated from IM7/8552-1 slit tape with the objective of achieving flat wrinkles within the material. PEUT was performed on this specimen in NASA's immersion tank specified above.

Figure E.33-3 shows indications of fiber wrinkling near the surface of the material. The wrinkles cause severe perturbations in the acoustic waves that are easily seen throughout the sample as shown in Figure E.33-4 and Figure E.33-5.

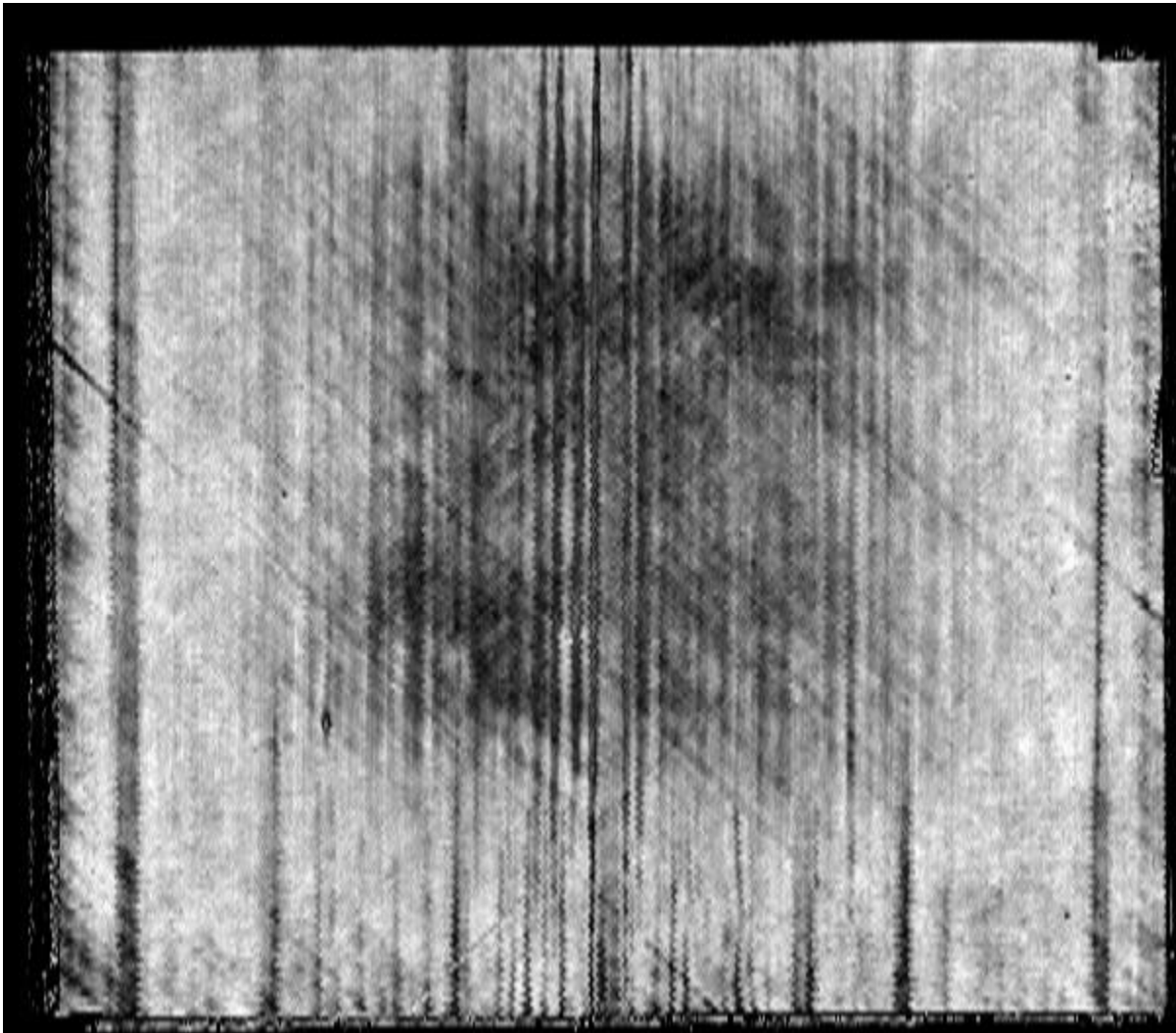


Figure E.33-3. UT image showing near surface indications of fiber waviness.

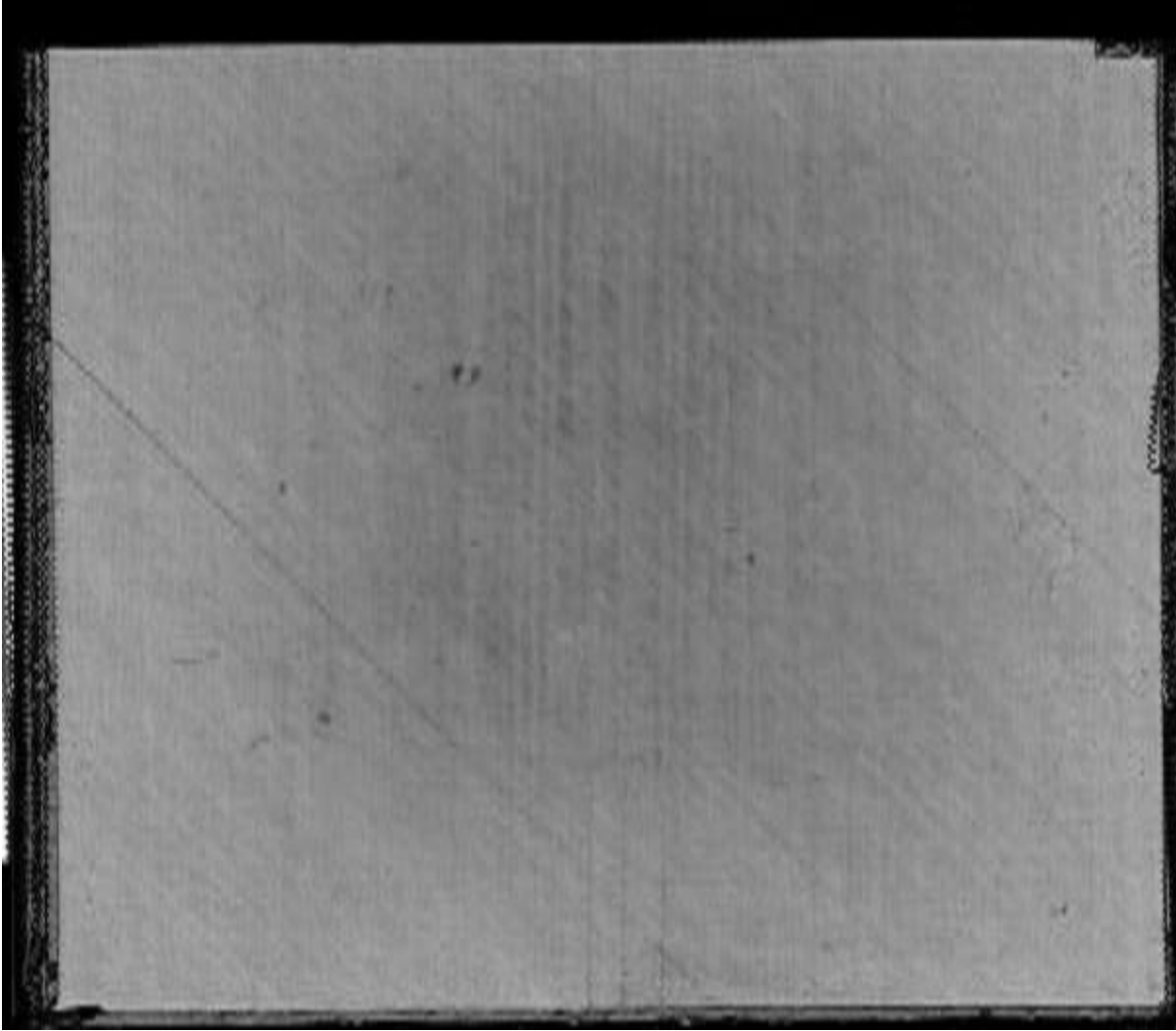


Figure E.33-4. UT image showing indications of fiber waviness within the material bulk.

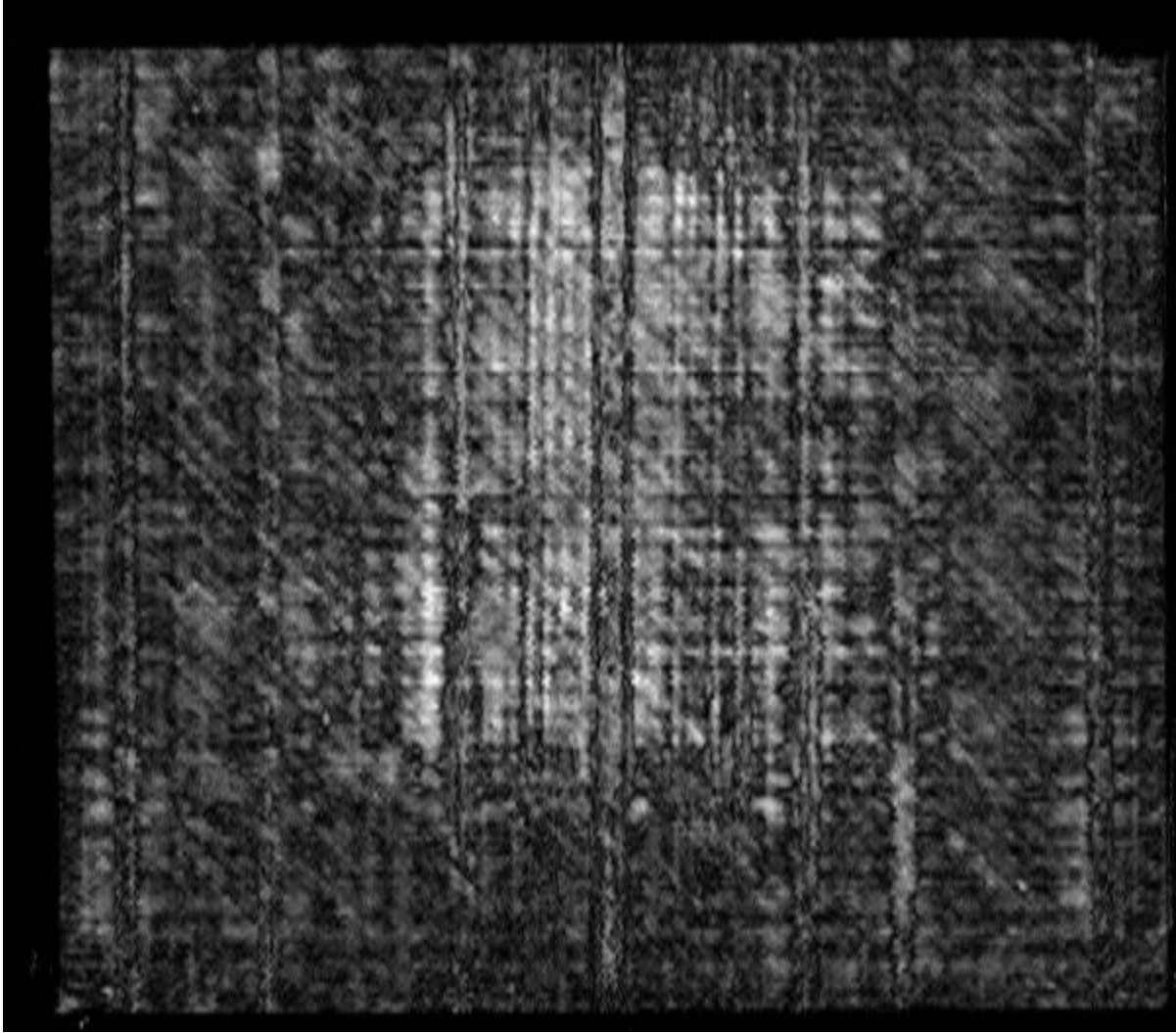


Figure E.33-5. UT image showing indications of fiber waviness within the material bulk.

E.33.2 Method: X-ray Computed Tomography (XCT)

E.33.2.1 Partner: NASA

E.33.2.2 Technique Applicability: ★★☆☆

XCT is somewhat capable of imaging the fiber wrinkles induced in this specimen.

E.33.2.3 Laboratory Setup

The microfocus XCT system at NASA LaRC is a commercially available Avonix (Nikon C2) Metrology System designed for high resolution NDE inspections. The system is an advanced microfocus X-ray system, capable of resolving details down to 5 μm , and with magnifications up to 60X. Supplied as complete, the system is a large-dimension radiation enclosure with X-ray source, specimen manipulator, and an amorphous silica detector, as shown in Figure E.33-6. The imaging controls are housed in a separate control console. The detector is a Perkin-Elmer, 16-bit, amorphous-silicon digital detector with a 2000 \times 2000-pixel array.

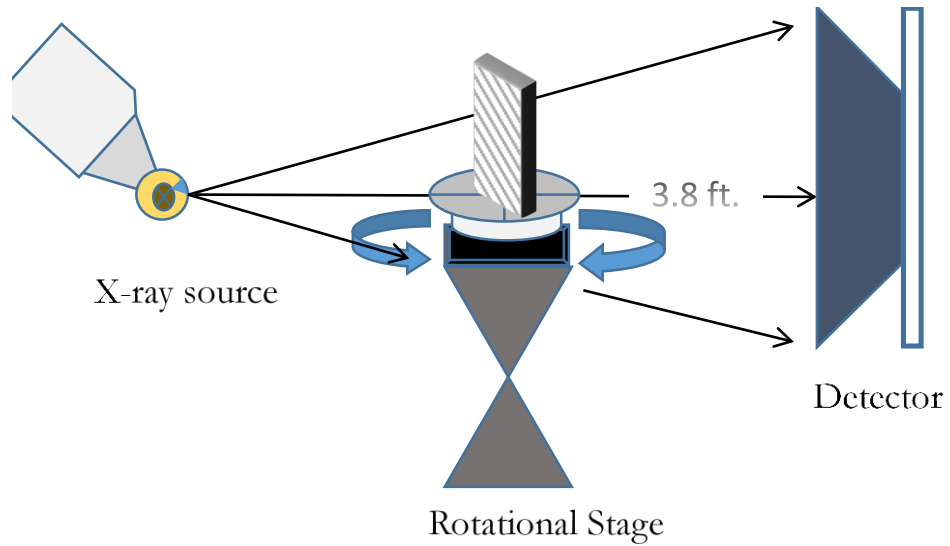


Figure E.33-6. XCT System Components

A consistent Cartesian coordinate system is used to define slice direction as illustrated in Figure E.33-7 and Figure E.33-8. Slices normal to the X-, Y-, and Z-directions are shown in Figures E.33-7a, b, and c, respectively.

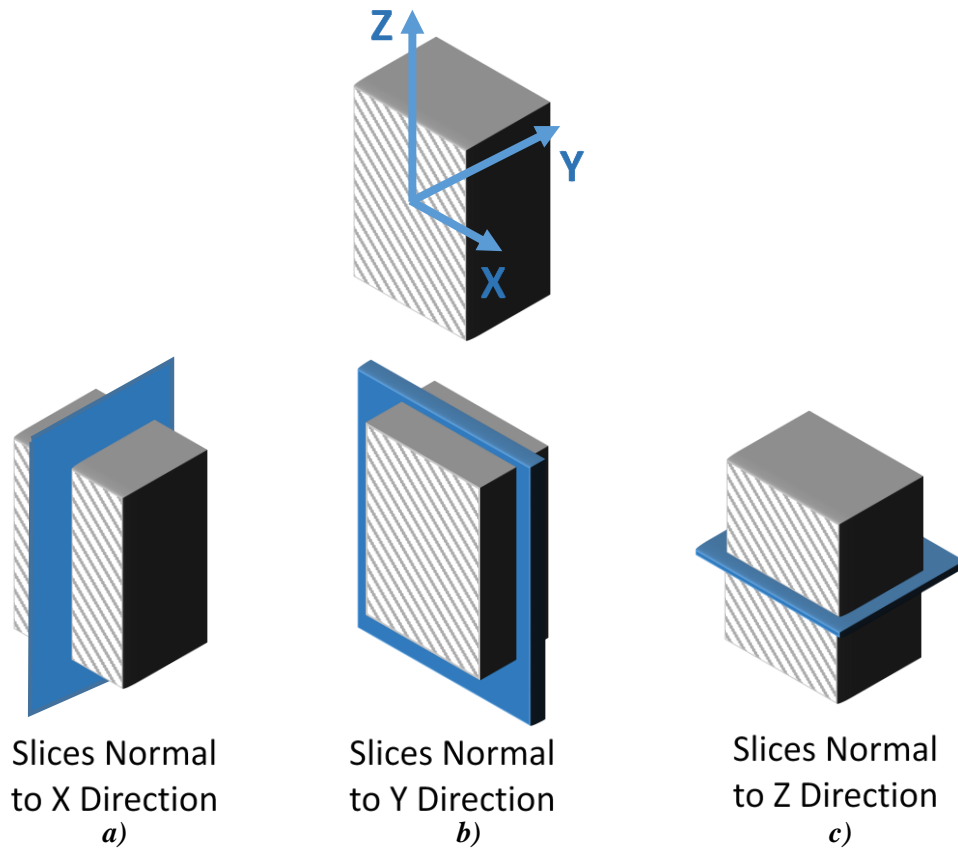


Figure E.33-7. Slice Direction Nomenclature.

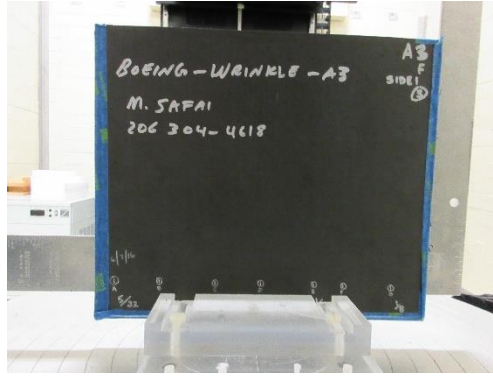


Figure E.33-8. Microfocus XCT system showing orientation of Specimen #33: Boeing-Wrinkles A3.

E.33.2.4 Equipment List and Specifications:

- Avonix 225 CT System
- 225 kV microfocus X-ray source with 5 μm focal spot size
- 15 or 30 kg Capacity, 5-axis, fully programmable manipulator
- Detector: Perkin Elmer XRD 1621 – 2000 \times 2000 pixels with 200 μm pitch
- 10 μm spatial resolution for specimens 1.5 cm wide
- Thin panels 10 \times 10 inches – full volume 200 μm spatial resolution

E.33.2.5 Settings

Table E.33-2. Data collection settings.

Source Energy	120 kV
Current	90 μA
Magnification	1.65 X
Filter	NF
# Rotational angles	3142
Exposure time / frame	1.0 sec
Max Histogram Grey Level	22 K
# Averages	8
Resolution (μm)	114.894 μm
Array Dimensions (pixels)	Set 1: 1999 \times 362 \times 1998 Set 2: 1998 \times 686 \times 1997

The specimen is placed vertically (rotated about the smallest dimension) on the rotational stage located between the radiation source and the detector. The rotational stage is computer-controlled and correlated to the position of the sample. As the sample is rotated the full 360° (~0.11° increments), the detector collects radiographs at each rotated angle as the X-ray path intersects the sample. 3D reconstruction of the collection of radiographs produces a volume of data that is then viewed along any plane in the volume. The closer the sample placement to the X-ray source, the higher the spatial resolution obtained.

E.33.2.6 Inspection Results

Section A

Specimen #33 is a panel with wrinkles induced within the material. XCT was performed on this specimen in NASA LaRC's large CT system with the settings defined in Section E.33.1.5. The scan was done using a large viewing window encompassing the whole specimen (Figure E.33-9)

and a small window covering a smaller area to increase the resolution of the scan (Figure E.33-10). This cannot always be done on larger specimens.

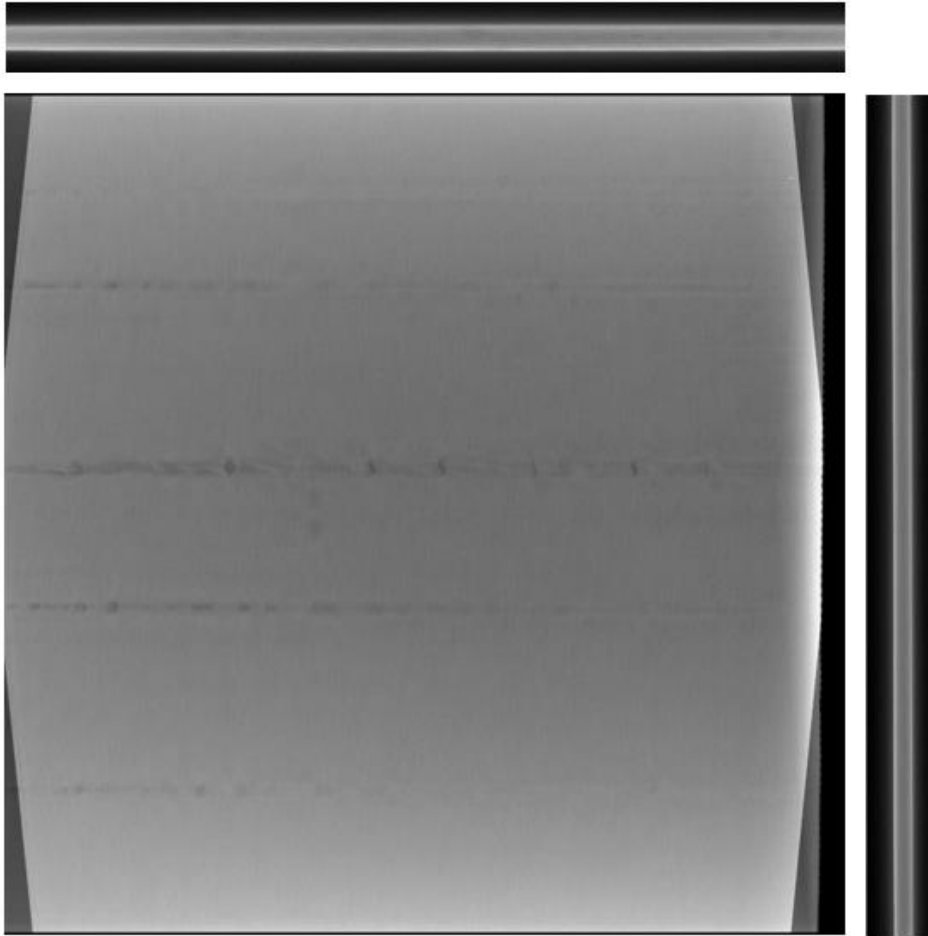


Figure E.33-9. 3D X-ray generated view of Specimen #33: Boeing-Wrinkles using a small viewing window showing the y direction (center), z direction (top) and x direction (right).

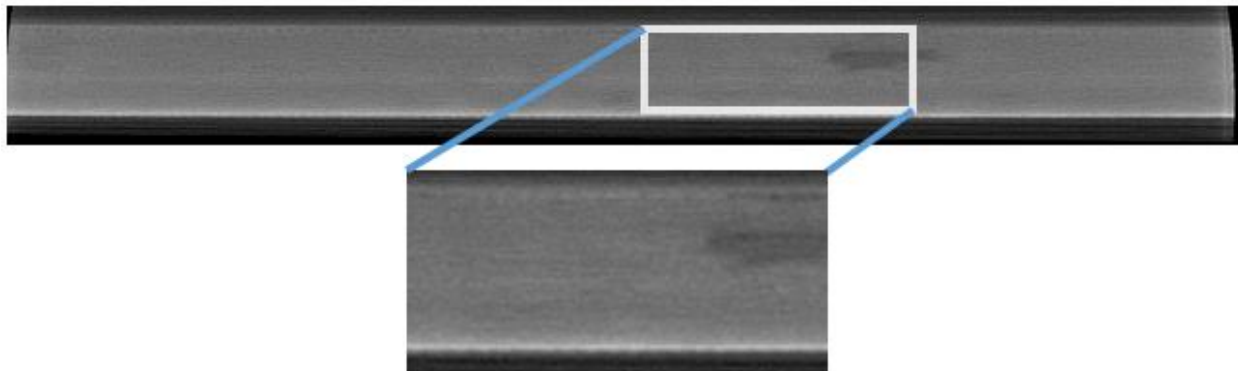


Figure E.33-10. 3D X-ray generated view of Specimen #33: Boeing-Wrinkles from the z direction.

The wrinkles are unseen from all viewing directions shown in Figure E.33-9. Both the x- and z-direction views give little evidence of any fiber waviness. In the y direction there are darker streaks and tear drop formations that are a result of the method used to induce wrinkling in the sample. These marks do show damage; however, they do not serve as an indicator for any fiber wrinkling.

The higher resolution image in Figure E.33-10 shows the beginning indications of fiber wrinkling though it is still not entirely clear. When viewing the full specimen the fiber waviness is even less apparent (Figure E.33-9).

E.33.3 Method: Guided Wave Ultrasonic Testing (GWUT)

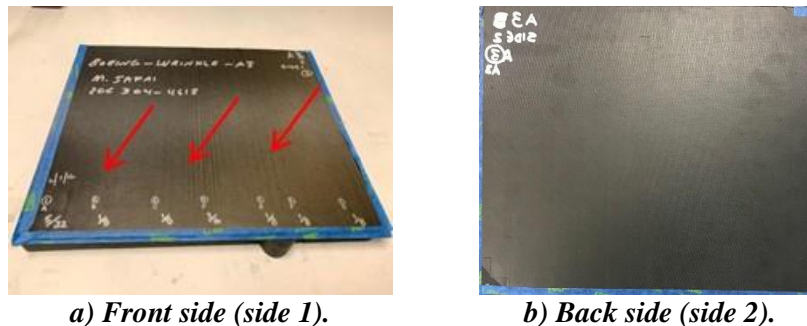
E.33.3.1 Partner: USC

E.33.3.2 Technique Applicability: ★★★

GWUT employs ultrasonic waves that propagate along waveguides by its boundaries, e.g. pipes, rods and plate-like structures, which allows waves propagate a long distance with little energy loss. GWUT shows advantage in many types of defect inspection, e.g. crack in metallic structures [1], and delamination in composite structures [2].

The Specimen, Boeing-Wrinkle-A3 (herein referred to as A3), is inspected using hybrid PZT-SLDV GWUT method in this report. General information of A3 and its wrinkle layout are illustrated in the paragraph below. The relative inspection, results and system rating are illustrated in the inspection results.

Specimen A3 is shown in Figure E.33-11 with its front and back view. The measured dimensions of A3 is $306 \times 260 \times 3.8$ mm. Significant wrinkles are observed on side one as shown in Figure E.33-11a (pointed by arrows), while no obvious wrinkles are observed on side two. No other information about A3 is available to the inspectors.



a) Front side (side 1).

b) Back side (side 2).

Figure E.33-11. Picture of specimen A3.

E.33.3.3 Laboratory Set Up

The same hybrid PZT-SLDV system is implemented to inspect A3, using contact type PZT as actuator and SLDV as sensor to excite and receive guided waves in the testing plate (Lamb waves) [1]. The overall setup also remains the same as reported previously and shown in Figure E.33-12 and Figure E.33-13 [3].

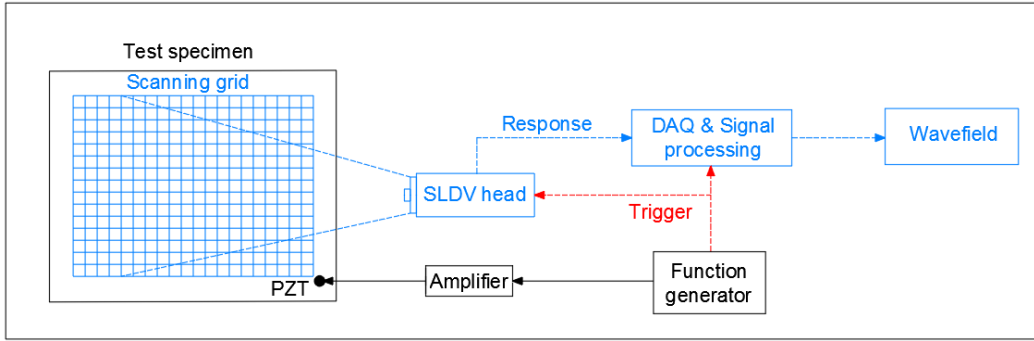


Figure E.33-12. Schematic design of the PZT-SLDV system.

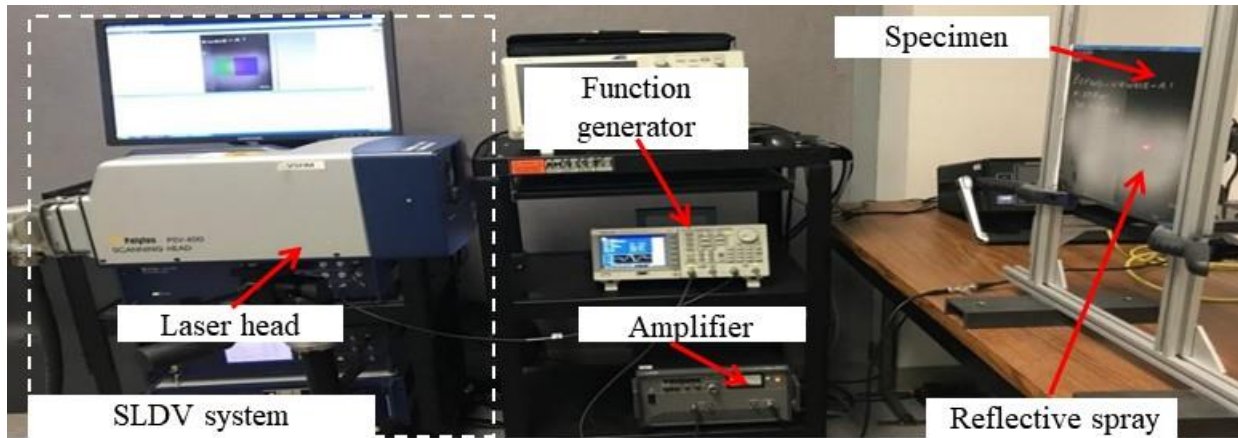


Figure E.33-13. Experimental setup of the PZT-SLDV system.

E.33.3.4 Equipment List and Specifications

The detailed specifications of the equipment and devices used for the hybrid PZT-SLDV system at USC VSHM laboratory are given in Table E.33-3. Data acquisition settings are shown in Table E.33-4.

Table E.33-3. Equipment/device specifications.

Equipment/device	Specifications
Polytec PSV-400-M2	2D scanning laser Doppler vibrometer with a frequency range up to 1 MHz with specific velocity decoders
PZT	Steminc 7-mm circular 0.5-mm thick piezoelectric transducers
Tektronix AFG3022C	2-channel arbitrary function generator with 1 μ Hz to 25MHz
HSA 4014	High speed bipolar amplifier up to 1 MHz and 200 VA
Target Simply Balanced TM organic honey	Natural and organic honey blend performed as couplant
Albedo 100 Reflective Spray	a non-permanent, clear spray with light-reflective properties

E.33.3.5 Settings

Table E.33-4. Data collection settings.

Sampling frequency (MHz)	12.56 MHz
Spatial sampling interval (mm)	1 mm
Average	200
Velocity decoder	VD-07 10mm/s/V
Spray coating	20 layers

In order to identify the optimal inspection frequency for wrinkle detection, 1D line inspection is performed first using a three-count toneburst excitation at selected frequencies 120, 240, and 300 kHz. Based on the results of A1 and A2, the scanning line is set perpendicular to the observed wrinkle pattern as shown in Figure E.33-14a. The spatial resolution is 1 mm, and the scanning line is 10 to 250 mm from the excitation point (O_1).

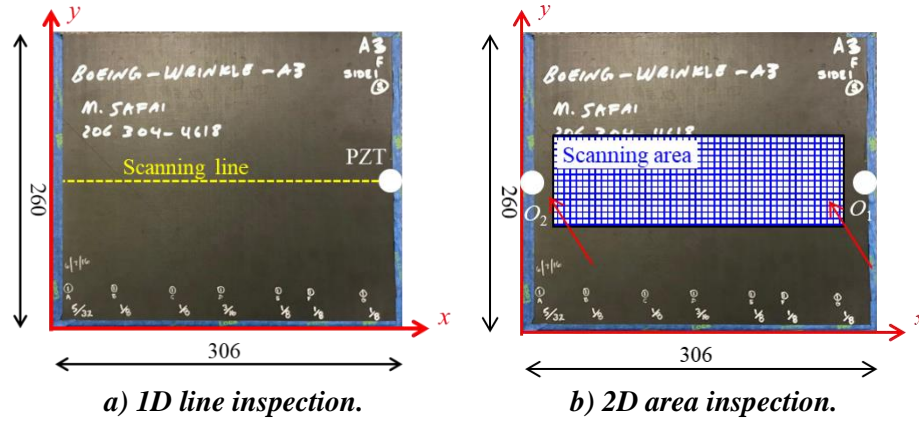


Figure E.33-14. Experimental setup along $0^\circ/180^\circ$ direction w.r.t actuation on side 1.

Based on the obtained optimal excitation frequency, 2D area inspection (310 mm \times 60 mm) is then performed to visualize the wrinkle defects with the same spatial resolution on both sides with two excitation locations at O_1 and O_2 respectively as shown in Figure E.33-14b.

E.33.3.6 Inspection Results

1D Inspection Results

The time-space wavefields are obtained and plotted in Figures E.33-15a, b, and c respectively. Through Fourier analysis, the corresponding frequency-wavenumber ($f-k$) spectra are calculated and plotted in Figures E.33-15d, e, and f respectively. At 120 kHz (Figure E.33-15a), only incident Lamb waves are observed, and no wave interactions with wrinkles is observed in the wavefield. In the relative $f-k$ spectrum, only incident wave modes are observed, which matches the wavefield observation. When the excitation frequency increases to 240 kHz, wave interactions are more distinguishable: reflections are observed from both time-space wavefield (Figure E.33-15b) and $f-k$ spectrum (Figure E.33-15e). Similar wave signatures are observed at 300 kHz. Since waves at lower frequency have less attenuation along wave propagation than higher frequency, the optimal excitation frequency (between 240 and 300 kHz) is identified as 240 kHz.

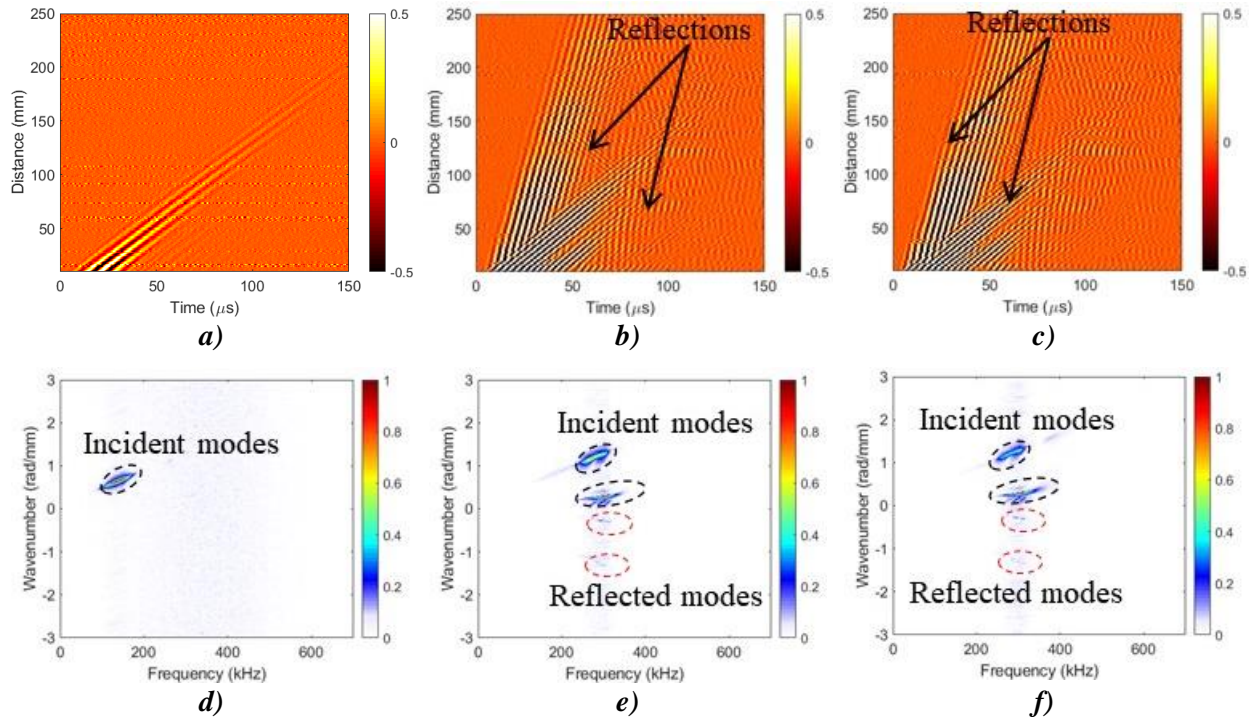


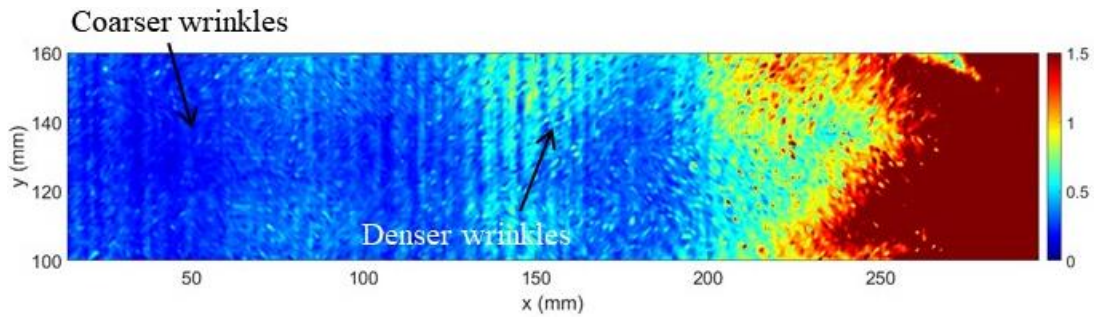
Figure E.33-15. 1D Inspection results wavefield results with excitation at (a) 120 kHz, (b) 240 kHz, and (c) 300 kHz; frequency-wavenumber spectra with excitation at (d) 120 kHz, (e) 240 kHz, and (f) 300 kHz, showing that wave-wrinkle interaction becomes obvious with excitation frequency increase.

2D Inspection Results on Side 1

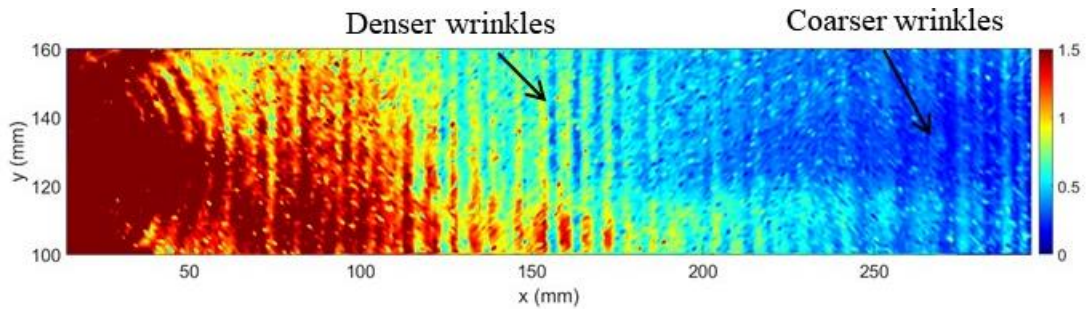
First conducted is the inspection on side 1 with two excitation locations at O_1 (right view) and O_2 (left view). The obtained wavefield images [3] are plotted in Figure E.33-16 (refer to previous reports for algorithm). As seen from Figure E.33-16a (excitation location at O_1), obvious wrinkle patterns are observed in the middle range along x direction (130–170 mm). The wrinkle patterns in this range are dense. In addition, coarser wrinkles are observed at around $x = 50$ mm.

When the excitation is at O_2 , the wrinkle patterns are very clear and easy to observe. Wrinkles exist from the beginning to the end along x direction. Denser wrinkles are observed in the middle range 100–150 mm, while coarser wrinkles are observed at around 250 mm.

Overall, the wrinkle detection results are consistent between O_1 and O_2 , the image intensity difference might be caused by the honey coupling of PZT actuator are not the same and hard to control.



a) Excitation at O_1 .

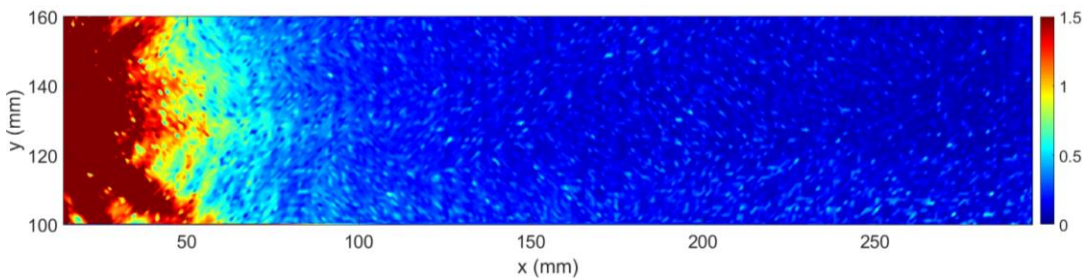


b) Excitation at O_2 .

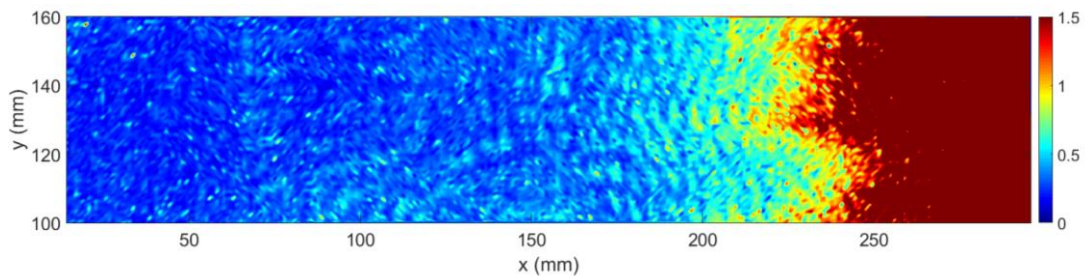
Figure E.33-16. Wavefield images obtained on side-1 with excitation.

2D Inspection Results on Side-2

In order to roughly identify the wrinkle locations along thickness, the 2D inspection is performed on side-2 with the same setup as side-1. The obtained wavefield images are shown in Figure E.33-17. No obvious wrinkle patterns are observed from the images, which are consistent to the visual inspection. Comparing the wavefield images obtained from side-1 and side-2, we can conclude that the wrinkle defects are closer to side-1 than side-2.



a) Excitation at O_1 .



b) Excitation at O_2 .

Figure E.33-17. Wavefield images obtained on side-2 with excitation.

In conclusion, wrinkle existence on A3 specimen using the hybrid PZT-SLDV system is successfully detected and quantified without material properties. The detailed rating of the system is shown in Table E.33-5. For defect visualization, five out of five stars is rated. The reason is that the wrinkle pattern is clearly observed, and its range is approximately quantified with different actuation locations. The inspection time for 1D inspection is around 1 minute, which is very rapid, while the inspection time for 2D inspection is around two hours for areas illustrated in this test, which is still relatively fast. Thus, the inspection time gets four stars overall. Last, the actuator PZT is \$3.60 per piece, which is cost effective. However, the SLDV system costs \$300,000 when purchasing. Thus, two of five stars are rated regarding the system cost. In the future, expensive SLDV can be replaced by customized fixed LDV and gantry system to reduce the system cost. Overall, this hybrid PZT-SLDV guided wave inspection is very robust in general with four out of five stars.

Table E.33-5. Hybrid PZT-SLDV guided wave inspection rating.

Hybrid PZT-SLDV guided wave inspection		
Sample A3 Defect: wrinkles	Rating	
	Detection:	★★★★★
	Defect visualization	★★★★★
	Inspection time:	★★★★☆
	Equipment cost:	★★☆☆☆
	Overall Performance:	★★★★☆

E.33.3.7 References

- [1] Yu, L.; Leckey, C. A.; and Tian, Z.: “Study on crack scattering in aluminum plates with Lamb wave frequency–wavenumber analysis,” *Smart Materials and Structures*, Vol. 22, No. 6, pp065019, 2013.
- [2] Tian, Z.; Yu, L.; and Leckey, C.: “Delamination detection and quantification on laminated composite structures with Lamb waves and wavenumber analysis,” *Journal of Intelligent Material Systems and Structures*, Vol.26, No. 13, 2015, pp. 1723-1738, 2015.
- [3] Guided wave inspection on specimen A1 (A1 report, submitted).

E.33.4 Method: Single-Sided Infrared Thermography (SSIR)

E.33.4.1 Partner: Boeing

E.33.4.2 Technique Applicability: ★★★

SSIR is capable of detecting wrinkles in the composite material.

E.33.4.3 Laboratory Setup

For each inspection, the part was placed in the IR imaging system (Figure E.33-18). For each test, the flash lamp fires, heating the surface of the part uniformly. The IR camera records the heat signature of the part over time to track the diffusion of heat through the part thickness. This test was repeated for the front and backsides of each panel. The wrinkles on the panel cause alternating areas of high and low resin content in the troughs and crest, respectively. Because the resin has a lower thermal conductivity than the carbon fiber, the high content regions (troughs) will retain heat more than the low content regions (crests). As a result, the crests will show as cold spots over time while the troughs show as hot spots.

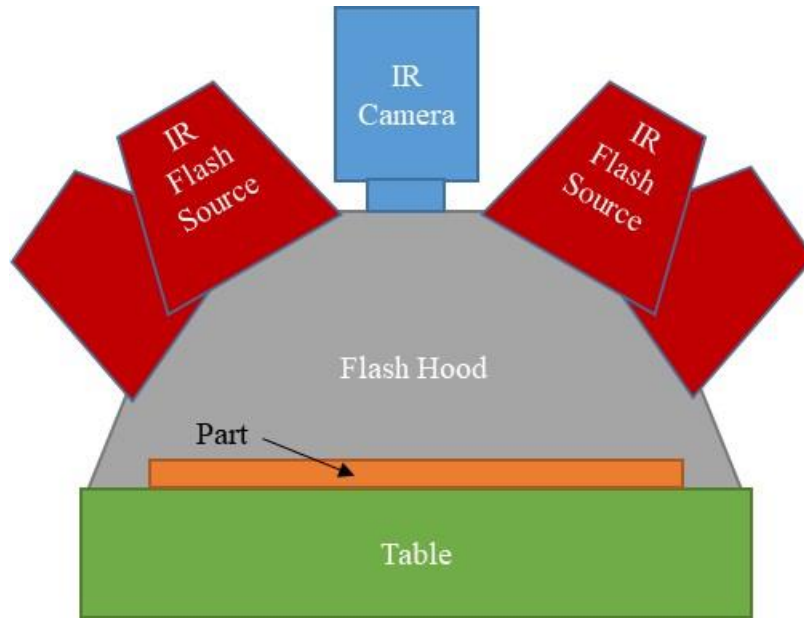


Figure E.33-18. Flash IRT system components.



Figure E.33-19. IR inspection system.

E.33.4.4 Equipment List and Specifications:

- Thermal Wave VoyageIR system
- SC6000 Series FLIR IR camera
- 4 6400 Watt-sec flash lamps
- Flash Hood
- X-Y gantry system

E.33.4.5 Settings

Data collection settings (i.e., resolution, frame rate, data acquisition time) were not provided by inspector.

E.33.4.6 Inspection Results

Figure E.33-20 shows the IR image of the panel at 1.6 sec. As anticipated, hot and cold spots can be observed (circled in red), corresponding with the manufactured wrinkle locations. Because the panel was uniformly heated on the side that the camera observed, the strongest thermal gradient will come from the wrinkles on that side. Therefore, the indications from side 1 are not clearly observable on side 2. From these data, it is possible to measure the wavelength of the wrinkles, though the amplitudes cannot be determined from these data.

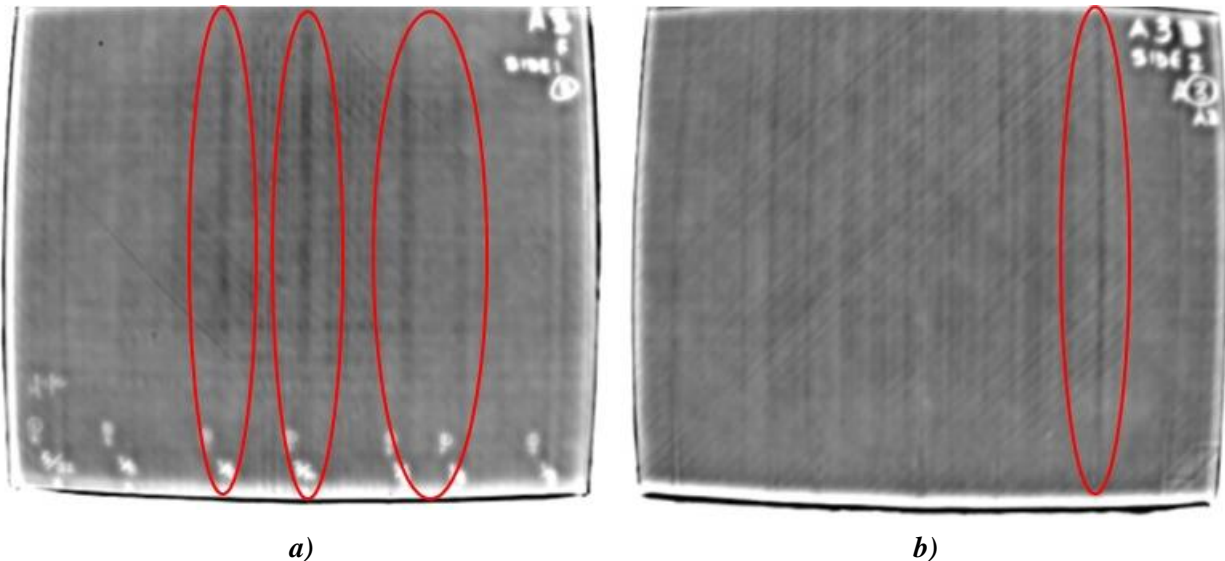


Figure E.33-20. Greyscale 1.6 sec IR image of Composite Wrinkle Standard A3 side 1 (a) and side 2 (b).

E.34 Specimen #34: Wrinkle A4

Structure	Material	Details	Dimensions (inches)	Partner Methods	
Thin laminates	IM7/8552-1 slit tape	Significant wrinkling in flat panels	15 × 12 × 0.15	NASA	E.34.1 PEUT
					E.34.2 XCT
				USC	E.34.3 GWUT
				Boeing	E.34.4 SSIR

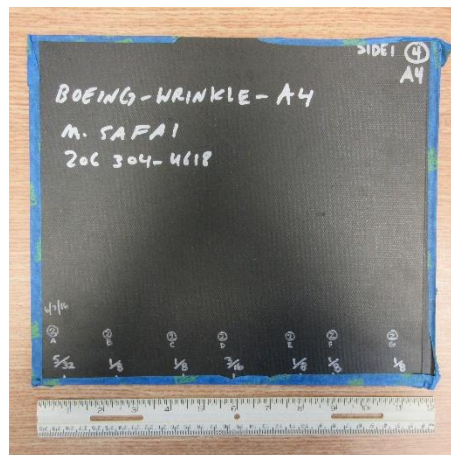


Figure E.34-1. Photograph of Specimen #34: Boeing-Wrinkle-A4.

E.34.1 Method: Pulse-Echo Ultrasonic Testing (PEUT)

E.34.1.1 Partner: NASA

E.34.1.2 Technique Applicability: ★★★

PEUT is capable of detecting the wrinkling in this specimen.

E.34.1.3 Laboratory Setup

Immersion Ultrasonic Testing: NASA LaRC uses a custom designed single probe ultrasonic scanning system. The system has an 8-axis motion controller, a multi-axis gantry robot mounted above a medium-size water tank, a dual-channel, 16-bit, high-speed digitizer, and an off-the-shelf ultrasonic pulser receiver. The system can perform TTUT and PEUT inspections. TT inspection employs two aligned ultrasonic probes, one transmitter and one receiver, placed on either side of a test specimen. Pulse-echo inspection is a single-sided method where a single ultrasonic probe is both transmitter and receiver. In each method, data are acquired while raster scanning the ultrasonic probe(s) in relation to a part. Figure E.34-2 shows a simplified block diagram of a scanning Pulse-echo inspection.

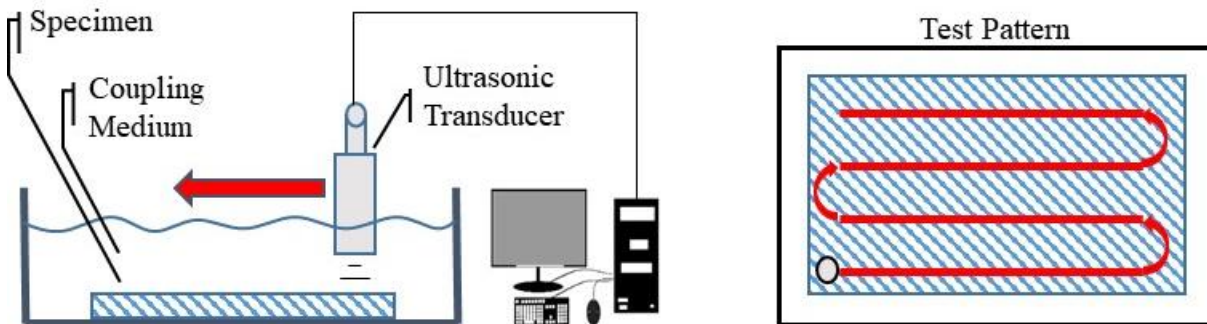


Figure E.34-2. Ultrasonic system components.

E.34.1.4 Equipment List and Specifications:

- Pulser/Receiver: Olympus 5073PR
- Digitizer: AlazarTech ATS9462, dual channel, 16 bit, 180 MS/s
- Sensor: Olympus 2-inch spherical focus immersion ultrasonic transducer
- Motion system: open looped stepper motor based X-YY-Z gantry robot
- Motion Controller: Galil DMC-4183
- Acquisition Software: FastScan, custom developed at NASA LaRC
- Signal Processing Software: DataViewer, custom developed at NASA LaRC

E.34.1.5 Settings

Table E.34-1. Data collection settings.

Resolution horizontal [in/pixel]	0.02
Resolution vertical [in/pixel]	0.05
Probe frequency [MHz]	10
Focal Length [in]	2
Array Dimensions [pixels]	601 × 201

The specimen is placed flat against the zero position of the tank raised above the glass bottom by several metal washers. The test probe is computer-controlled and correlated to the position on the

sample. It is also focused to a point 1 mm below the surface of the test material. The specimen remains in place while the transducer follows a preprogrammed test grid across the surface as indicated in Figure E.34-2. At each point, ultrasonic data are collected from individual pulses. Larger step sizes between data collection result in lower image resolution. These data points are reconstructed into a data cube displaying spatial coordinates as time progresses. 2D reconstruction of the collection of ultrasonic responses create flattened slices at varying depths within the material.

E.34.1.6 Inspection Results

Specimen #34, is a flat panel fabricated from IM7/8552-1 slit tape with the objective of achieving wrinkles within the material. PEUT was performed on this specimen in NASA's immersion tank specified above.

Figure E.34-3 shows indications of fiber wrinkling near the surface of the material. The wrinkles cause severe perturbations in the acoustic waves that are easily seen throughout the sample as shown in Figure E.34-4.

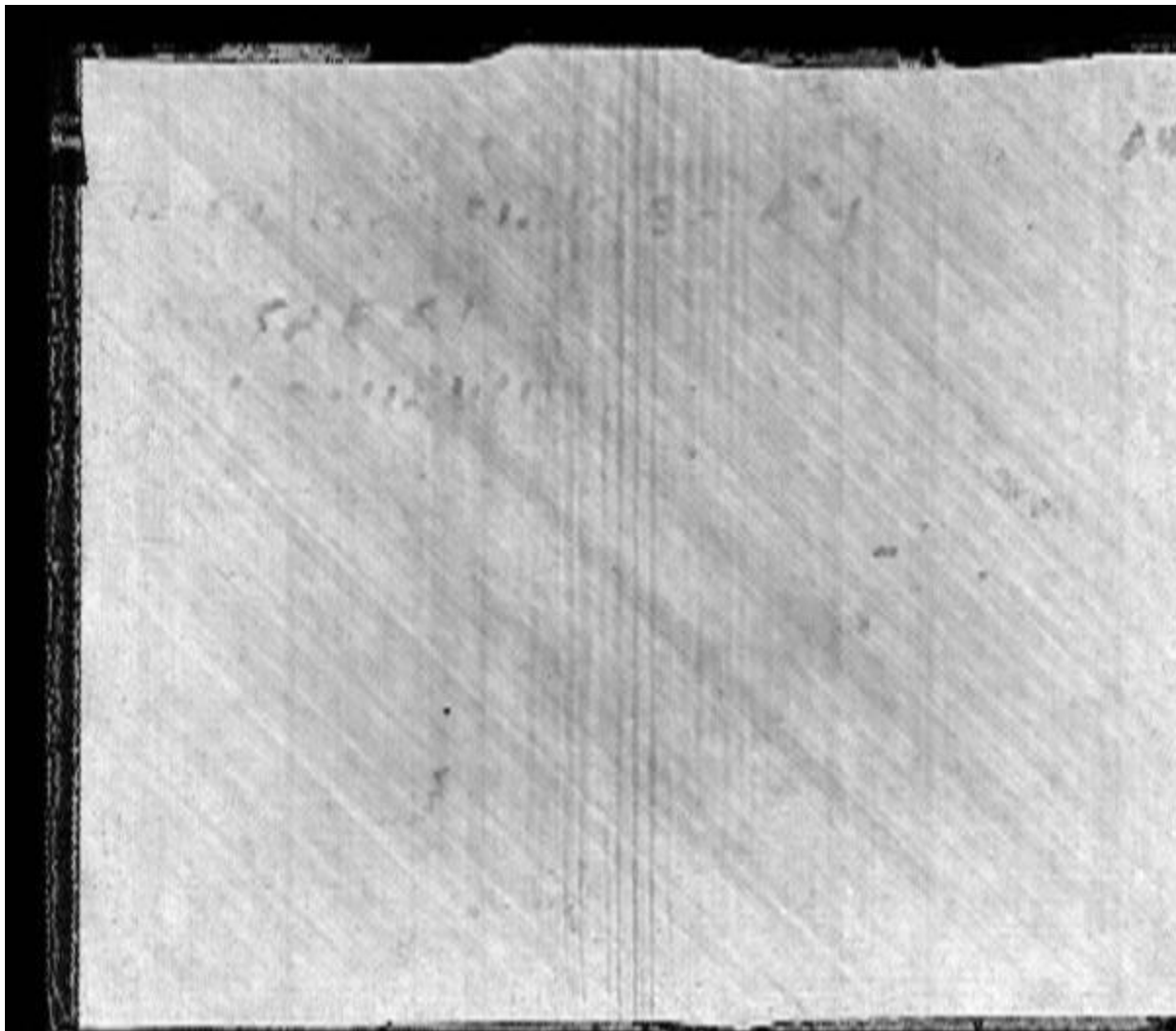


Figure E.34-3. UT image showing near surface indications of fiber waviness.

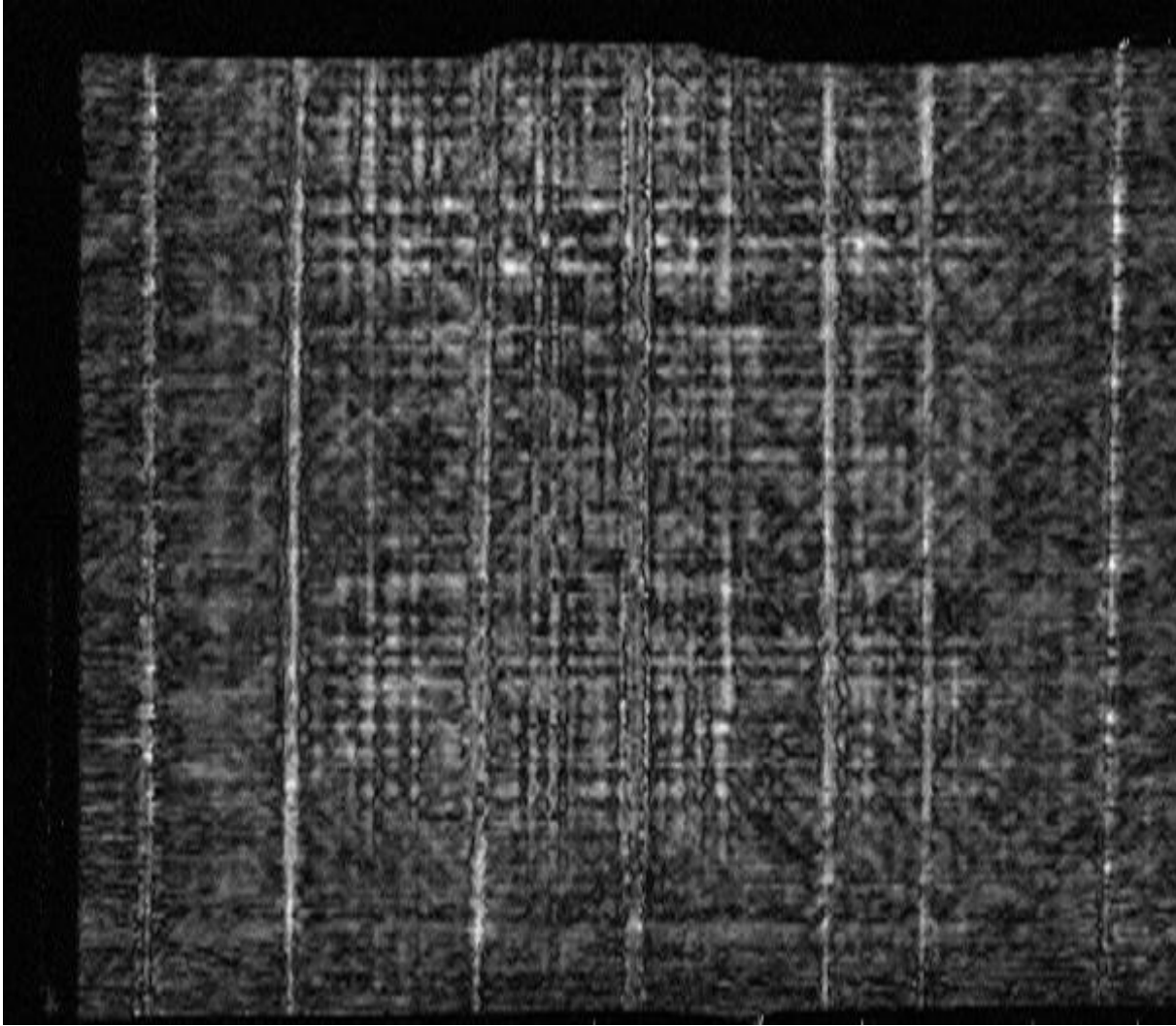


Figure E.34-4. UT image showing indications of fiber waviness within the material bulk.

E.34.2 Method: X-ray Computed Tomography (XCT)

E.34.2.1 Partner: NASA

E.34.2.2 Technique Applicability: ☆☆☆

XCT is not capable of imaging the fiber wrinkles induced in this specimen.

E.34.2.3 Laboratory Setup

The microfocus XCT system at NASA LaRC is a commercially available Avonix (Nikon C2) Metrology System designed for high resolution NDE inspections. The system is an advanced microfocus X-ray system, capable of resolving details down to 5 μm , and with magnifications up to 60X. Supplied as complete, the system is a large-dimension radiation enclosure with X-ray source, specimen manipulator, and an amorphous silica detector, as shown in Figure E.34-5. The imaging controls are housed in a separate control console. The detector is a Perkin-Elmer, 16-bit, amorphous-silicon digital detector with a 2000 \times 2000-pixel array.

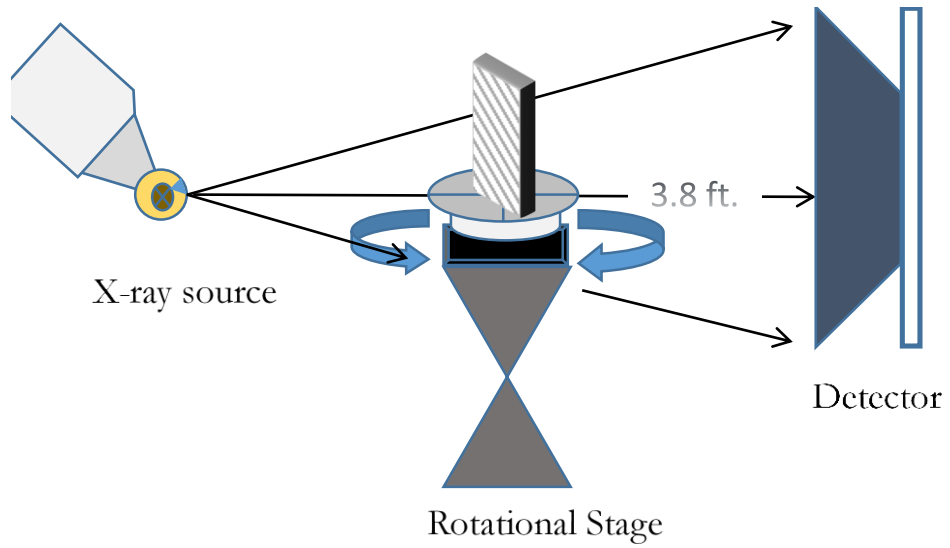


Figure E.34-5. XCT system components.

A consistent Cartesian coordinate system is used to define slice direction as illustrated in Figure E.34-6. Slices normal to the X-, Y-, and Z-directions are shown in Figures 34-6a, b, and c, respectively.

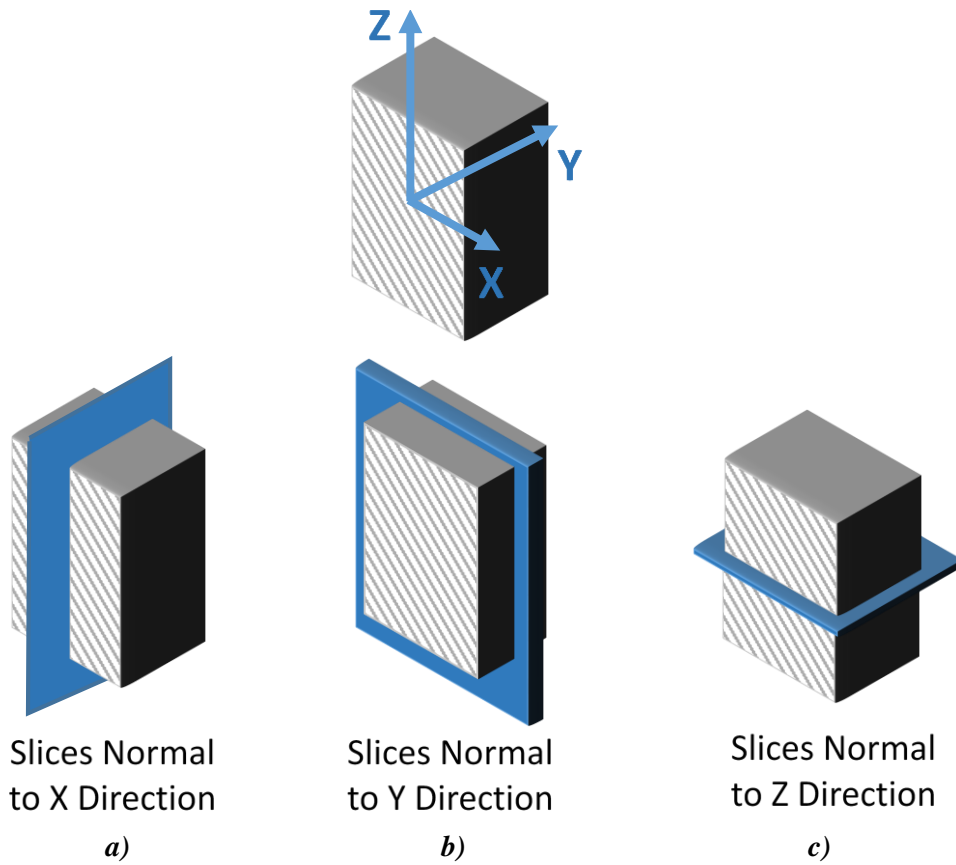


Figure E.34-6. Slice direction nomenclature.

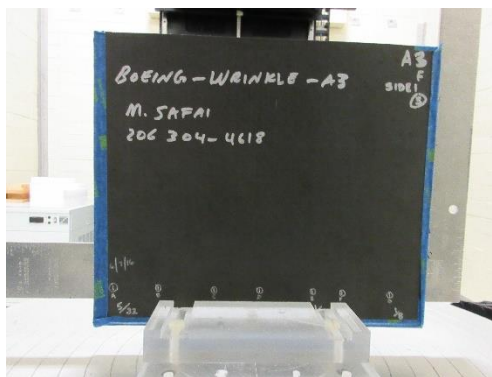


Figure E.34-7. Microfocus XCT system showing orientation of Specimen #34: Boeing-Wrinkles A4.

E.34.2.4 Equipment List and Specifications:

- Avonix 225 CT System
- 225 kV microfocus X-ray source with 5 μm focal spot size
- 15 or 30kg Capacity, 5-axis, fully programmable manipulator
- Detector: Perkin Elmer XRD 1621 – 2000 \times 2000 pixels with 200 μm pitch
- 10 μm spatial resolution for specimens 1.5 cm wide
- Thin panels 10 \times 10 inches – full volume 200 μm spatial resolution

E.34.2.5 Settings

Table E.34-2. Data collection settings.

Source Energy	120 kV
Current	90 μA
Magnification	1.65 X
Filter	NF
# Rotational angles	3142
Exposure time / frame	1.0 sec
Max Histogram Grey Level	22 K
# Averages	8
Resolution (μm)	114.894 μm
Array Dimensions (pixels)	Set 1: 1999 \times 362 \times 1998 Set 2: 1998 \times 686 \times 1997

The specimen is placed vertically (rotated about the smallest dimension) on the rotational stage located between the radiation source and the detector. The rotational stage is computer-controlled and correlated to the position of the sample. As the sample is rotated the full 360° (~0.11° increments), the detector collects radiographs at each rotated angle as the X-ray path intersects the sample. 3D reconstruction of the collection of radiographs produces a volume of data that is viewed along any plane in the volume. The closer the sample can be placed to the X-ray source, the higher the spatial resolution that can be obtained.

E.34.2.6 Inspection Results

Specimen #34 is a panel with significant wrinkles induced within the material. XCT was performed on this specimen in NASA LaRC's large CT system with the settings defined in Section E.34.1.6. The scan was done using a large viewing window encompassing the whole specimen (Figure

E.34-8) and a small window covering a smaller area to increase the resolution of the scan (Figure E.34-9). This cannot always be done on larger specimens.



Figure E.34-8. 3D X-ray generated view of specimen #32: Boeing-Wrinkles using a small viewing window showing the y direction (center), z direction (top) and x direction (right).

The wrinkles cannot be seen from all viewing directions shown in Figure E.34-8. Both the x- and z-direction views give little evidence of any fiber waviness. In the y direction there are darker streaks and that are a result of the method used to induce wrinkling in the sample. These marks do show damage; however, they do not serve as an indicator for any fiber wrinkling. The higher resolution image in Figure E.34-9 shows possible indications of fiber wrinkling though it is still not entirely clear. When viewing the full specimen the fiber waviness is even less apparent (Figure E.34-8).

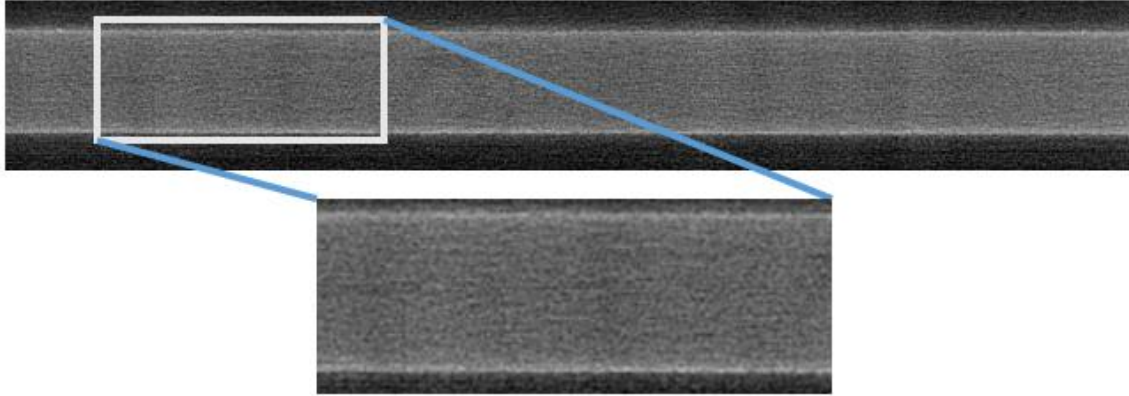


Figure E.34-9. 3D X-ray generated view of specimen #34: Boeing-Wrinkles from the z direction.

E.34.3 Method: Guided Wave Ultrasonic Testing (GWUT)

E.34.3.1 Partner: USC

E.34.3.2 Technique Applicability: ★★★

GWUT employs ultrasonic waves that propagate along waveguides by its boundaries, e.g. pipes, rods and plate-like structures, which allows waves propagate a long distance with little energy loss. GWUT shows advantage in many types of defect inspection, e.g. crack in metallic structures [1], and delamination in composite structures [2].

The Boeing-wrinkle-A4 (herein referred to as A4) is inspected using hybrid PZT-SLDV GWUT method in this report. General information of A4 and its wrinkle layout are illustrated in the paragraph below. The relative inspection, results and system rating are illustrated in the inspection results.

Specimen A4 is shown in Figure E.34-10 with its front and back view. The measured dimension of A4 is $306 \times 260 \times 4.4$ mm. Significant wrinkles are observed on side one as shown in Figure E.34-10a, while no obvious wrinkles are observed on side two. No other information about A4 is available to the inspectors.

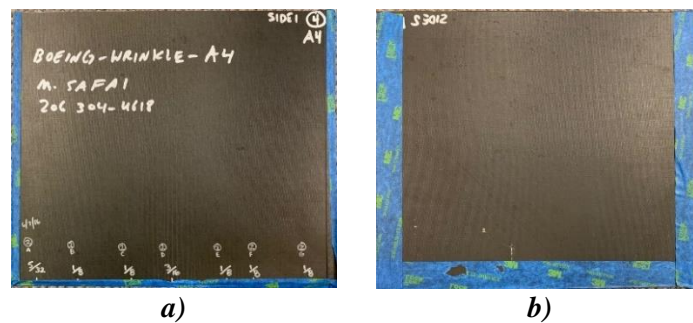


Figure E.34-10. Picture of specimen A4. (a) front side (side 1), and (b) back side (side 2).

E.34.3.3 Laboratory Set Up

The same hybrid PZT-SLDV system is implemented to inspect A4, using contact type PZT as actuator and SLDV as sensor to excite and receive guided waves in the testing plate (Lamb waves) [1]. The overall setup also remains the same as reported previously and shown in Figure E.34-11 and Figure E.34-12 [3].

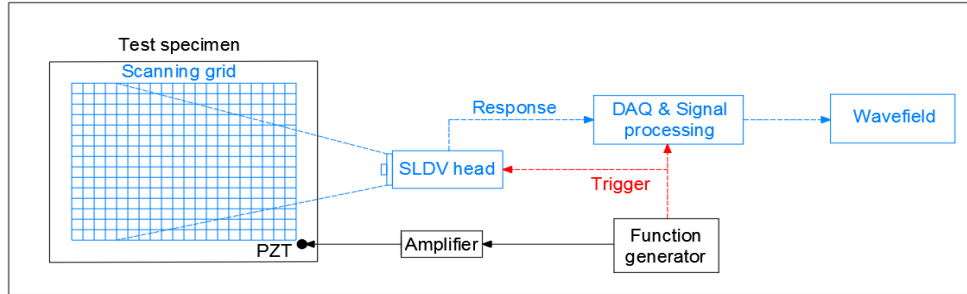


Figure E.34-11. Schematic design of the PZT-SLDV system.

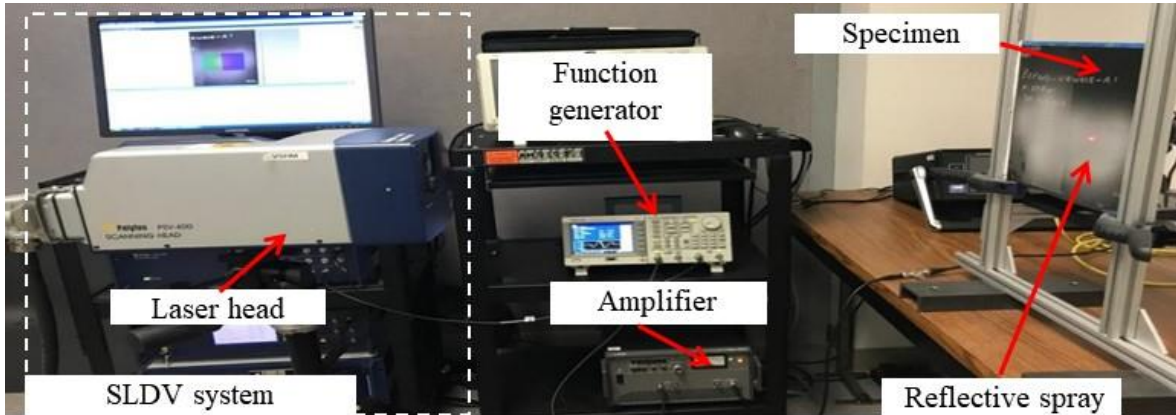


Figure E.34-12. Experimental setup of the PZT-SLDV system.

E.34.3.4 Equipment List and Specifications

The detailed specifications of the equipment and devices used for the hybrid PZT-SLDV system at USC VSHM laboratory are given in Table E.34-3. Data acquisition settings are shown in Table E.34-4.

Table E.34-3. Equipment/device specifications.

Equipment/device	Specifications
Polytec PSV-400-M2	2D scanning laser Doppler vibrometer with a frequency range up to 1 MHz with specific velocity decoders
PZT	Steminc 7-mm circular 0.5-mm thick piezoelectric transducers
Tektronix AFG3022C	2-channel arbitrary function generator with 1 μ Hz to 25MHz
HSA 4014	High speed bipolar amplifier up to 1 MHz and 200 VA
Target Simply Balanced TM organic honey	Natural and organic honey blend performed as couplant
Albedo 100 Reflective Spray	a non-permanent, clear spray with light-reflective properties

E.34.3.5 Settings

Table E.34-4. Data collection settings.

Sampling frequency (MHz)	12.56 MHz
Spatial sampling interval (mm)	1 mm
Average	200
Velocity decoder	VD-07 10mm/s/V
Spray coating	20 layers

Since A4 is similar to A3 from visual inspection, the same optimal excitation frequency (240 kHz) is adopted based on the results of A3 inspection. 2D area inspection (310 mm× 60 mm) is performed in order to visualize the wrinkle defects with 1-mm spatial resolution on both sides with excitation location at O as shown in Figure E.34-13.

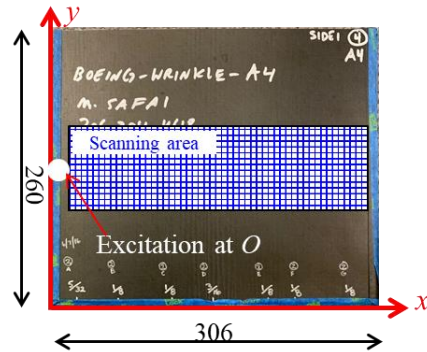


Figure E.34-13. 2D area inspection setup.

E.34.3.6 Inspection Results

2D Inspection Results on Side-1

First conducted is the inspection on side one with excitation location at O . The obtained wavefield image is plotted in Figure E.34-14a (refer to previous reports for algorithm). Denser wrinkle patterns are observed in the middle range along x direction (100-200 mm), while coarser wrinkles are observed at around $x = 50-70$ mm and 210-280 mm.

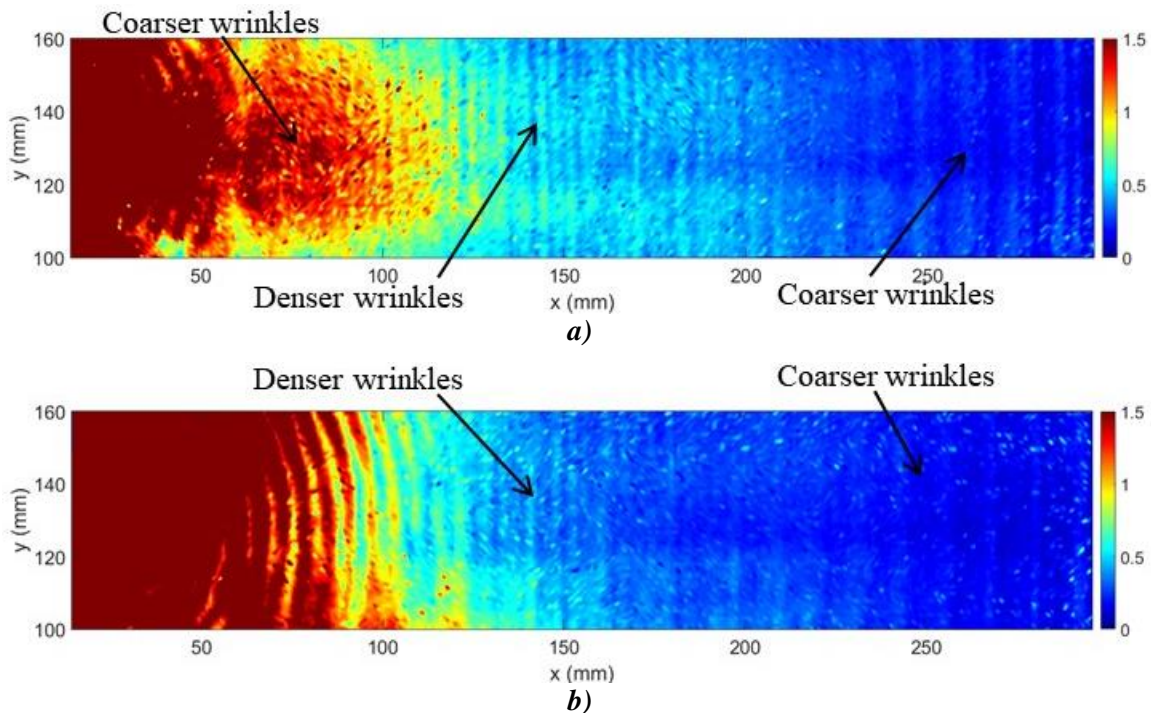


Figure E.34-14. Wavefield images obtained on: (a) side-1, and (b) side-2.

2D Inspection Results on Side-2

For rough identification of the wrinkle locations through thickness, 2D inspection is performed on side-2 with the same setup as side-1. The obtained wavefield image is plotted in Figure E.34-14b. Similar to imaging results on side-1, denser wrinkle patterns are observed at $x = 100\text{--}200$ mm, and coarser wrinkle patterns are observed at $x = 250$ mm. However, the wrinkle patterns are not as strong and clear as side-1. Comparing the wavefield images obtained from side-1 and side-2, we can conclude that the wrinkle defects are closer to side-1 than side-2.

In conclusion, wrinkle existence on A4 specimen using the hybrid PZT-SLDV system is successfully detected and quantified without material properties. The detailed rating of the system is shown in Table E.34-5. For defect visualization, five out of five stars is rated. The reason is that the wrinkle pattern is clearly observed, and its range is approximately quantified. The inspection time for the performed 2D inspection is around two hours for areas illustrated in this test, which is relatively fast. Thus, the inspection time gets four stars overall. Last, the actuator PZT is \$3.60 per piece, which is cost effective. However, the SLDV system costs \$300,000 when purchasing. Overall, two of five stars are rated regarding the system cost. In the future, expensive SLDV can be replaced by customized fixed LDV and gantry system to reduce the system cost. Considering the above five aspects, this hybrid PZT-SLDV guided wave inspection is very robust and get four out of five stars in general.

Table E.34-5. Hybrid PZT-SLDV guided wave inspection rating.

Hybrid PZT-SLDV guided wave inspection		
Sample A4 Defect: wrinkles	Rating	
	Detection:	★★★★★
	Defect visualization	★★★★★
	Inspection time:	★★★★☆
	Equipment cost:	★★☆☆☆
	Overall Performance:	★★★★☆

E.34.3.7 References

- [1] Yu, L.; Leckey, C. A.; and Tian, Z.: “Study on crack scattering in aluminum plates with Lamb wave frequency–wavenumber analysis,” *Smart Materials and Structures*, Vol. 22, No. 6, pp065019, 2013.
- [2] Tian, Z.; Yu, L.; and Leckey, C.: “Delamination detection and quantification on laminated composite structures with Lamb waves and wavenumber analysis,” *Journal of Intelligent Material Systems and Structures*, Vol.26, No. 13, 2015, pp. 1723-1738, 2015.
- [3] Guided wave inspection on specimen A1 (A1 report, submitted).

E.34.4 Method: Single-Sided Infrared Thermography

E.34.4.1 Partner: Boeing

E.34.4.2 Technique Applicability: ★★★

Flash thermography is capable of detecting wrinkles in the composite material.

E.34.4.3 Laboratory Setup

For each inspection, the part was placed in the IR imaging system (Figure E.34-15). For each test, the flash lamp fires, heating the surface of the part uniformly. The IR camera records the heat

signature of the part over time to track the diffusion of heat through the part thickness. This test was repeated for the front and backsides of each panel. The wrinkles on the panel cause alternating areas of high and low resin content in the troughs and crest, respectively. Because the resin has a lower thermal conductivity than the carbon fiber, the high content regions (troughs) will retain heat more than the low content regions (crests). As a result, the crests will show as cold spots over time while the troughs show as hot spots.

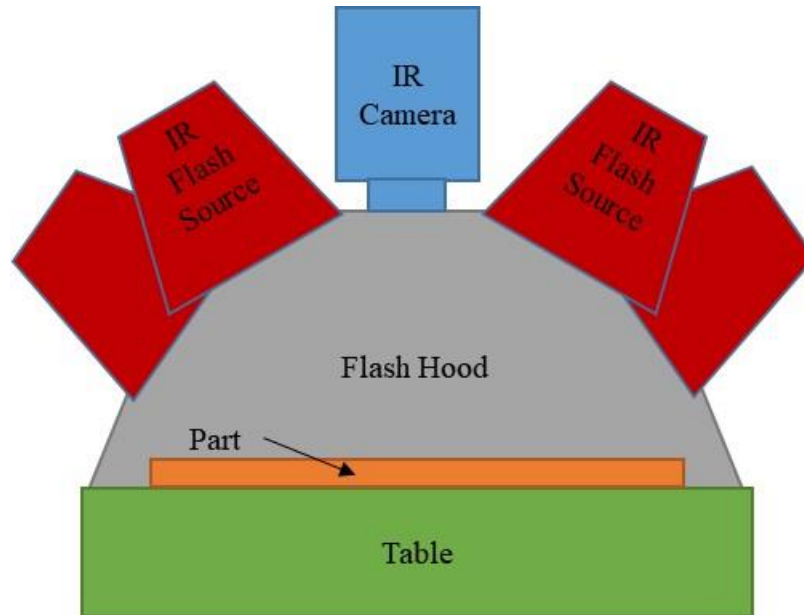


Figure E.34-15. Flash IRT system components.



Figure E.34-16. IR inspection system.

E.34.4.4 Equipment List and Specifications:

- Thermal Wave VoyageIR system
- SC6000 Series FLIR IR camera
- 4 6400 Watt-sec flash lamps
- Flash Hood
- X-Y gantry system

E.34.4.5 Settings

Data collection settings (i.e., resolution, frame rate, data acquisition time) were not provided by inspector.

E.34.4.6 Inspection Results

Figure E.34-17 shows the IR image of the panel at 1.0 sec. As anticipated, hot and cold spots can be observed (circled in red), corresponding with the manufactured wrinkle locations. Because the panel was uniformly heated on the side that the camera observed, the strongest thermal gradient will come from the wrinkles on that side. Because of this, one can observe fainter, mirrored indications of the wrinkles when observed from the opposite side, such as the left side grouping of wrinkles in Figure E.34-17a appearing fainter on the right side in Figure E.34.17b. From these data, it is possible to measure the wavelength of the wrinkles, though the amplitudes cannot be determined from these data.

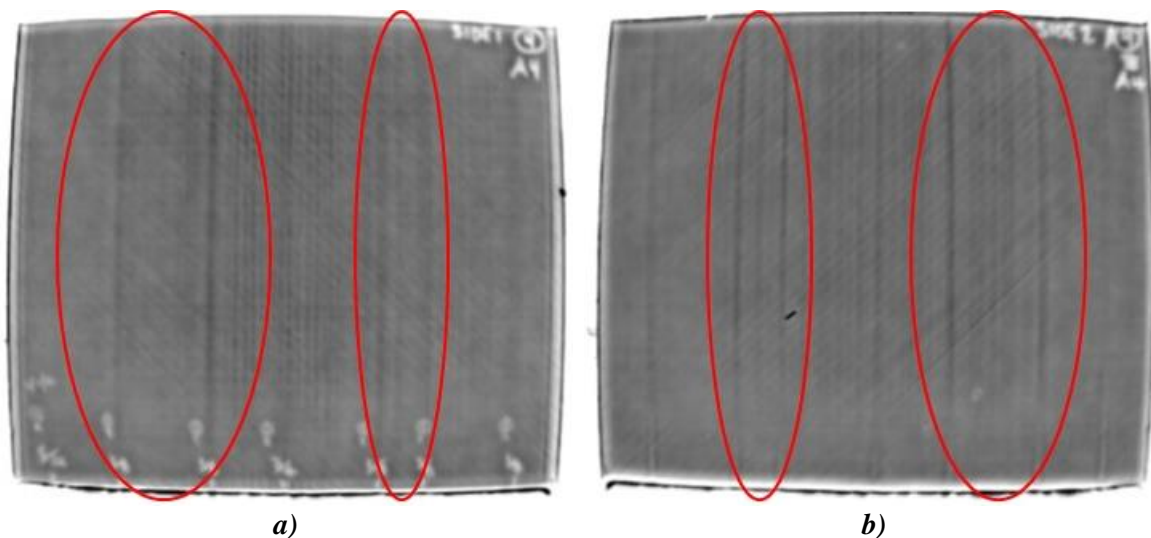


Figure E.34-17. Greyscale 1.0 sec IR image of Composite Wrinkle Standard A4 side 1 (a) and side 2 (b).

E.35 Specimen #35: Boeing 8276-200-58-8A

Structure	Material	Details	Dimensions (inches)	Partner Methods
8 fabric plies 2 fiberglass plies	BMS8-276 BMS8-331	58° Curve with 0.2-inch radius Brass, RPF and PT inserts at varying depths	24 × 6.5	Boeing E.35.1 XCT E.35.2 TTUT E.35.3 SSIR E.35.4 X-ray DR E.35.5 X-ray CR

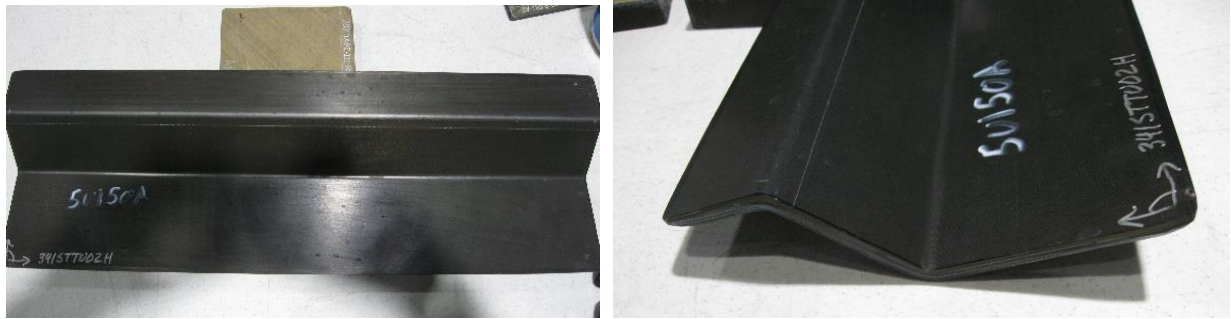


Figure E.35-1. Photographs of Angle Panel Reference Standard

E.35.1 Method: X-ray Computed Tomography (XCT)

E.35.1.1 Partner: Boeing

E.35.1.2 Technique Applicability: ★★★

XCT is capable of identifying all inserts, notably brass inserts.

E.35.1.3 Laboratory Setup

The Digital Radiography Center (DRC) utilizes an YXLON Modular CT System. This system has the capability to utilize various X-ray sources for varying applications, including a 450-kV source, a microfocus source, and a nanofocus source. The microfocus source used has a variable focal spot size of less than 4 μm and is suitable for magnifications up to 10X, with the nanofocus ranging up to 187X. The detector has 3 degrees of freedom (DOF), allowing for increase in the effective detector area through combined scans. The manipulator controls the position of the detector, object, and source. It has 7 DOF including a rotating stage to rotate the object during the scan. The entire system includes the source, detector, manipulator, control and reconstruction computers, and user control station. The computers and control station are outside of the radiation enclosure (vault) and utilize a safety interlock system to operate. Cameras are located in the vault to allow the operator to monitor the part from outside the enclosure.

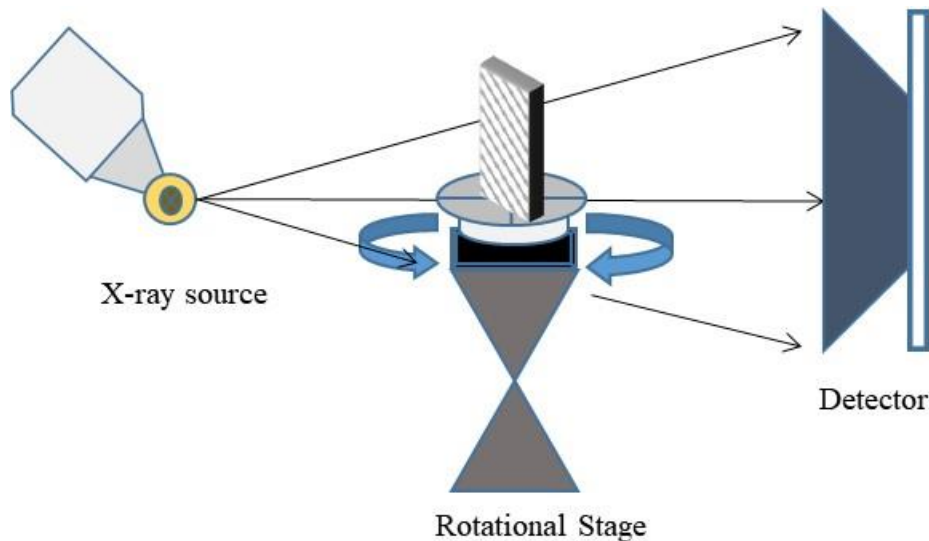


Figure E.35-2. XCT system components.

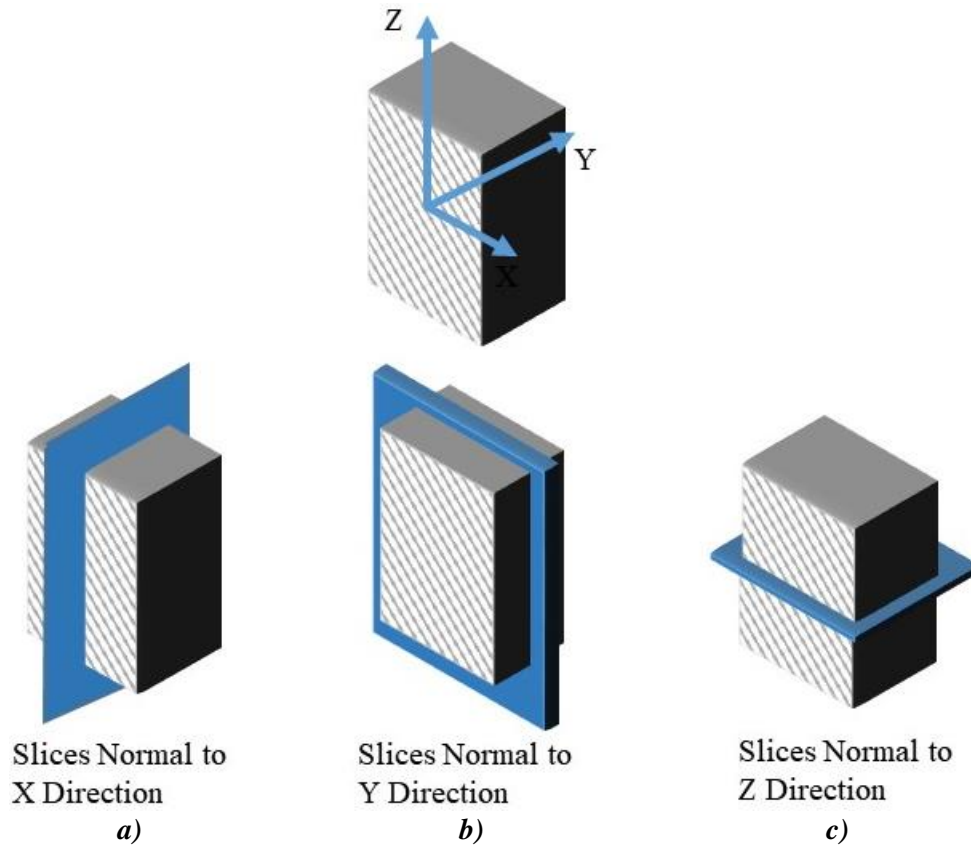


Figure E.35-3. Slice direction nomenclature.

The standards were divided into two sections, labeled Upper and Lower, and placed on the rotator in a soft clamp (Figure E.35-4). The specimen was right-side-up for the Upper scan, and upside-down for the Lower scan. Plastic markers, which show up in 3D reconstruction, were placed on the sections to denote the boundaries between sections. The position of the specimen, source, and detector are controlled to produce geometric magnification of the image and increase the spatial resolution. The image data are gathered as X-rays penetrate the part and expose the detector for a set amount of time. For each scan, these image data are collected at 1080 different angles throughout a 360° rotation. These images are then reconstructed to create the 3D volume data set. This data set is viewed and analyzed in Volume Graphics, a volume rendering software, to identify the relevant components.



Figure E.35-4. Microfocus XCT setup for Radii Delamination Standard.

E.35.1.4 Equipment List and Specifications

- YXLON Modular CT System
- 225 kV microfocus X-ray source with variable focal spot size
- 100 kg capacity, 7-axis, granite-based manipulator
- XRD 1621 Detector – 2048 × 2048 pixels with 200 μm pitch, 400 × 400 mm active area
- 126 μm spatial resolution for half volume scan
- Volume Graphics 3.0 visualizing software
- Reconstruction Computer

E.35.1.5 Settings

Table E.35-1. Data collection settings.

Source Energy	205 kV
Current	0.47 mA
Magnification	1.59 X
Filter	Copper
# Rotational angles	1080
Exposure time/frame	800 ms
Spatial Resolution (μm)	125.777 μm
Array Dimensions (pixels)	2048 × 2048

E.35.1.6 Inspection Results

The Radii Delamination Standards are carbon fiber composite panels with foreign material inserts in various layers to evaluate the detectability using ultrasonic inspection. These inserts, largely grouped around the angle in the panel; however, are not exclusive to this area. The standards vary in thickness, utilizing 8, 26, and 48 plies of carbon fiber fabric with exterior layers of fiberglass. Because of their length, the data set consists of the upper and lower half volumes of the standards, flipped 180° for the scan.

After aligning the volume coordinate system to correspond with the panel geometry, the slice view can be used to inspect conditions at each lamina. The brightness and contrast settings are also adjusted to make defects clear, but retain the visible noise at a reasonable level. The inserts are

clearly visible (Figure E.35-5), showing with less density for pressure sensitive tape (PT) and release ply fabric (RPF) and higher density for brass. The brass is the most readily observable, followed by the PT with the RPF having the lowest detectability. The RPF may show the least response due to similar density to base material or due to a strong interface with little voiding or delamination to be detected.

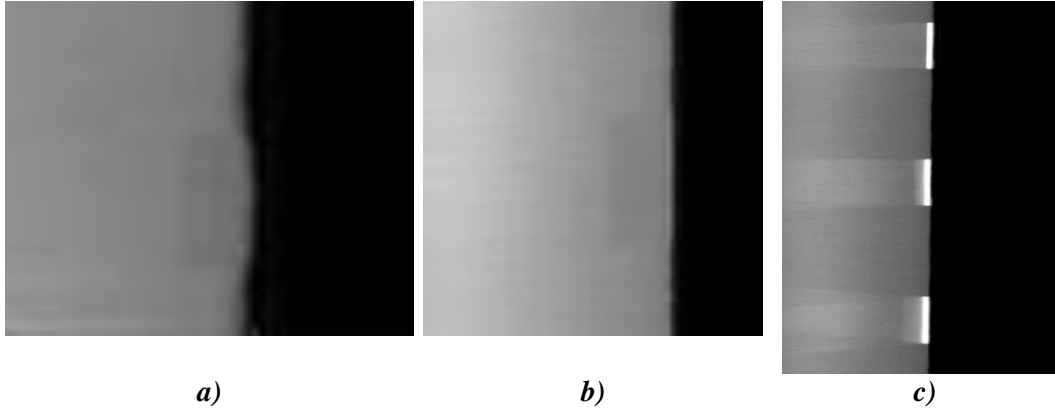


Figure E.35-5. CT slice view showing PT (a), RPF (b), and brass (c) inserts.

The CT scanning and reconstruction process is subject to artificial and undesirable artifacts. These are the result of multiple conditions. The direction of rotation leaves an underlying direction to the noise of the data set, aligning with the rotation. This is seen as a light, roughly horizontal streaking seen in (Figure E.35-5). The presence of high-density material in an otherwise low-density structure often creates even more intense ray artifacts, seen as shadow-like streaks emanating from the high-density material (Figure E.35-5c). If defects are present in these dark artifacts, their detectability is reduced. Lastly, the part may rotate in and out of the cone-beam of the X-rays during the scan, leaving the top and bottom edges of the volume not fully defined. This is seen as darker “wedges” of the volume at the top and bottom of the data set (Figure E.35-5).

The detectability of the inserts relies on viewing the slices at the appropriate angle, which aligns with the lamina. This means the inserts within the curve of the panel, while still detectable, are less apparent (Figure E.35-6), and operators must be careful to attempt to identify them. The inserts are also more visible when they induce delamination with air or if they have a much greater density than the composite material.

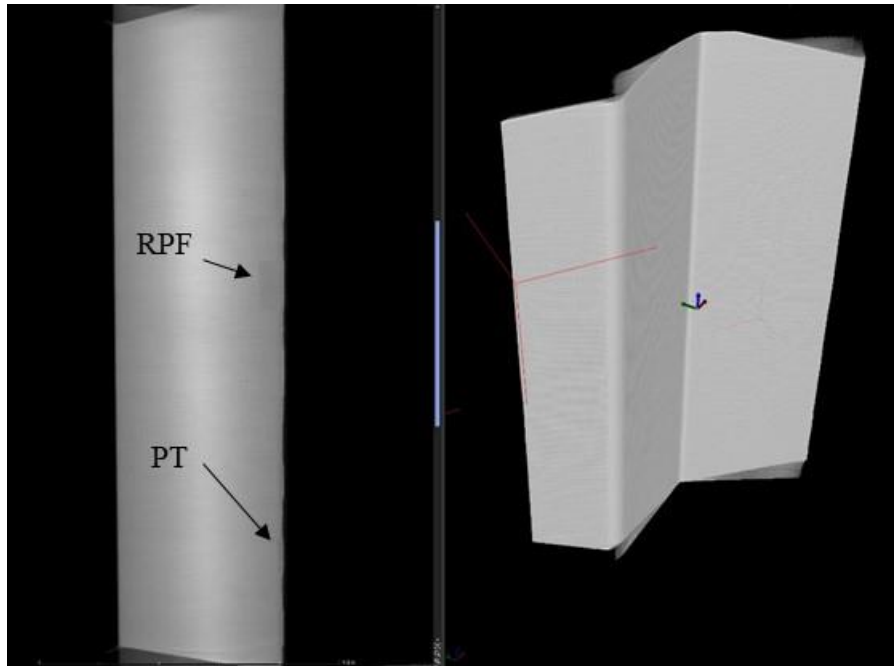


Figure E.35-6. CT slice view showing PT and RPF inserts.

E.35.2 Method: Through-Transmission Ultrasound Testing (TTUT)

E.35.2.1 Partner: Boeing

E.35.2.2 Technique Applicability: ★★★

All inserts are visually detectable with TTUT data.

E.35.2.3 Laboratory Setup

The TTUT scanner at the Boeing laboratory consists of an enclosure, part supports, a water pump and nozzle system, ultrasonic transducers (transmitter and receiver), robotic manipulator, and control computer. After adjusting the water to produce a uniform flow, the pulser and receiver (on opposite sides of the specimen) perform a C-scan under the control of the robotic manipulator and control computer. The C-scan is produced by taking multiple 1D scans (A-scans) and stitching them together to produce the final area result.

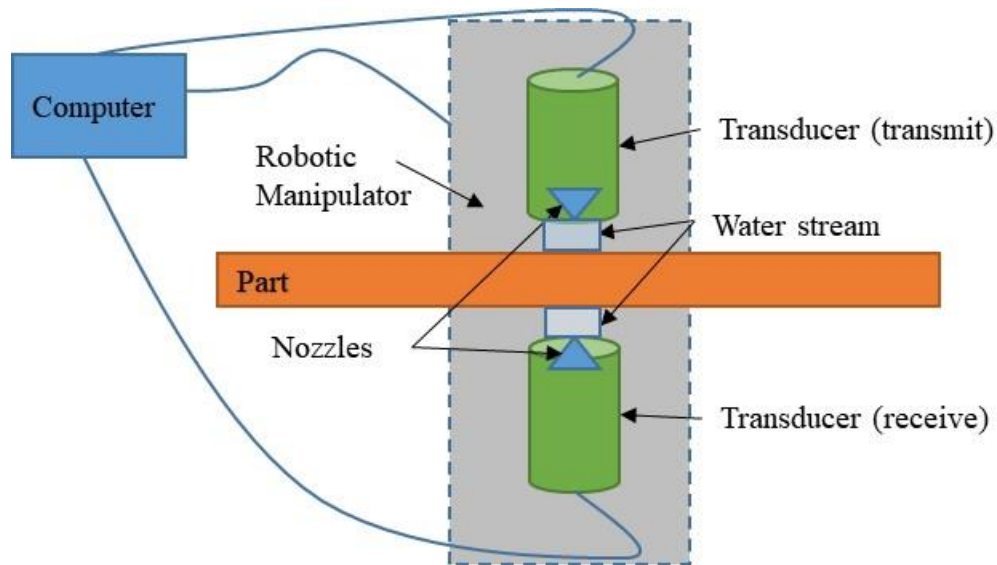


Figure E.35-7. TTUT Scanning schematic with water pump.

TTUT works on the principal of the capture and quantification of the transmitted waves. It uses a pulsing transducer on one side of the part and has the receiving transducer on the opposite side of the part. Scanning is accomplished with contact, water streams, or full immersion method, as long as sufficient ultrasonic coupling is used. Although the TTUT works on non-parallel, front-to-back surface, the optimized data are produced when the front-to-back surfaces are parallel to each other.

As the ultrasonic waves travel through a material, they are attenuated. Defects and material discontinuities such as delamination, porosity and foreign material interfaces cause increased attenuation. UT has an orientation dependency, where certain defect orientations will attenuate the signal more if they are oriented for maximum reflection. Delamination tend to be oriented favorably for detection, making ultrasound the common method for composite inspection.

E.35.2.4 Equipment List and Specifications:

- 1 MHz ultrasonic transducer and receiver
- Water pump, nozzles, and circulation system
- Robotic manipulator
- Enclosure
- Control computer

E.35.2.5 Settings

Table E.35-2. Data collection settings.

Frequency	1 MHz
Resolution	0.04 inch × 0.04 inch

E.35.2.6 Inspection Results

The NASA Radii Delamination Standards are carbon fiber composite panels with foreign material inserts in various layers to evaluate the detectability using ultrasonic inspection. These inserts are largely grouped around the angle in the panel; however, not exclusive to this area. The standards vary in thickness, utilizing 8, 26, and 48 plies of carbon fiber fabric with exterior layers of

fiberglass. Using TTUT, the all insert types (PT, RPF, and brass) were detectable. However, this visual detectability generally reduced as thickness increased.

The brass inserts were the most resolved and detected (Figure E.35-8c) and the RPF inserts showed the lowest detectability (Figure E.35-8b). This is consistent with the theory that the RPF inserts bond to the material the best, leading to a small TTUT signal, while the brass has the worst bond (likely due to applied coating), leading to the large signals seen. The brass also has a significantly different attenuation than the surrounding material, allowing easy detection. The 48 ply standards included inserts in locations on and away from the curved radius. The inserts away from the radius tended to be better resolved and defined (Figure E.35-8) due to the more uniform background signal. While the RPF inserts had small responses and resolving their exact shape is difficult, their presence tended to be detectable in the distortion of the surrounding signal and features (Figure E.35-8b).

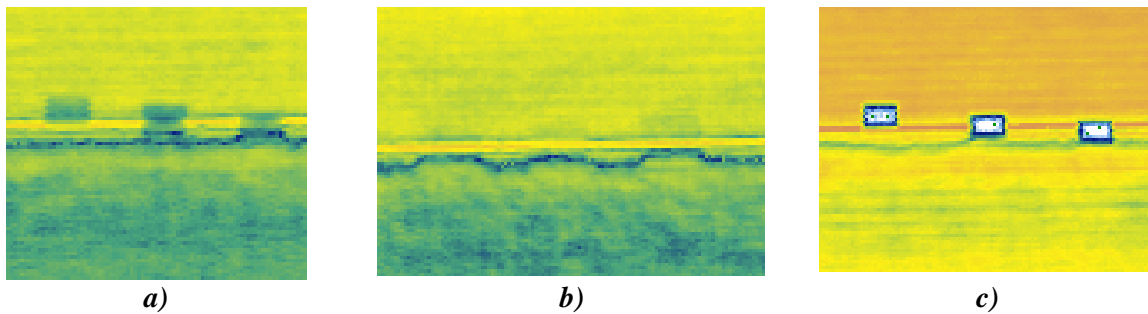


Figure E.35-8. TTUT scans showing PT (a), RPF (b), and brass (c) inserts.

E.35.3 Method: Single-Sided Infrared Thermography (SSIR)

E.35.3.1 Partner: Boeing

E.35.3.2 Technique Applicability: ★★★

SSIR can detect all insert types in the radii standard.

E.35.3.3 Laboratory Setup

For each inspection, the part was placed in the IR imaging system (Figure E.35-9). For each test, the flash lamp fires, heating the surface of the part uniformly. The IR camera records the heat signature of the part over time to track the diffusion of heat through the part thickness. As the diffusion wave moves through the part, the inserts in the standards will cause disturbances in the otherwise approximately uniform heat flow. A few factors can influence the nature of the heat signature. If the insert has a different thermal conductivity than the part material, it will show as a hot spot (lower thermal conductivity) or cold spot (higher thermal conductivity) as it aids or hampers the diffusion of heat through the part. The inserts may also cause a significant delamination in the part, which has an insulating effect and will show as a hotter indication. With either case, the now disturbance in the originally uniform heat flow will be captured with the IR camera as a function of time.

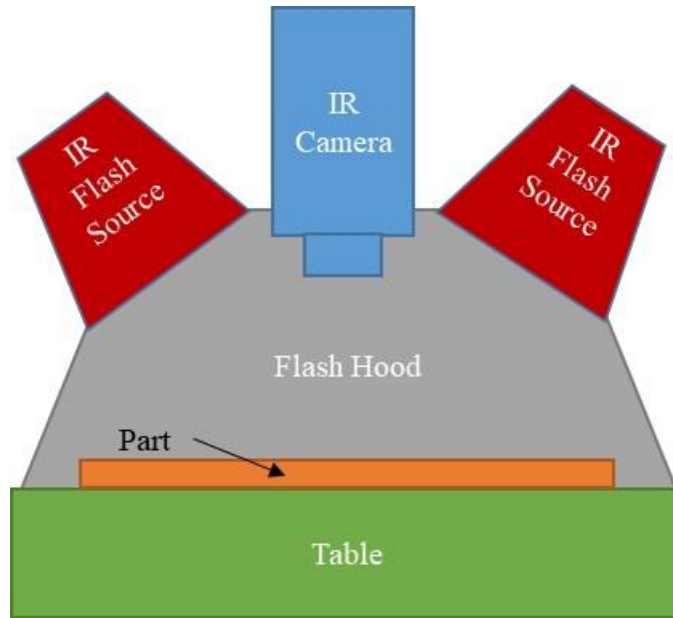


Figure E.35-9. Flash IRT system components.



Figure E.35-10. IR inspection system.

E.35.3.4 Equipment List and Specifications:

- SC6000 Series FLIR IR camera
- Flash lamps
- Flash hood

E.35.3.5 Settings

Table E.35-3. Imaging and exposure parameters.

Frame Rate	120 fps
Image Size	640 × 512 pixels
Capture Duration	5 sec
Camera Frequency	120 Hz
Flash Duration	<0.2 sec

E.35.3.6 Inspection Results

The Radii Delamination Standards are carbon fiber composite panels with foreign material inserts in various layers to evaluate the detectability using ultrasonic inspection. These inserts are largely grouped around the angle in the panel; however, not exclusive to this area. The standards vary in thickness, utilizing 8, 26, and 48 plies of carbon fiber fabric with exterior layers of fiberglass.

Because the flash heat diffuses through the thickness of the part, inserts at different layers should appear most clearly at varying times. This is observed in the lower image of Figure E.35-11, where only one set of inserts gives a thermal signature, because the thermal diffusion wave has not interacted with the deeper inserts yet. Similarly, the uppermost sets of inserts show the most clearly in the upper image. As the heat wave progresses through the material, the inserts heat up and cool faster than the surrounding material, leading to initially lighter indications followed by darker indications as time progresses. This is seen in the upper image where the PT inserts close to the surface have begun to cool faster (dark) while the lower inserts are heating up faster (light).

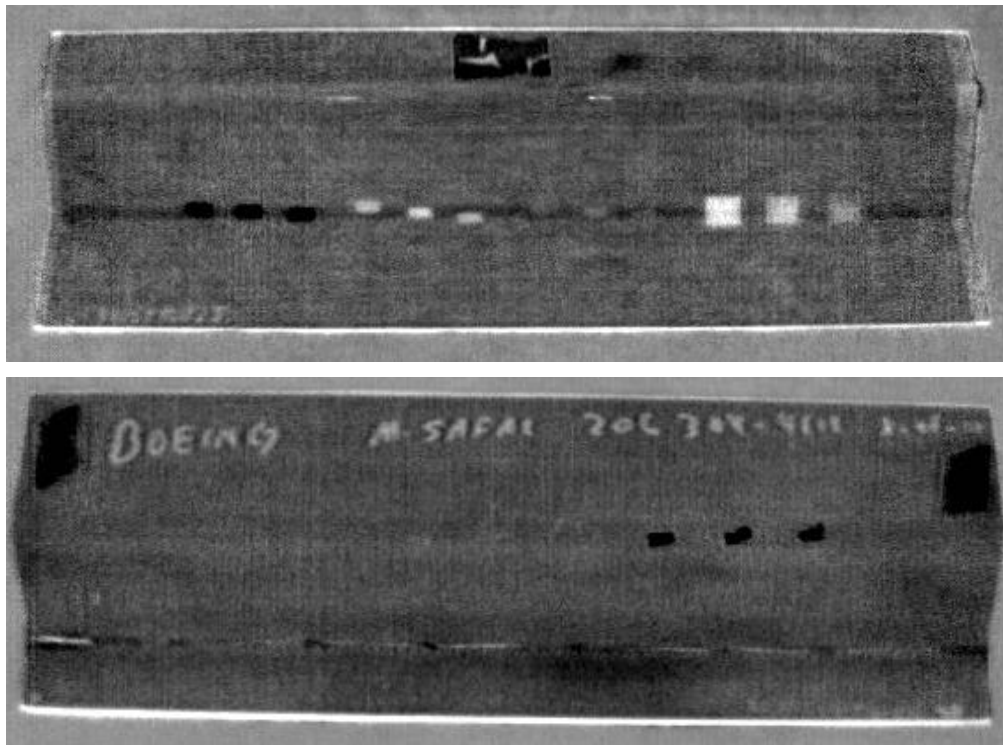


Figure E.35-11. Greyscale IR image of Radii Delamination Standard inserts (Top: PT and RPF, Bottom: brass)

E.35.4 Method: X-ray Digital Radiography (DR)

E.35.4.1 Partner: Boeing

E.35.4.2 Technique Applicability: ★☆☆

X-ray DR is capable of detecting the brass and RPF inserts but is unable to detect the PT inserts.

E.35.4.3 Laboratory Setup

The DRC utilizes an YXLON Modular CT System with DR capability. This system includes a microfocus source and a digital detector array with positions controlled by a manipulator system.

The microfocus source used has a variable focal spot size of less than four μm and is suitable for magnifications up to 10X. The manipulator has 7 DOF including a rotating stage to rotate the object as well as the ability to control its position along with the detector for magnification. The entire system includes the source, detector, manipulator, and user control station. The computers and control station are outside of the radiation enclosure (vault) and utilize a safety interlock system to operate. Cameras are located in the vault to allow the operator to monitor the part from outside the enclosure.

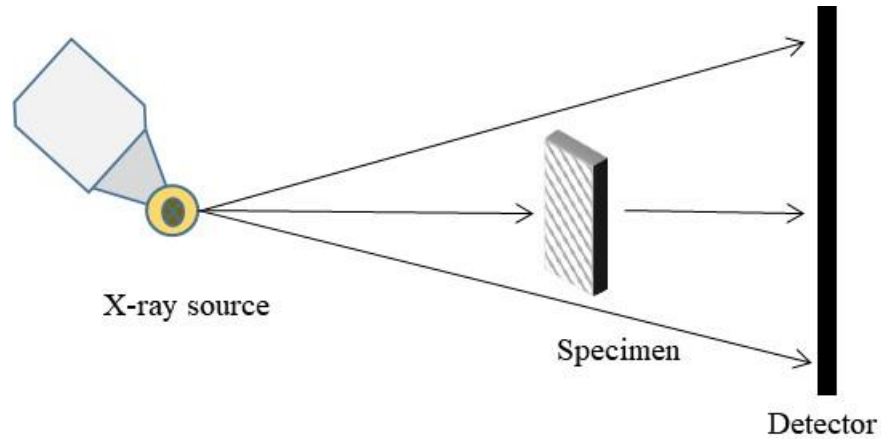


Figure E.35-12. X-ray DR imaging.

The standards were divided into two sections, labeled Upper and Lower, and placed on the rotator in a soft clamp (Figure E.35-13). The specimen was right side up for the Upper scan, and upside-down for the Lower scan. Lead markers were placed on the sections to denote the boundaries between and label sections. The position of the specimen, source, and detector are controlled to produce geometric magnification of the image and increase the spatial resolution while capturing the entire section of the part in the detector area. The image data are gathered as X-rays penetrate the part and expose the detector for a set amount of time to produce a frame; multiple frames are average to produce the final image. This image, viewed in Image 3500, has much lower noise levels than a single frame due to the averaging. The operator adjusts the brightness and contrast settings of the image to identify the inserts, seen in the 2D image as rectangular defects.



Figure E.35-13. Laboratory setup of angle plate standard for DR imaging.

E.35.4.4 Equipment List and Specifications:

- 225 kV microfocus X-ray source with variable focal spot size
- 100 kg capacity, 7-axis, granite-based manipulator
- XRD 1621 Detector – 2048 × 2 048 pixels with 200 μm pitch, 400 × 400 mm active area
- Image 3500 visualizing software

E.35.4.5 Settings

Table E.35-4. Imaging and exposure parameters.

Source Energy	100 kV
Current	0.7 mA
Source-Detector Distance	42 in
Source-Object Distance	27 in
Magnification	1.55X
Integration Time	500 ms
Integration Frames	50
Spatial Resolution (μm)	129 μm
Array Dimensions (pixels)	2048 × 2048

E.35.4.6 Inspection Results

The NASA Angle Panel Standards are carbon fiber composite panels with foreign material inserts in various layers to evaluate the detectability using ultrasonic inspection. These inserts are largely grouped around the angle in the panel; however, not exclusive to this area. The standards vary in thickness, utilizing 8, 26, and 48 plies of carbon fiber fabric with exterior layers of fiberglass. Because of their length, the data set consists of the upper and lower half images of the standards.

DR X-ray imaging is sensitive to density variations, caused by material differences, voids, or other defects affecting the density of material the X-rays pass through. Because this imaging is 2D, the results are superimposed internal images of the specimens. The resulting digital images are 16-bit greyscale images with the greyscale values representing the material density at each location (lighter corresponding to denser regions). Using Image 3500, the brightness and contrast settings vary to make defects visible. In the standards, the inserts show as rectangular areas with darker values (positive image).

The RPF insert is detectable in this laminate thickness (Figures E.35-14, E.35-15b). However, the PT inserts are not detectable (Figure E.35-15a). Because the densities of the carbon fiber base material and the inserts are similar, a single-ply insert does not create a large density variation, thereby limiting the detectability. This detectability also drops as the laminate increases in thickness. The brass inserts, however, cause a very large density variation and are readily observable in all laminate thicknesses (Figure E.35-15c). Metal FOD in composite structures often show this degree of detectability due to the relatively high density of the metal compared to the composite.

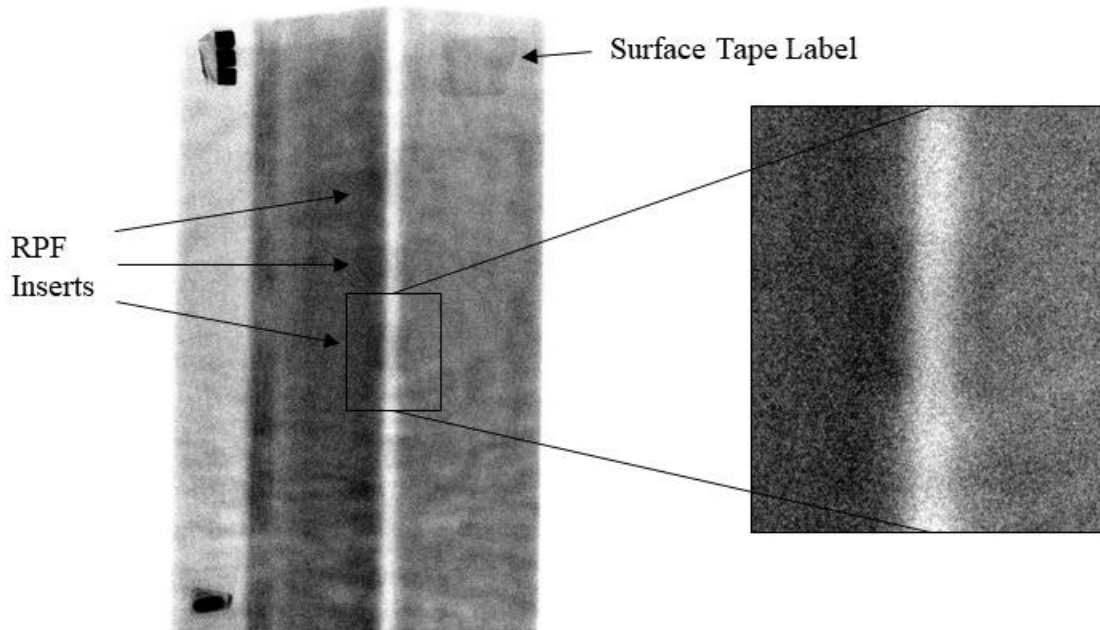


Figure E.35-14. DR Image of RPF inserts with close up.

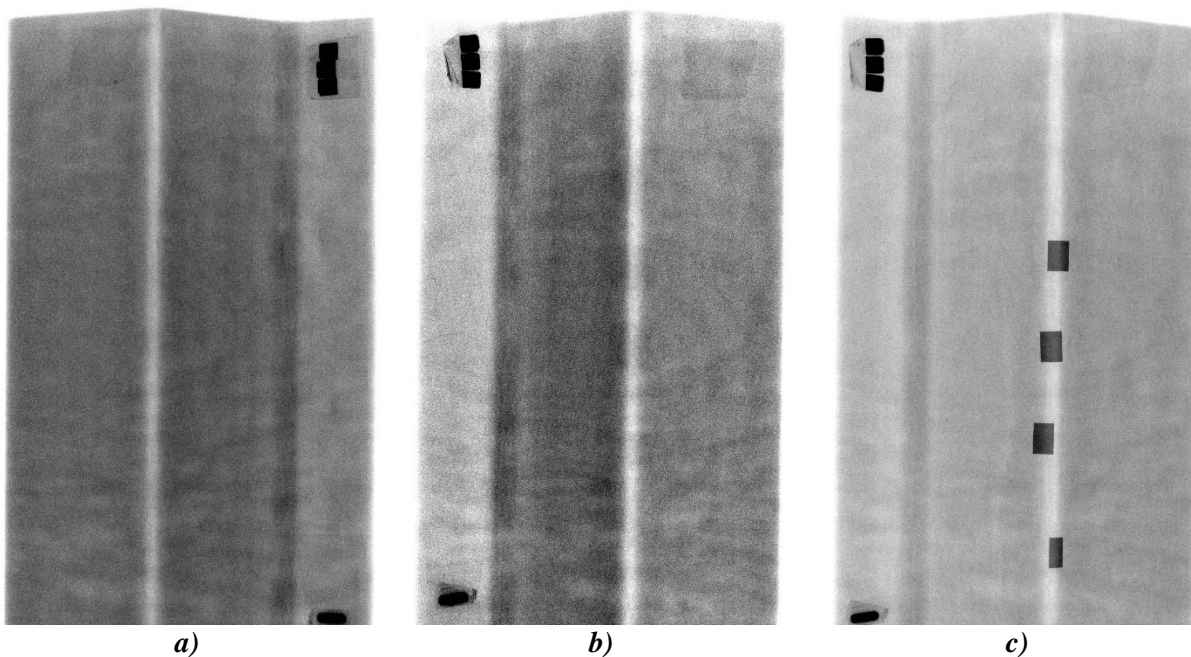


Figure E.35-15. DR images of PT (a), RPF (b), and brass (c) insert locations in 8276-200-58-8 standard.

E.35.5 Method: X-ray Computed Radiography (CR)

E.35.5.1 Partner: Boeing

E.35.5.2 Technique Applicability: ★☆☆

X-ray CR is capable of detecting the RPF and brass inserts but is unable to detect the PT inserts.

E.35.5.3 Laboratory Setup

The DRC has a small X-ray enclosure (vault) for the primary purpose of 2D X-ray imaging. It includes a Philips 160 kV X-ray source and the ability to use film, CR, and digital detector arrays. The CR imaging plates are placed on a table and the source, suspended from the ceiling by a 3-axis crane, can be positioned to control the Source to Object Distance. Outside of the enclosure are the controls for the source, utilizing a safety interlock system. These controls allow the user to set the energy, current, and exposure time for the source. In addition to the vault, the DRC utilizes a CRxFlex system to scan and erase the CR imaging plates, storing the images on a computer. The phosphorus imaging plates, after exposure to X-rays, will luminesce the images when exposed to blue light, allowing the 50- μm scanner to create digital versions and “erase” the plates using bright white light to be used again. The CR digital images are then reviewed using Rhythm Review.

The standards were divided into two sections, labeled Upper and Lower, and placed directly on the plastic cassette containing the imaging plate with the X-ray source directly overhead (Figure E.35.16). The source was located 60 inches from the specimen and imaging plate to reduce geometric distortion. Lead markers were used to show section boundaries and label the images, showing up in the results as bright white. Because of the large differences in laminate thicknesses between the specimens, three separate source energies were used, with the highest energy for the thickest specimens.

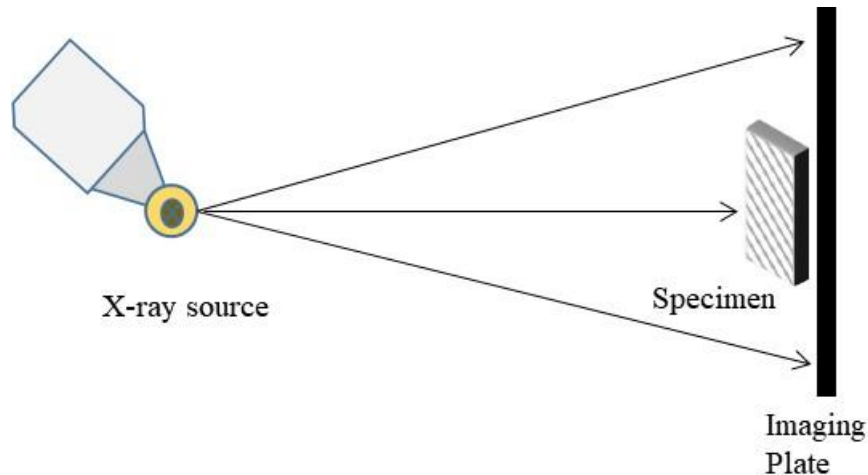


Figure E.35-16. X-ray CR imaging.

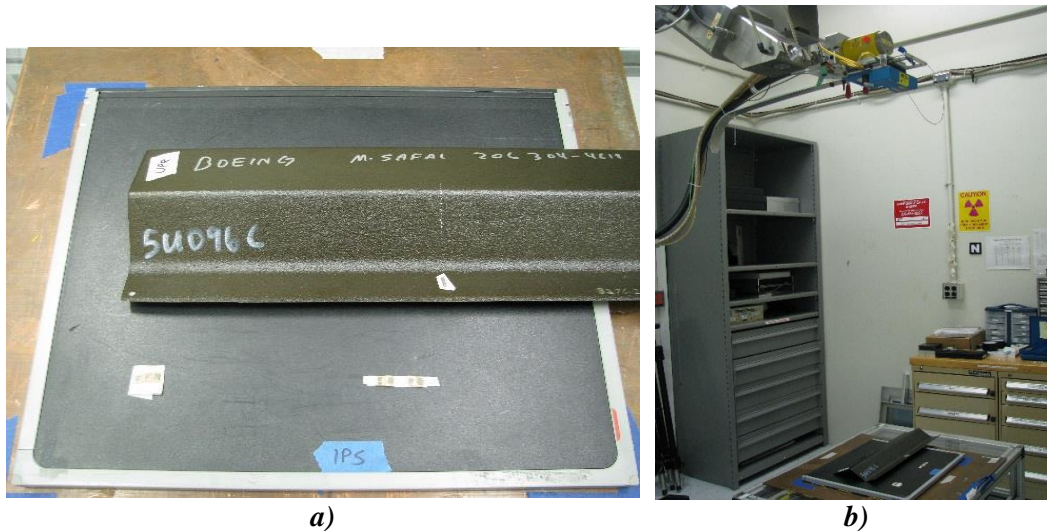


Figure E.35-17. Laboratory setup of angle plate standards for CR imaging.

E.35.5.4 Equipment List and Specifications:

- Philips 160 kV X-ray source, 0.4 mm focal spot size
- IPS Phosphorus Imaging Plate
- GE CRxFlex Scanner, 50 μm resolution
- GE Rhythm Review 5.0 visualizing software

E.35.5.5 Settings

Table E.35-5. Imaging and Exposure Parameters

Source Energy	30,40,50 kV
Current	10 mA
Source-Detector Distance	60 in
Magnification	1X
Exposure time	10 s
Resolution (μm)	50 μm
Imaging Area (in)	14 \times 17

E.35.5.6 Inspection Results

The NASA Angle Panel Standards are carbon fiber composite panels with foreign material inserts in various layers to evaluate the detectability using ultrasonic inspection. These inserts are largely grouped around the angle in the panel; however, not exclusive to this area. The standards vary in thickness, utilizing 8, 26, and 48 plies of carbon fiber fabric with exterior layers of fiberglass. Because of their length, the data set consists of the upper and lower half images of the standards.

CR X-ray imaging is sensitive to density variations, caused by material differences, voids, or other defects effecting the density of material the X-rays pass through. Because this imaging is 2D, the results are superimposed internal images of the specimens. The resulting digital images are 16-bit greyscale images with the greyscale values representing the material density at each location (lighter corresponding to denser regions). Using Rhythm Review, the brightness and contrast settings vary to make defects visible. In addition, multiple filters are available to make defect identification easier for the operator. In the standards, the inserts show as rectangular areas with lighter values (negative image).

The RPF insert is detectable in this laminate thickness (Figure E.35-18 and Figure E.35-19b); however, the PT inserts are not detectable (Figure E.35-19a). Because the densities of the carbon fiber base material and the inserts are similar, a single-ply insert does not create a large density variation, thereby limiting the detectability. The brass inserts, however, cause a very large density variation and are readily observable in all laminate thicknesses (Figure E.35-19c). Metal FOD in composite structures often show this degree of detectability due to the relatively high density of the metal compared to the composite.

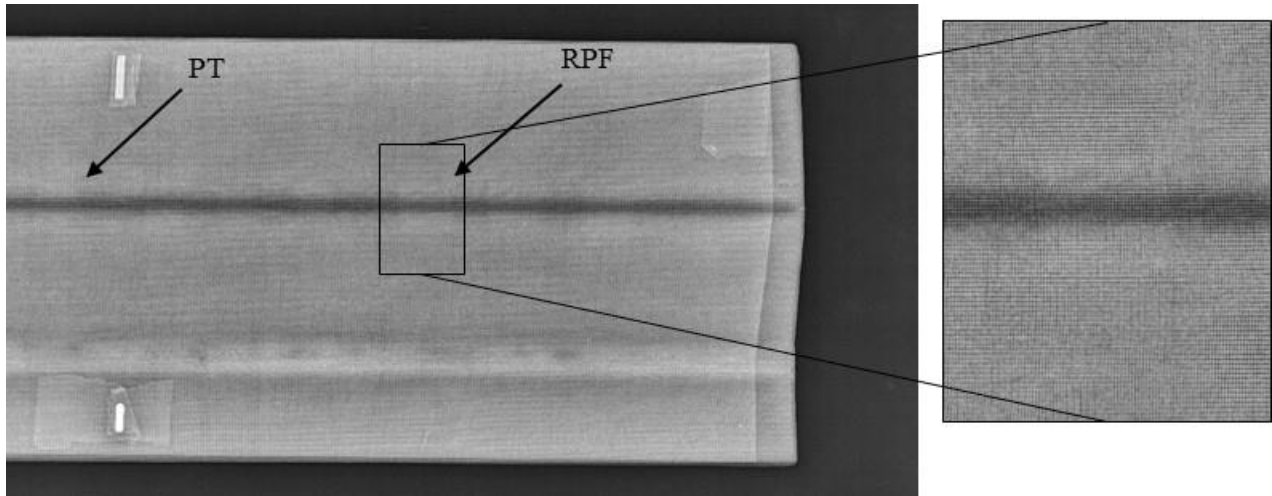


Figure E.35-18. CR image of RPF inserts with close up (filter applied).

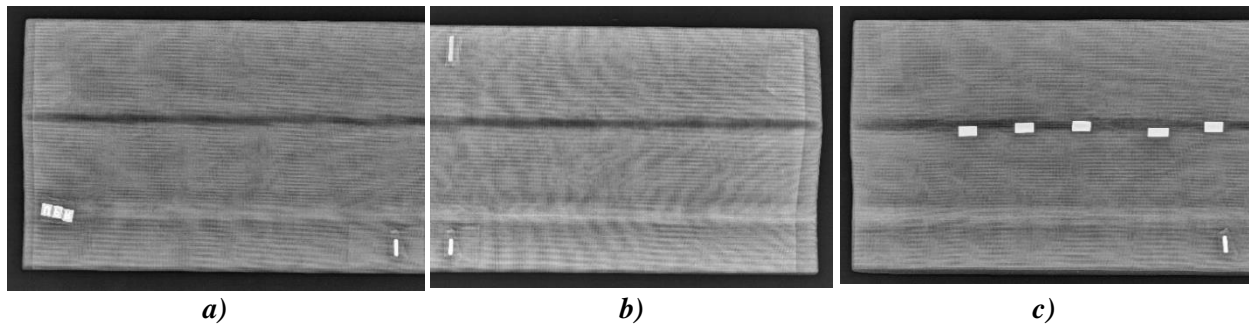


Figure E.35-19. CR images of PT (a), RPF (b), and brass (c) insert locations for 8276-200-58-8 standard (filter applied).

Structure	Material	Details	Dimensions (inches)	Partner Methods
26 fabric plies 2 fiberglass plies	BMS8-276 BMS8-331	58° Curve with 0.2-inch radius Brass, RPF and PT inserts at varying depths	24 × 6.5	Boeing E.36.3 XCT E.36.4 TTUT E.36.5 SSIR E.36.6 X-ray DR E.36.7 X-ray CR E.36.8 Backscatter

E.36 Specimen #36: Boeing 8276-200-58-26A

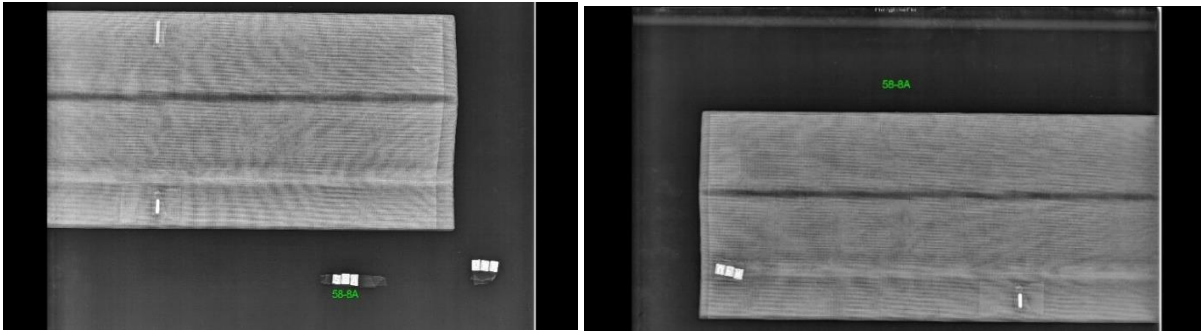


Figure E.36-1. Photographs of Angle Panel Reference Standard.

E.36.1 Method: X-ray Computed Tomography (XCT)

E.36.1.1 Partner: Boeing

E.36.1.2 Technique Applicability: ★★★

XCT is capable of identifying all inserts, notably brass inserts.

E.36.1.3 Laboratory Setup

The DRC utilizes an YXLON Modular CT System. This system has the capability to utilize various X-ray sources for varying applications, including a 450-kV source, a microfocus source, and a nanofocus source. The microfocus source used has a variable focal spot size of less than four μm and is suitable for magnifications up to 10X, with the nanofocus ranging up to 187X. The detector has 3 DOF, allowing for increase in the effective detector area through combined scans. The manipulator controls the position of the detector, object, and source. It has 7 DOF including a rotating stage to rotate the object during the scan. The entire system includes the source, detector, manipulator, control and reconstruction computers, and user control station. The computers and control station are outside of the radiation enclosure (vault) and utilize a safety interlock system to operate. Cameras are located in the vault to allow the operator to monitor the part from outside the enclosure.

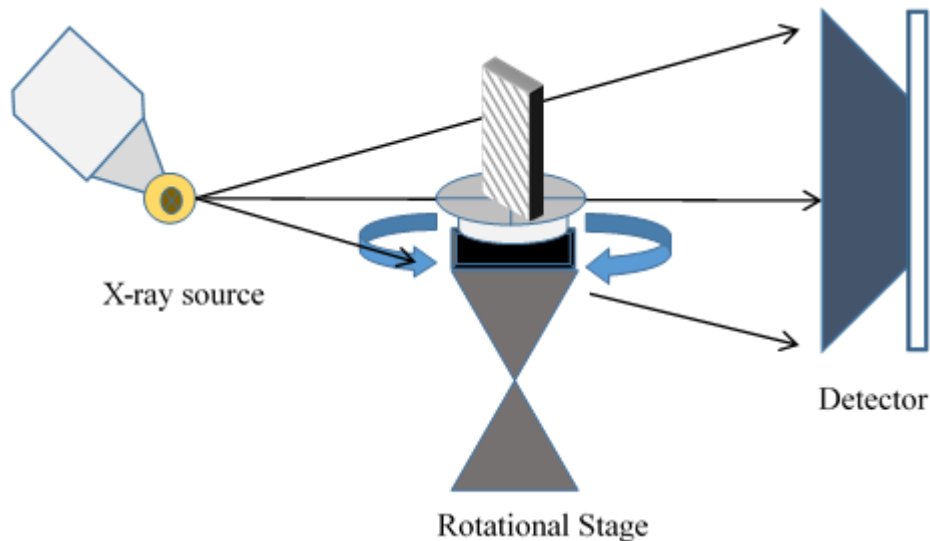


Figure E.36-2. XCT system components.

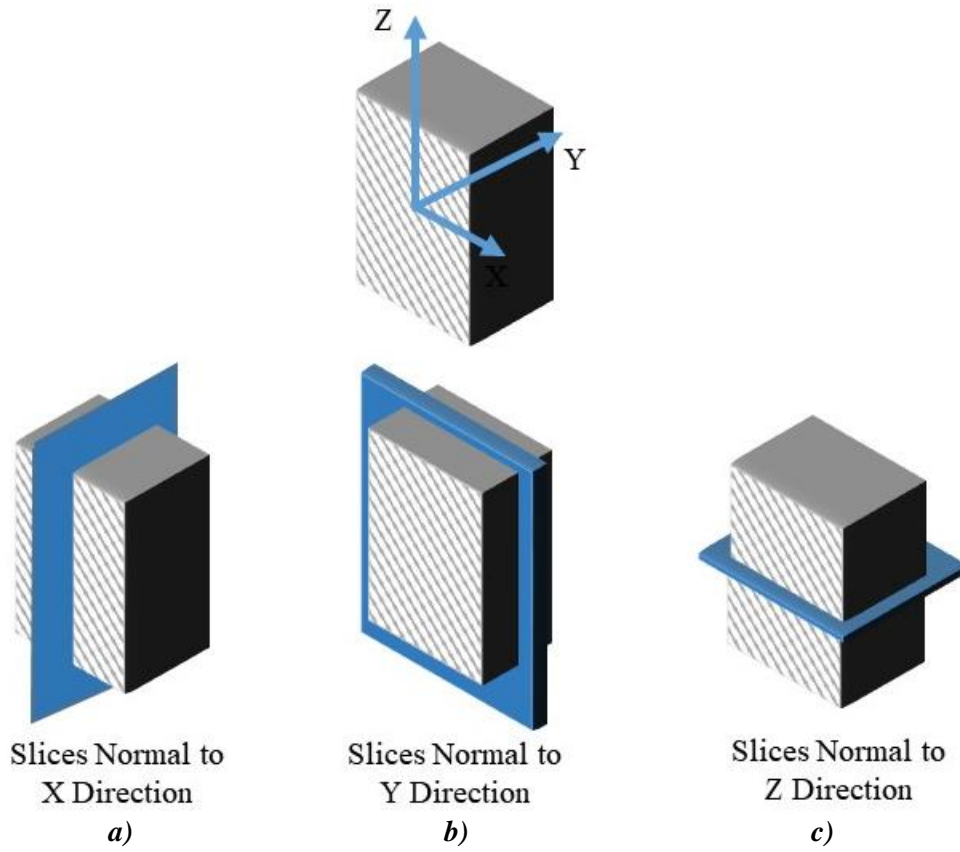


Figure E.36-3. Slice direction nomenclature.

The standards were divided into two sections, labeled Upper and Lower, and placed on the rotator in a soft clamp (Figure E.36-4). The specimen was right side up for the Upper scan, and upside-down for the Lower scan. Plastic markers, which show up in 3D reconstruction, were placed on the sections to denote the boundaries between sections. The position of the specimen, source, and detector are controlled to produce geometric magnification of the image and increase the spatial resolution. The image data are gathered as X-rays penetrate the part and expose the detector for a set amount of time. For each scan, these image data are collected at 1080 different angles throughout a 360° rotation. These images are then reconstructed to create the 3D volume data set. This data set is viewed and analyzed in Volume Graphics, a volume rendering software, to identify the relevant components.

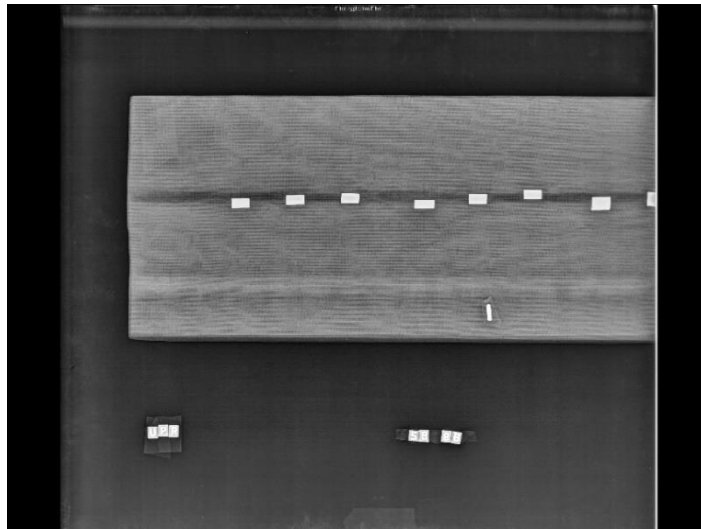


Figure E.36-4. Microfocus XCT setup for Radii Delamination Standard.

E.36.1.4 Equipment List and Specifications:

- YXLON Modular CT System
- 225 kV microfocus X-ray source with variable focal spot size
- 100 kg capacity, 7-axis, granite-based manipulator
- XRD 1621 Detector – 2048 × 2048 pixels with 200 μm pitch, 400 × 400 mm active area
- 126 μm spatial resolution for half volume scan
- Volume Graphics 3.0 visualizing software
- Reconstruction Computer

E.36.1.5 Settings

Table E.36-1. Data collection settings.

Source Energy	205 kV
Current	0.47 mA
Magnification	1.59 X
Filter	Copper
# Rotational angles	1080
Exposure time/frame	800 ms
Spatial Resolution (μm)	125.777 μm
Array Dimensions (pixels)	2048 × 2048

E.36.1.6 Inspection Results

The Radii Delamination Standards are carbon fiber composite panels with foreign material inserts in various layers to evaluate the detectability using ultrasonic inspection. These inserts are largely grouped around the angle in the panel; however, not exclusive to this area. The standards vary in thickness, utilizing 8, 26, and 48 plies of carbon fiber fabric with exterior layers of fiberglass. Because of their length, the data set consists of the upper and lower half volumes of the standards, flipped 180° for the scan.

After aligning the volume coordinate system to correspond with the panel geometry, the slice view is used to inspect conditions at each lamina. The brightness and contrast settings are also adjusted to make defects clear, but retain the visible noise at a reasonable level. The inserts are clearly

visible (Figure E.36-5), showing with less density for PT and RPF and higher density for brass. The brass is the most readily observable, followed by the PT with the RPF having the lowest detectability. The RPF may show the least response due to similar density to base material or due to a strong interface with little voiding or delamination to be detected.

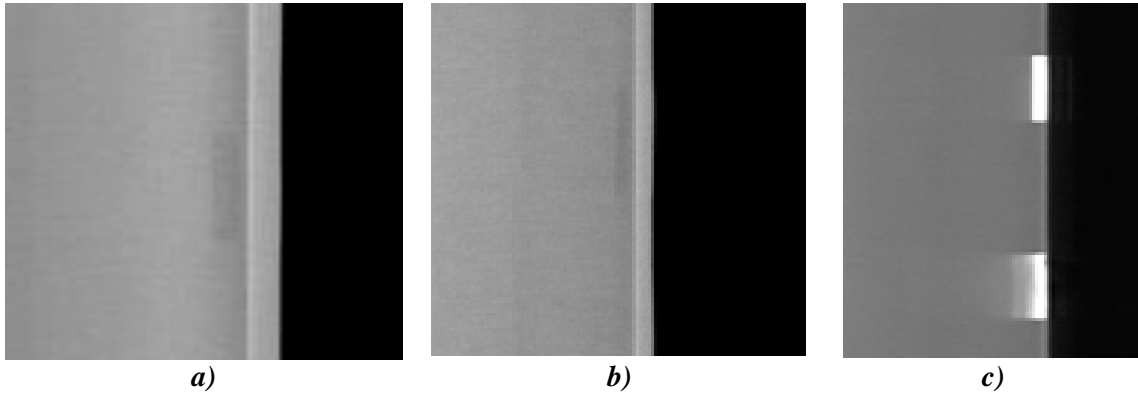


Figure E.36-5. CT slice view showing PT (a), RPF (b), and brass (c) inserts.

The CT scanning and reconstruction process is subject to artificial and undesirable artifacts. These are the result of multiple conditions. The direction of rotation leaves an underlying direction to the noise of the data set, aligning with the rotation. This is seen as a light, roughly horizontal streaking seen in (Figure E.36-5). The presence of high-density material in an otherwise low-density structure often creates even more intense ray artifacts, seen as shadow-like streaks emanating from the high-density material (Figure E.36-5c). If defects are present in these dark artifacts, their detectability is reduced. Lastly, the part may rotate in and out of the cone-beam of the X-rays during the scan, leaving the top and bottom edges of the volume not fully defined. This is seen as darker “wedges” of the volume at the top and bottom of the data set (Figure E.36-5).

The detectability of the inserts relies on viewing the slices at the appropriate angle, which aligns with the lamina. This means the inserts within the curve of the panel, while still detectable, are less apparent (Figure E.36-6), and operators must be careful to attempt to identify them. The inserts are also more visible when they induce delamination with air or if they have a much greater density than the composite material.

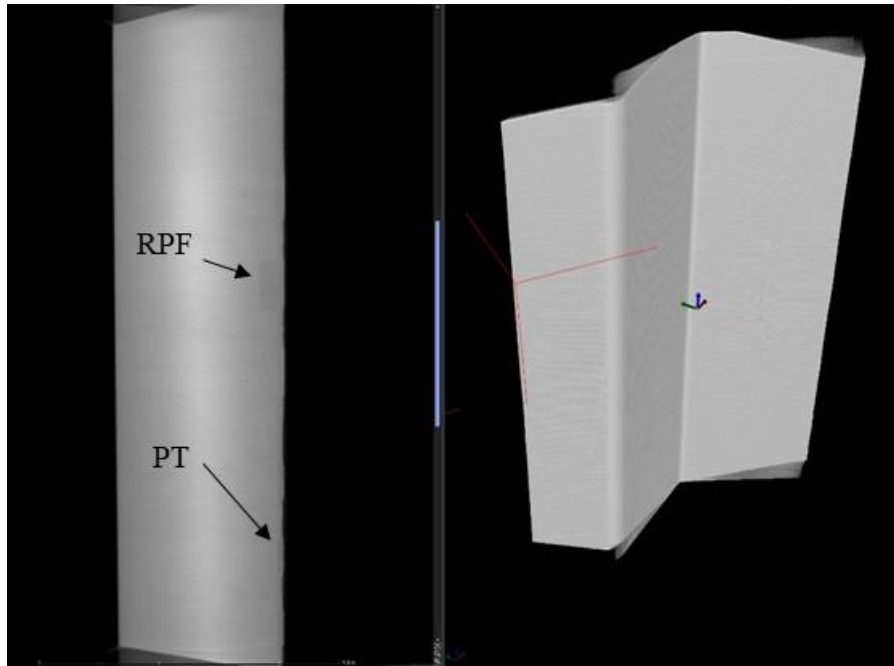


Figure E.36-6. CT slice view showing PT and RPF inserts.

E.36.2 Method: Through-Transmission Ultrasound Testing (TTUT)

E.36.2.1 Partner: Boeing

E.36.2.2 Technique Applicability: ★★★

All inserts are visually detectable with TTUT data.

E.36.2.3 Laboratory Setup

The TTUT scanner at the Boeing laboratory consists of an enclosure, part supports, a water pump and nozzle system, ultrasonic transducers (transmitter and receiver), robotic manipulator, and control computer. After adjusting the water to produce a uniform flow, the pulser and receiver (on opposite sides of the specimen) perform a C-scan under the control of the robotic manipulator and control computer. The C-scan is produced by taking multiple 1-dimensional scans (A-scans) and stitching them together to produce the final area result.

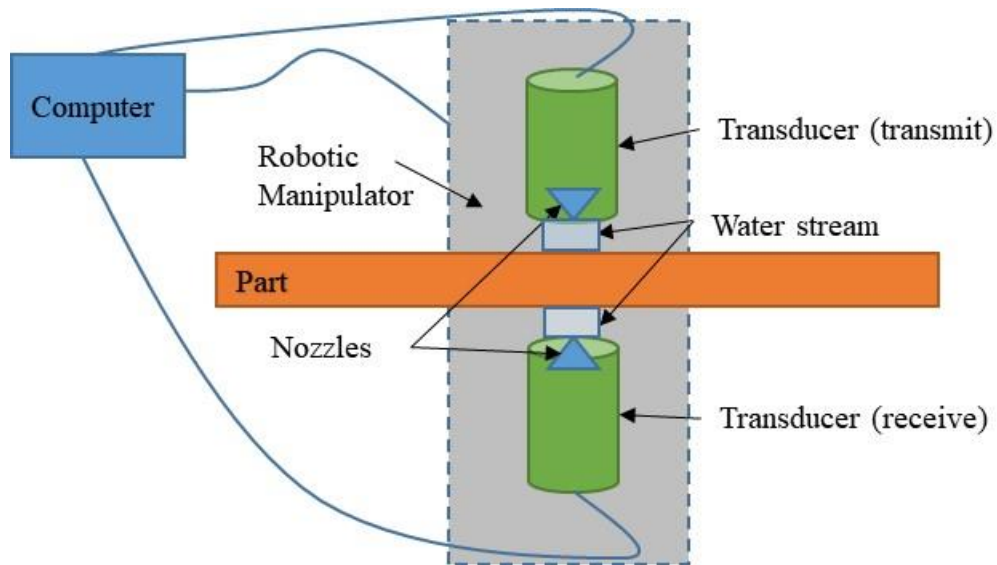


Figure E.36-7. TTU Scanning schematic with water pump.

TTUT works on the principal of the capture and quantification of the transmitted waves. It uses a pulsing transducer on one side of the part and has the receiving transducer on the opposite side of the part. Scanning can be accomplished with contact, water streams, or full immersion method, as long as sufficient ultrasonic coupling is used. Although the TTUT works on non-parallel, front-to-back surface the optimized data are produced when the front-to-back surfaces are parallel to each other.

As the ultrasonic waves travel through a material, they are attenuated. Defects and material discontinuities such as delamination, porosity and foreign material interfaces cause increased attenuation. UT has an orientation dependency, where certain defect orientations will attenuate the signal more if they are oriented for maximum reflection. Delamination tend to be oriented favorably for detection, making ultrasound the common method for composite inspection.

E.36.2.4 Equipment List and Specifications:

- 1 MHz ultrasonic transducer and receiver
- Water pump, nozzles, and circulation system
- Robotic manipulator
- Enclosure
- Control computer

E.36.2.5 Settings

Table E.36-2. Data collection settings.

Frequency	1 MHz
Resolution	0.04 inch × 0.04 inch

E.36.2.6 Inspection Results

The NASA Radii Delamination Standards are carbon fiber composite panels with foreign material inserts in various layers to evaluate the detectability using ultrasonic inspection. These inserts are largely grouped around the angle in the panel; however, not exclusive to this area. The standards vary in thickness, utilizing 8, 26, and 48 plies of carbon fiber fabric with exterior layers of

fiberglass. Using TTUT, the all insert types (PT, RPF, and brass) were detectable. However, this visual detectability generally reduced as thickness increased.

The brass inserts were the most resolved and detected (Figure E.36-8c) and the RPF inserts showed the lowest detectability (Figure E.36-8b). This is consistent with the theory that the RPF inserts bond to the material the best, leading to a small TTUT signal, while the brass has the worst bond (likely due to applied coating), leading to the large signals seen. The brass also has a significantly different attenuation than the surrounding material, allowing easy detection. The 48 ply standards included inserts in locations on and away from the curved radius. The inserts away from the radius tended to be better resolved and defined (Figure E.36-8) due to the more uniform background signal. While the RPF inserts had small responses and resolving their exact shape is difficult, their presence tended to be detectable in the distortion of the surrounding signal and features (Figure E.36-8b).

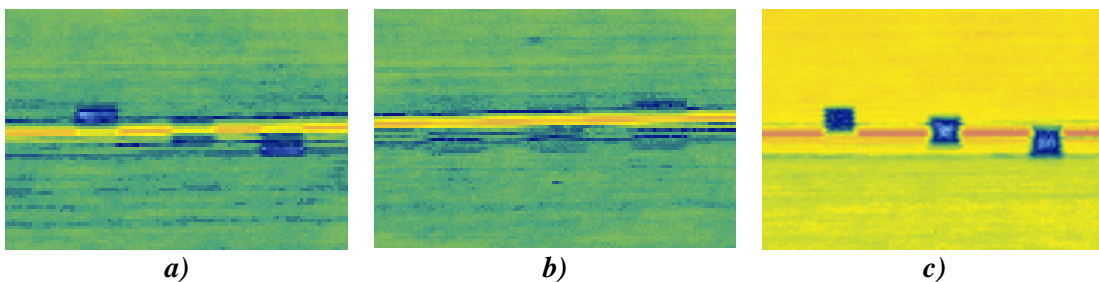


Figure E.36-8. TTUT scans showing PT (a), RPF (b), and brass (c) inserts.

E.36.3 Method: Single-Sided Infrared Thermography (SSIR)

E.36.3.1 Partner: Boeing

E.36.3.2 Technique Applicability: ★★☆☆

SSIR can detect all insert types in the radii standard.

E.36.3.3 Laboratory Setup

For each inspection, the part was placed in the IR imaging system (Figure E.36-9). For each test, the flash lamp fires, heating the surface of the part uniformly. The IR camera records the heat signature of the part over time to track the diffusion of heat through the part thickness. As the diffusion wave moves through the part, the inserts in the standards will cause disturbances in the otherwise approximately uniform heat flow. A few factors can influence the nature of the heat signature. If the insert has a different thermal conductivity than the part material, it will show as a hot spot (lower thermal conductivity) or cold spot (higher thermal conductivity) as it aids or hampers the diffusion of heat through the part. The inserts may also cause a significant delamination in the part, which has an insulating effect and will show as a hotter indication. With either case, the now disturbance in the originally uniform heat flow will be captured with the IR camera as a function of time.

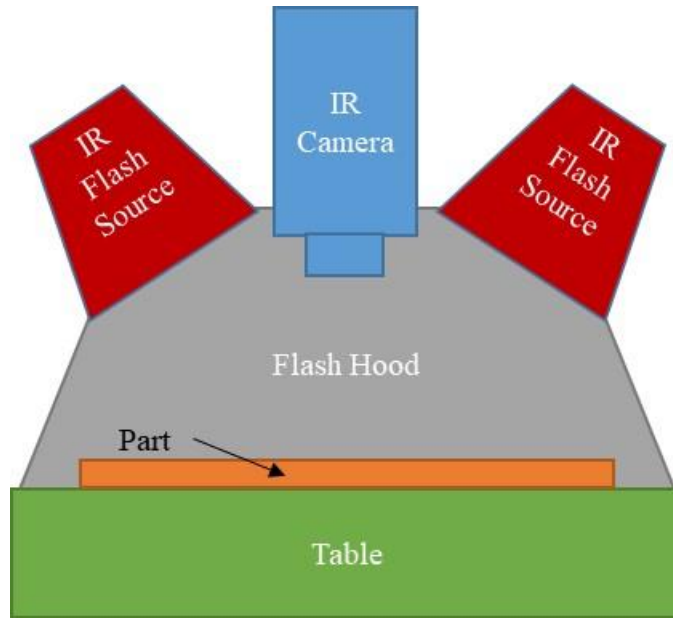


Figure E.36-9. Flash IRT system components.



Figure E.36-10. IR inspection system.

E.36.3.4 Equipment List and Specifications:

- SC6000 Series FLIR IR camera
- 6400 Watt-sec flash lamps
- Flash Hood

E.36.3.5 Settings

Table E.36-3. Imaging and exposure parameters.

Frame Rate	120 fps
Image Size	640 × 512 pixels
Capture Duration	5 sec
Camera Frequency	120 Hz
Flash Duration	<0.2 sec

E.36.3.6 Inspection Results

The Radii Delamination Standards are carbon fiber composite panels with foreign material inserts in various layers to evaluate the detectability using ultrasonic inspection. These inserts are largely grouped around the angle in the panel; however, not exclusive to this area. The standards vary in thickness, utilizing 8, 26, and 48 plies of carbon fiber fabric with exterior layers of fiberglass.

Because the flash heat diffuses through the thickness of the part, inserts at different layers should appear most clearly at varying times. This is observed in the lower image of Figure E.36-11, where one set of inserts gives a significant thermal signature while the others are just starting to show, because the thermal diffusion wave has not interacted with the deeper inserts yet. Similarly, the uppermost sets of inserts show the most clearly in the upper image. As the heat wave progresses through the material, the inserts heat up and cool faster than the surrounding material, leading to initially lighter indications followed by darker indications as time progresses. This is seen in the upper image where the PT inserts close to the surface have begun to cool faster (dark) while the lower inserts are heating up faster (light).

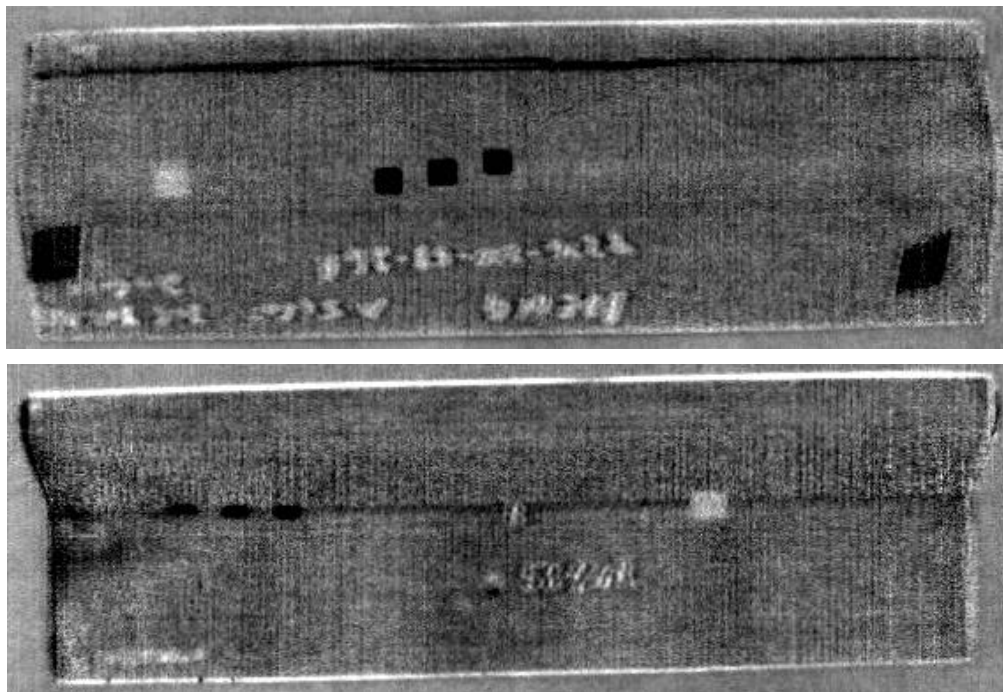


Figure E.36-11. Greyscale IR image of Radii Delamination Standard inserts (Top: PT and RPF, Bottom: brass).

E.36.4 Method: X-ray Digital Radiography (DR)

E.36.4.1 Partner: Boeing

E.36.4.2 Technique Applicability: ★☆☆

X-ray DR is capable of detecting the brass inserts but is unable to detect the RPF or PT inserts.

E.36.4.3 Laboratory Setup

The DRC utilizes an YXLON Modular CT System with Digital Radiography capability. This system includes a microfocus source and a digital detector array with positions controlled by a manipulator system. The microfocus source used has a variable focal spot size of less than four

μm and is suitable for magnifications up to 10X. The manipulator has 7 DOF including a rotating stage to rotate the object as well as the ability to control its position along with the detector for magnification. The entire system includes the source, detector, manipulator, and user control station. The computers and control station are outside of the radiation enclosure (vault) and utilize a safety interlock system to operate. Cameras are located in the vault to allow the operator to monitor the part from outside the enclosure.

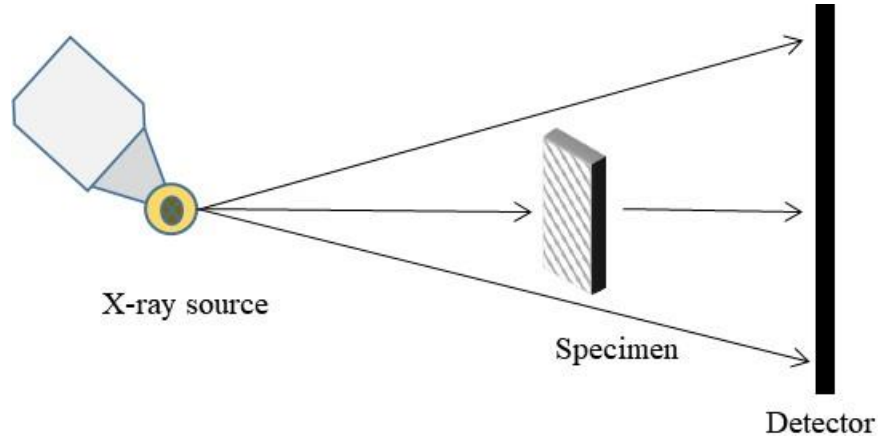


Figure E.36-12. X-ray DR imaging.

The standards were divided into two sections, labeled Upper and Lower, and placed on the rotator in a soft clamp (Figure E.36-13). The specimen was right side up for the Upper scan, and upside-down for the Lower scan. Lead markers were placed on the sections to denote the boundaries between and label sections. The position of the specimen, source, and detector are controlled to produce geometric magnification of the image and increase the spatial resolution while capturing the entire section of the part in the detector area. The image data are gathered as X-rays penetrate the part and expose the detector for a set amount of time to produce a frame; multiple frames are average to produce the final image. This image, viewed in Image 3500, has much lower noise levels than a single frame due to the averaging. The operator adjusts the brightness and contrast settings of the image to identify the inserts, seen in the 2D image as rectangular defects.



Figure E.36-13. Laboratory setup of angle plate standard for DR imaging.

E.36.4.4 Equipment List and Specifications:

- 225 kV microfocus X-ray source with variable focal spot size
- 100 kg capacity, 7-axis, granite-based manipulator
- XRD 1621 Detector – 2048 × 2048 pixels with 200 μm pitch, 400 × 400 mm active area
- Image 3500 visualizing software

E.36.4.5 Settings

Table E.36-4. Imaging and exposure parameters.

Source Energy	100 kV
Current	0.7 mA
Source-Detector Distance	42 in
Source-Object Distance	27 in
Magnification	1.55X
Integration Time	500 ms
Integration Frames	50
Spatial Resolution (μm)	129 μm
Array Dimensions (pixels)	2048 × 2048

E.36.4.6 Inspection Results

The NASA Angle Panel Standards are carbon fiber composite panels with foreign material inserts in various layers to evaluate the detectability using ultrasonic inspection. These inserts are largely grouped around the angle in the panel; however, not exclusive to this area. The standards vary in thickness, utilizing 8, 26, and 48 plies of carbon fiber fabric with exterior layers of fiberglass. Because of their length, the data set consists of the upper and lower half images of the standards.

DR X-ray imaging is sensitive to density variations, caused by material differences, voids, or other defects affecting the density of material the X-rays pass through. Because this imaging is 2D, the results are superimposed internal images of the specimens. The resulting digital images are 16-bit greyscale images with the greyscale values representing the material density at each location (lighter corresponding to denser regions). Using Image 3500, the brightness and contrast settings vary to make defects visible. In the standards, the inserts show as rectangular areas with darker values (positive image).

The PT and RPF inserts are undetectable in this laminate thickness (Figure E.36-14a, b). Because the densities of the carbon fiber base material and the inserts are similar, a single-ply insert does not create a large density variation, thereby limiting the detectability. This detectability also drops as the laminate increases in thickness. The brass inserts, however, cause a very large density variation and are readily observable in all laminate thicknesses (Figure E.36-14c). Metal FOD in composite structures often show this degree of detectability due to the relatively high density of the metal compared to the composite.

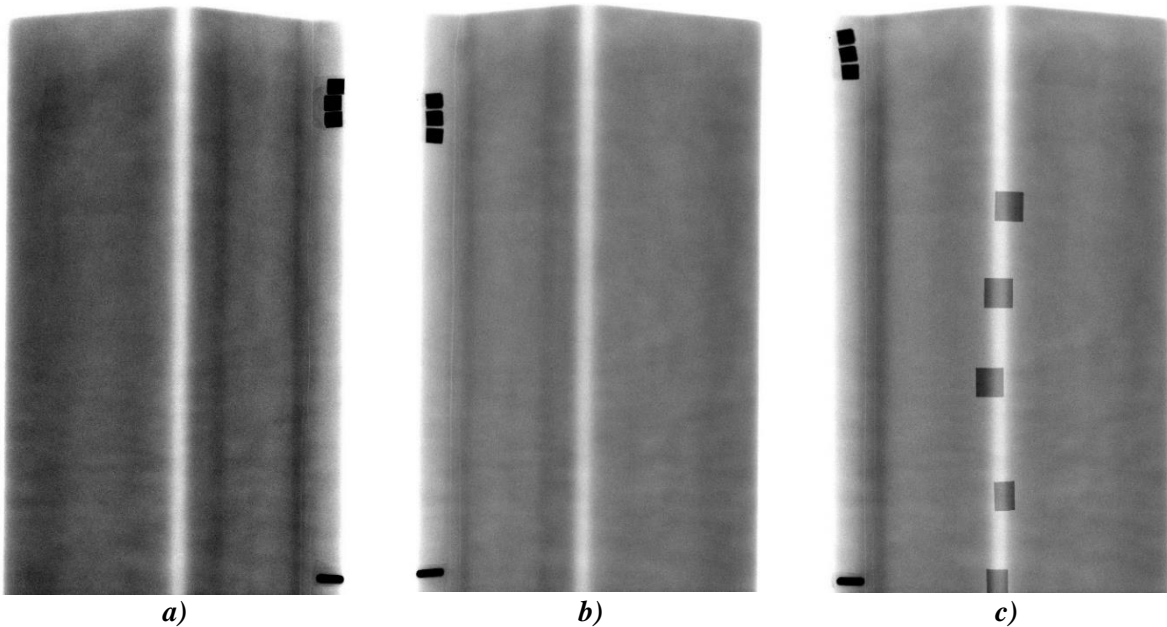


Figure E.36-14. DR images of PT (a), RPF (b), and brass (c) insert locations in 8276-200-58-26 standard.

E.36.5 Method: Computed Radiography (CR)

E.36.5.1 Partner: Boeing

E.36.5.2 Technique Applicability: ★☆☆

X-ray CR is capable of detecting the brass inserts but is unable to detect the PT and RPF inserts.

E.36.5.3 Laboratory Setup

The DRC has a small X-ray enclosure (vault) for the primary purpose of 2D X-ray imaging. It includes a Philips 160-kV X-ray source and the ability to use film, CR, and digital detector arrays. The CR imaging plates are placed on a table and the source, suspended from the ceiling by a 3-axis crane, can be positioned to control the Source to Object Distance. Outside of the enclosure are the controls for the source, utilizing a safety interlock system. These controls allow the user to set the energy, current, and exposure time for the source. In addition to the vault, the DRC utilizes a CRxFlex system to scan and erase the CR imaging plates, storing the images on a computer. The phosphorus imaging plates, after exposure to X-rays, will luminesce the images when exposed to blue light, allowing the 50- μ m scanner to create digital versions and “erase” the plates using bright white light to be used again. The CR digital images are then reviewed using Rhythm Review.

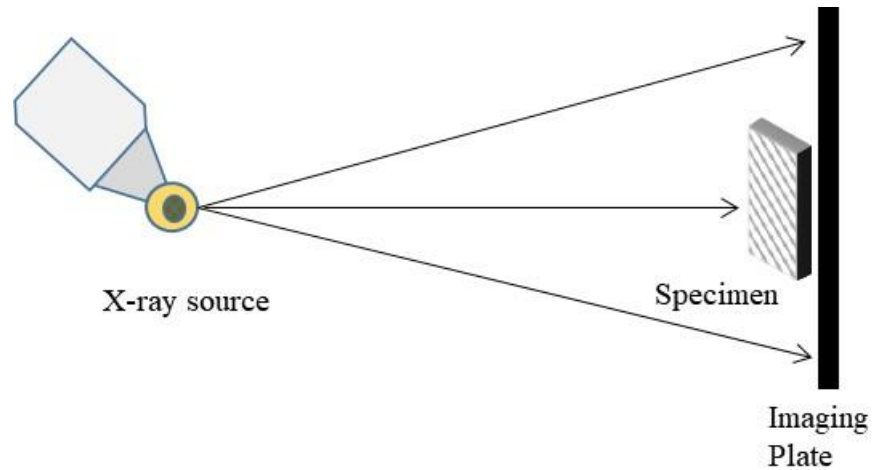
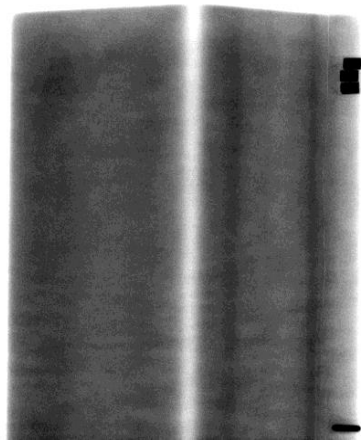


Figure E.36-15. X-ray CR imaging.

The standards were divided into two sections, labeled Upper and Lower, and placed directly on the plastic cassette containing the imaging plate with the X-ray source directly overhead (Figure E.36-15). The source was located 60 inches from the specimen and imaging plate to reduce geometric distortion. Lead markers were used to show section boundaries and label the images, showing up in the results as bright white. Because of the large differences in laminate thicknesses between the specimens, three separate source energies were used, with the highest energy for the thickest specimens.



a)



b)

Figure E.36-16. Laboratory setup of angle plate standards for CR imaging.

E.36.5.4 Equipment List and Specifications:

- Philips 160 kV X-ray source, 0.4 mm focal spot size
- IPS Phosphorus Imaging Plate
- GE CRxFlex Scanner, 50 μm resolution
- GE Rhythm Review 5.0 visualizing software

E.36.5.5 Settings

Table E.36-5. Imaging and exposure parameters.

Source Energy	30,40,50 kV
Current	10 mA
Source-Detector Distance	60 in
Magnification	1X
Exposure time	10 s
Resolution (μm)	50 μm
Imaging Area (in)	14 \times 17

E.36.5.6 Inspection Results

The NASA Angle Panel Standards are carbon fiber composite panels with foreign material inserts in various layers to evaluate the detectability using ultrasonic inspection. These inserts are largely grouped around the angle in the panel; however, not exclusive to this area. The standards vary in thickness, utilizing 8, 26, and 48 plies of carbon fiber fabric with exterior layers of fiberglass. Because of their length, the data set consists of the upper and lower half images of the standards.

CR X-ray imaging is sensitive to density variations, caused by material differences, voids, or other defects effecting the density of material the X-rays pass through. Because this imaging is 2D, the results are superimposed internal images of the specimens. The resulting digital images are 16-bit greyscale images with the greyscale values representing the material density at each location (lighter corresponding to denser regions). Using Rhythm Review, the brightness and contrast settings vary to make defects visible. In addition, multiple filters are available to make defect identification easier for the operator. In the standards, the inserts show as rectangular areas with lighter values (negative image).

The PT and RPF inserts are undetected for this laminate thickness (Figure E.36-17a, b). Because the densities of the carbon fiber base material and the inserts are similar, a single-ply insert does not create a large density variation, thereby limiting the detectability. The brass inserts, however, cause a very large density variation and are readily observable in all laminate thicknesses (Figure E.36-17c). Metal FOD in composite structures often show this degree of detectability due to the relatively high density of the metal compared to the composite.

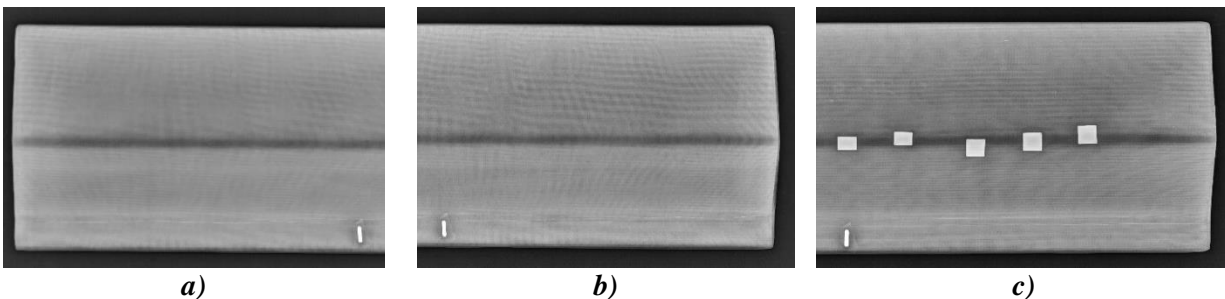


Figure E.36-17. CR images of PT (a), RPF (b), and brass (c) insert locations for 8276-200-58-26 standard (filter applied).

E.36.6 Method: X-ray Backscatter

E.36.6.1 Partner: Boeing

E.36.6.2 Technique Applicability: ★☆☆

X-ray Backscatter is capable of detecting the brass inserts but is unable to detect the PT and RPF inserts.

E.36.6.3 Laboratory Setup

The DRC has a large X-ray enclosure (vault) which is utilized for high-energy CT scanning, large 2D X-ray imaging, and X-ray backscatter scanning. A custom NuSAFE portable backscatter system is set up in this enclosure. Because of the relatively low radiation output, it can be safely operated with the operator in the vault, outside of a boundary established by the controlling Radiation Health and Safety organization. Figure E.36-18 shows the backscatter unit (left), while the high voltage, generator, cooling system, and control computer are housed in a portable cart (right), which can also hold the unit for transportation.

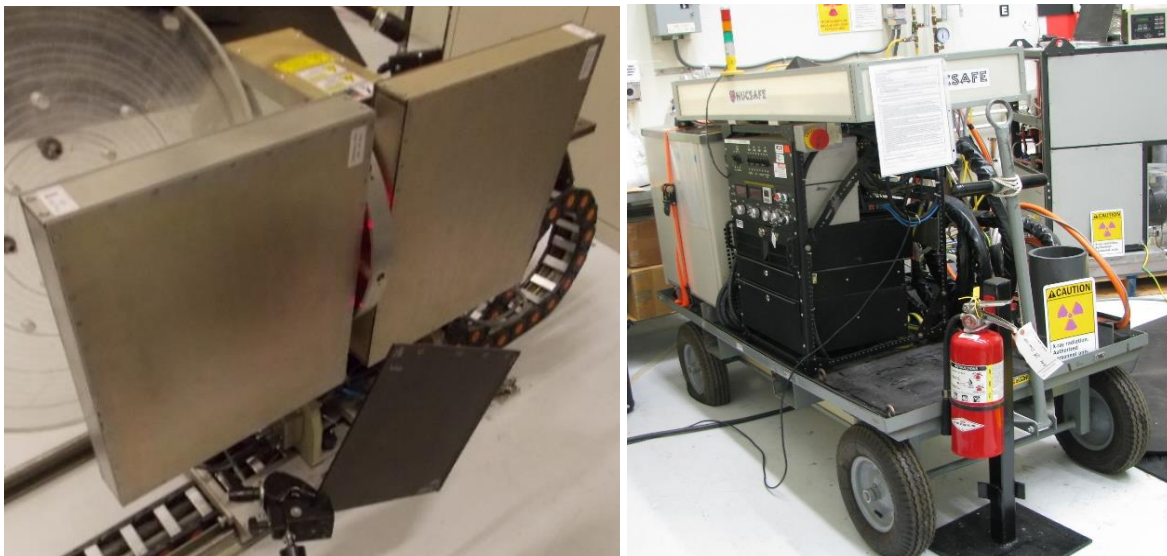


Figure E.36-18. NuSAFE portable X-ray backscatter system.

Unlike most other X-ray methods, which are TT, Backscatter X-ray is a method of 2D imaging that only requires one-sided access. When X-rays interact with a material, most pass through with some attenuation; however, a small fraction scatters back and can be detected (Compton Scattering). Backscatter uses this by exposing a small area of a specimen to a rotating collimated X-ray beam (Figure E.36-18). The scattered X-rays are collected with detectors and used along with the swept area of the beam to construct a column of an image. By translating the whole source, another column is made and sequentially a full 2D image is created as seen from the source side. In this test, the part is placed a short distance from the unit with the X-rays initially aligned to one side. During scanning, the unit then translated across the part to build the image.

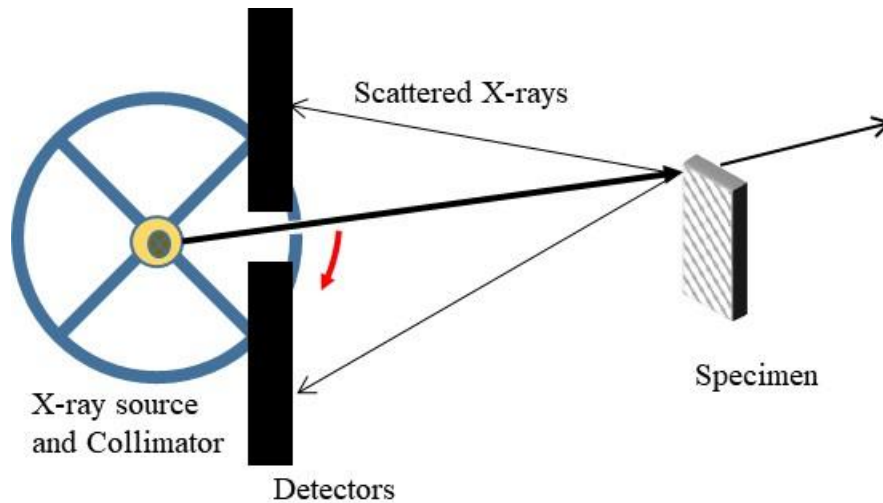


Figure E.36-19. X-ray backscatter imaging.

E.36.6.4 Equipment List and Specifications:

- NuSAFE Portable X-ray Backscatter imaging system

E.36.6.5 Settings

Table E.36-6. Imaging and exposure parameters.

Source Energy	80 kV
Current	21.1 mA
Scan Velocity	216 mm/min
Collimator Speed	27 RPM
Exposure per pixel	0.617 ms
Image width and height	550 × 400 pixels
Pixel Size	1 mm × 0.1°
Imaging Sweep Area	40°

E.36.6.6 Inspection Results

The Radii Delamination Standards are carbon fiber composite panels with foreign material inserts in various layers to evaluate the detectability using ultrasonic inspection. These inserts are largely grouped around the angle in the panel; however, not exclusive to this area. The standards vary in thickness, utilizing 8, 26, and 48 plies of carbon fiber fabric with exterior layers of fiberglass.

Backscatter X-ray is particularly sensitive to material differences that cause large variations in scatter. Metallic foreign material or water in honeycomb panels are examples of detectable phenomena. It is not sensitive in thicker parts however, as the scattered X-rays deeper in the part fail to generate a clear image. In this standard, the brass inserts provide a detectable scatter; however, this scatter is only resolved in the shallow layers, becoming fainter and undetectable at the back layers. This is seen in Figure E.36-20 as the shallow inserts on the left side are clear, but the deeper inserts in the middle are faint with the back inserts located to the right not visible at all. The indications on the sides of the panel are the grips use to hold the part for scanning.

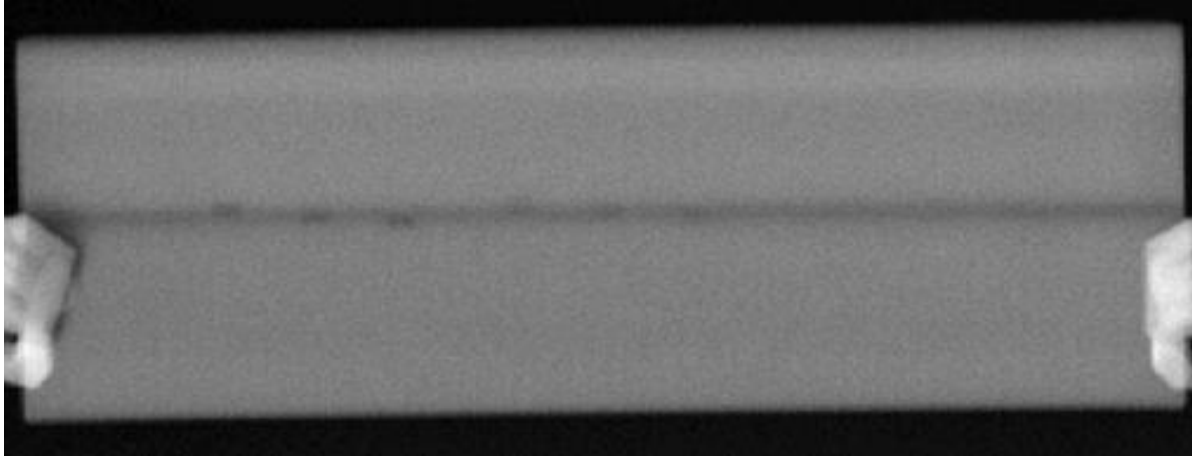


Figure E.36-20. X-ray backscatter image of 8276-200-58-26 standard with brass inserts.

E.37 Specimen #37: Boeing 8276-200-58-48A

Structure	Material	Details	Dimensions (inches)	Partner Methods	
				NASA	Boeing
Thin laminates	8276 slit tape	S curve ($_ / _$) 58° slant with two 0.2-inch radii	20x6x2.4	E.37.1 PE UT	E.37.2 XCT E.37.3 TTUT E.37.4 SSIR E.37.5 X-ray DR E.37.6 X-ray CR



Figure E.37-1. Photograph of Specimen #37: Boeing 8276-200-58-48A.

E.37.1 Method: Pulse-Echo Ultrasound Testing (PEUT)

E.37.1.1 Partner: NASA

E.37.1.2 Technique Applicability: ★★★

PEUT is capable of detecting the delaminations simulated within this sample.

E.37.1.3 Laboratory Setup

Immersion Ultrasonic Testing: NASA LaRC uses a custom designed single probe ultrasonic scanning system. The system has an 8-axis motion controller, a multi-axis gantry robot mounted above a medium-size water tank, a dual-channel, 16-bit, high-speed digitizer, and an off-the-shelf ultrasonic pulser receiver. The system can perform through transmission and pulse-echo ultrasonic inspections. TT inspection employs two aligned ultrasonic probes, one transmitter and one

receiver, placed on either side of a test specimen. Pulse-echo inspection is a single-sided method where a single ultrasonic probe is both transmitter and receiver. In each method, data are acquired while raster scanning the ultrasonic probe(s) in relation to a part. Figure E.37-2 shows a simplified block diagram of a scanning Pulse-echo inspection.

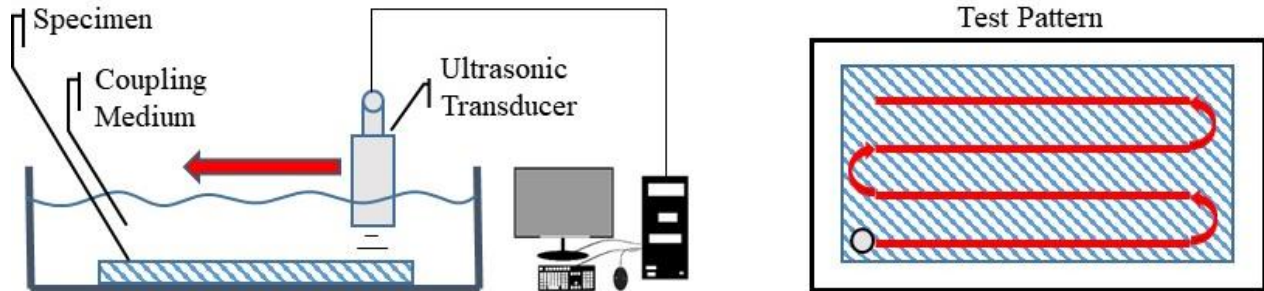


Figure E.37-2. Ultrasonic system components.

E.37.1.4 Equipment List and Specifications:

- Pulsar/Receiver: Olympus 5073PR
- Digitizer: AlazarTech ATS9462, dual channel, 16 bit, 180 MS/s
- Sensor: Olympus 2-inch spherical focus immersion ultrasonic transducer
- Motion system: open looped stepper motor based X-YY-Z gantry robot
- Motion Controller: Galil DMC-4183
- Acquisition Software: FastScan, custom developed at NASA LaRC
- Signal Processing Software: DataViewer, custom developed at NASA LaRC

E.37.1.5 Settings

Table E.37-1. Data collection settings.

Resolution horizontal [in/pixel]	0.025
Resolution vertical [in/pixel]	0.025
Probe frequency [MHz]	5
Focal Length [in]	2
Array Dimensions [pixels]	821 × 150

The specimen is placed flat against the zero position of the tank raised above the glass bottom by several metal washers. The test probe is computer-controlled and correlated to the position on the sample. It is also focused to a point one mm below the surface of the test material. The specimen remains in place while the transducer follows a preprogrammed test grid across the surface as indicated in Figure E.37-2. At each point, ultrasonic data are collected from individual pulses. Larger step sizes between data collection result in lower image resolution. These data points are reconstructed into a data cube displaying spatial coordinates as time progresses. 2D reconstruction of the collection of ultrasonic responses create flattened slices at varying depths within the material.

E.37.1.6 Inspection Results

Specimen #37, is an S curve panel with a 58° slant and two 0.2-inch radii fabricated from 8276 slit tape with the objective of achieving delaminations via inserts throughout the sample. PEUT was performed on this specimen in NASA's immersion tank specified above.

The scan was performed normal to the larger edge region providing the largest amount of surface. Figure E.37-3 shows delaminations just below the surface of the material. They appear white due to the acoustic waves reflecting off the air pocket generating a strong early response. Figures E.37-4 and E.37-5 show delaminations within the bulk of the sample at depths of 0.033 inch and 0.119 inch respectively. Indications from delaminations in the curved radii are also visible.



Figure E.37-3. UT image showing near surface delaminations on the large flat edge.

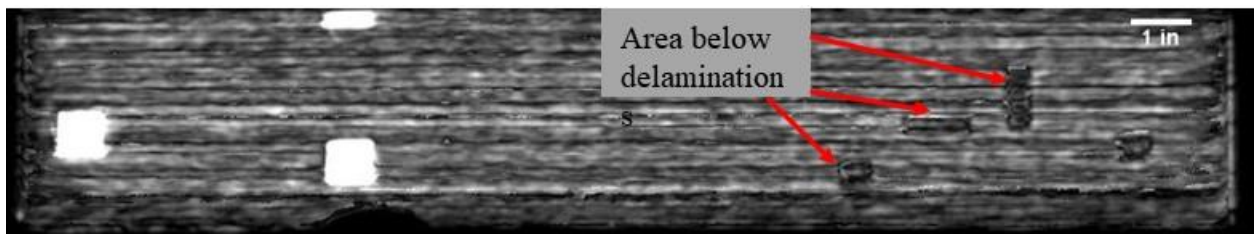


Figure E.37-4. UT image showing delaminations within the bulk of the sample.

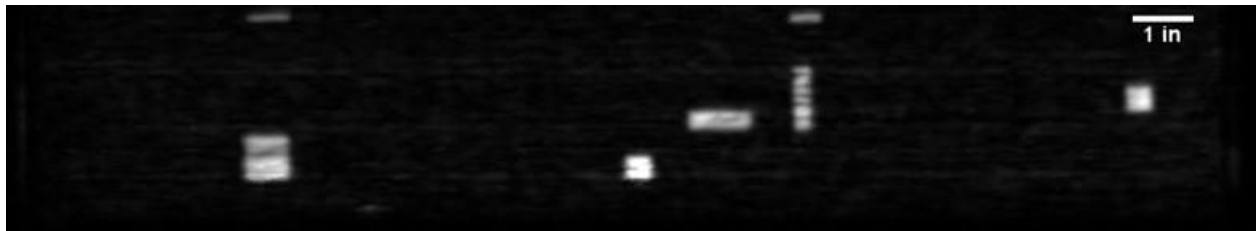


Figure E.37-5. UT image showing delaminations within the bulk of the sample

E.37.2 Method: X-ray Computed Tomography (XCT)

E.37.2.1 Partner: Boeing

E.37.2.2 Technique Applicability: ★★★

XCT is capable of identifying all inserts, notably brass inserts.

E.37.2.3 Laboratory Setup

The DRC utilizes an YXLON Modular CT System. This system has the capability to utilize various X-ray sources for varying applications, including a 450-kV source, a microfocus source, and a nanofocus source. The microfocus source used has a variable focal spot size of less than 4 μm and is suitable for magnifications up to 10X, with the nanofocus ranging up to 187X. The detector has 3 DOF, allowing for increase in the effective detector area through combined scans. The manipulator controls the position of the detector, object, and source. It has 7 DOF including a rotating stage to rotate the object during the scan. The entire system includes the source, detector, manipulator, control and reconstruction computers, and user control station. The computers and control station are outside of the radiation enclosure (vault) and utilize a safety interlock system to

operate. Cameras are located in the vault to allow the operator to monitor the part from outside the enclosure.

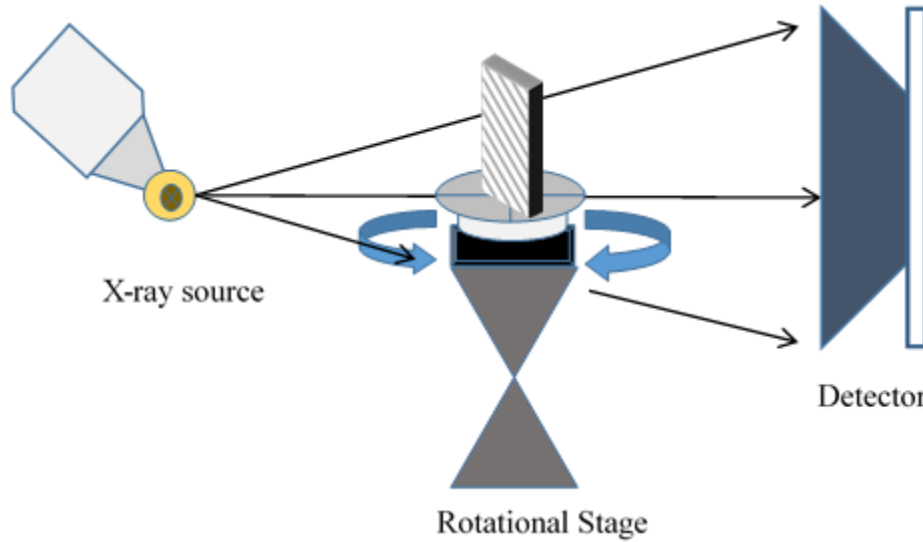


Figure E.37-6. XCT system components.

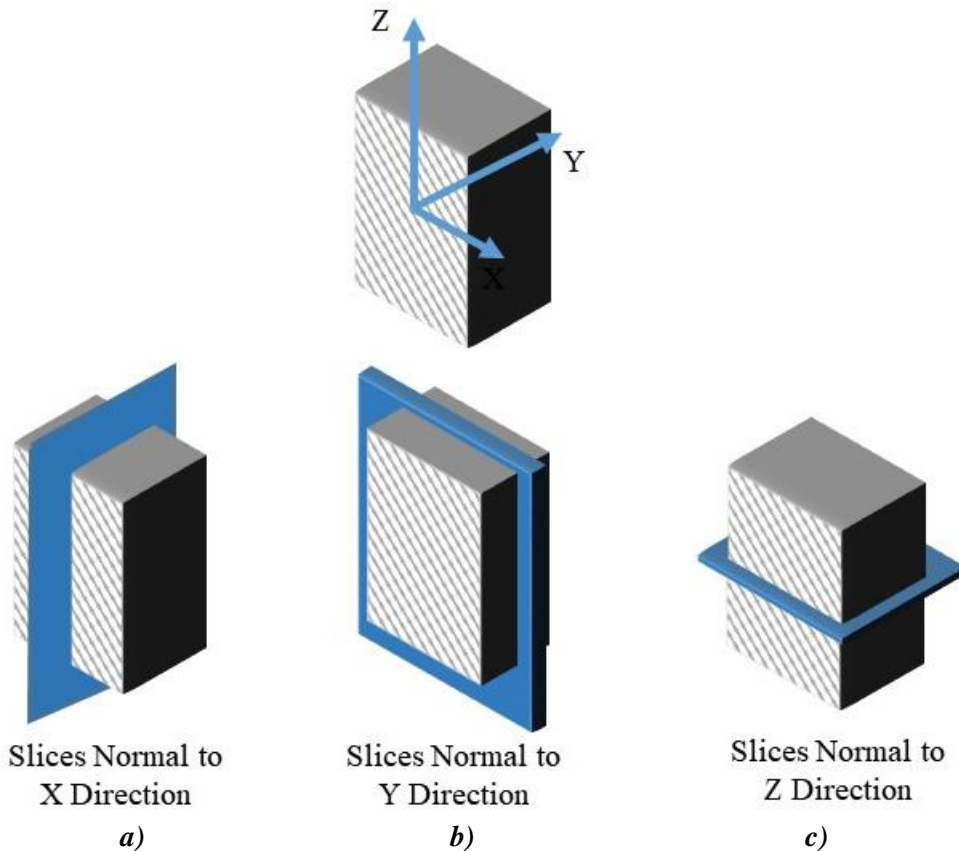


Figure E.37-7. Slice direction nomenclature.

The standards were divided into two sections, labeled Upper and Lower, and placed on the rotator in a soft clamp (Figure E.37-8). The specimen was right side up for the Upper scan, and upside-down for the Lower scan. Plastic markers, which show up in 3D reconstruction, were placed on

the sections to denote the boundaries between sections. The position of the specimen, source, and detector are controlled to produce geometric magnification of the image and increase the spatial resolution. The image data are gathered as X-rays penetrate the part and expose the detector for a set amount of time. For each scan, these image data are collected at 1080 different angles throughout a 360° rotation. These images are then reconstructed to create the 3D volume data set. This data set is viewed and analyzed in Volume Graphics, a volume rendering software, to identify the relevant components.

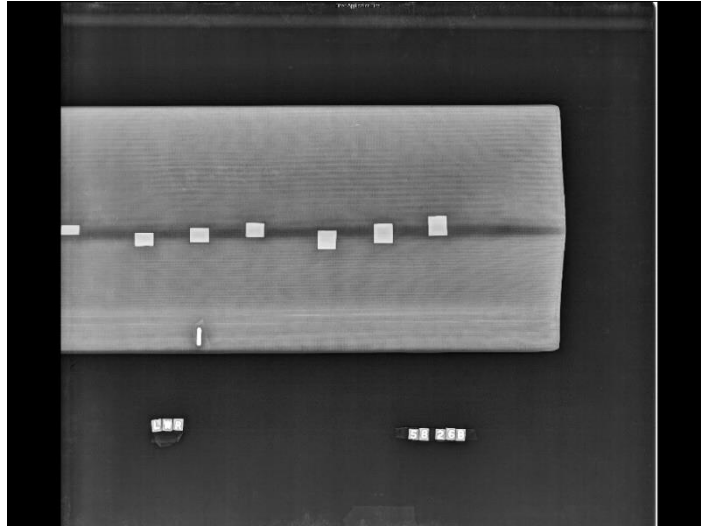


Figure E.37-8. Microfocus XCT setup for Radii Delamination Standard.

E.37.2.4 Equipment List and Specifications:

- YXLON Modular CT System
- 225 kV microfocus X-ray source with variable focal spot size
- 100 kg capacity, 7-axis, granite-based manipulator
- XRD 1621 Detector – 2048 × 2048 pixels with 200 μm pitch, 400 × 400 mm active area
- 126 μm spatial resolution for half volume scan
- Volume Graphics 3.0 visualizing software
- Reconstruction Computer

E.37.2.5 Settings

Table E.37-2. Data collection settings.

Source Energy	205 kV
Current	0.47 mA
Magnification	1.59 X
Filter	Copper
# Rotational angles	1080
Exposure time/frame	800 ms
Spatial Resolution (μm)	125.777 μm
Array Dimensions (pixels)	2048 × 2048

E.37.2.6 Inspection Results

The Radii Delamination Standards are carbon fiber composite panels with foreign material inserts in various layers to evaluate the detectability using ultrasonic inspection. These inserts grouped

around the angle in the panel; however, not exclusive to this area. The standards vary in thickness, utilizing 8, 26, and 48 plies of carbon fiber fabric with exterior layers of fiberglass. Because of their length, the data set consists of the upper and lower half volumes of the standards, flipped 180° for the scan.

After aligning the volume coordinate system to correspond with the panel geometry, the slice view is used to inspect conditions at each lamina. The brightness and contrast settings are also adjusted to make defects clear, but retain the visible noise at a reasonable level. The inserts are clearly visible (Figure E.37-9), showing with less density for PT and RPF and higher density for brass. The brass is the most readily observable, followed by the PT with the RPF having the lowest detectability. The RPF may show the least response due to similar density to base material or due to a strong interface with little voiding or delamination to be detected.

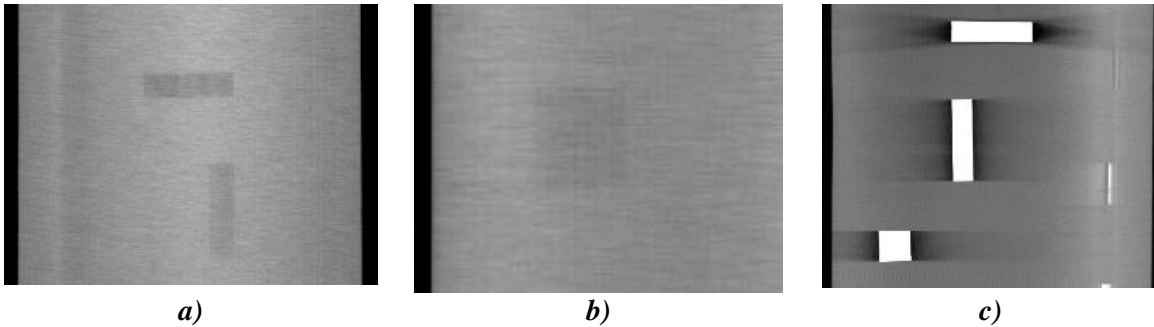


Figure E.37-9. CT Slice view showing PT (a), RPF (b), and brass (c) inserts.

The CT scanning and reconstruction process is subject to artificial and undesirable artifacts. These are the result of multiple conditions. The direction of rotation leaves an underlying direction to the noise of the data set, aligning with the rotation. This is seen as a light, roughly horizontal streaking seen in (Figure E.37-9). The presence of high-density material in an otherwise low-density structure often creates even more intense ray artifacts, seen as shadow-like streaks emanating from the high-density material (Figure E.37-9c). If defects are present in these dark artifacts, their detectability is reduced. Lastly, the part may rotate in and out of the cone-beam of the X-rays during the scan, leaving the top and bottom edges of the volume not fully defined. This is seen as darker “wedges” of the volume at the top and bottom of the data set (Figure E.37-9).

The detectability of the inserts relies on viewing the slices at the appropriate angle, which aligns with the lamina. This means the inserts within the curve of the panel, while still detectable, are less apparent (Figure E.37-10), and operators must be careful to attempt to identify them. The inserts are also more visible when they induce delamination with air or if they have a much greater density than the composite material.

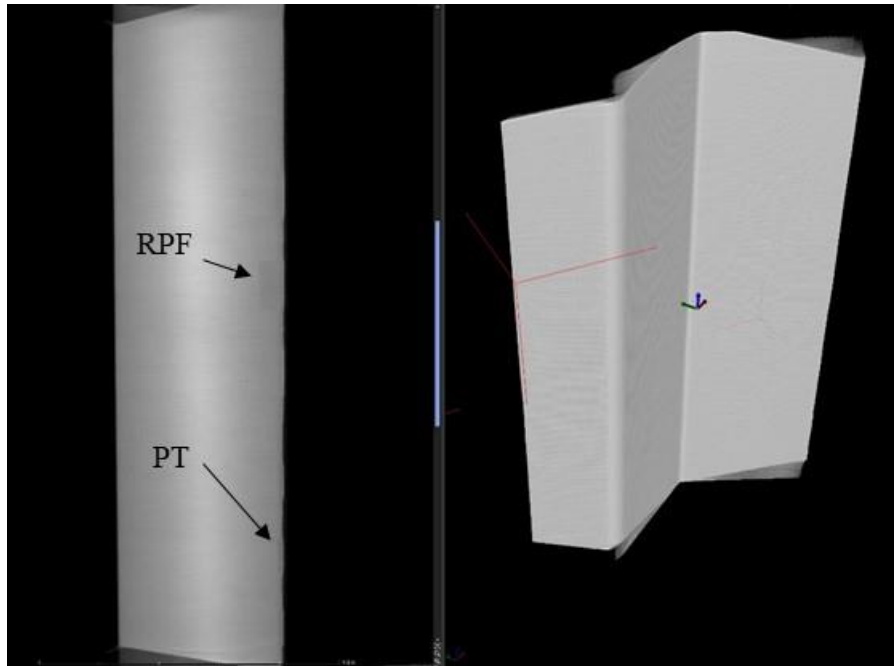


Figure E.37-10. CT slice view showing PT and RPF inserts.

E.37.3 Method: Through-Transmission Ultrasound Testing (TTUT)

E.37.3.1 Partner: Boeing

E.37.3.2 Technique Applicability: ★★★

All inserts are visually detectable with TTUT data.

E.37.3.3 Laboratory Setup

The TTUT scanner at the Boeing laboratory consists of an enclosure, part supports, a water pump and nozzle system, ultrasonic transducers (transmitter and receiver), robotic manipulator, and control computer. After adjusting the water to produce a uniform flow, the pulser and receiver (on opposite sides of the specimen) perform a C-scan under the control of the robotic manipulator and control computer. The C-scan is produced by taking multiple 1-dimensional scans (A-scans) and stitching them together to produce the final area result.

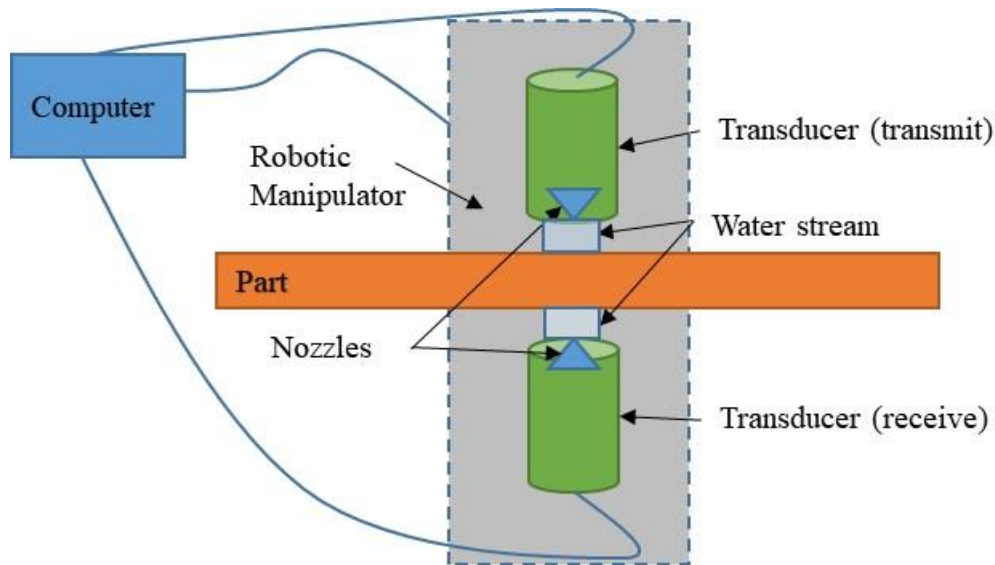


Figure E.37-11. TTUT scanning schematic with water pump.

TTUT works on the principal of the capture and quantification of the transmitted waves. It uses a pulsing transducer on one side of the part and has the receiving transducer on the opposite side of the part. Scanning can be accomplished with contact, water streams, or full immersion method, as long as sufficient ultrasonic coupling is used. Although the TTUT works on non-parallel, front-to-back surface, the optimized data are produced when the front-to-back surfaces are parallel to each other.

As the ultrasonic waves travel through a material, they are attenuated. Defects and material discontinuities such as delamination, porosity and foreign material interfaces cause increased attenuation. UT has an orientation dependency, where certain defect orientations will attenuate the signal more if they are oriented for maximum reflection. Delamination tend to be oriented favorably for detection, making ultrasound the common method for composite inspection.

E.37.3.4 Equipment List and Specifications:

- 1 MHz ultrasonic transducer and receiver
- Water pump, nozzles, and circulation system
- Robotic manipulator
- Enclosure
- Control computer

E.37.3.5 Settings

Table E.37-3. Data collection settings.

Frequency	1 MHz
Resolution	0.04 inch × 0.04 inch

E.37.3.6 Inspection Results

The NASA Radii Delamination Standards are carbon fiber composite panels with foreign material inserts in various layers to evaluate the detectability using ultrasonic inspection. These inserts grouped around the angle in the panel; however, not exclusive to this area. The standards vary in thickness, utilizing 8, 26, and 48 plies of carbon fiber fabric with exterior layers of fiberglass.

Using TTUT, the all insert types (PT, RPF, and brass) were detectable. However, this visual detectability was generally reduced as thickness increased.

The brass inserts were the most resolved and detected (Figure E.37-12c) and the RPF inserts showed the lowest detectability (Figure E.37-12b). This is consistent with the theory that the RPF inserts bond to the material the best, leading to a small TTUT signal, while the brass has the worst bond (likely due to applied coating), leading to the large signals seen. The brass also has a significantly different attenuation than the surrounding material, allowing it to easily be detected. The 48 ply standards included inserts in locations on and away from the curved radius. The inserts away from the radius tended to be better resolved and defined (Figure E.37-12) due to the more uniform background signal. While the RPF inserts had small responses and resolving their exact shape is difficult, their presence tended to be detectable in the distortion of the surrounding signal and features (Figure E.37-12b).

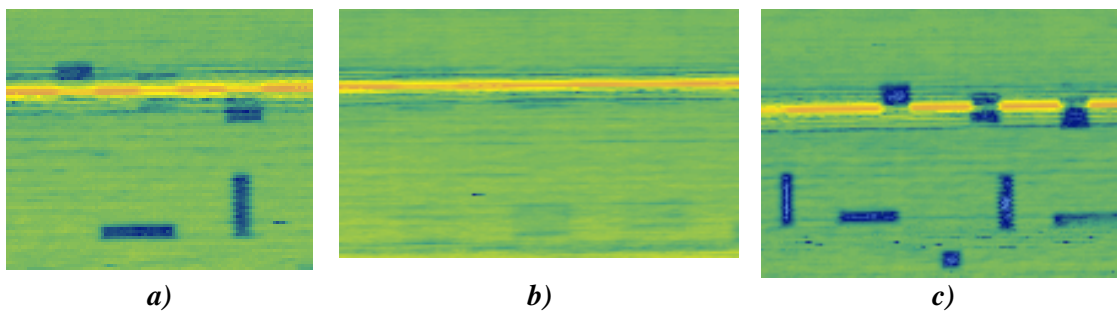


Figure E.37-12. TTUT scans showing PT (a), RPF (b), and brass (c) inserts.

E.37.4 Method: Single-Sided Infrared Thermography (SSIR)

E.37.4.1 Partner: Boeing

E.37.4.2 Technique Applicability: ★★☆☆

Flash Thermography can detect all insert types in the radii standard.

E.37.4.3 Laboratory Setup

For each inspection, the part was placed in the IR imaging system (Figure E.37-13). For each test, the flash lamp fires, heating the surface of the part uniformly. The IR camera records the heat signature of the part over time to track the diffusion of heat through the part thickness. As the diffusion wave moves through the part, the inserts in the standards will cause disturbances in the otherwise approximately uniform heat flow. A few factors can influence the nature of the heat signature. If the insert has a different thermal conductivity than the part material, it will show as a hot spot (lower thermal conductivity) or cold spot (higher thermal conductivity) as it aids or hampers the diffusion of heat through the part. The inserts may also cause a significant delamination in the part, which has an insulating effect and will show as a hotter indication. With either case, the now disturbance in the originally uniform heat flow will be captured with the IR camera as a function of time.

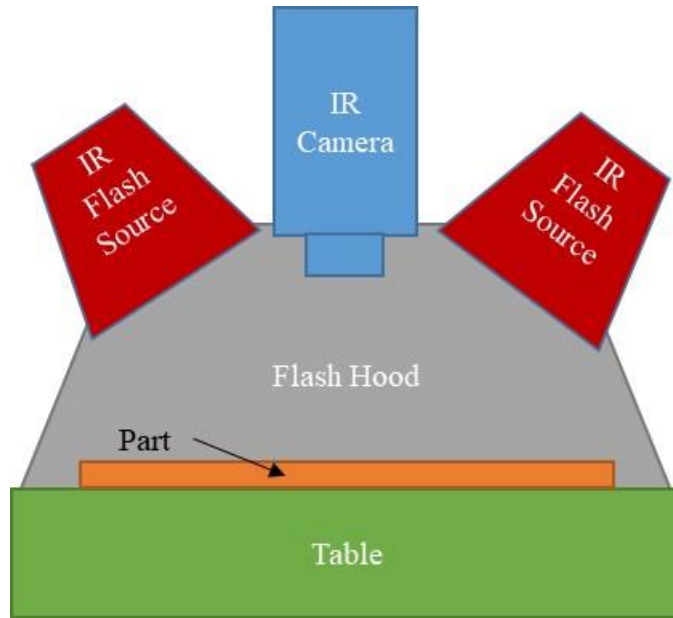


Figure E.37-13. Flash IRT system components.

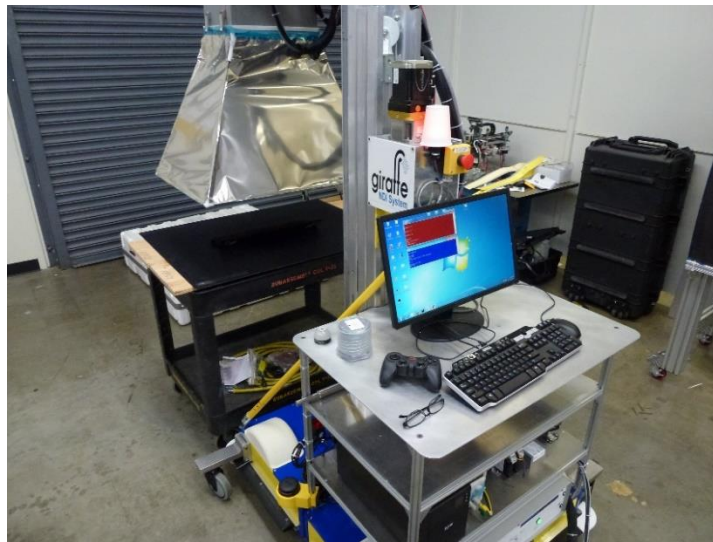


Figure E.37-14. IR inspection system.

E.37.4.4 Equipment List and Specifications:

- SC6000 Series FLIR IR camera
- 6400 Watt-sec flash lamps
- Flash Hood

E.37.4.5 Settings

Table E.37-4. Data collection settings.

Frame Rate	120 fps
Image Size	640 × 512 pixels
Capture Duration	5 sec
Camera Frequency	120 Hz
Flash Duration	<0.2 sec

E.37.4.6 Inspection Results

The Radii Delamination Standards are carbon fiber composite panels with foreign material inserts in various layers to evaluate the detectability using ultrasonic inspection. These inserts grouped around the angle in the panel; however, not exclusive to this area. The standards vary in thickness, utilizing 8, 26, and 48 plies of carbon fiber fabric with exterior layers of fiberglass.

Because the flash heat diffuses through the thickness of the part, inserts at different layers should appear most clearly at varying times. This can be observed in the lower image of Figure E.37-15, where only one set of inserts (left side) gives a thermal signature, because the thermal diffusion wave has not interacted with the deeper inserts yet. Similarly, the uppermost sets of inserts show the most clearly in the upper image. As the heat wave progresses through the material, the inserts heat up and cool faster than the surrounding material, leading to initially lighter indications followed by darker indications as time progresses. This is seen in the upper image where the PT inserts close to the surface have begun to cool faster (dark) while the lower RPF inserts are heating up faster (light).

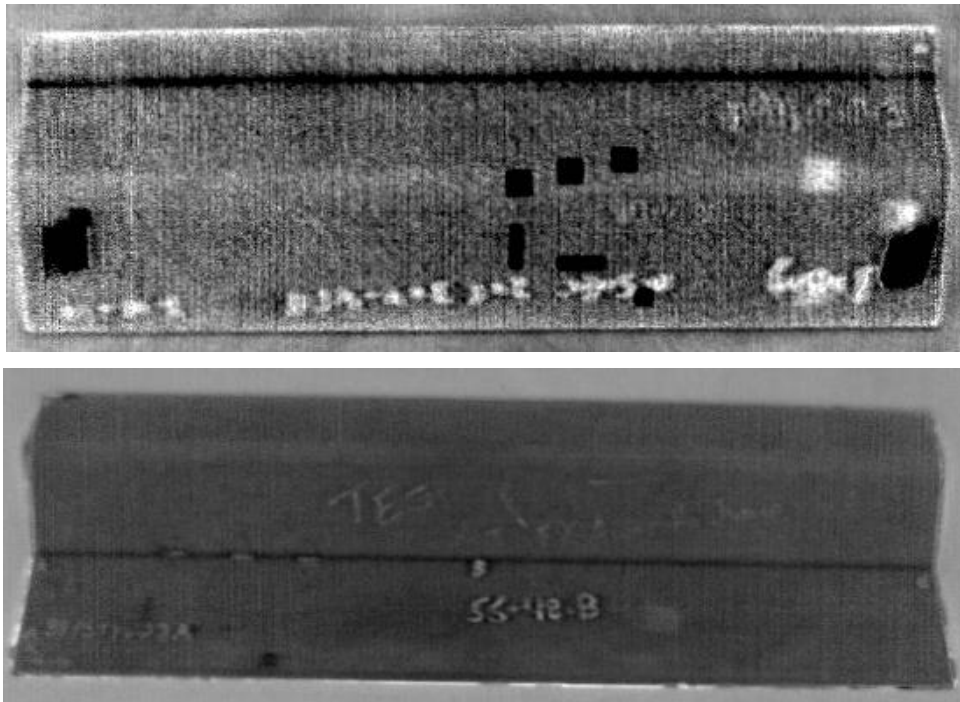


Figure E.37-15. Greyscale IR image of Radii Delamination Standard inserts (Top: PT and RPF, Bottom: brass).

E.37.5 Method: X-ray Digital Radiography (DR)

E.37.5.1 Partner: Boeing

E.37.5.2 Technique Applicability: ★☆☆

DR is capable of detecting the brass inserts but is unable to detect the RPF or PT inserts.

E.37.5.3 Laboratory Setup

The DRC utilizes an YXLON Modular CT System with Digital Radiography capability. This system includes a microfocus source and a digital detector array with positions controlled by a

manipulator system. The microfocus source used has a variable focal spot size of less than four μm and is suitable for magnifications up to 10X. The manipulator has 7 DOF including a rotating stage to rotate the object as well as the ability to control its position along with the detector for magnification. The entire system includes the source, detector, manipulator, and user control station. The computers and control station are outside of the radiation enclosure (vault) and utilize a safety interlock system to operate. Cameras are located in the vault to allow the operator to monitor the part from outside the enclosure.

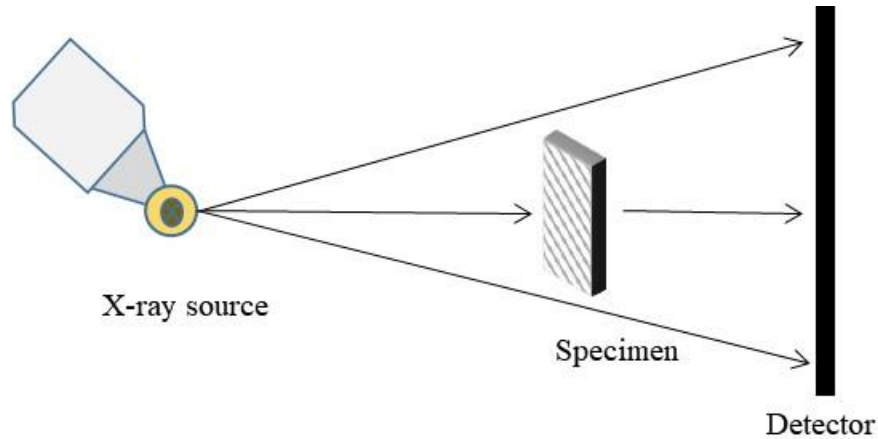


Figure E.37-16. X-ray DR imaging.

The standards were divided into two sections, labeled Upper and Lower, and placed on the rotator in a soft clamp (Figure E.37-16). The specimen was right side up for the Upper scan, and upside-down for the Lower scan. Lead markers were placed on the sections to denote the boundaries between and label sections. The position of the specimen, source, and detector are controlled to produce geometric magnification of the image and increase the spatial resolution while capturing the entire section of the part in the detector area. The image data are gathered as X-rays penetrate the part and expose the detector for a set amount of time to produce a frame; multiple frames are average to produce the final image. This image, viewed in Image 3500, has much lower noise levels than a single frame due to the averaging. The operator adjusts the brightness and contrast settings of the image to identify the inserts, seen in the 2D image as rectangular defects.



Figure E.37-17. Laboratory setup of angle plate standard for DR imaging.

E.37.5.4 Equipment List and Specifications:

- 225 kV microfocus X-ray source with variable focal spot size
- 100kg capacity 7 axis granite based manipulator
- XRD 1621 Detector – 2048x2048 pixels with 200 μm pitch, 400x400 mm active area
- Image 3500 visualizing software

E.37.5.5 Settings

Table E.37-5. Data collection settings.

Source Energy	100 kV
Current	0.7 mA
Source-Detector Distance	42 in
Source-Object Distance	27 in
Magnification	1.55X
Integration Time	500 ms
Integration Frames	50
Spatial Resolution (μm)	129 μm
Array Dimensions (pixels)	2048 \times 2048

E.37.5.6 Inspection Results

The NASA Angle Panel Standards are carbon fiber composite panels with foreign material inserts in various layers to evaluate the detectability using ultrasonic inspection. These inserts grouped around the angle in the panel; however, not exclusive to this area. The standards vary in thickness, utilizing 8, 26, and 48 plies of carbon fiber fabric with exterior layers of fiberglass. Because of their length, the data set consists of the upper and lower half images of the standards.

DR X-ray imaging is sensitive to density variations, caused by material differences, voids, or other defects affecting the density of material the X-rays pass through. Because this imaging is 2D, the results are superimposed internal images of the specimens. The resulting digital images are 16-bit greyscale images with the greyscale values representing the material density at each location (lighter corresponding to denser regions). Using Image 3500, the brightness and contrast settings vary to make defects visible. In the standards, the inserts show as rectangular areas with darker values (positive image).

The PT and RPF inserts are undetectable in this laminate thickness (Figure E.37-18a, b). Because the densities of the carbon fiber base material and the inserts are similar, a single-ply insert does not create a large density variation, thereby limiting the detectability. This detectability also drops as the laminate increases in thickness. The brass inserts, however, cause a very large density variation and are readily observable in all laminate thicknesses (Figure E.37-18c). Metal FOD in composite structures often show this degree of detectability due to the relatively high density of the metal compared to the composite.

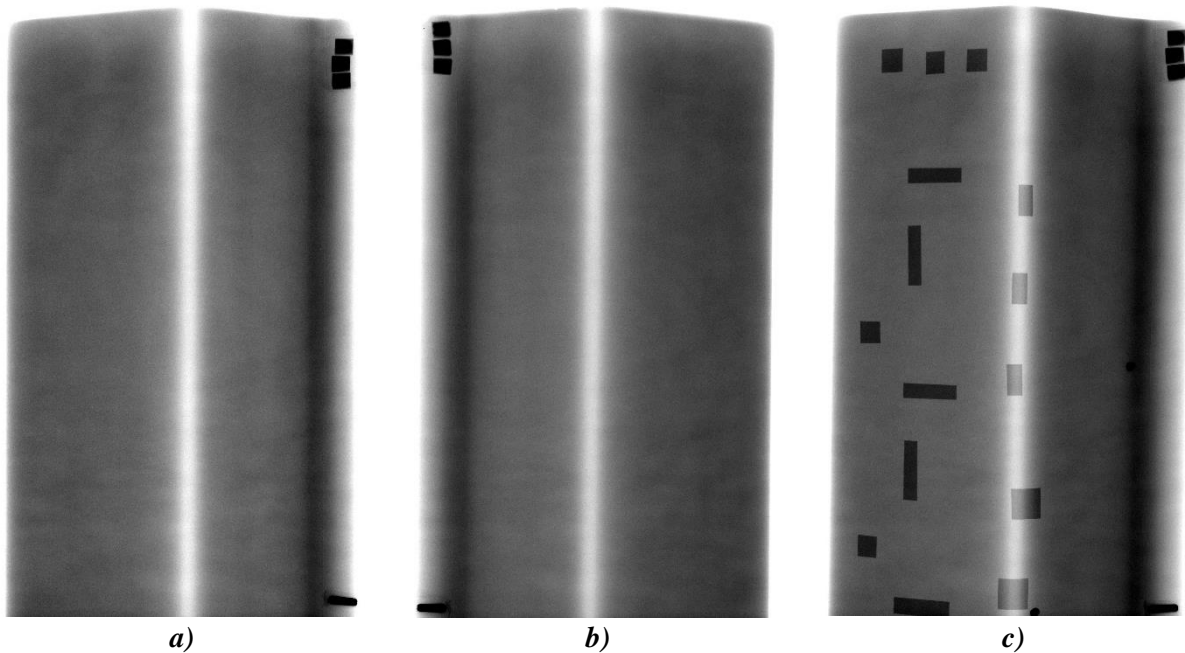


Figure E.37-18. DR images of PT (a), RPF (b), and brass (c) insert locations in 8276-200-58-48 standard.

E.37.6 Method: Computed Radiography (CR)

E.37.6.1 Partner: Boeing

E.37.6.2 Technique Applicability: ★☆☆

X-ray CR is capable of detecting the brass inserts but is unable to detect the PT and RPF inserts.

E.37.6.3 Laboratory Setup

The DRC has a small X-ray enclosure (vault) for the primary purpose of 2D X-ray imaging. It includes a Philips 160-kV X-ray source and the ability to use film, CR, and digital detector arrays. The CR imaging plates are placed on a table and the source, suspended from the ceiling by a 3-axis crane, can be positioned to control the Source to Object Distance. Outside of the enclosure are the controls for the source, utilizing a safety interlock system. These controls allow the user to set the energy, current, and exposure time for the source. In addition to the vault, the DRC utilizes a CRxFlex system to scan and erase the CR imaging plates, storing the images on a computer. The phosphorus imaging plates, after exposure to X-rays, will luminesce the images when exposed to blue light, allowing the 50- μ m scanner to create digital versions and “erase” the plates using bright white light to be used again. The CR digital images are then reviewed using Rhythm Review.

The standards were divided into two sections, labeled Upper and Lower, and placed directly on the plastic cassette containing the imaging plate with the X-ray source directly overhead (Figure E.37-19). The source was located 60 inches from the specimen and imaging plate to reduce geometric distortion. Lead markers were used to show section boundaries and label the images, showing up in the results as bright white. Because of the large differences in laminate thicknesses between the specimens, three separate source energies were used, with the highest energy for the thickest specimens.

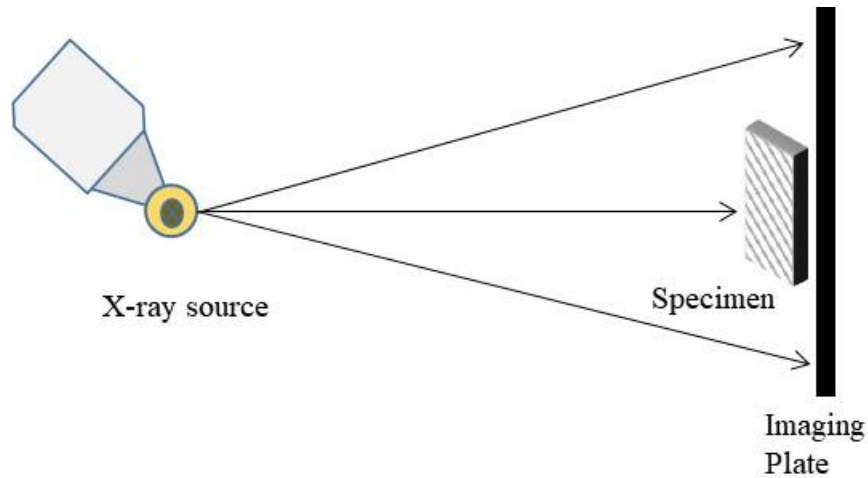
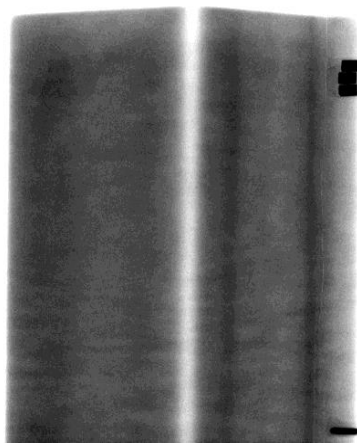


Figure E.37-19. X-ray CR imaging.



a)



b)

Figure E.37-20. Laboratory setup of angle plate standards for CR imaging.

E.37.6.4 Equipment List and Specifications:

- Philips 160 kV X-ray source, 0.4 mm focal spot size
- IPS Phosphorus Imaging Plate
- GE CRxFlex Scanner, 50 μm resolution
- GE Rhythm Review 5.0 visualizing software

E.37.6.5 Settings

Table E.37-6. Data collection settings.

Source Energy	30,40,50 kV
Current	10 mA
Source-Detector Distance	60 in
Magnification	1X
Exposure time	10 s
Resolution (μm)	50 μm
Imaging Area (in)	14 \times 17

E.37.6.6 Inspection Results

The NASA Angle Panel Standards are carbon fiber composite panels with foreign material inserts in various layers to evaluate the detectability using ultrasonic inspection. These inserts grouped around the angle in the panel; however, not exclusive to this area. The standards vary in thickness, utilizing 8, 26, and 48 plies of carbon fiber fabric with exterior layers of fiberglass. Because of their length, the data set consists of the upper and lower half images of the standards.

CR X-ray imaging is sensitive to density variations, caused by material differences, voids, or other defects effecting the density of material the X-rays pass through. Because this imaging is 2D, the results are superimposed internal images of the specimens. The resulting digital images are 16-bit greyscale images with the greyscale values representing the material density at each location (lighter corresponding to denser regions). Using Rhythm Review, the brightness and contrast settings vary to make defects visible. In addition, multiple filters are available to make defect identification easier for the operator. In the standards, the inserts show as rectangular areas with lighter values (negative image).

The PT and RPF inserts are undetected for this laminate thickness (Figure E.37-21a, b). Because the densities of the carbon fiber base material and the inserts are similar, a single-ply insert does not create a large density variation, thereby limiting the detectability. The brass inserts, however, cause a very large density variation and are readily observable in all laminate thicknesses (Figure E.37-21c). Metal FOD in composite structures often show this degree of detectability due to the relatively high density of the metal compared to the composite.

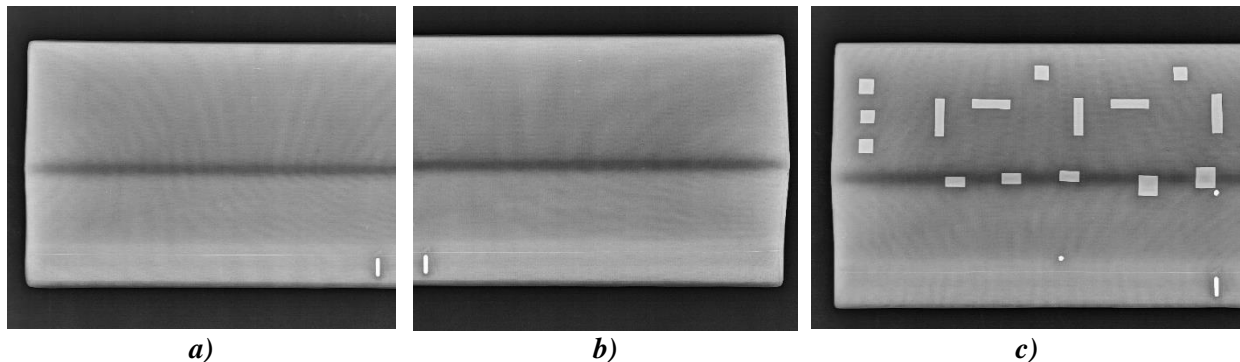


Figure E.37-21. CR images of PT (a), RPF (b), and brass (c) insert locations for 8276-200-58-48 standard (filter applied).

E.38 Specimen #38: Boeing 8276-200-56-48A

Structure	Material	Details	Dimensions (inches)	Partner Methods
48 fabric plies	BMS8-276	56° Curve with 0.2-inch radius	24 × 6.5	Boeing
2 fiberglass plies	BMS8-331	Brass, RPF and PT inserts at varying depths		
				E.38.1 XCT E.38.2 TTUT E.38.3 X-ray DR E.38.4 X-ray CR

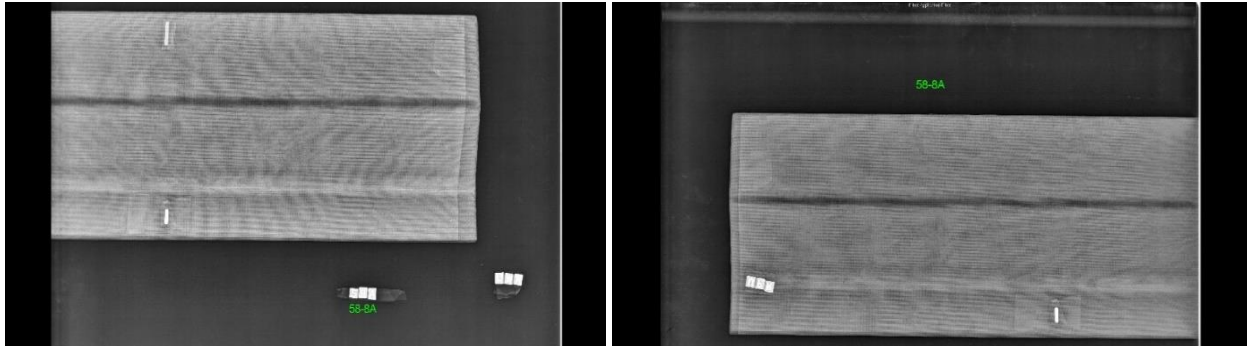


Figure E.38-1. Photographs of Angle Panel Reference Standard.

E.38.1 Method: X-ray Computed Tomography (XCT)

E.38.1.1 Partner: Boeing

E.38.1.2 Technique Applicability: ★★★

XCT is capable of identifying all inserts, notably brass inserts.

E.38.1.3 Laboratory Setup

The DRC utilizes an YXLON Modular CT System. This system has the capability to utilize various X-ray sources for varying applications, including a 450-kV source, a microfocus source, and a nanofocus source. The microfocus source used has a variable focal spot size of less than four μm and is suitable for magnifications up to 10X, with the nanofocus ranging up to 187X. The detector has 3 DOF, allowing for increase in the effective detector area through combined scans. The manipulator controls the position of the detector, object, and source. It has 7 DOF including a rotating stage to rotate the object during the scan. The entire system includes the source, detector, manipulator, control and reconstruction computers, and user control station. The computers and control station are outside of the radiation enclosure (vault) and utilize a safety interlock system to operate. Cameras are located in the vault to allow the operator to monitor the part from outside the enclosure.

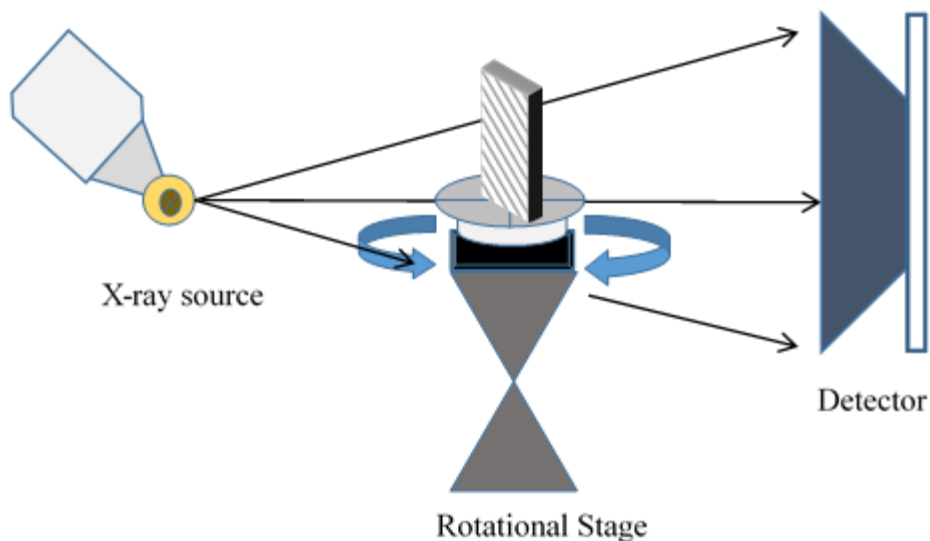


Figure E.38-2. XCT system components.

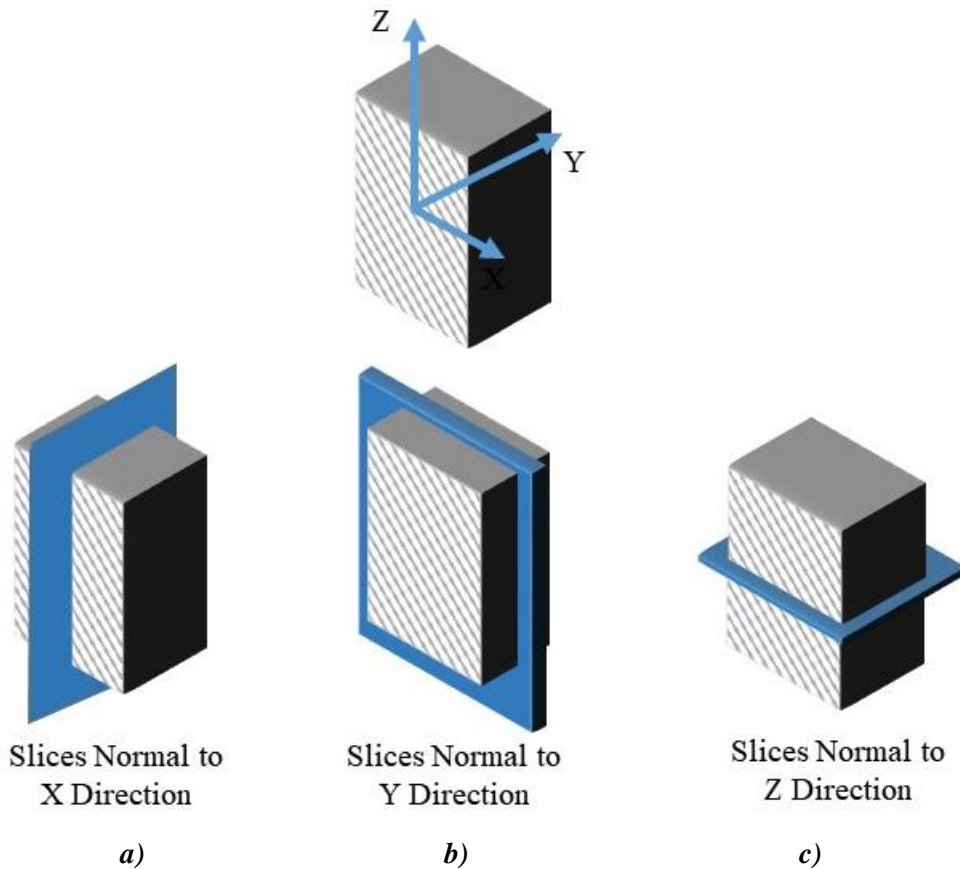


Figure E.38-3. Slice direction nomenclature.

The standards were divided into two sections, labeled Upper and Lower, and placed on the rotator in a soft clamp (Figure E.38-4). The specimen was right side up for the Upper scan, and upside-down for the Lower scan. Plastic markers, which show up in 3D reconstruction, were placed on the sections to denote the boundaries between sections. The position of the specimen, source, and detector are controlled to produce geometric magnification of the image and increase the spatial resolution. The image data are gathered as X-rays penetrate the part and expose the detector for a set amount of time. For each scan, these image data are collected at 1080 different angles throughout a 360° rotation. These images are then reconstructed to create the 3D volume data set. This data set is viewed and analyzed in Volume Graphics, a volume rendering software, to identify the relevant components.

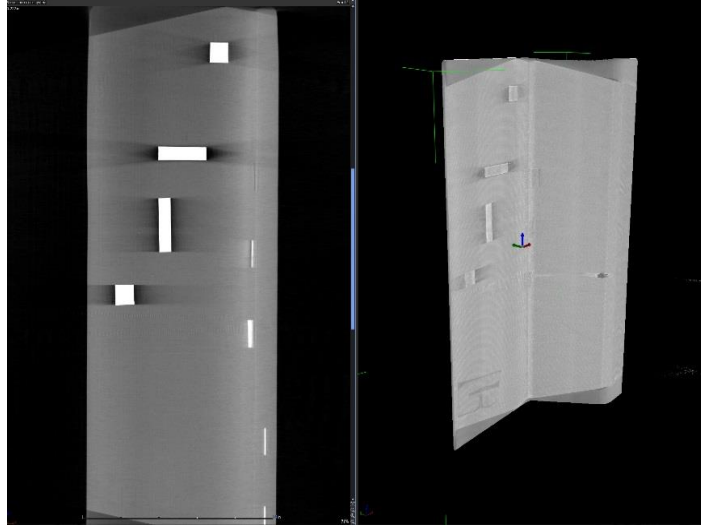


Figure E.38-4. Microfocus XCT setup for Radii Delamination Standard.

E.38.1.4 Equipment List and Specifications:

- YXLON Modular CT System
- 225 kV microfocus X-ray source with variable focal spot size
- 100 kg capacity, 7-axis, granite-based manipulator
- XRD 1621 Detector – 2048 × 2048 pixels with 200 μm pitch, 400 × 400 mm active area
- 126 μm spatial resolution for half volume scan
- Volume Graphics 3.0 visualizing software
- Reconstruction Computer

E.38.1.5 Settings

Table E.38-1. Data collection settings.

Source Energy	205 kV
Current	0.47 mA
Magnification	1.59 X
Filter	Copper
# Rotational angles	1080
Exposure time/frame	800 ms
Spatial Resolution (μm)	125.777 μm
Array Dimensions (pixels)	2048 × 2048

E.38.1.6 Inspection Results

The Radii Delamination Standards are carbon fiber composite panels with foreign material inserts in various layers to evaluate the detectability using ultrasonic inspection. These inserts grouped around the angle in the panel; however, not exclusive to this area. The standards vary in thickness, utilizing 8, 26, and 48 plies of carbon fiber fabric with exterior layers of fiberglass. Because of their length, the data set consists of the upper and lower half volumes of the standards, flipped 180° for the scan.

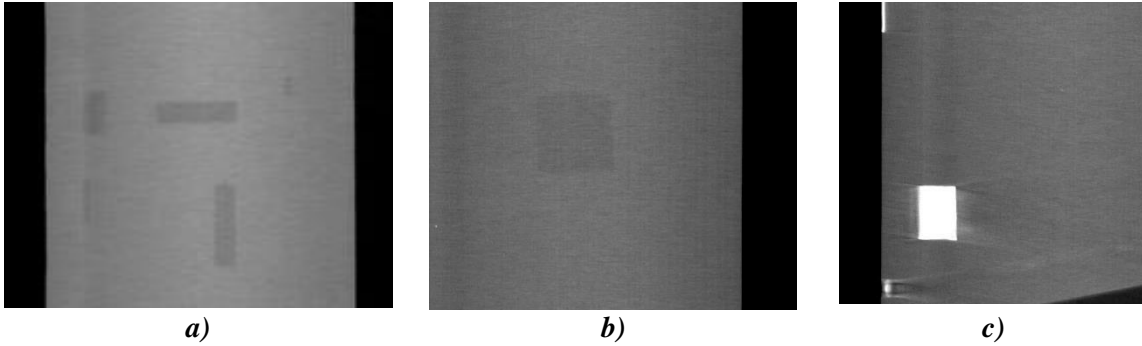


Figure E.38-5. CT slice view showing PT (a), RPF (b), and brass (c) inserts.

After aligning the volume coordinate system to correspond with the panel geometry, the slice view can be used to inspect conditions at each lamina. The brightness and contrast settings are also adjusted to make defects clear, but retain the visible noise at a reasonable level. The inserts are clearly visible (Figure E.38-5), showing with less density for PT and RPF and higher density for brass. The brass is the most readily observable, followed by the PT with the RPF having the lowest detectability. The RPF may show the least response due to similar density to base material or due to a strong interface with little voiding or delamination to be detected.

The CT scanning and reconstruction process is subject to artificial and undesirable artifacts. These are the result of multiple conditions. The direction of rotation leaves an underlying direction to the noise of the data set, aligning with the rotation. This is seen as a light, roughly horizontal streaking seen in (Figure E.38-5). The presence of high-density material in an otherwise low-density structure often creates even more intense ray artifacts, seen as shadow-like streaks emanating from the high-density material (Figure E.38-5c). If defects are present in these dark artifacts, their detectability is reduced. Lastly, the part may rotate in and out of the cone-beam of the X-rays during the scan, leaving the top and bottom edges of the volume not fully defined. This is seen as darker “wedges” of the volume at the top and bottom of the data set (Figure E.38-5).

The detectability of the inserts relies on viewing the slices at the appropriate angle, which aligns with the lamina. This means the inserts within the curve of the panel, while still detectable, are less apparent (Figure E.38-6), and operators must be careful to attempt to identify them. The inserts are also more visible when they induce delamination with air or if they have a much greater density than the composite material.

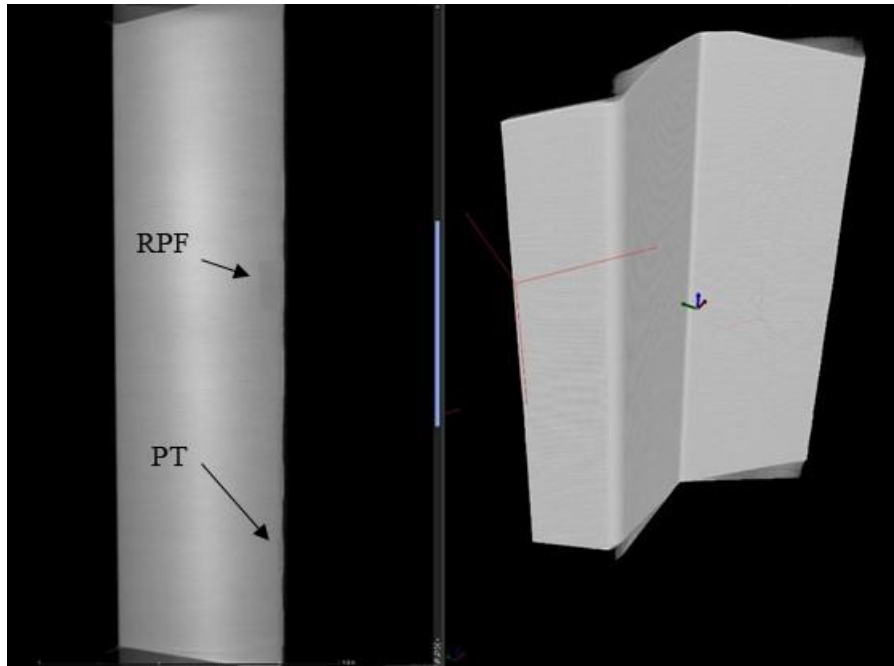


Figure E.38-6. CT Slice view showing PT and RPF inserts.

E.38.2 Method: Through-Transmission Ultrasound Testing (TTUT)

E.38.2.1 Partner: Boeing

E.38.2.2 Technique Applicability: ★★★

All inserts are visually detectable with TTUT data.

E.38.2.3 Laboratory Setup

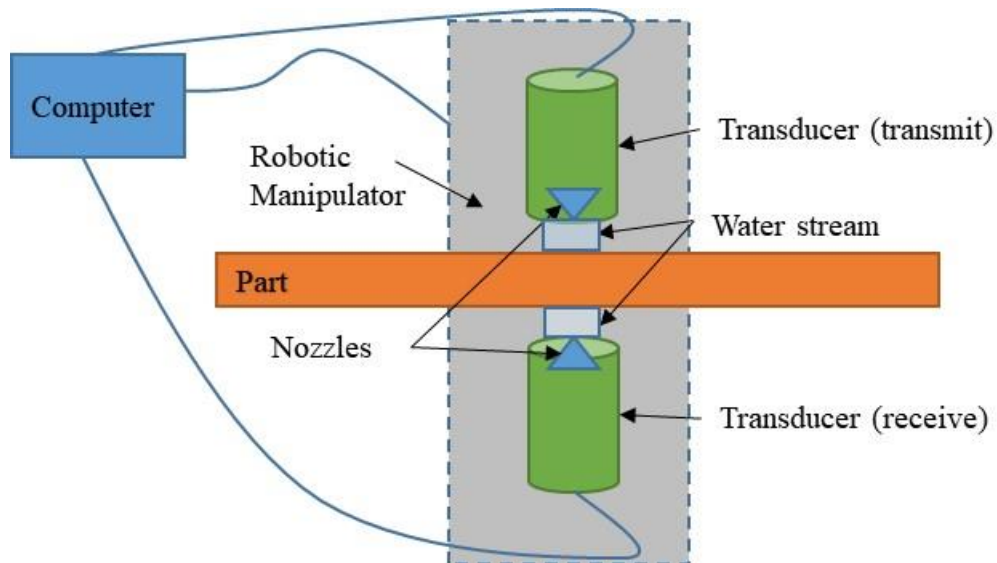


Figure E.38-7. TTUT scanning schematic with water pump.

The TTUT scanner at the Boeing laboratory consists of an enclosure, part supports, a water pump and nozzle system, ultrasonic transducers (transmitter and receiver), robotic manipulator, and control computer. After adjusting the water to produce a uniform flow, the pulser and receiver (on

opposite sides of the specimen) perform a C-scan under the control of the robotic manipulator and control computer. The C-scan is produced by taking multiple 1-dimensional scans (A-scans) and stitching them together to produce the final area result.

TTUT works on the principal of the capture and quantification of the transmitted waves. It uses a pulsing transducer on one side of the part and has the receiving transducer on the opposite side of the part. Scanning can be accomplished with contact, water streams, or full immersion method, as long as sufficient ultrasonic coupling is used. Although the TTUT works on non-parallel, front-to-back surface, the optimized data are produced when the front-to-back surfaces are parallel to each other.

As the ultrasonic waves travel through a material, they are attenuated. Defects and material discontinuities such as delamination, porosity and foreign material interfaces cause increased attenuation. UT has an orientation dependency, where certain defect orientations will attenuate the signal more if they are oriented for maximum reflection. Delamination tend to be oriented favorably for detection, making ultrasound the common method for composite inspection.

E.38.2.4 Equipment List and Specifications:

- 1 MHz ultrasonic transducer and receiver
- Water pump, nozzles, and circulation system
- Robotic manipulator
- Enclosure
- Control computer

E.38.2.5 Settings

Table E.38-2. Data collection settings.

Frequency	1 MHz
Resolution	0.04 inch × 0.04 inch

E.38.2.6 Inspection Results

The NASA Radii Delamination Standards are carbon fiber composite panels with foreign material inserts in various layers to evaluate the detectability using ultrasonic inspection. These inserts are largely grouped around the angle in the panel; however, not exclusive to this area. The standards vary in thickness, utilizing 8, 26, and 48 plies of carbon fiber fabric with exterior layers of fiberglass. Using TTUT, the all insert types (PT, RPF, and brass) were detectable. However, this visual detectability was generally reduced as thickness increased.

The brass inserts were the most resolved and detected (Figure E.38-8c) and the RPF inserts showed the lowest detectability (Figure E.38-83b). This is consistent with the theory that the RPF inserts bond to the material the best, leading to a small TTUT signal, while the brass has the worst bond (likely due to applied coating), leading to the large signals seen. The brass also has a significantly different attenuation than the surrounding material, allowing it to easily be detected. The 48-ply standards included inserts in locations on and away from the curved radius. The inserts away from the radius tended to be better resolved and defined (Figure E.38-8) due to the more uniform background signal. While the RPF inserts had small responses and resolving their exact shape is difficult, their presence tended to be detectable in the distortion of the surrounding signal and features (Figure E.38-8b).

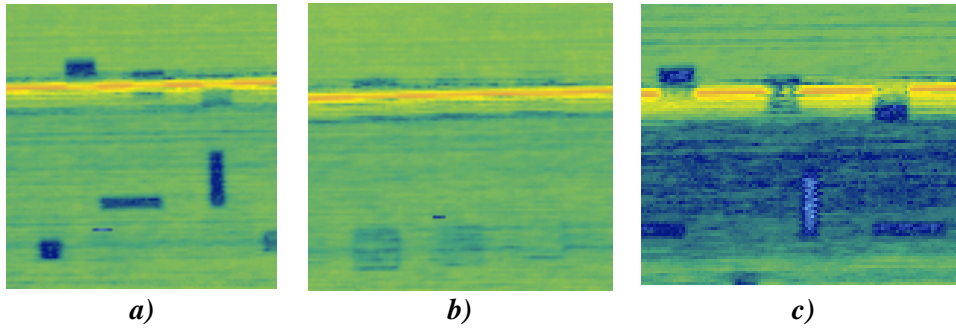


Figure E.38-8. TTUT scans showing PT (a), RPF (b), and brass (c) inserts.

E.38.3 Method: X-ray Digital Radiography (DR)

E.38.3.1 Partner: Boeing

E.38.3.2 Technique Applicability: ★★☆☆

X-ray DR is capable of detecting the brass inserts but is unable to detect the RPF or PT inserts.

E.38.3.3 Laboratory Setup

The DRC utilizes an YXLON Modular CT System with DR capability. This system includes a microfocus source and a digital detector array with positions controlled by a manipulator system. The microfocus source used has a variable focal spot size of less than four μm and is suitable for magnifications up to 10X. The manipulator has 7 DOF including a rotating stage to rotate the object as well as the ability to control its position along with the detector for magnification. The entire system includes the source, detector, manipulator, and user control station. The computers and control station are outside of the radiation enclosure (vault) and utilize a safety interlock system to operate. Cameras are located in the vault to allow the operator to monitor the part from outside the enclosure.

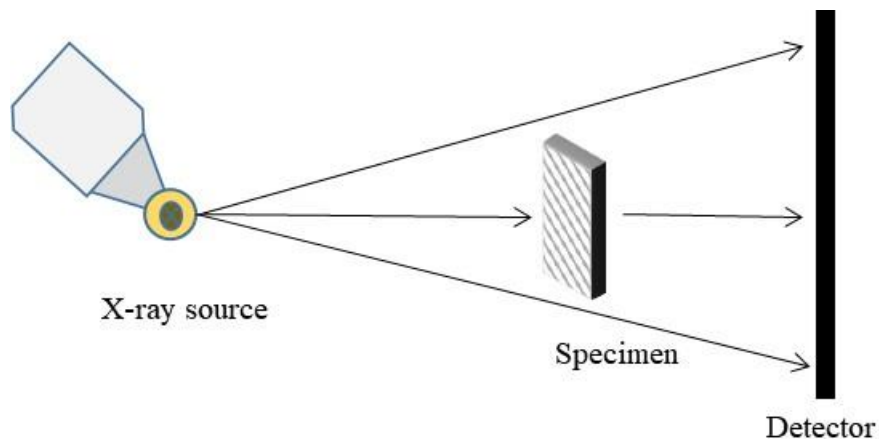


Figure E.38-9. X-ray DR Imaging

The standards were divided into two sections, labeled Upper and Lower, and placed on the rotator in a soft clamp (Figure E.38-10). The specimen was right side up for the Upper scan, and upside-down for the Lower scan. Lead markers were placed on the sections to denote the boundaries between and label sections. The position of the specimen, source, and detector are controlled to produce geometric magnification of the image and increase the spatial resolution while capturing the entire section of the part in the detector area. The image data are gathered as X-rays penetrate

the part and expose the detector for a set amount of time to produce a frame; multiple frames are average to produce the final image. This image, viewed in Image 3500, has much lower noise levels than a single frame due to the averaging. The operator adjusts the brightness and contrast settings of the image to identify the inserts, seen in the 2D image as rectangular defects.



Figure E.38-10. Laboratory setup of angle plate standard for DR imaging.

E.38.3.4 Equipment List and Specifications:

- 225 kV microfocus X-ray source with variable focal spot size
- 100 kg capacity, 7-axis, granite-based manipulator
- XRD 1621 Detector $\times 2048 \times 2048$ pixels with $200 \mu\text{m}$ pitch, 400×400 mm active area
- Image 3500 visualizing software

E.38.3.5 Settings

Table E.38-3. Imaging and exposure parameters.

Source Energy	100 kV
Current	0.7 mA
Source-Detector Distance	42 in
Source-Object Distance	27 in
Magnification	1.55X
Integration Time	500 ms
Integration Frames	50
Spatial Resolution (μm)	129 μm
Array Dimensions (pixels)	2048x2048

E.38.3.6 Inspection Results

The NASA Angle Panel Standards are carbon fiber composite panels with foreign material inserts in various layers to evaluate the detectability using ultrasonic inspection. These inserts grouped around the angle in the panel; however, not exclusive to this area. The standards vary in thickness, utilizing 8, 26, and 48 plies of carbon fiber fabric with exterior layers of fiberglass. Because of their length, the data set consists of the upper and lower half images of the standards.

DR X-ray imaging is sensitive to density variations, caused by material differences, voids, or other defects affecting the density of material the X-rays pass through. Because this imaging is 2D, the

results are superimposed internal images of the specimens. The resulting digital images are 16-bit greyscale images with the greyscale values representing the material density at each location (lighter corresponding to denser regions). Using Image 3500, the brightness and contrast settings vary to make defects visible. In the standards, the inserts show as rectangular areas with darker values (positive image).

The PT and RPF inserts are undetectable in this laminate thickness (Figure E.38-11a, b). Because the densities of the carbon fiber base material and the inserts are similar, a single-ply insert does not create a large density variation, thereby limiting the detectability. This detectability also drops as the laminate increases in thickness. The brass inserts, however, cause a very large density variation and are readily observable in all laminate thicknesses (Figure E.38-11c). Metal FOD in composite structures often show this degree of detectability due to the relatively high density of the metal compared to the composite.

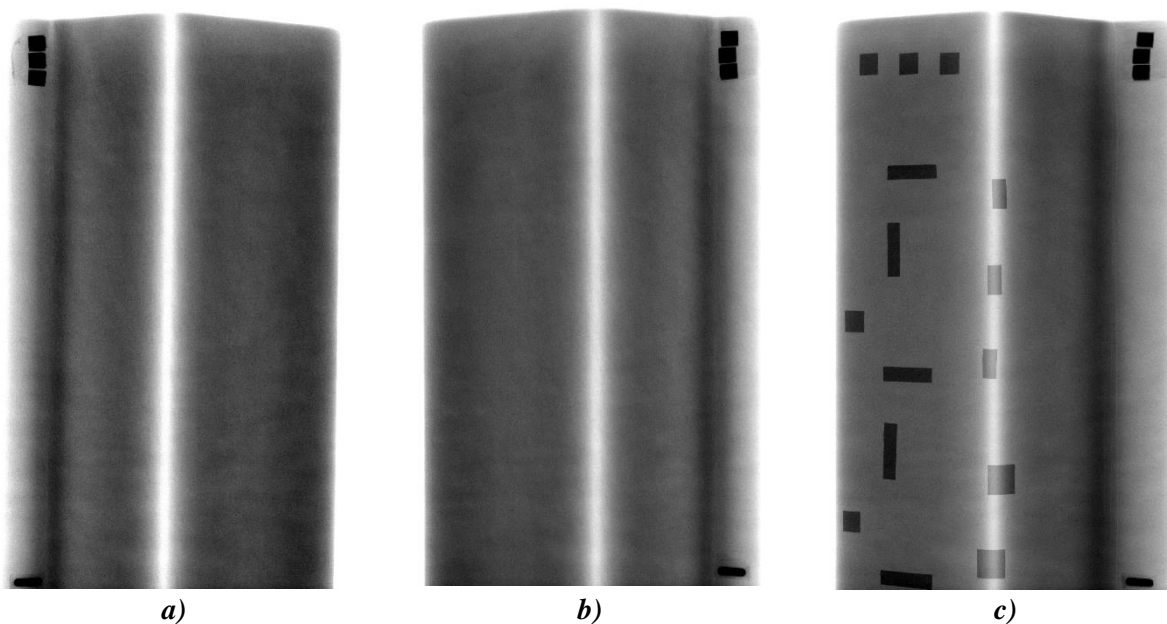


Figure E.38-11. DR images of PT (a), RPF (b), and brass (c) insert locations in 8276-200-56-48 standard.

E.38.4 Method: X-ray Computed Radiography (CR)

E.38.4.1 Partner: Boeing

E.38.4.2 Technique Applicability: ★☆☆

X-ray CR is capable of detecting the brass inserts but is unable to detect the PT and RPF inserts.

E.38.4.3 Laboratory Setup

The DRC has a small X-ray enclosure (vault) for the primary purpose of 2D X-ray imaging. It includes a Philips 160-kV X-ray source and the ability to use film, CR, and digital detector arrays. The CR imaging plates are placed on a table and the source, suspended from the ceiling by a 3-axis crane, can be positioned to control the Source to Object Distance. Outside of the enclosure are the controls for the source, utilizing a safety interlock system. These controls allow the user to set the energy, current, and exposure time for the source. In addition to the vault, the DRC utilizes a CRxFlex system to scan and erase the CR imaging plates, storing the images on a computer. The

phosphorus imaging plates, after exposure to X-rays, will luminesce the images when exposed to blue light, allowing the 50- μ m scanner to create digital versions and “erase” the plates using bright white light to be used again. The CR digital images are then reviewed using Rhythm Review.

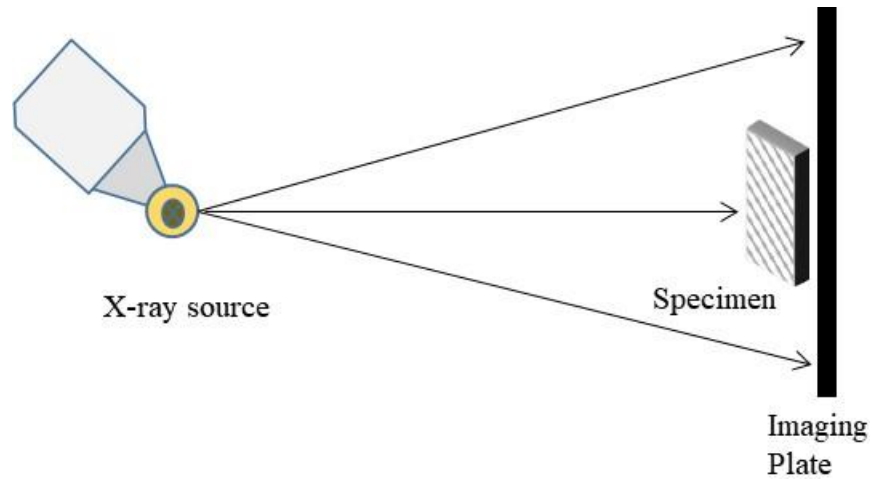
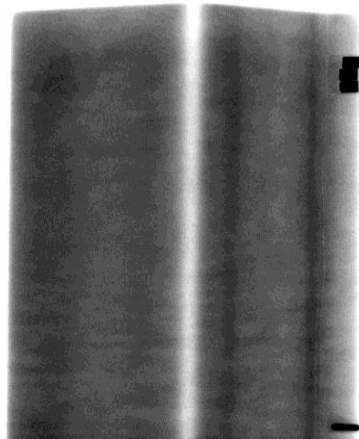


Figure E.38-12. X-ray CR imaging.

The standards were divided into two sections, labeled Upper and Lower, and placed directly on the plastic cassette containing the imaging plate with the X-ray source directly overhead (Figure E.38-13). The source was located 60 inches from the specimen and imaging plate to reduce geometric distortion. Lead markers were used to show section boundaries and label the images, showing up in the results as bright white. Because of the large differences in laminate thicknesses between the specimens, three separate source energies were used, with the highest energy for the thickest specimens.



a)



b)

Figure E.38-13. Laboratory setup of angle plate standards for CR imaging.

E.38.4.4 Equipment List and Specifications:

- Philips 160-kV X-ray source, 0.4 mm focal spot size
- IPS Phosphorus Imaging Plate
- GE CRxFlex Scanner, 50 μ m resolution
- GE Rhythm Review 5.0 visualizing software

E.38.4.5 Settings

Table E.38-4. Imaging and exposure parameters.

Source Energy	30,40,50 kV
Current	10 mA
Source-Detector Distance	60 in
Magnification	1X
Exposure time	10 s
Resolution (μm)	50 μm
Imaging Area (in)	14 \times 17

E.38.4.6 Inspection Results

The NASA Angle Panel Standards are carbon fiber composite panels with foreign material inserts in various layers to evaluate the detectability using ultrasonic inspection. These inserts grouped around the angle in the panel; however, not exclusive to this area. The standards vary in thickness, utilizing 8, 26, and 48 plies of carbon fiber fabric with exterior layers of fiberglass. Because of their length, the data set consists of the upper and lower half images of the standards.

CR X-ray imaging is sensitive to density variations, caused by material differences, voids, or other defects effecting the density of material the X-rays pass through. Because this imaging is 2D, the results are superimposed internal images of the specimens. The resulting digital images are 16-bit greyscale images with the greyscale values representing the material density at each location (lighter corresponding to denser regions). Using Rhythm Review, the brightness and contrast settings are varied to make defects visible. In addition, multiple filters are available to make defect identification easier for the operator. In the standards, the inserts show as rectangular areas with lighter values (negative image).

The PT and RPF inserts are undetected for this laminate thickness (Figure E.38-14a, b). Because the densities of the carbon fiber base material and the inserts are similar, a single-ply insert does not create a large density variation, thereby limiting the detectability. The brass inserts, however, cause a very large density variation and are readily observable in all laminate thicknesses (Figure E.38-14c). Metal FOD in composite structures often show this degree of detectability due to the relatively high density of the metal compared to the composite.

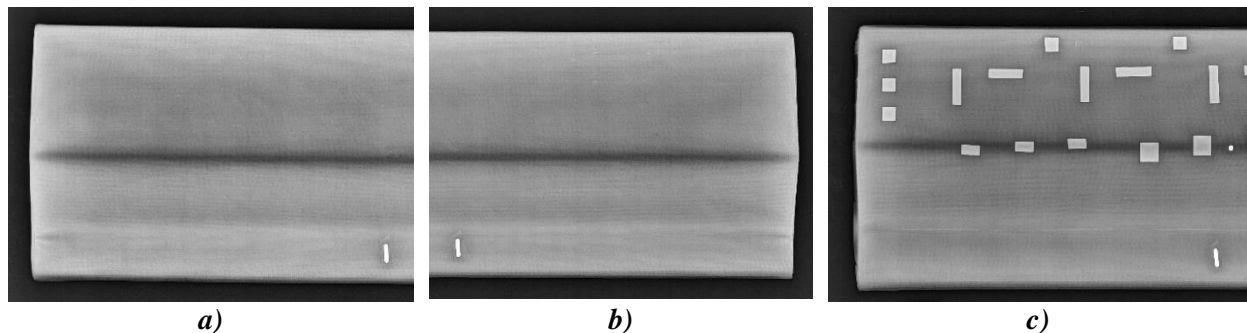


Figure E.38-14. CR images of PT (a), RPF (b), and brass (c) insert locations for 8276-200-56-48 standard (filter applied).

E.39 Specimen #39: Boeing 8276-200-59-48A

Structure	Material	Details	Dimensions (inches)	Partner Methods	
Laminates	8276 Tape	S curve (∟) 59° slant with two 0.2-inch radii. Multiple types of delamination simulators.	20 × 6 × 2.4	NASA	E.39.1 XCT
				Boeing	E.39.2 XCT E.39.3 TTUT E.39.4 X-ray DR E.39.5 X-ray CR



Figure E.39-1. Photograph of specimen #39: Boeing-8276-200-59-48A.

E.39.1 Method: X-ray Computed Tomography (XCT)

E.39.1.1 Partner: Boeing

E.39.1.2 Technique Applicability: ★★★

XCT is capable of identifying all inserts, notably brass inserts.

E.39.1.3 Equipment List and Specifications:

- YXLON Modular CT System
- 225 kV microfocus X-ray source with variable focal spot size
- 100 kg capacity, 7-axis, granite-based manipulator
- XRD 1621 Detector - 2048 × 2048 pixels with 200 μm pitch, 400 × 400 mm active area
- 126 μm spatial resolution for half volume scan
- Volume Graphics 3.0 visualizing software
- Reconstruction Computer

E.39.1.4 Settings

Table E.39-1. Data collection settings.

Source Energy	205 kV
Current	0.47 mA
Magnification	1.59 X
Filter	Copper
# Rotational angles	1080
Exposure time / frame	800 ms
Spatial Resolution (μm)	125.777 μm
Array Dimensions (pixels)	2048 × 2048

E.39.1.5 Laboratory Setup

The DRC utilizes an YXLON Modular CT System. This system has the capability to utilize various X-ray sources for varying applications, including a 450-kV source, a microfocus source, and a nanofocus source. The microfocus source used has a variable focal spot size of less than four μm and is suitable for magnifications up to 10X, with the nanofocus ranging up to 187X. The detector has 3 DOF, allowing for increase in the effective detector area through combined scans. The manipulator controls the position of the detector, object, and source. It has 7 DOF including a rotating stage to rotate the object during the scan. The entire system includes the source, detector, manipulator, control and reconstruction computers, and user control station. The computers and control station are outside of the radiation enclosure (vault) and utilize a safety interlock system to operate. Cameras are located in the vault to allow the operator to monitor the part from outside the enclosure.

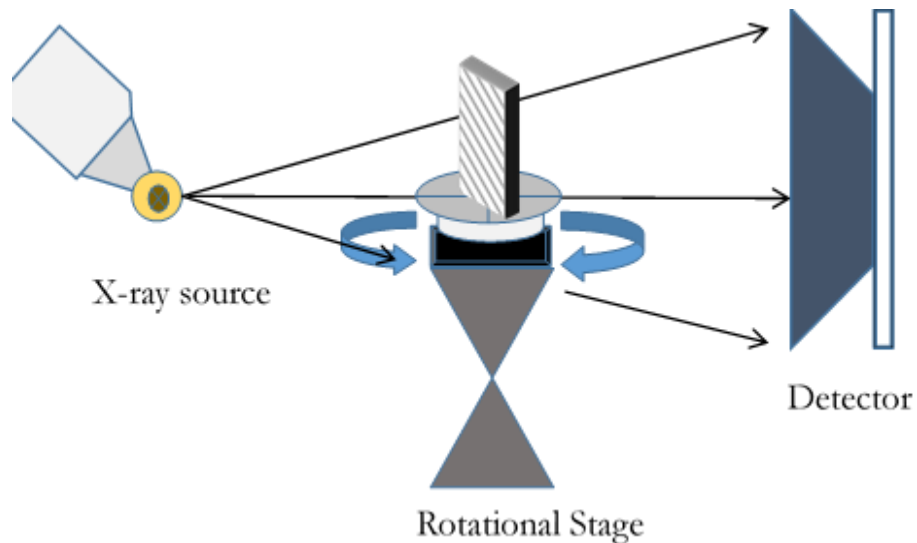


Figure E.39-2. XCT system components.

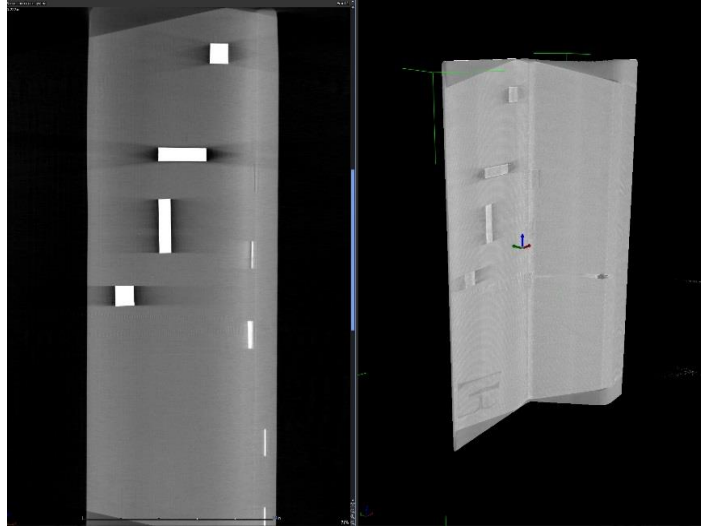


Figure E.39-4. Microfocus XCT setup for Radii Delamination Standard.

E.39.1.6 Inspection Results

The Radii Delamination Standards are carbon fiber composite panels with foreign material inserts in various layers to evaluate the detectability using ultrasonic inspection. These inserts are largely grouped around the angle in the panel; however, not exclusive to this area. The standards vary in thickness, utilizing 8, 26, and 48 plies of carbon fiber fabric with exterior layers of fiberglass. Because of their length, the data set consists of the upper and lower half volumes of the standards, flipped 180° for the scan.

After aligning the volume coordinate system to correspond with the panel geometry, the slice view can be used to inspect conditions at each lamina. The brightness and contrast settings are also adjusted to make defects clear, but retain the visible noise at a reasonable level. The inserts are clearly visible (Figure E.39-5), showing with less density for PT and RPF and higher density for brass. The brass is the most readily observable, followed by the PT with the RPF having the lowest detectability. The RPF may show the least response due to similar density to base material or due to a strong interface with little voiding or delamination to be detected.

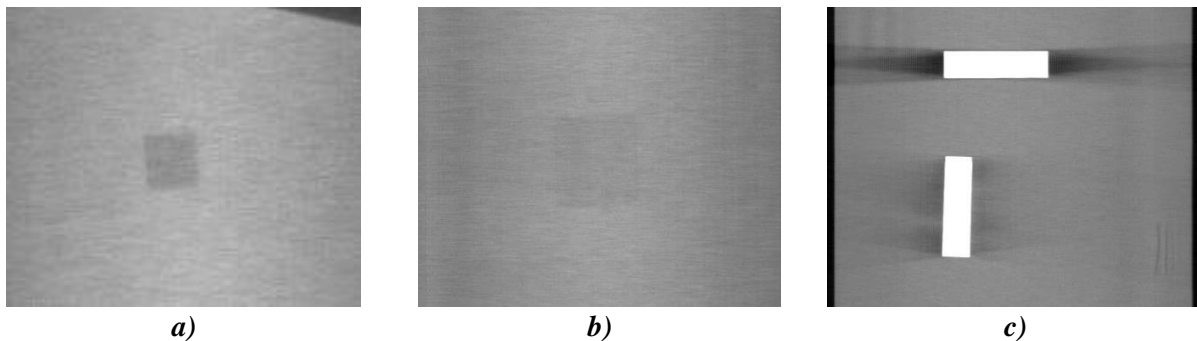


Figure E.39-5. CT slice view showing PT (a), RPF (b), and brass (c) inserts.

The CT scanning and reconstruction process is subject to artificial and undesirable artifacts. These are the result of multiple conditions. The direction of rotation leaves an underlying direction to the noise of the data set, aligning with the rotation. This is seen as a light, roughly horizontal streaking seen in (Figure E.39-5). The presence of high-density material in an otherwise low density structure often creates even more intense ray artifacts, seen as shadow-like streaks emanating from

the high-density material (Figure E.39-5c). If defects are present in these dark artifacts, their detectability is reduced. Lastly, the part may rotate in and out of the cone-beam of the X-rays during the scan, leaving the top and bottom edges of the volume not fully defined. This is seen as darker “wedges” of the volume at the top and bottom of the data set (Figure E.39-5).

The detectability of the inserts relies on viewing the slices at the appropriate angle, which aligns with the lamina. This means the inserts within the curve of the panel, while still detectable, are less apparent (Figure E.39-6), and operators must be careful to attempt to identify them. The inserts are also more visible when they induce delamination with air or if they have a much greater density than the composite material.

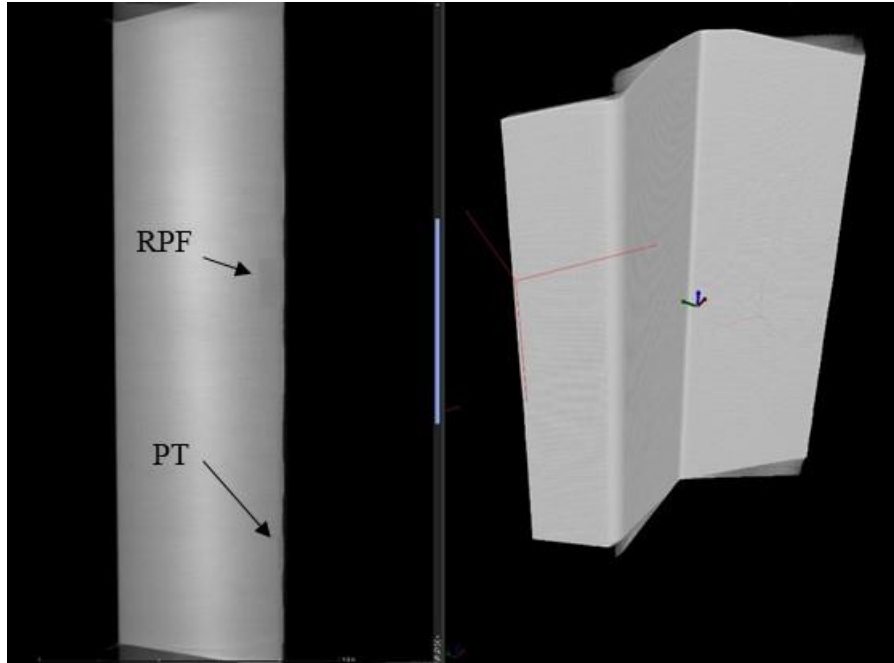


Figure E.39-6. CT slice view showing PT and RPF inserts.

E.39.2 Method: Through-Transmission Ultrasound Testing (TTUT)

E.39.2.1 Partner: Boeing

E.39.2.2 Technique Applicability: ★★★

All inserts are visually detectable with TTUT data.

E.39.2.3 Equipment List and Specifications:

- 1 MHz ultrasonic transducer and receiver
- Water pump, nozzles, and circulation system
- Robotic manipulator
- Enclosure
- Control computer

E.39.2.4 Settings

Table E.39-2. Data collection settings.

Frequency	1 MHz
Resolution	0.04 inch × 0.04 inch

E.39.2.5 Laboratory Setup

The TTUT scanner at the Boeing laboratory consists of an enclosure, part supports, a water pump and nozzle system, ultrasonic transducers (transmitter and receiver), robotic manipulator, and control computer. After adjusting the water to produce a uniform flow, the pulser and receiver (on opposite sides of the specimen) perform a C-scan under the control of the robotic manipulator and control computer. The C-scan is produced by taking multiple 1-dimensional scans (A-scans) and stitching them together to produce the final area result.

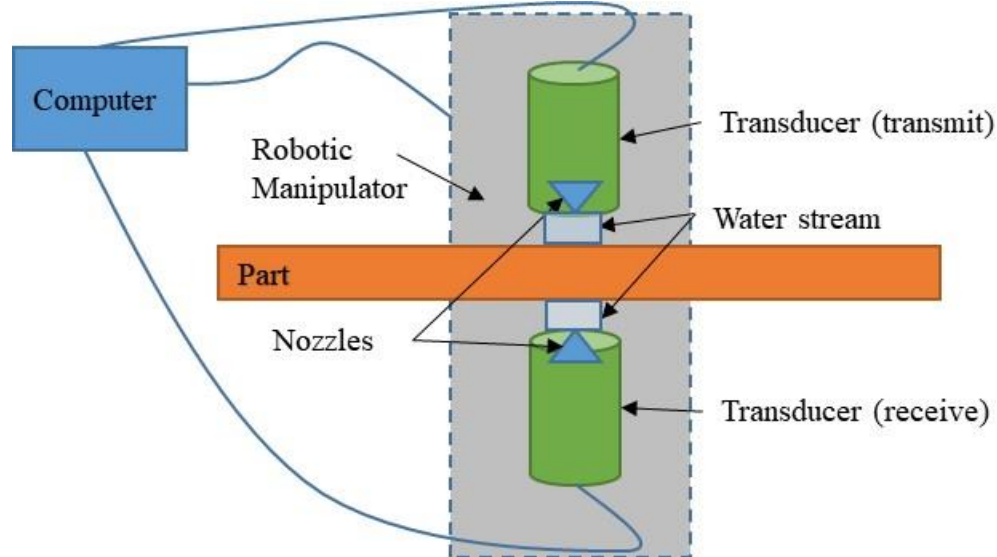


Figure E.39-7. TTUT scanning schematic with water pump.

TTUT works on the principal of the capture and quantification of the transmitted waves. It uses a pulsing transducer on one side of the part and has the receiving transducer on the opposite side of the part. Scanning can be accomplished with contact, water streams, or full immersion method, as long as sufficient ultrasonic coupling is used. Although the TTUT works on non-parallel, front-to-back surface, the optimized data are produced when the front-to-back surfaces are parallel to each other.

As the ultrasonic waves travel through a material, they are attenuated. Defects and material discontinuities such as delamination, porosity and foreign material interfaces cause increased attenuation. UT has an orientation dependency, where certain defect orientations will attenuate the signal more if they are oriented for maximum reflection. Delamination tend to be oriented favorably for detection, making ultrasound the common method for composite inspection.

E.39.2.6 Inspection Results

The NASA Radii Delamination Standards are carbon fiber composite panels with foreign material inserts in various layers to evaluate the detectability using ultrasonic inspection. These inserts are largely grouped around the angle in the panel; however, not exclusive to this area. The standards vary in thickness, utilizing 8, 26, and 48 plies of carbon fiber fabric with exterior layers of fiberglass. Using TTUT, the all insert types (PT, RPF, and brass) were detectable. However, this visual detectability was generally reduced as thickness increased.

The brass inserts were the most resolved and detected (Figure E.39-8c) and the RPF inserts showed the lowest detectability (Figure E.39-8b). This is consistent with the theory that the RPF inserts

bond to the material the best, leading to a small TTUT signal, while the brass has the worst bond (likely due to applied coating), leading to the large signals seen. The brass also has a significantly different attenuation than the surrounding material, allowing it to easily be detected. The 48-ply standards included inserts in locations on and away from the curved radius. The inserts away from the radius tended to be better resolved and defined (Figure E.39-8) due to the more uniform background signal. While the RPF inserts had small responses and resolving their exact shape is difficult, their presence tended to be detectable in the distortion of the surrounding signal and features (Figure E.39-8b).

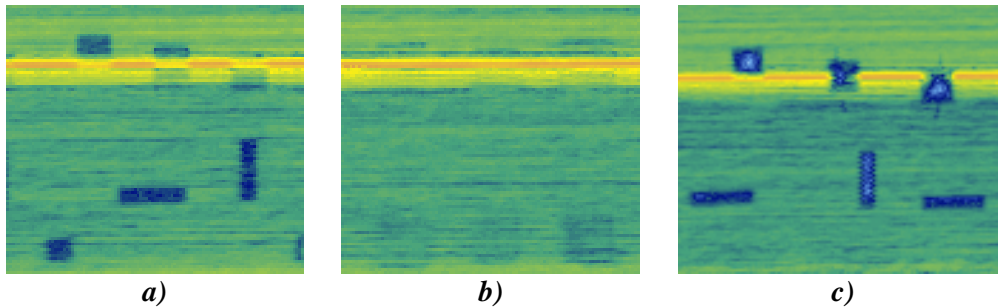


Figure E.39-8. TTUT scans showing PT (a), RPF (b), and brass (c) inserts.

E.39.3 Method: X-ray Digital Radiography (DR)

E.39.3.1 Partner: Boeing

E.39.3.2 Technique Applicability: ★☆☆

X-ray DR is capable of detecting the brass inserts but is unable to detect the RPF or PT inserts.

E.39.3.3 Equipment List and Specifications:

- 225 kV microfocus X-ray source with variable focal spot size
- 100kg capacity 7 axis granite based manipulator
- XRD 1621 Detector – 2048 × 2048 pixels with 200 μm pitch, 400 × 400 mm active area
- Image 3500 visualizing software

E.39.3.4 Settings

Table E.39-3. Imaging and exposure parameters.

Source Energy	100 kV
Current	0.7 mA
Source-Detector Distance	42 in
Source-Object Distance	27 in
Magnification	1.55X
Integration Time	500 ms
Integration Frames	50
Spatial Resolution (μm)	129 μm
Array Dimensions (pixels)	2048 × 2048

E.39.3.5 Laboratory Setup

The DRC utilizes an YXLON Modular CT System with DR capability. This system includes a microfocus source and a digital detector array with positions controlled by a manipulator system. The microfocus source used has a variable focal spot size of less than four μm and is suitable for

magnifications up to 10X. The manipulator has 7 DOF including a rotating stage to rotate the object as well as the ability to control its position along with the detector for magnification. The entire system includes the source, detector, manipulator, and user control station. The computers and control station are outside of the radiation enclosure (vault) and utilize a safety interlock system to operate. Cameras are located in the vault to allow the operator to monitor the part from outside the enclosure.

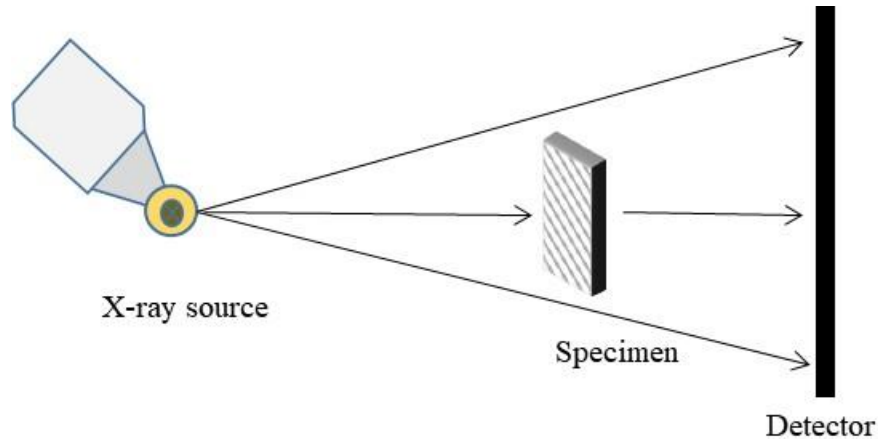


Figure E.39-9. X-ray DR imaging.

The standards were divided into two sections, labeled Upper and Lower, and placed on the rotator in a soft clamp (Figure E.39-10). The specimen was right side up for the Upper scan, and upside-down for the Lower scan. Lead markers were placed on the sections to denote the boundaries between and label sections. The position of the specimen, source, and detector are controlled to produce geometric magnification of the image and increase the spatial resolution while capturing the entire section of the part in the detector area. The image data are gathered as X-rays penetrate the part and expose the detector for a set amount of time to produce a frame; multiple frames are average to produce the final image. This image, viewed in Image 3500, has much lower noise levels than a single frame due to the averaging. The operator adjusts the brightness and contrast settings of the image to identify the inserts, seen in the 2D image as rectangular defects.



Figure E.39-10. Laboratory setup of angle plate standard for DR imaging.

E.39.3.6 Inspection Results

The NASA Angle Panel Standards are carbon fiber composite panels with foreign material inserts in various layers to evaluate the detectability using ultrasonic inspection. These inserts are largely grouped around the angle in the panel; however, not exclusive to this area. The standards vary in thickness, utilizing 8, 26, and 48 plies of carbon fiber fabric with exterior layers of fiberglass. Because of their length, the data set consists of the upper and lower half images of the standards.

DR X-ray imaging is sensitive to density variations, caused by material differences, voids, or other defects affecting the density of material the X-rays pass through. Because this imaging is 2D, the results are superimposed internal images of the specimens. The resulting digital images are 16-bit greyscale images with the greyscale values representing the material density at each location (lighter corresponding to denser regions). Using Image 3500, the brightness and contrast settings are varied to make defects visible. In the standards, the inserts show as rectangular areas with darker values (positive image).

The PT and RPF inserts are undetectable in this laminate thickness (Figure E.39-11a, b). Because the densities of the carbon fiber base material and the inserts are similar, a single-ply insert does not create a large density variation, thereby limiting the detectability. This detectability also drops as the laminate increases in thickness. The brass inserts, however, cause a very large density variation and are readily observable in all laminate thicknesses (Figure E.39-11c). Metal FOD in composite structures often show this degree of detectability due to the relatively high density of the metal compared to the composite.

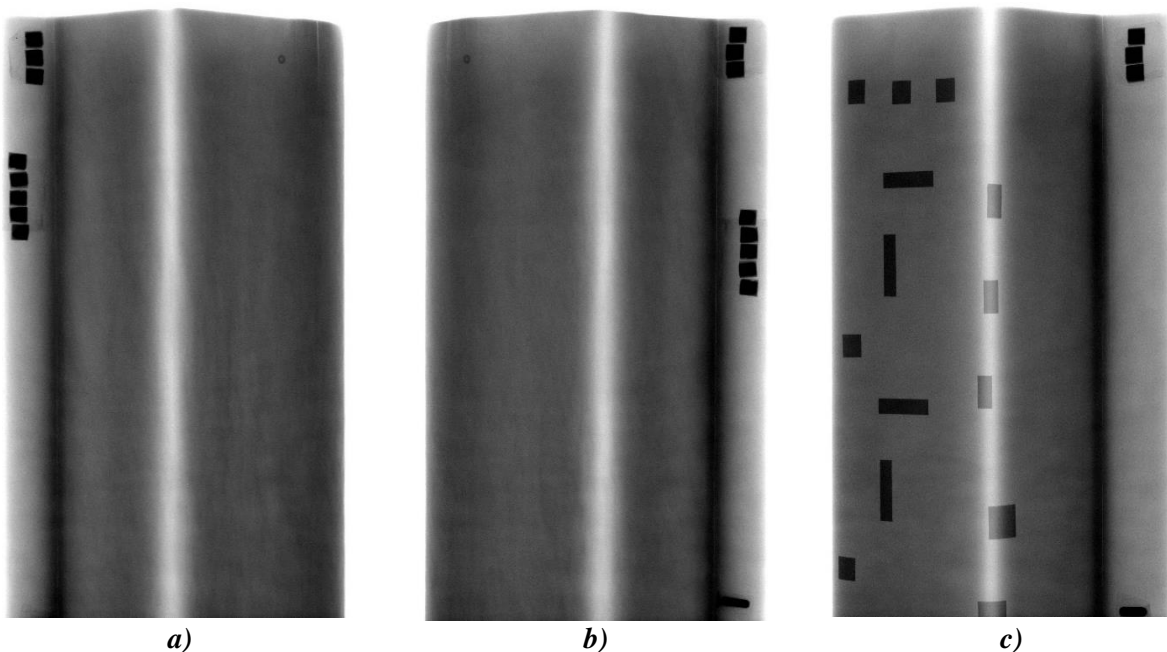


Figure E.39-11. DR images of PT (a), RPF (b), and brass (c) insert locations in 8276-200-59-48 standard.

E.39.4 Method: X-ray Computed Radiography (CR)

E.39.4.1 Partner: Boeing

E.39.4.2 Technique Applicability: ★☆☆

X-ray CR is capable of detecting the brass inserts but is unable to detect the PT and RPF inserts.

E.39.4.3 Equipment List and Specifications:

- Philips 160-kV X-ray source, 0.4 mm focal spot size
- IPS Phosphorus Imaging Plate
- GE CRxFlex Scanner, 50 μm resolution
- GE Rhythm Review 5.0 visualizing software

E.39.4.4 Settings

Table E.39-4. Imaging and exposure parameters.

Source Energy	30,40,50 kV
Current	10 mA
Source-Detector Distance	60 in
Magnification	1X
Exposure time	10 s
Resolution (μm)	50 μm
Imaging Area (in)	14 \times 17

E.39.4.5 Laboratory Setup

The DRC has a small X-ray enclosure (vault) for the primary purpose of 2D X-ray imaging. It includes a Philips 160-kV X-ray source and the ability to use film, CR, and digital detector arrays. The CR imaging plates are placed on a table and the source, suspended from the ceiling by a 3-axis crane, can be positioned to control the Source to Object Distance. Outside of the enclosure are the controls for the source, utilizing a safety interlock system. These controls allow the user to set the energy, current, and exposure time for the source. In addition to the vault, the DRC utilizes a CRxFlex system to scan and erase the CR imaging plates, storing the images on a computer. The phosphorus imaging plates, after exposure to X-rays, will luminesce the images when exposed to blue light, allowing the 50- μm scanner to create digital versions and “erase” the plates using bright white light to be used again. The CR digital images are then reviewed using Rhythm Review.

The standards were divided into two sections, labeled Upper and Lower, and placed directly on the plastic cassette containing the imaging plate with the X-ray source directly overhead (Figure E.39-12). The source was located 60 inches from the specimen and imaging plate to reduce geometric distortion. Lead markers were used to show section boundaries and label the images, showing up in the results as bright white. Because of the large differences in laminate thicknesses between the specimens, three separate source energies were used, with the highest energy for the thickest specimens.

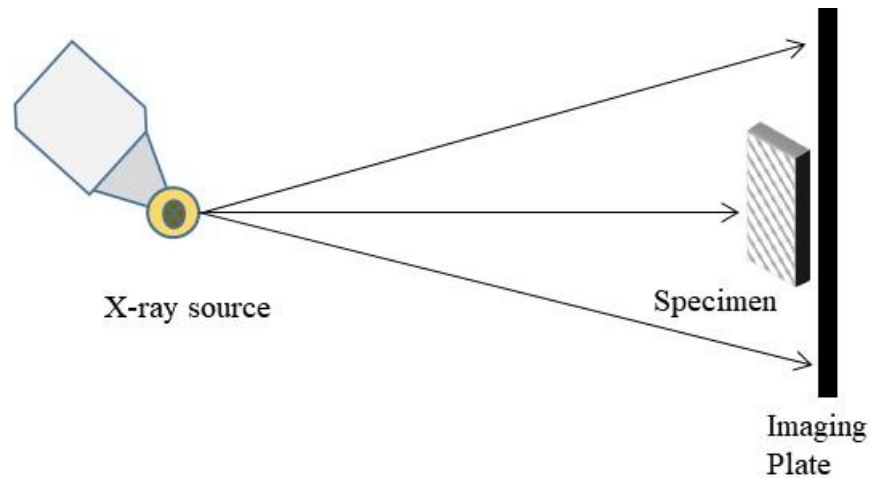


Figure E.39-12. X-ray CR imaging.

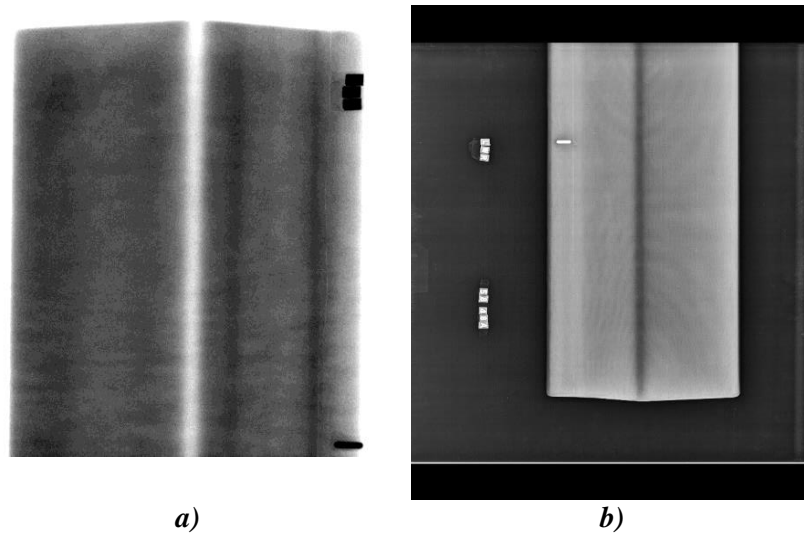


Figure E.39-13. Laboratory setup of angle plate standards for CR imaging.

E.39.4.6 Inspection Results

The NASA Angle Panel Standards are carbon fiber composite panels with foreign material inserts in various layers to evaluate the detectability using ultrasonic inspection. These inserts are largely grouped around the angle in the panel; however, not exclusive to this area. The standards vary in thickness, utilizing 8, 26, and 48 plies of carbon fiber fabric with exterior layers of fiberglass. Because of their length, the data set consists of the upper and lower half images of the standards.

CR X-ray imaging is sensitive to density variations, caused by material differences, voids, or other defects effecting the density of material the X-rays pass through. Because this imaging is 2D, the results are superimposed internal images of the specimens. The resulting digital images are 16-bit greyscale images with the greyscale values representing the material density at each location (lighter corresponding to denser regions). Using Rhythm Review, the brightness and contrast settings are varied to make defects visible. In addition, multiple filters are available to make defect identification easier for the operator. In the standards, the inserts show as rectangular areas with lighter values (negative image).

The PT and RPF inserts are undetected for this laminate thickness (Figure E.39-14a, b). Because the densities of the carbon fiber base material and the inserts are similar, a single-ply insert does not create a large density variation, thereby limiting the detectability. The brass inserts, however, cause a very large density variation and are readily observable in all laminate thicknesses (Figure E.39-14c). Metal FOD in composite structures often show this degree of detectability due to the relatively high density of the metal compared to the composite.

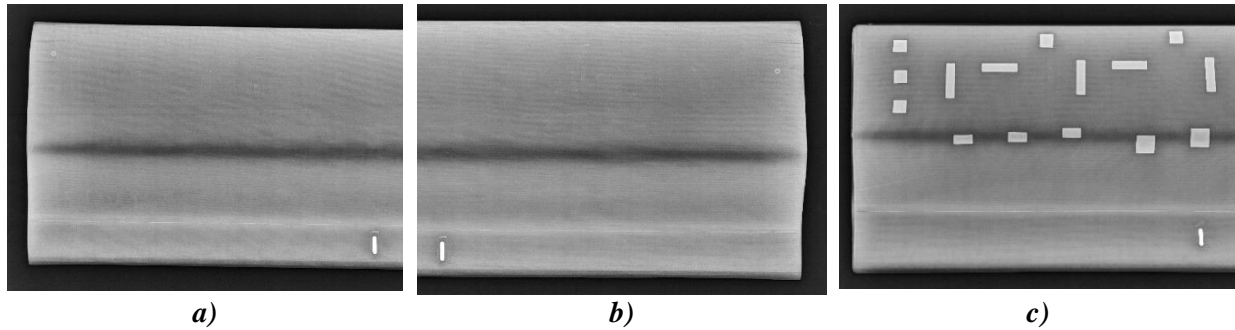


Figure E.39-14. CR images of PT (a), RPF (b), and brass (c) insert locations for 8276-200-59-48 standard (filter applied).

E.40 Specimen #40: Boeing-8276-200-58-8B – Not Tested

Structure	Material	Details	Dimensions (inches)	Partner Methods
Laminates	8276 Tape	S curve ($_/_$) 58° slant with two 0.2 inch radii. Multiple types of delamination simulators.	20 × 6 × 2.4	Not Tested